UNIVERSITY OF BIRMINGHAM

Determining the role of *Helicobacter pylori* and the microbiota during gastric cancer progression

by

Harriet Jayne Giddings

A thesis submitted to the University of Birmingham for the degree of
DOCTOR OF PHILOSOPHY

Institute of Microbes, Infections and Microbiomes
College of Medical and Dental Sciences
University of Birmingham
October 2024

Abstract

The global burden of gastric cancer (GC) is increasing and approximately 89% of non-cardia GC cases are linked to *Helicobacter pylori* infection. *H. pylori*-induced gastric adenocarcinoma (GAC) is typically preceded by a progression of histological changes within the gastric mucosa, which begins with chronic gastritis (CG) and advances to gastric intestinal metaplasia (GIM). Sequencing studies have also shown that the gastric microbiota undergoes significant alterations during carcinogenesis, with *H. pylori* gradually becoming displaced by non-*H. pylori* bacteria. However, studying *H. pylori* infection in vitro presents several challenges and sequencing data often lack spatial information regarding bacterial distribution and location. Therefore, although *H. pylori* genotypes encoding the virulence factors VacA, CagA and HtrA are associated with increased risk of GAC, the precise role of *H. pylori* and the gastric microbiota during carcinogenesis remains unclear. The aim of this study was to explore the relationship between *H. pylori* and the gastric microbiota across the early, middle, and late stages of gastric carcinogenesis. Patient-derived organoid monolayers were used to study the vacuolating effect of *H. pylori* VacA in vitro. Whilst VacA induced prominent vacuolation in the AGS cell line, vacuolation was not observed in monolayers exposed to different VacA allelic forms, raising questions over the significance of vacuolation during infection. To further understand the relationship between *H. pylori* and the gastric microbiota in carcinogenesis, multiplex imaging using RNAscope in situ hybridisation (ISH) combined with immunohistochemistry (IHC) of CG, GIM, and GAC histological gastric tissue was conducted. Although E-cadherin and MUC5AC expression remained relatively stable in CG, MUC2 expression was elevated in both GIM and GAC. Additionally, a significant correlation was found between *H. pylori*

presence and invasion of non-*H. pylori* bacteria into the lamina propria. In order to identify these bacteria, tissue regions containing invasive bacteria were isolated using laser capture microdissection (LCM) followed by full-length 16S ribosomal rRNA sequencing. Although multiple non-*H. pylori* bacterial genera were identified in CG, GIM and GAC samples, low sample biomass and amplicon contamination posed a significant challenge, highlighting the need for improved methods in future studies. Finally, a modified Gram stain was validated as a rapid, cost-effective tool for identification of non-*H. pylori* bacteria in histological samples, which confirmed previous findings and holds promise as a surveillance tool for GAC. In conclusion, in addition to *H. pylori*, the gastric microbiota likely also contribute to gastric carcinogenesis and future studies should therefore focus on confirming the identity and functional role of these bacteria.

.

Dedication

Since embarking on this PhD, I always knew I would dedicate this thesis to my Grandma, Vera. From as young as I can remember she inspired me to be curious, ask questions and seek enjoyment from learning. She taught me the importance of always trying my best. I also fondly remember spending hours with her looking at cat claws, leaves and flies through her light microscope, which are memories I will cherish forever and inspired me to pursue a career in science.

Acknowledgements

First and foremost, I would like to thank my supervisor Dr Amanda Rossiter for her advice, support and encouragement throughout my PhD. I am forever grateful to her for providing me with a second chance when things didn't originally go to plan. Thank you to Dr Claire Shannon-Lowe, for her unwavering support and enthusiasm with all things organoid related, I am very grateful for the time I spent working in her laboratory and will miss our coffees together in the Med Cafe. I thank Dr Karen Robinson for her brilliant advice, providing strains and fun times had at conferences. I am extremely grateful to Professor Jeffrey Cole, for his support, encouragement and excellent advice on how to improve my writing and presentation skills; I have learned a lot from him and will be forever grateful.

I would like to thank everyone I worked alongside in T101 and T102 over the years for providing such a supportive and encouraging environment even when things were difficult. Tabi, Cassie, Hannah, Basil, Sara, Osama, Tobi, Chen, Mat, Damon and Santosh, thank you for being such wonderful colleagues and friends, I hope we stay in contact. I also thank Will from the CSL lab, for being such a good friend and shoulder to cry on when my organoids didn't grow; I wish him the best for his own PhD. I would also like to thank members of the HAPI lab, Robin, Guillaume and Chris for being welcoming and kind, even though my stay was short.

I am very grateful to Alex and Becky at COMPARE, for their constant support and advice with my imaging work. Thank you for being so patient with me when I needed the confocal microscope instructions explained to me a million times. I am also very grateful to Ana, Jordanne and Joe at the BTA for scanning all of my images and for all their hard work in ensuring the various projects ran smoothly. Thank you to Dr Josh Quick, Natalie and Sam for your guidance and patience with my sequencing work.

Outside of my PhD, I am incredibly grateful to my amazing friends. Lauren, Izzy, Ella, Immy, Jade and Sof – I can't wait to celebrate with you over a pint soon.

The biggest thanks go to my family. Mum, Dad, Alice, Grandma and Grampy, thank you so much for your endless support and constantly believing in me, even when I didn't believe in myself. It has been a difficult journey, but I am grateful for you encouraging me to 'take it one day at a time'. To my wonderful partner Christopher, I have never met someone so kind, selfless and supportive. Your words of encouragement have been never ending, and I am truly grateful to have you in my life; I don't think I would have made it this far without you. Finally, to my lovely Nan and Grandad, although you are sadly no longer with us, I think about you both daily and know you would be proud of me. I love you and miss you.

Publications and awards resulting from the research conducted in this thesis

Publications

Giddings, H.J., Teodósio, A., Jones, J., McMurray, J.L., Hunter, K., Alame, R., Gardiner, I., Abdawn, Z., Butterworth, W., Henderson, I.R., Cole, J.A., Shannon-Lowe, C.D. and Rossiter-Pearson, A.E. (2025), The Gastric Microbiota Invade the Lamina Propria in *Helicobacter pylori*-Associated Gastritis and Precancer. Helicobacter, 30: e70016. https://doi.org/10.1111/hel.70016.

Awards

Second place best overall poster, awarded at Microbiomes in Health and Disease conference, 14–16 February 2024, Cambridge UK.

Second place best overall talk, awarded at MRC IMPACT DTP student symposium, 26th January 2023, Leicester, UK.

Highly commended for poster presentation, awarded at *Helicobacter pylori* genomics, signalling and carcinogenesis conference, June 29–July 2, 2022, Helsingør, Denmark.

First place best overall poster, awarded at MRC IMPACT DTP student symposium, 1st April 2022, Birmingham, UK.

List of abbreviations

AdDF	advanced ADF
AG	atrophic gastritis
AR	antigen retrieval
ASR	age-standardised rate
BSA	bovine serum albumin
BTA	Birmingham tissue analytics
Cag PAI	cag pathogenicity island
CagA	cytotoxin-associated gene A
CG	chronic gastritis
CHO	chinese hamster ovary
cRPMI	complete RPMI
D-TAC	diffusible type adenocarcinoma
EBV	Epstein-Barr virus
EMT	epithelial-mesenchymal-transition
FCS	foetal calf serum
FFPE	formalin-fixed paraffin-embedded
FISH	fluorescent in situ hybridisation
GAC	gastric adenocarcinoma
GC	gastric cancer
GIM	gastric intestinal metaplasia
H&E	haematoxylin and eosin
HBRC	human biomaterials research centre
HDGC	hereditary diffuse gastric cancer

HIER	heat induced epitope retrieval
HRP	horseradish peroxidase
HtrA	high temperature requirement A
I-TGAC	intestinal-type gastric carcinoma
IHC	immunohistochemistry
ISH	in situ hybridisation
LCM	laser capture microdissection
MAG	multifocal atrophic gastritis
MOI	multiplicity of infection
NAT	normal adjacent to tumour
ONT	oxford nanopore technologies
PBS	phosphate buffered saline
PPI	proton pump inhibitor
PUD	peptic ulcer disease
ROI	region of interest
SG	superficial gastritis
SIBO	small intestine bacterial overgrowth
SNP	single-nucleotide polymorphism
SSC	sodium citrate saline
UBT	urea breath test
VacA	vacuolating cytotoxin A
VEGF	vascular endothelial growth factor

Table of Contents

List of Figures

List of Tables

Chapter 1: Introduction

1.1. Gastric cancer epidemiology and incidence

Gastric cancer (GC) is the fifth most common malignant cancer and fourth leading cause of cancer-associated deaths globally. In 2021, there were an estimated 768, 793 deaths from GC reported worldwide (Siegel *et al*., 2021). On average, over one million cases of gastric cancer are diagnosed globally per year, yet incidence rate has steadily declined over the last thirty years. Incidence rate, or age-standardised rate (ASR), is defined as the number of cases per 100,000 per year and is a hypothetical measure based on the population distribution of a standard population. ASR is generally used to determine the risk of GC within a population or group; whereby a low-risk region is defined as an ASR of <10 per 100,000 people and a high-risk region is defined as an ASR of >20 per 100,000 people (Sung *et al*., 2021).

The ASR of GC varies geographically. Generally, high ASR countries are usually found in Asia, such as Mongolia, Japan, and Korea, whereas the United States of America (USA), United Kingdom (UK), South Africa and most European countries have a low ASR. For example, in 2022, incidence rates were highest in eastern Asia with 22.4 cases per 100,000 people, whereas the lowest rate was in South Africa with 3.3 cases per 100,000 people. In fact, in 2020, 75.3% of all stomach cancer cases reported globally were from Asian countries (Ferlay *et al*., 2021). Further variation in GC ASR and mortality have also been also identified. Even though Eastern Asian countries such as Mongolia, Japan and Korea reported the highest ASR, the highest death rates were observed in Western Asian countries such as Iran and Tajikistan. Additionally, global ASR of GC is roughly 2-fold higher in males in comparison to females, with a global average of 15.8 and 7.0 cases per 100,000 people, respectively (Morgan *et al*., 2022).

The reason for this remains unclear, however, some studies have suggested that higher consumption of alcohol and tobacco generally observed in males, or differences in sex hormones between males and females might be a contributing risk factor (Camargo *et al*., 2012; Wang *et al*., 2017). Furthermore, globally, GC is the fourth most common cancer for males, whereas in the UK it is the thirteenth most common (Cancer Research UK, 2024).

In the last thirty years, global incidence of GC has steadily declined, and it is now likened to a 'rare disease' primarily due to the discovery of *H. pylori* and availability of antibiotics. Even in recent years, a decrease in incidence and mortality is now predicted, as there were 27,600 new cases and 11,010 deaths reported in 2018 in the USA, compared with a prediction of 26, 890 new cases and approximately 10,880 deaths by the end of 2024 (Clinton *et al.,* 2020). As such, by 2035, 16 countries, including the UK and USA are hypothesised to fall below the rare diseased threshold, which is defined by having an ASR of 6 per 100,000 people (Morgan *et al*., 2022).

However, global incidence of GC in young people (<40 years old) has risen from 2 to 18% between 2002 and 2020 (Calderillo-Ruíz *et al*., 2023). The reason behind this is unclear, but it is hypothesised that likelihood of GC is overlooked due to a misconception that this cancer primarily effects older individuals. As such, younger patients are often incorrectly diagnosed or prescribed proton pump inhibitors (PPIs), without an invasive procedure such as endoscopy, resulting in pre-cancerous changes to the gastric mucosa sadly going unnoticed until it is too late (Zaręba *et al*., 2019).

Gastric adenocarcinoma (GAC) develops in gastric gland cells and is the most common type of GC in the UK, although it is often diagnosed at the later stages when the cancer has progressed (Banks et al., 2019). Given that GC is generally diagnosed in the later stages of cancer progression, the relative five-year survival rate of GC is ~23.9% in the UK, which is far lower than other cancers such as prostate (88.5%), kidney (66.6%) and colorectal cancer (CRC) (57.6%) as outlined in Figure 1.1 (NHS England Digital, 2024). As such, GC has recently been added to the Cancer Research UK (CRUK) list of cancers of strategic priority, with the aim to achieve earlier diagnosis, by improving awareness and surveillance methods (Cancer Research UK, 2024).

1.2. Types of gastric cancer

Gastric cancer was first characterised using the Laurén classification, which separated GC histologically into two main subtypes: diffusible type adenocarcinoma (D-TAC) and intestinal-type gastric carcinoma (I-TGAC). Broadly, the diffuse type is characterised by the presence of poorly cohesive cells which do not form glands, whereas cells within the intestinal type exhibit differentiation, either with or without mucin production (Lee *et al*., 2018). Around 30% of gastric cancers are the diffusible type which is more aggressive and generally affects the majority of the stomach. In comparison to the intestinal type, it is difficult to diagnose as mucosa within the diffuse type often appears histologically normal (Safadi *et al*., 2022). Intestinal-type gastric carcinoma, such as GAC, is less aggressive but primarily affects the distal stomach and is characterised by a series of histological changes to the gastric mucosa which are noticeable during endoscopy examination (Lee *et al.,* 2018).

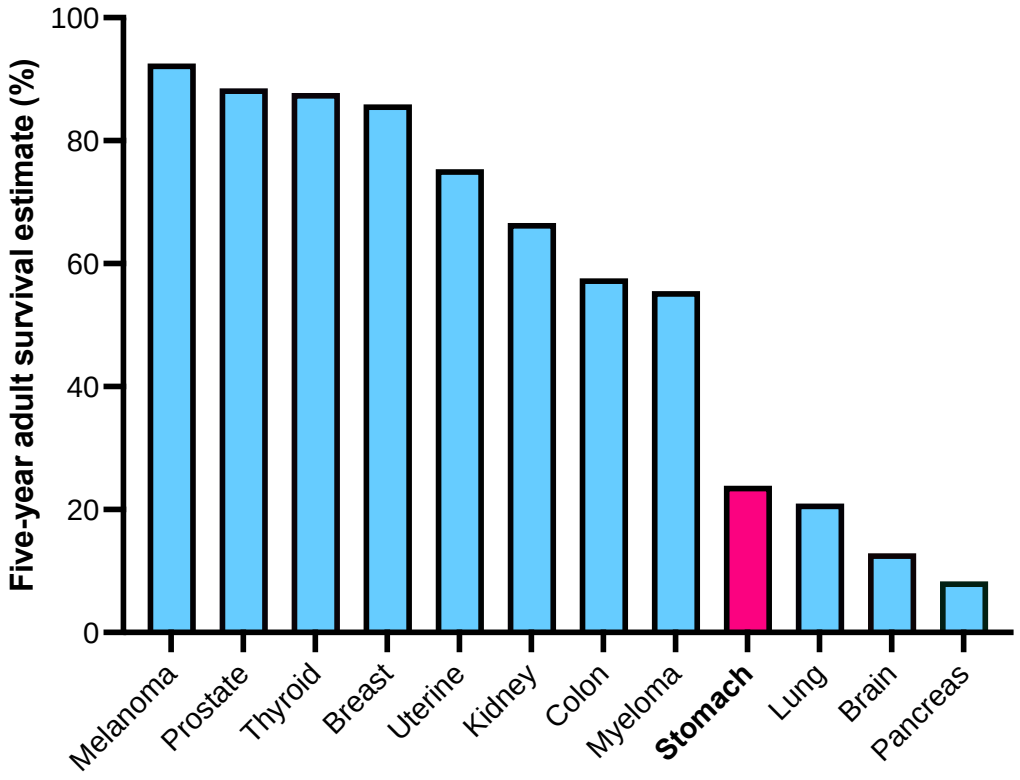

Figure 1.1. Five-year cancer survival estimates for adults in England. Five-year survival estimates for adults (aged 18-99) diagnosed between 2016-2020 and followed up until 2021. Figure reproduced in GraphPad Prism software from accredited official statistics published by NHS Digital in February 2023 (NHS England Digital, 2024).

1.3. Risk factors for development of gastric cancer

Lifestyle and dietary factors

Over the years, several studies have reported that lifestyle factors such as excessive alcohol use, smoking tobacco and a sedentary lifestyle or obesity are related to onset of gastric symptoms which can result in GC (González and López-Carrillo, 2010; Ebrahimi, 2023). The link between alcohol use and GC risk remains unclear, but it is hypothesised that alcohol exacerbates production of gastric acid, resulting in irritation and inflammation of the mucosa. In addition, acetaldehyde, the toxic metabolite of alcohol, is associated with mucosal injury, adverse cellular differentiation, host apoptosis and production of damaging free-radicals (Clinton *et al*., 2020). Many epidemiological studies have reported that gastric cancer risk is 1.5 to 2.5-fold higher in people who currently smoke cigarettes, compared with those who have never smoked (Sasazuki *et al*., 2002). Similar to alcohol, cigarettes contain multiple harmful chemicals, composed of aromatic amines, phenolic compounds and N-nitroso compounds with known toxic and carcinogenic effects on host mucosa and DNA, which might also drive tumourigenesis and cancer development (Zhang *et al*., 2012).

Nicotine has also been identified as another major risk factor, as it can activate tumour cell nicotinic acetylcholine receptors and promote release of growth factors such as vascular endothelial growth factor (VEGF) which directly exacerbates tumour angiogenesis and growth (Wong *et al*., 2007). Another risk factor is obesity, which is associated with increased risk of several cancers and it is thought that excess adipose tissue results in elevated pro-inflammatory cytokines such as TNF-α, IL-6 and IL-1β which can trigger tumorigenesis (Mohammadi, 2020; Scaglione *et al*., 2002).

Genetic mutations

Around 1-3% of gastric cancers are hereditary diffuse gastric cancers (HDGC), which are often caused by a germline mutation in the E-cadherin *CDH1* gene. Mutation results in epithelial-mesenchymal-transition (EMT), whereby cell-cell adherence of gastric mucosal cells is reduced, resulting in loss of cell polarity, cell structure and migration (Guilford *et al*., 1999). HDGC increases risk for development of both diffuse gastric cancer and lobular breast cancer (Schrader *et al*., 2008). Whilst HDGC is the most common hereditary cancer syndrome, other hereditary syndromes are associated with mutations in specific genes, resulting in increased risk. These include but are not limited to Lynch syndrome, familial adenomatous polyposis (FAP) and Peutz-Jehgders syndrome (Slavin *et al*., 2019). Inactivation of the tumour suppressor p53 gene is also associated with increased risk of GC and can occur in up to 77% of cases. It has been reported that the majority of p53 alterations occur in the early inflammatory stages of GC and increase in frequency as carcinogenesis progresses (Fenoglio-Preiser *et al*., 2003). The reason behind inactivation of p53 during GC development remains unclear, but is thought to be the result of a random, missense or deletion mutation in p53 or additional single-nucleotide polymorphisms (SNPs) within the gastric mucosa (Matozaki *et al*., 1992).

Epstein-Barr virus

Epstein-Barr virus (EBV) is a major risk factor for the development of nasopharyngeal carcinoma, T-cell lymphoma and GC. The mechanism behind carcinogenesis remains unclear, but it thought that EBV primarily infects oral B-lymphocytes and epithelial cells, which enter the digestive tract and arrive in the stomach, enabling translocation and

activation of EBV within the gastric mucosa. It is reported that EBV induces genomic methylation of the host, resulting in abnormal gene expression, imbalances in cellular signalling and initiation of tumorigenesis (Hutt-Fletcher, 2017). Latent EBV products are also associated with downregulation of microRNA, which can also result in reduced E-cadherin expression (Shinozaki *et al*., 2010).

1.4. *Helicobacter pylori*

Helicobacter pylori belongs to the Campylobacteria phylum and is a coloniser of the human digestive tract; it is estimated to be present in over half of the world's population (Diaconu *et al*., 2017). *H. pylori* is Gram-negative, microaerophilic, non-invasive and its cells are often spiral or coccoid in appearance (Amieva and El-Omar, 2008). Today's understanding of *H. pylori* primarily arose from Australian research in the 1980s, whereby it was first discovered by Barry Marshall and Robin Warren in 1982. Biopsy specimens were obtained from 100 patients who had presented with gastritis or peptic ulcers; both spiral and curved bacilli were observed in samples from 58 patients which were initially thought to be related to, or a new species of *Campylobacter* (Marshall and Warren, 1984). In the 1980s, it was thought that gastric ulceration and development of GC were solely related to lifestyle factors. However, in 1985, Marshall deliberately infected himself with *H. pylori* in order to demonstrate that the bacterium caused gastritis and gastric inflammation. Within 14 days, he experienced sickness, exhaustion, halitosis and diarrhoea. Soon after, Marshall underwent an endoscopy where he was diagnosed with *H. pylori*-induced gastritis. This was a vital finding, resulting in Marshall and Warren being awarded the Nobel Prize for Physiology in 2005

for proving that *H. pylori* directly induced chronic gastritis and severe mucosal damage within the human stomach (Marshall and Adams, 2008).

H. pylori epidemiology

It is estimated that *H. pylori* colonise between 50 and 70% of the global population, with prevalence depending on geographical region, socioeconomical status, race, age and lifestyle factors (Hu *et al*., 2017). *H. pylori* prevalence is generally higher in adults compared with children and adolescents, although this is likely due to the 'cohort effect', as most *H. pylori* infections are acquired in childhood (Malaty *et al*., 2002). A meta-analysis of several global *H. pylori* infection studies revealed the highest infection rates were in in African, Southeast Asian and South American counties, with some of the highest rates obtained in Nigeria (89.7%), South Africa (86.8%), Nicaragua (83.3%) and Colombia (83.1%). In contrast, infection rates were lowest in Europe, Oceana and North America, including the UK (27%), Belgium (11%), Sweden (15%) and USA (25%). Whist meta-analyses provide an indication of infection rates, it is worth noting that number of studies and sample size can vary greatly between countries (Zamani *et al*., 2018). High incidences of infection are likely attributed to lower socioeconomic status, lack of sufficient healthcare and hygiene and crowded living conditions (Mendall *et al*., 1992). Additionally, number of siblings are also a predictor of infection, with some studies suggesting that transmission of *H. pylori* between siblings and family members is a significant cause of high infection rates in these areas (Goodman and Correa, 2000). In contrast, in areas with low infection rates, improved public hygiene, healthcare, education and living conditions reduce the likelihood of transmission between the general public and family members (Diaconu *et al*., 2017).

The role of *H. pylori* in the human stomach

Given that a large proportion of the population are infected by *H. pylori*, yet only few people develop symptoms, questions have arisen over whether *H. pylori* should be considered a pathogen or commensal of the human stomach (Amieva and El-Omar, 2008). Evidence suggests that a relationship between *H. pylori* and the human host has existed for at least 3,000 years, as antigens of *H. pylori,* in addition to other bacterial species as *Giardia* and *Cryptosporidia*, were detected in mummified faecal specimens (Alisson *et al.,* 2019). Furthermore, genetic diversity of *H. pylori* has been shown to decrease with distance from East Africa, which correlates with genetic diversity of humans. This suggests that *H. pylori* has coevolved with humans over the last ~60,000 years, and likely shares a common ancestor (Linz *et al.,* 2007).

Studies have suggested that *H. pylori* colonisation benefits the human host, by modulating the immune system and protecting against the development of other diseases or pathologies (Li *et al.,* 2018). For example, it is proposed that *H. pylori* protect against asthma and allergy via the ‘hygiene hypothesis’, whereby early childhood exposure to certain pathogens may regulate the immune system. Several studies have suggested that *H. pylori* alter the ratio of Th1 and Th2 helper and regulatory T cells, resulting in dampening of inflammatory pathways commonly involved in asthma or allergy (Liu *et al.,* 2024). In addition, *H. pylori* has been shown to reduce the risk of oesophageal diseases, such as gastroesophageal reflux disease (GERD), Barrett’s oesophagus and oesophageal adenocarcinoma (Miller *et al.,* 2022). Although the precise mechanism is unclear, it is hypothesised that *H. pylori* influence gastric acid production and stomach movement, resulting in reduced acid reflux back

into the oesophageal tract, and as such, eradication of *H. pylori* may reverse this effect *(*Doorakers *et al.,* 2020). Moreover, although *H. pylori* indeed have some protective effects on the human host, given the findings by Marshall and Warren (1984) linking *H. pylori* with gastritis and inflammation, it is important to test and treat for *H. pylori* infection if a patient is presenting with undesirable and unpleasant symptoms.

Diagnosis of *H. pylori*

According to National Institute for Health and Care Excellence (NICE) guidelines, the current gold standard for non-invasive detection of *H. pylori* is the urea breath test (UBT) which detects breakdown of urea by *H. pylori*-secreted urease (García-Morales *et al.*, 2023). It is generally preferred for patients who do not require an endoscopy, but have other diseases strongly associated with *H. pylori* infection, such as peptic ulcer disease (PUD) (Chey *et al*., 2017). Although the UHB test is rapid and cost effective, false positive results have been obtained due to the presence of other urease-producing microbiota within the stomach and prescription of proton-pump inhibitors. This can lead to over-reporting of *H. pylori* infection during epidemiological studies. In contrast, the coccoid form of *H. pylori* is metabolically inactive, does not produce urease and can produce false-negative results (Osaki *et al*., 2008) .

As such, stool culture is an additional non-invasive indicator of *H. pylori* infection and is commonly in combination with the UBT for *H. pylori* diagnosis in the UK (Aumpan *et al.,* 2020). *H. pylori* is detected in stool using monoclonal or polyclonal antibodies, however, this test is often criticised as isolation of *H. pylori* from stool is difficult due to presence of biliary salts, competition with other microbiota and transformation of the

bacterium into a viable but not culturable form (Kelly *et al*., 1994). Furthermore, an additional non-invasive test relies on detection of *H. pylori*-specific IgG and IgA antibodies. Whilst these tests are generally regarded as highly sensitive (80-90%) and provide an immediate result, they are also limited as they are not as effective as invasive testing, do not distinguish between past and active infection and are not widely available or approved by many government agencies (Xu and Graham, 2021). Once *H. pylori* is detected, patients are usually prescribed a standard 14-day triple therapy of proton pump inhibitors (PPIs), such as omeprazole or lansoprazole, in combination with antibiotics such as amoxicillin, metronidazole or clarithromycin. A re-test for *H. pylori* infection is then conducted four to eight weeks after discontinuing treatment to ensure infection is eradicated (Chey *et al.,* 2017).

If *H. pylori* infection persists or symptoms worsen despite treatment, infection is investigated further with an invasive endoscopy. Although this procedure is uncomfortable for the patient and requires a hospital or clinic visit, an endoscopy is a reliable tool for detection of *H. pylori*, pre-cancerous lesions and histological changes indicative of GC (East *et al*., 2016). During an endoscopic procedure, physicians are able to identify changes to the gastric mucosa associated with *H. pylori* infection, including erythema, swelling, ulceration, atrophy, lesions and bleeding (Glover *et al*., 2020). Furthermore, during an endoscopic procedure, a biopsy can be obtained of the infected tissue for further histological analysis by a pathologist. A variety of staining techniques, including H&E, Warthine Starry and Giemsa stain have been used to evaluate gastric inflammation and presence of *H. pylori* within gastric tissue, in addition to mucin expression (Lee and Kim, 2015). The updated Sydney system is then used

to grade *H. pylori* density, immune cell activity, glandular atrophy and inflammation from five separate biopsy sites (Dixon *et al*., 1996).

H. pylori pathogenesis

H. pylori have high genetic diversity, with DNA sequence polymorphism between 2.7 and 8.0%. Its genetic diversity is acquired through several mechanisms, often involving spontaneous mutations, mobile genetic elements, allelic recombination and recombination with other bacteria (Hirschl *et al*., 1994). However, *H. pylori* are genetically heterogenous resulting in expression of multiple genes which produce varying phenotypes. As such, *H. pylori* strains vary in pathogenicity, with some strains having higher virulence than others (Mi *et al*., 2021). *H. pylori* possess several virulence factors which facilitate colonisation, adherence and damage to host tissue. *H. pylori* cells have three to seven sheathed flagella, which enhance motility through gastric mucin (Gu, 2017). It was also observed that number of flagella correlated with enhanced sialic acid-binding adhesion (SabA) mediated interactions, thus suggesting an association between number of flagella and pathological outcome (Martínez *et al*., 2016). Urease is also produced by *H. pylori* and accounts for around 10% of the bacterial cell protein production (Schoep *et al*., 2010). Urease hydrolyses urea, which results in ammonia and carbamate production, which in turn neutralises stomach acid, facilitating survival of *H. pylori* in the harsh gastric environment (Athmann *et al*., 2000).

CagA

A well-characterised virulence factor associated with *H. pylori* is the *cag* pathogenicity island (cag PAI). It is found in approximately 60-70% of Western *H. pylori* strains and

almost 100% of East-Asian strains, such as strains obtained from China, Japan and Korea (Tomb *et al*., 1997). The cag PAI is a 40kb DNA insertion element, which contains approximately 31 genes, including ~3,500-5,000 base pair *cagA,* which encodes the 128-145 kDa CagA protein. *H. pylori* strains are either *cagA*-positive, or *cagA*-negative, with the *cagA*-positive strains encoding the *cagA* gene at the end of the *cag* PAI (Backert and Tegtmeyer, 2017). Within the cag PAI, the Cag type 4 secretion system (T4SS) is encoded in addition to its effector protein, CagA. Generally, *H. pylori* adhesins such as BabA/B and SabA initiate the bacterial contact to epithelial cells, whilst the T4SS acts as an extra-cellular, pilus-like structure which then translocates CagA into the cell cytosol (Nejati *et al*., 2018). It is well established that that CagA induces releases pro-inflammatory cytokines such as interleukin-8 (IL-8) secretion via a series of signalling cascades. One such cascade, is activation of the NF-$_K$B pathway, which plays a key role in the regulation of genes associated with the inflammatory response to microbial infections in both gastric and intestinal epithelial cells and is often associated with carcinogenesis (Peng *et al*., 2020; Taniguchi and Karin, 2018). In healthy cells, NF-$_K$B is inhibited by I$_K$B proteins within the cell cytoplasm. However, infection with *H. pylori* CagA results in activation of intracellular signalling pathways, which leads to nuclear translocation of NF-$_K$B and an increase in IL-8 secretion during the inflammatory response. Once injected inside the cell, CagA can act in either a phosphorylation-dependent or independent pathway (Sharma *et al*., 1998) (Figure 1.2)

CagA induces a multitude of destructive effects on host cells as it can interfere with cellular morphology and physiology. CagA has been observed to interact with

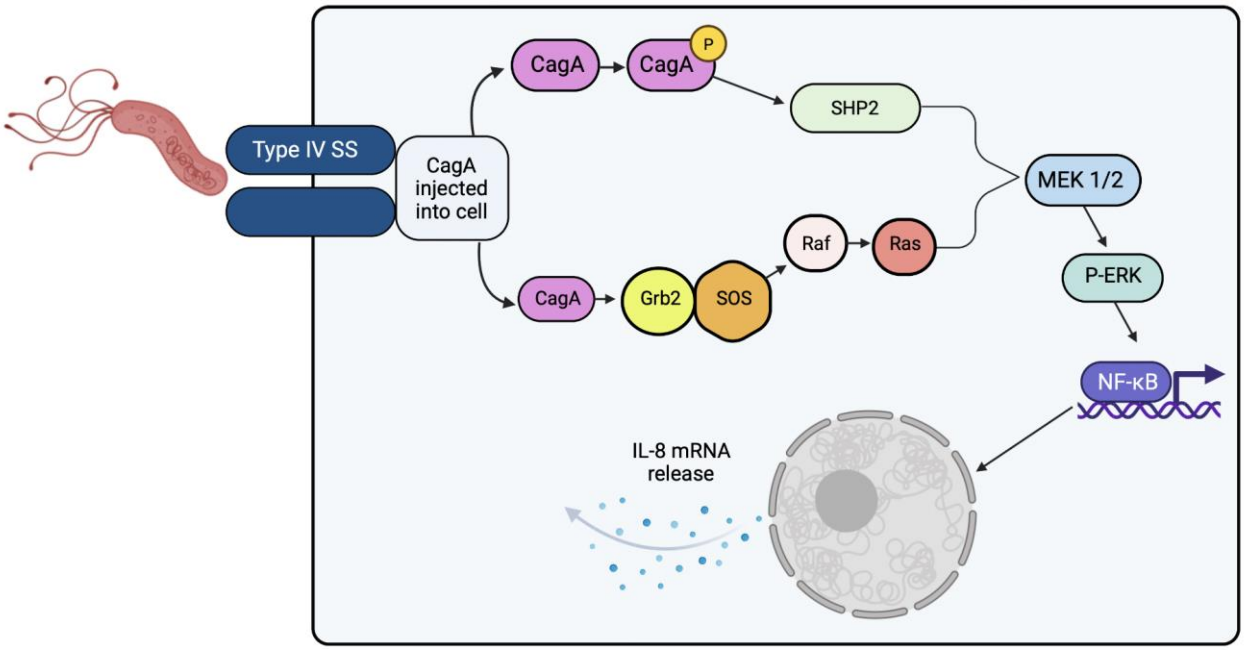

Figure 1.2. Simplified schematic showing *H. pylori* CagA induced IL-8 release within a host cell. CagA is injected into the host cell via the Type IV secretion system, resulting in activation of nuclear signalling pathways and translocation of NF-KB in a phosphorylation dependent or independent manner. IL-8 mRNA levels rise within the host cell and are eventually secreted extracellularly during a pro-inflammatory response. Figure created in Biorender.com.

partitioning defective-1 (PAR1) and microtubule affinity-regulating kinase (MARK) which induces depolarisation of epithelial cell monolayers by interfering with basolateral proteins and tight junctional barriers (Amieva and El-Omar, 2008). CagA is also associated with disruption of Wnt signalling, promoting hyperproliferation of gastric cells, in addition to modulation of the aforementioned p53 pathway (Li *et al*., 2016; Song *et al*., 2015). Another well-studied phenotype induced by CagA is the formation of 'hummingbird' shaped-cells, whereby the host cell elongates and becomes spindle-shaped. This likely occurs due to inactivation of focal adhesion kinase (FAK) as a result of activation of SHP-2 by phosphorylated CagA (Tsutsumi *et al*., 2006).

VacA

Vacuolating cytotoxin-A (VacA) is another important and well-studied *H. pylori* virulence factor. VacA is a secreted Type V autotransporter protein, which is produced by most *H. pylori* strains and shares no similarity with any other known bacterial or eukaryotic protein (Atherton *et al.,* 1995). VacA belongs to the autotransporter pathway of secreted proteins and can either remain on the bacterial surface or is transported across the inner membrane of Gram-negative *H. pylori* in a *sec*-dependent process, followed by transport across the outer membrane by a transporter domain (Telford *et al*., 1994). The VacA precursor polypeptide is ~140 kDa and during export is processed resulting in production of a mature ~88 kDa toxin, a ~12 kDa unknown peptide and the C-terminal ~33 kDa β-barrel (Fischer *et al*., 2001). The β-barrel structure forms a pore in the outer membrane enabling translocation of the active 88 kDa toxin, which either remains on the bacterial surface or is released into the extracellular space as two cleaved products: signal and intermediate region p33, and middle region p55.

The p33 and p55 toxin domains can exist as separate domains, but are required to interact with each other to induce virulent effects (Torres *et al*., 2005) (Figure 1.3). The p55 domain is involved in host-cell binding activity, whereas the p33 domain has been shown to induce downstream virulent effects (Palframan *et al*., 2012; Papini *et al*., 2001). The ~12 kDa subunit of unknown function is also released as a soluble protein (Cover and Blaser, 1992). *VacA* is also polymorphic and contains at least two variable components in the signal (s), intermediate (i) and middle (m) regions, which undergo allelic recombination, resulting in strains exhibiting mosaicism (Atherton et al., 1995). The intermediate region exists as subtypes i1 or i2 whereas the middle and signal regions generally exist as m1 or m2 and s1 or s2. The *vacA* gene is composed of different allelic types from each region and is a determinant of toxin production and virulence (Papini *et al*., 2001). Recently, new genotypes *d1* and *d2* have also been identified from a fourth deletion (d) region between the signal and intermediate regions using bioinformatic approaches. Using theoretical assumptions, it was shown that strains expressing *d1* are likely to be found in areas with high *H. pylori* presence, whereas *d2* is associated with areas with low infection rate (Soyfoo *et al*., 2021).

H. pylori expressing s1/m1 and s1/m2 VacA are generally more pathogenic, causing more chronic inflammation when compared with other genotypes. The s1/m1 allelic combination is thought to induce the most severe damage to the gastric mucosa and has since been associated with increased risk for development of GC (Gerhard *et al*., 1999; Louw *et al*., 2001). In contrast, during an in vivo C57BL/6J mouse infection study using isogenic *H. pylori* strains, it was observed that despite VacA s1/i1 forms inducing severe inflammation, their colonisation success and bacterial density was significantly

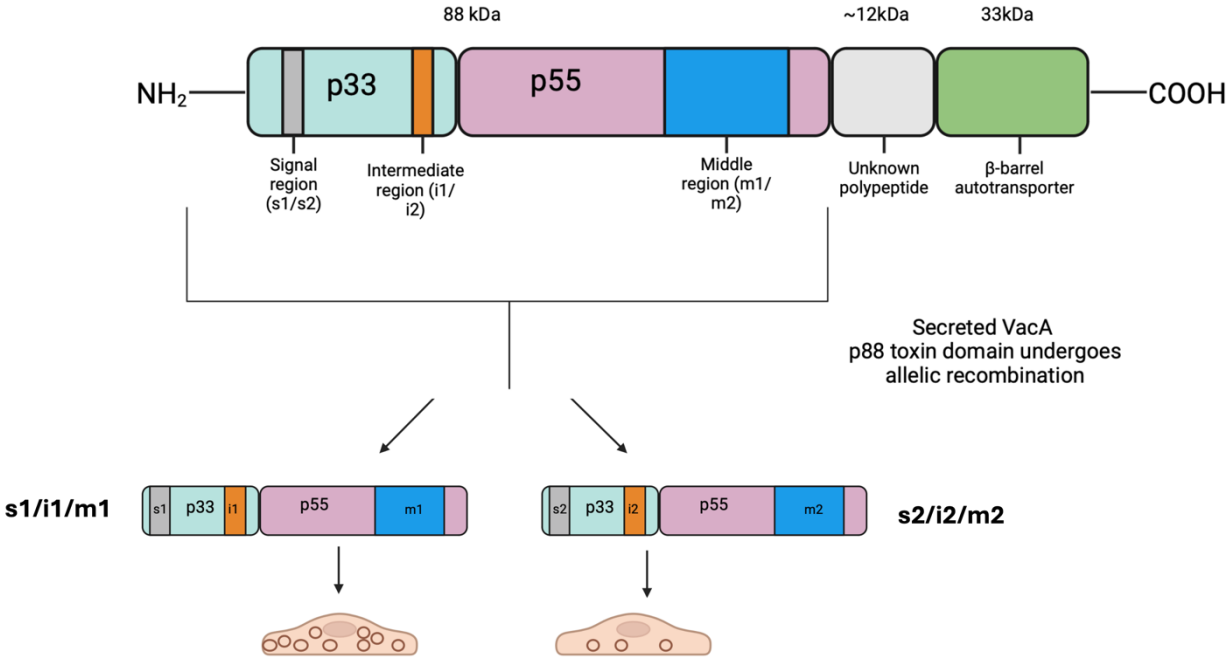

Figure 1.3. Simplified schematic showing *H. pylori* VacA protein structure and allelic recombination within the secreted p88 toxin. The VacA precursor polypeptide is ~140kDa which is processed during export resulting in production of a mature ~88 kDa toxin, a ~12 kDa unknown peptide and the C-terminal ~33 kDa β-barrel (Fischer *et al*., 2001). The active 88 kDa toxin (p88) is composed of the signal (s), intermediate (i) region and middle (m) region which undergo allelic recombination, resulting in mosaicism. Generally, the s1/i1/m1 allelic form is associated with higher vacuolating activity compared with the s2/i2/m2 form. p88 either remains on the bacterial surface or is released into the extracellular space as two cleaved products: signal (s) and intermediate (i) region p33 and middle (m) region p55. Figure reproduced from Sewald *et al.,* (2008) and created in Biorender.com.

lower compared with s2/i2 expressing strains (Winter *et al*., 2014). However, this study was conducted on mice, which are not natural hosts of *H. pylori.* As such, it is possible that mice are more susceptible to the s2/i2 form of *H. pylori* compared with humans, but this phenomenon was not investigated further. VacA induces multiple effects on host epithelial cells, although arguably the most extensively studied effect is vacuolation. Although the mechanism behind vacuolation remains unclear, the current model hypothesises that VacA is internalised into the endosomal compartment by endocytosis, leading to an influx of H^+ ions into the endosome and accumulation of ammonium ions and water into the lumen. This results in formation of prominent 'holes' or vacuoles across the host cell membrane (Ricci *et al*., 1993). Over the last twenty years, many in vitro studies have reported vacuolation of various mammalian cell lines or primary gastric cells in response to various forms of VacA, including gastric AGS and MKN, ovarian Chinese hamster ovary (CHO) and cervical cancer HeLa cells. (Harris *et al*., 1996; Kimura *et al*., 1999; Kuck *et al*., 2001).

Additionally, strains expressing the s1/m1 form of VacA are generally associated with higher vacuolating activity in comparison to the s2/m2 form (Atherton *et al.*, 1995; Letley *et al.*, 2003). However, it has also been observed in some studies that m1 and m2 forms of VacA exhibit varying cell-type specify, as the m1 form induced greater vacuolation of HeLa cells in comparison to the m2 form during one study. In contrast, both the m1 and m2 forms were reported to induce similar levels of vacuolation in kidney RK-13 cells (Pagliaccia *et al*., 1998). Whilst VacA-induced vacuolation is a prominent phenotype observed in vitro, this effect is not well-studied using in vivo animal models and is rarely observed using human biopsy tissue or histological tissue

sections. Additionally, Holland *et al.* (2020) reported vacuolation of parietal cells following infusion of VacA into C57BL/6 mice, this observation has not been reported since using any human-derived models or histological samples (Pagliaccia *et al*., 1998).

Although vacuolation is a well-reported effect of VacA in vitro, given this phenotype is rarely observed in vivo, the significance of vacuolation in *H. pylori* pathogenesis and carcinogenesis still remains a research area of interest. Aside from vacuolation, other virulent effects of VacA include autophagy, resulting in destruction of cytoplasmic material and apoptosis (death) of cultured cells. Although exact cellular mechanisms remain unclear, it is hypothesised that VacA-induced autophagy relies on binding to low-density lipoprotein receptor-related protein 1 (LRP1) on host cells. However, it is also hypothesised that autophagy can also be initiated by the host cell in response to VacA in order to prevent further toxin-induced damage and vacuolation (Terebiznik *et al*., 2006). Furthermore, it is currently proposed that VacA induces apoptosis by interfering with host cell mitochondria, where it can reduce mitochondrial transmembrane potential, promote cytochrome *c* release and induce mitochondrial fragmentation (Jones *et al*., 2010; Kimura *et al*., 1999). A further effect of VacA is disruption of intercellular junctions and increased permeability of host-cell monolayers, resulting in an efflux of anions, chloride, urea and bicarbonate. (Tombola *et al*., 1999). In turn, VacA increases paracellular permeability resulting in loss of host membrane polarity, which is an effect often observed during early carcinogenesis (Papini *et al*., 2001). Finally, VacA can also impair the function of several immune cells, such as

lymphocytes, macrophages and eosinophils, in an effort to 'hide' from the host immune system (Altobelli *et al*., 2019; Terebiznik *et al*., 2009).

HtrA

An additional and less-studied virulence factor of *H. pylori* is secreted serine protease high temperature requirement A (HtrA). HtrA proteins are generally proteolytic and also exhibit chaperone-like properties on host cells (Skorko-Glonek *et al*., 2013). These proteins are usually involved in quality control and house-keeping roles within the bacterial cell, but *H. pylori* HtrA has been reported to secrete into the extracellular space as a soluble protease and promote colonisation of host gastric tissue (Löwer *et al*., 2008). HtrA also cleaves cell junction proteins, such as claudin-8, occludin and E-cadherin, which causes depolarisation of polarised monolayers and damage to the host tissue (Hoy *et al*., 2010). Interestingly, a recent study demonstrated that a single nucleotide polymorphism (SNP) mutation found within HtrA (position serine/leucine 171) triggered HtrA trimer formation, which is significantly correlated with increased risk of gastric cancer. The study showed that the trimeric 171Leucine-type (171L) of HtrA inflicted more epithelial damage, enhanced injection of CagA and cleavage of E-cadherin in comparison to the 171Serine-type (171S). Although these findings were relatively recent, it is possible that the 171L/S HtrA mutation could be included as a potential biomarker for *H. pylori* infection and *H. pylori*-induced GC in the future (Sharafutdinov *et al*., 2023).

1.5. *H. pylori* and gastric adenocarcinoma

In 2014, *H. pylori* was designated as a type 1 carcinogen by the World Health Organisation (WHO) for its association between severe gastric disease and development of GC. Currently, a widely accepted model for explaining the mechanism of *H. pylori*-induced gastric adenocarcinoma (GAC) progression is outlined in Correa's cascade of carcinogenesis which was published in 2004 by Dr Pelayo Correa. This cascade outlines the stepwise histological changes which occur within the gastric mucosa following initial *H. pylori* infection (Correa, 2004) (Figure 1.4).

Superficial and atrophic gastritis

Immediately following infection with *H. pylori*, healthy gastric mucosa becomes inflamed due to mucosal injury resulting in chronic gastritis (CG), which is also known as chronic superficial gastritis (SG). The active form of CG is associated with the presence of immune cells such as granulocytes distributed throughout the epithelium, whereas the non-active form is associated with infiltration of lymphoid and plasma cells throughout the lamina propria. Although both forms of CG are highly associated with neutrophil infiltration, CG generally lasts no more than seven to 10 days, and most CG cases resolve naturally. However, some patients may experience hypochlorhydria, acid reflux, nausea, stomach discomfort and a reduction in appetite, which are usually treated with over the counter (OTC) medications (Tombola *et al.*, 1999).

Following acute infection, CG may develop into chronic atrophic gastritis (AG) which is often diagnosed by endoscopy. AG is histologically associated with infiltration of mononuclear immune cells, such as lymphocytes, macrophages, and plasma cells.

Persistent inflammation results in atrophy of the gastric glands and can be multifocal, known as multifocal atrophic gastritis (MAG) whereby foci of the atrophy are present in multiple regions of the stomach. An additional indicator of AG is hypo, or achlorhydria, which is a reduction or complete loss of stomach acid. This occurs during atrophic gastritis, due to the destruction of gastric glands and subsequent loss of acid-producing parietal cells (Cifuentes *et al*., 2022). Additionally, pepsinogen-secreting chief cells are often lost as a result of AG, thus reduced serum pepsinogen I levels are often used as a diagnostic tool or biomarker for AG in some countries.

Gastric intestinal metaplasia

If untreated, patients with AG will often develop gastric intestinal metaplasia (GIM), which is a process that can happen over months or years depending on the patient (Eun *et al.,* 2014). During GIM progression, the gastric mucosa undergoes physiological changes and resembles the intestinal mucosa. As this change is irreversible, GIM is often referred to as 'the point of no return' and is not cured with antibiotic therapy. GIM can be either complete (Type I), which appears histologically similar to the small intestines and is associated with goblet cell expression, MUC2 secretion, brush border and eosinophilic enterocyte presence. Conversely, incomplete (Type 2) GIM resembles the colon and is associated with multiple, irregular MUC5AC or MUC2 droplets and an absence of brush border (Correa and Piazuelo, 2012). Although expression of MUC2 is absent in the healthy gastric mucosa, as it is highly expressed in both complete and incomplete GIM and is used as a histological indicator of GIM which is easily identified with H&E staining (Correa, 2004).

Dysplasia

Dysplasia is the penultimate stage of gastric carcinogenesis and is a term used to describe the presence of abnormal cells in a tissue. Within the dysplastic gastric epithelium, the nuclei are usually enlarged and dark in appearance (hyperchromatic), irregular shaped and lack polarity. The overall epithelial architecture is irregular, forming tubular-shaped branches with irregular lumens and psuedopapillae. Gastric dysplasia is often graded using a two-tier system, or low and high-grade dysplasia based on both cellular and nuclear morphology (Lauwers and Riddell, 1999). Dysplasia can be characterised based on mucin and gene expression as either adenomatous/type I (intestinal phenotype) or foveolar/pyloric/type II (gastric phenotype). Dysplasia presence is highly correlated with cancer risk and is relatively uncommon in countries with low gastric cancer risk such as the UK and Australia. Dysplasia management is difficult, and it is therefore recommended that tissue lesions require endoscopic resection, due to the potential for such lesions to progress into adenocarcinoma or metastasise (Correa and Piazuelo, 2012).

Gastric adenocarcinoma

Gastric adenocarcinoma (GAC) is the final stage of carcinogenesis and is often called invasive carcinoma, as the surrounding stroma becomes degraded and penetrated by neoplastic cells. GAC often has an irregular mucosal and microvascular pattern, in addition to irregular nuclei and distorted tubular glands (Correa and Piazuelo, 2012; Lee *et al.*, 2018).

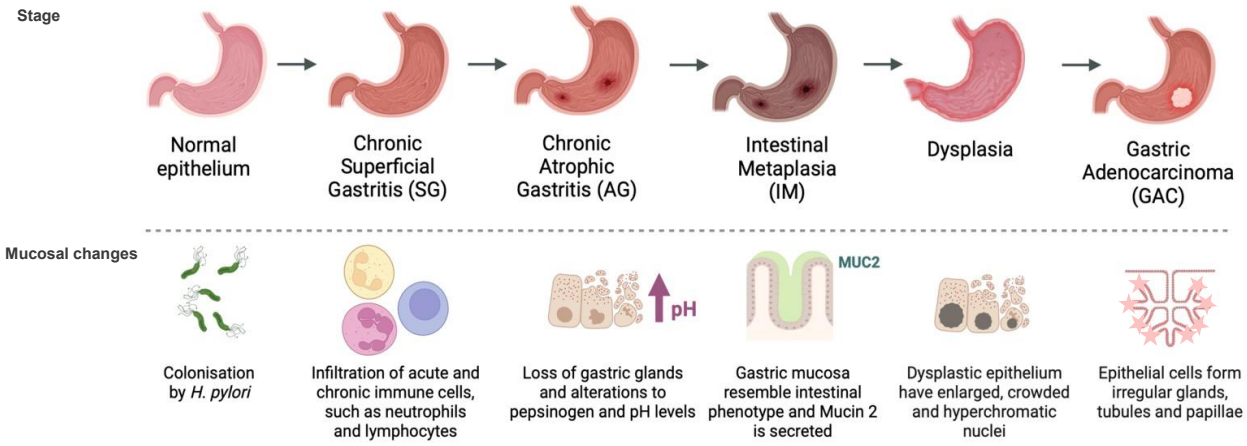

Figure 1.4. Correa's cascade of carcinogenesis and associated mucosal changes. *H. pylori* colonise the gastric mucosa, initially resulting in SG (also called CG). Most cases of SG remain asymptomatic, but it can also lead to AG if untreated, whereby gastric glands are lost, and local pH rises. SG progresses to GIM, whereby the gastric mucosa resembles an intestinal phenotype and *de novo* secretion of MUC2 occurs. Eventually, the gastric mucosa can become dysplastic, subsequently resulting in development of GAC. Figure created in Biorender.com.

1.6. Models to study *H. pylori* infection

In vivo animal models

Since its discovery, several animal models quickly became available to study the effects of virulence factors and manipulate *H. pylori* infection. The first *H. pylori* animal model was the gnotobiotic piglet, which was used to demonstrate the importance of virulence factors urease and flagella during infection (Eaton *et al.,* 1991). Although inflammation was observed following artificial infection with *H. pylori*, it was soon noted that although stomach ulcers were observed, the overall inflammatory response differed greatly between piglets and humans, whereby inflammatory responses, primarily involving neutrophils, were lower in the piglet in comparison to adult humans.

Furthermore, piglets soon became unfavourable as a disease model due to the requirement of specialised, large facilities and high maintenance costs (Taillieu *et al.,* 2022). Several studies then attempted to artificially infect cats and dogs with *H. pylori*, which failed to induce an inflammatory response (Nedrud, 1999). This was likely because other *Helicobacter* species such as such as *H. suis, H. felis* and *H. salomonis,* rather than *H. pylori*, are natural colonisers of these animals, which could therefore explain the lack of inflammatory response (Taillieu *et al.,* 2022).

Mouse models soon became favourable, due to reduced costs and lower space requirements (O'Rourke and Lee, 2003). Several studies have shown that prolonged infection of germ free C57BL/6 mice induced CG, AG and inflammation which are characteristics of chronic *H. pylori* infection and mucosal damage (Ghiara et al., 1995; Sakagami et al., 1996). The earliest mouse colonisation studies used the standardised *H. pylori* 'Sydney Strain 1' (SS1) strain, which is known to readily adhere to the gastric

mucosa and maintain colonising ability in long-term studies (Lee *et al*., 1997). However, despite the availability of several animal models to study *H. pylor*i infection, several problems remain with these models. Aside from ethical implications and high costs, animals often do not respond to *H. pylori* infection to the same extent as humans, thus later stages in Correa's cascade of carcinogenesis are not easily modelled using animal models (Correa and Piazuelo, 2012; Taylor and Fox, 2012).

In vitro cell lines

Cell lines are a common in vitro model to study *H. pylori* infection, as they are relatively cost-effective, reproducible and far easier to maintain compared with animals. Cultured AGS and MKN cell lines are derived from gastric adenocarcinomas and are frequently used for gastric in vitro infection studies. The effect of CagA has been extensively studied using these cell lines, where cellular elongation, scattering and production of IL-8 has been observed following infection with various *H. pylori* strains (Bourzac *et al*., 2007; Murata-Kamiya *et al*., 2007; Sharma *et al*., 1998). Furthermore, as previously discussed, the vacuolating effects of VacA are prominent following infection of a variety of cultured cells (Kuck *et al.,* 2001; Terebiznik *et al*., 2009). Aside from gastric cells, other non-gastric, human-derived cell lines have been reported in *H. pylori* infection studies, including cervical cancer HeLa cells, although it is unclear why this type of cell was used to model a gastric infection, given they originate from the cervix (Cover *et al*., 1992). Additionally, murine-derived and other animal cell lines such as J774 macrophages, murine $CD4^+$ T-lymphocytes and chinese hamster ovary (CHO) cells have been used to model *H. pylori* infection in vitro (Löfling *et al*., 2008; Rosenplänter *et al*., 2007). However, whilst cell lines are an excellent alternative to animal models

for studying bacterial infection, they are often genetically unstable, have a short life span and low passage limit (Idowu *et al*., 2022). Furthermore, the majority of cell lines also do not recapitulate the gastric architecture, due to lack of cellular polarisation and mucin production which is found on the apical surface of gastric epithelia. These are important host features that can influence response to *H. pylori* infection (Kim *et al.*, 2020).

Organoid models

In recent years, organoid models have become a popular alternative to animal models and cell lines for modelling a variety of bacterial infections (Kim *et al.,* 2020). Organoids are 3-dimensional (3D) structures derived from pluripotent stem cells, which are capable of recapitulating the architecture and function of the original organ the stem cells were obtained from (Bartfeld and Clevers, 2015). Organoids are self-maintaining and generally have a far higher passage limit in comparison to cell lines. In addition, unlike most cell lines, cells within organoids are highly polarised, with a defined apical and basal membrane and express a multitude of features, proteins and cell types also found within the original organ, such as chief, stem, parietal cells, cell junctional proteins and mucin layers (Fuji *et al.,* 2018).

Gastric organoids were originally developed from $Lgr5^{+}$ gastric stem cells, which successfully developed into small organoids containing mucus neck and pit cells (Barker *et al.*, 2010). In the last decade, both human and murine derived 3D models have gained attention for studying *H. pylori* infection in vitro. Bartfeld and Clevers (2015) were among the first to establish gastric organoids directly from gastric glands

and also developed an infection protocol detailing micro-injection of organoids with *H. pylori* cultures. However, microinjection of cultures is a laborious, expensive and unsustainable process, as this system does not support long-term infection studies. In addition, because 3D organoids significantly differ in sizes, infection protocols are difficult to standardise as it is almost impossible to infect them equally with a precise ratio of bacteria to cells, or multiplicity of infection (MOI). This results in some organoids receiving a higher dose of bacteria than others and becoming overwhelmed by infection (Bartfeld and Clevers, 2015).

Recently, alternative approaches have become available, whereby 2-dimensional (2D) organoid monolayers were successfully generated by shearing 3D organoids and reseeding onto glass coverslips. The 2D monolayers were then used as a *H. pylori* infection model, whereby hallmarks of CagA response were observed including cellular elongation and upregulation of IL-8 (Schlaermann *et al.,* 2016). Unfortunately, these models were unable to support long-term infection studies as after 24 hours of infection they lost tissue architecture and polarisation, in addition to gradual dispersal of apical mucin within the culture medium.

To solve this issue, Boccellato *et al.* (2019) published an alternative approach outlined in Figure 1.5, which involves seeding 2D cultures onto a cell culture transwell insert thus allowing access to the apical and basolateral surface of the organoids. They then employed air-liquid interface (ALI) technology to remove apical medium, facilitating polarisation and mucin production within the monolayers, which were coined ‘mucosoid’ cultures. Furthermore, the mucosoids were then infected with live cultures

of *H. pylori* and successfully sustained long-term infection over a two to four-week period. This method has since been employed in additional *H. pylori* infection studies involving Na-K-ATPase reduction (Vagin *et al.,* 2024), mucosal homeostasis (Boccellato *et al.,* 2019) and endosomal trafficking (Capurro *et al.,* 2019).

However, it is worth mentioning that although gastric organoid models recapitulate the host architecture and cell types found within the stomach, they do not incorporate other physiological aspects such as blood flow, pH maintenance and biomechanics (Carvalho *et al.*, 2023). As such, stomach-on-a-chip (SoC) devices have recently been engineered which replicate architectural and functional traits of a human stomach, such as maintenance of long-term 3D epithelial and mesenchymal cells, peristaltic flow and churning (Ferreira *et al.*, 2023; Lee *et al.,* 2018). Whilst these models have been reported in gastrointestinal research studies, as of 2024 there are no reports detailing their applications to model *H. pylori* infection (Carvalho *et al.*, 2023).

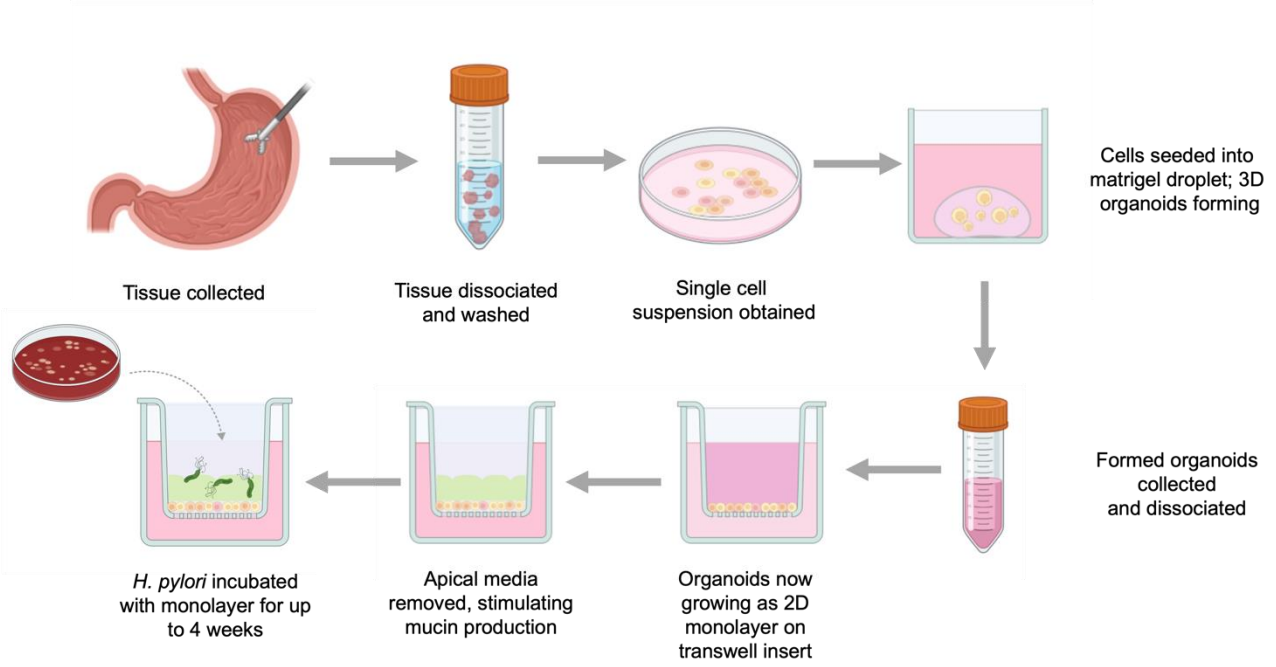

Figure 1.5. Schematic outlining generation of 2D organoid mucosoid monolayers, derived from 3D gastric organoids. Tissue is collected during routine endoscopy, dissociated and re-seeded as a single cell suspension within matrigel matrix. Eventually, 3D organoids form which are further dissociated and reseeded as a cell monolayer onto a transwell insert. Once a polarised monolayer forms, an ALI culture is created by removing the apical media which stimulates mucin production. ALI cultures are then used for downstream experiments and infected with cultures of bacteria, such as *H. pylori*. Figure reproduced from methods outlined by Boccellato *et al.,* (2019) and created in Biorender.com.

1.7. The human microbiome

The human microbiome is comprised of eukaryotes, archaea, viruses and bacteria which colonise the inside and outside of our bodies. It consists of approximately 10-100 trillion microbial cells, with the majority found within our gastrointestinal tract (Turnbaugh *et al.,* 2007). The human microbiome is sometimes described as 'the hidden organ', as it generally has a symbiotic relationship with the body and is involved in several key functions, including metabolism, digestion, homeostasis and immune regulation (Bocci, 1992). However, occasionally the microbiome becomes disturbed, which results in an imbalance of microbiota and alterations in bacterial composition or function. This effect is usually associated with an overall loss of bacteria, overgrowth of pathogenic opportunistic bacteria or loss of beneficial symbiotic bacteria (DeGruttola *et al.,* 2016). In the last twenty years, research into the link between the human microbiome in health and disease has gained significant traction, primarily driven by advancements in microbial profiling technology and reductions in technology and analysis costs (Cullen *et al.,* 2020).

The human microbiome and cancer

Recent evidence has shown that the microbiome is also associated with cancer. Currently, although 11 microorganisms are designated as a group 1 carcinogen, this currently only includes one species of bacteria – *H. pylori* (Martel *et al.,* 2020). However, several other bacteria are currently being investigated for their role in cancer development. For example, many pathogenic bacteria are frequently isolated from colorectal cancer (CRC) patients and include species belonging to the Bacteroidota and Fusobacteriota phyla. For example, several commensal bacteria, such as

Fusobacterium nucleatum and *Lactobacillus reuteri* have been found to increase intestinal tumourigenesis and aggravate inflammatory pathways in the gastrointestinal tract (Lo *et al.*, 2022; Zepeda-Rivera *et al.*, 2024).

In addition, the intestinal microbiota has also been reported to contribute to other cancer, such as hepatocellular carcinoma (HCC). For example, in murine models of acute liver disease, an enrichment of bacteria such as streptococci, bifidobacteria and enterobacteria have been reported in patients with acute liver disease at risk of developing HCC (Llopis *et al.*, 2016). Furthermore, the skin microbiota is also emerging as a risk factor for breast cancer progression. A recent study reported an enrichment of skin commensal species, such as *Staphylococcus epidermidis* and *Micrococcus luteus* within mammary tumour biopsies (Bernardo *et al.,* 2023). Taken together, in recent years, advancements in technology have identified a clear link between the human microbiota and progression of several cancers.

Sequencing-based methods to study the microbiome

Most microbiome studies use microbial gene amplicon sequencing techniques to identify hypervariable regions of the small subunit ribosomal RNA gene (16S). 16S rRNA sequencing is favoured as it is culture-free method which provides genera or species level identification of a given microbiome (Johnson *et al.,* 2019). However, 16S sequencing relies on PCR amplification of conserved sequences within hypervariable regions (such as V3-V5) or the full length of the 16S rRNA gene followed by mapping to an online taxonomic database, such as SILVA 138.2. This method is used to determine operational taxonomic units (OTUs) which have a 97% sequence identity

with known bacterial taxa. Additionally, in recent years, high-throughput shotgun metagenomic sequencing techniques have also gained popularity and involve functional analyses of entire genomes of viral, eukaryotic and bacterial microbiota. Rather than capturing defined regions of the 16S rRNA gene, the whole genome of organisms can be targeted with random primers to sequence regions of genome overlap. Sequences are then mapped to a database or reassembled *de novo* (Durazzi *et al.,* 2021). Shotgun metagenomic sequencing is an alternative, highly sensitive technique which provides strain level detection and can also reveal functional profiles of the identified bacteria. However, due to the large volumes of data generated, the associated costs and bioinformatic requirements are far greater than for 16S rRNA sequencing.

Whilst sequencing-based studies reduce the need for bacterial culture, a major drawback is that PCR and amplicon-based studies are prone to sample contamination and therefore overestimation of bacterial abundance (Eun *et al.*, 2014). Contamination may arise from the laboratory environment, sample, or even within various kits used for preparation of sequencing libraries (Salter *et al.,* 2014). An additional concern with sequencing-based reports is large discrepancies between sample size, techniques and data analysis pipelines, which can also result in under or over reporting of bacterial abundance (Kool *et al.,* 2023; Nearing *et al.*, 2022).

Metabolomics is another tool commonly used in microbiota studies which identifies, quantifies and profiles bacterial metabolic events during host-pathogen interactions. In addition to virulence factors, bacterial metabolites are important to understand as they

have several roles within the human body, including regulation of the gut microbiota, nutrient absorption, energy metabolism and regulation of the immune response (Liu *et al*., 2022). Some of the earliest metabolomic studies were conducted on plants, whereby plants were screened for metabolomic biomarkers to predict future plant growth and effect of herbicide or genetic modification was investigated by analysing various secreted plant compounds (Liu *et al.,* 2022). Common techniques in metabolomic studies include nuclear magnetic resonance spectroscopy (NMR) and mass spectrometry (MS), which can be targeted or untargeted *(*Smirnov *et al.,* 2016). Targeted techniques usually involve studies on compounds, such as fatty acids or amino acids, whereas non-targeted techniques usually identify differences between metabolite profiles in control and test groups (Lau *et al.*, 2016).

Imaging-based methods to study the microbiota

Although sequencing data provides information on bacterial abundance and metabolic events, it is unable to provide spatial and contextual information regarding location and distribution of bacteria in a given microbiome. Recently, imaging-based techniques have been explored to label and track gut microbiota in situ using live murine models. Many of these studies rely on fluorescent probes which target components of bacterial cell walls or deliver fluorescent or infrared antibodies to bacteria. However, these methods have only been conducted on transplanted bacteria and rely on specialist MRI or bioluminescence techniques to visualise bacterial distribution within the organism, which would be unsuitable, expensive and potentially dangerous approach if applied to human microbiome research (Apostolos *et al*., 2022; Chen *et al*., 2023).

Visualisation of microbiota in situ is difficult due to the requirement of specialist equipment and risk of harming the organism. As such, the majority of standard imaging-based methods to visualise bacteria rely on ex vivo samples, often obtained from biopsy or swabbed material. A powerful technique to fluorescently label specific bacteria within samples is fluorescent in situ hybridisation (FISH), which is a targeted approach that uses probes to detect specific bacterial DNA or RNA sequences that then emit fluorescence when viewed using a confocal or fluorescence microscope. FISH has been widely used for identification of microbial taxa within several biopsy samples, including oral (Thurnheer *et al.*, 2004), gastrointestinal (Ng and Tropini, 2021) and skin (Gellrich *et al.*, 2004).

FISH is a popular and user-friendly technique, but is often prone to unspecific binding, resulting in high likelihood of false-positive labelling. Conversely, FISH has limited sensitivity for low-abundance targets, such as certain bacteria, which can result in under-reporting of bacterial presence. Recently, a novel, alternative in situ hybridisation technique, ‘RNAscope’, was developed by ACD Bio and is outlined in Figure 1.6. Rather than a single fluorescent-labelled probe, RNAscope probes bind to specific RNA sequences and consist of a target binding site comprised of a double Z probe and a pre-amplifier binding site. The double Z probe is composed of two independent probes, which must both bind in tandem for the pre-amplifier to then bind, ensuring highly specific binding to the target sequence.

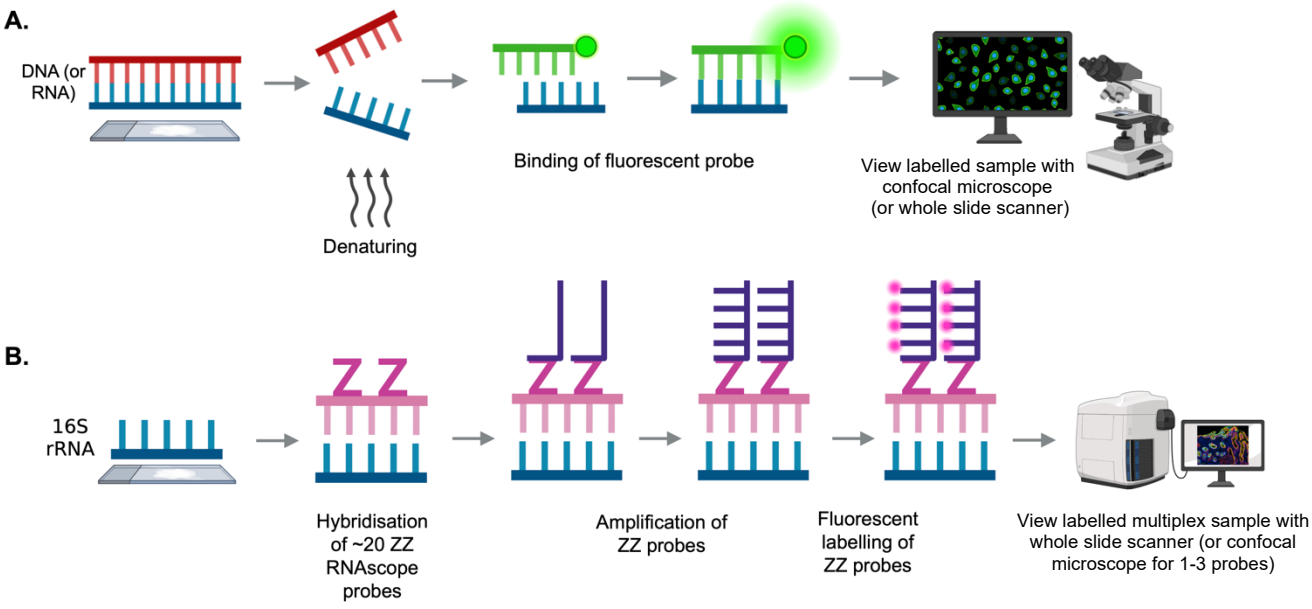

Figure 1.6. Simplified schematic showing differences between conventional FISH and RNAscope ISH. Traditional FISH commonly uses fluorophore-labelled probes which are designed to target specific DNA or RNA sequences on host tissue. Images are usually obtained using a standard confocal or fluorescent microscope (A). In comparison, RNAscope ISH uses double-Z probes which target specific bacterial rRNA sequences, which are then amplified and fluorescently labelled with a fluorophore. A whole slide scanner capable of spectrally unmixing fluorophores is usually used for obtaining images of multiplex (multiple target) RNAscope images (B), but a confocal microscope can also be used for imaging samples labelled with 1-3 targets which do not require spectral unmixing.

The pre-amplifier then undergoes a series of amplification steps and contains multiple binding sites which are then directly labelled with a fluorophore or fluorescent enzyme such as horseradish peroxidase (HRP). In comparison to conventional FISH, RNAscope technology is highly specific, eliminating the likelihood of unspecific binding and high background noise. Many studies employing RNAscope technology focus on eukaryotic structures, however, a small number of studies have used RNAscope to target 16S rRNA bacterial sequences. Amongst these studies, several have used RNAscope technology to investigate various microbiomes, including the respiratory and colon microbiota (Bonifacio and Schmolke, 2021, Shimbori *et al.,* 2022).

1.8. The gastric microbiota

It was initially assumed that the gastric microenvironment was sterile, until the discovery of *H. pylori* which paved the way for further research on the gastric microbiota. Before the availability of high-throughput sequencing-based techniques, early research into the gastric microbiota relied on culture-based techniques, or temporal temperature gradient electrophoresis (TEEG). In the early 2000s, Monstein *et al.* (2002) used TEEG-based methods to identify gastric 'indigenous' bacteria within histologically normal patient samples and identified consistent presence of bacteria such as streptococci, pseudomonads, staphylococci and stomatococci. Furthermore, in 2006, 16S rDNA sequencing of gastric biopsy sample from 23 adults with normal healthy mucosa or chronic gastritis revealed 128 phylotypes, primarily belonging to the phyla Pseudomonadota, Bacillota, Bacteroidota, Actinomycetota and Fusobacteriota *(*Bik *et al.,* 2006). No differences between the two patient groups were observed and *H. pylori* presence did not impact microbial diversity. Interestingly, many of thesee

identified bacteria were associated with the oral cavity, such as various streptococci, fusobacteria and prevotella. It is therefore possible that these bacteria are either commensals of the gastric environment, or opportunistic bacteria which have entered the stomach as a result of swallowing (Castaño-Rodríguez *et al.,* 2017). As sequencing-based tools gained popularity, several additional studies followed suit and have also identified further genera prevalent in the stomach, including *Helicobacter, Prevotella,* S*treptococcus, Fusobacterium, Neisseria, Haemophilus* and *Acinetobacter*, which are found in varying abundances between individuals (Ferreira *et al*., 2018; Rajilic-Stojanovic *et al.,* 2020; Zhang *et al*., 2023).

Gastric microbiota and carcinogenesis

Throughout Correa's cascade of carcinogenesis, the gastric microbiota also alters significantly during progression of CG to GAC. It is currently understood that during the early stages of carcinogenesis, *H. pylori* is prevalent, which is later displaced and dominated by other bacteria, such as those of the gastrointestinal tract or oral microbiota (Coker *et al.,* 2018; Serrano *et al.,* 2021) (Figure 1.7). The mechanism behind this remains unclear, but it is hypothesised that *H. pylori* utilises urease to neutralise the acidic gastric mucosa, which in turn facilitates survival of other alkaliphilic gastric microbiota (Schoep *et al.*, 2010). A similar hypothesis suggests that during progression from CG to GAC, persistent *H. pylori* infection induces inflammation of the gastric mucosa, resulting in glandular atrophy and a loss of acid-secreting parietal cells, which also raises local pH and facilitates colonisation by other bacterial species, however, this does not explain the apparent loss of *H. pylori* (Murakami *et al.,* 2013). Whilst several studies have observed alterations in the gastric microbiota during

carcinogenesis, literature within this field remains limited and there are many discrepancies between studies. As previously discussed, studying the gastric microbiome relies on sequencing-based technology, which are prone to contamination issues, and disparities in sample preparation and biomass, often over or underestimating bacterial relative abundance. In addition, multiple methods and data analysis tools are used, resulting in a lack of standardisation between experiments and studies (Johnson *et al.*, 2019; Salter *et al.*, 2014).

Although most studies report loss of *H. pylori* and an enrichment of non-*H. pylori* bacteria from CG through to GAC, some studies have also reported the opposite effect, or no effect at all, raising several important questions regarding the link between *H. pylori* and the gastric microbiota and the reliability of many sequencing-based studies. To provide a summary of the latest work studying the relationship between *H. pylori* and the gastric microbiota, eight individual sequencing-based studies of various sample size and methodologies were examined, and their main findings are detailed in Table 1.1. Whilst several studies identified a significant enrichment of phyla such as Bacillota and Bacteroidota during development of GAC, several of the studies also reported conflicting findings regarding the relationship between *H. pylori* and non-*Helicobacter* genera. For example, although Guantaya *et al.,* (2019) reported an enrichment of oral bacteria, such as streptococci*,* actinomyces, prevotella and veillonella *in H. pylori*-positive individuals with CG, the opposite effect was reported by and Maldronando-Contreras *et al.,* (2011).

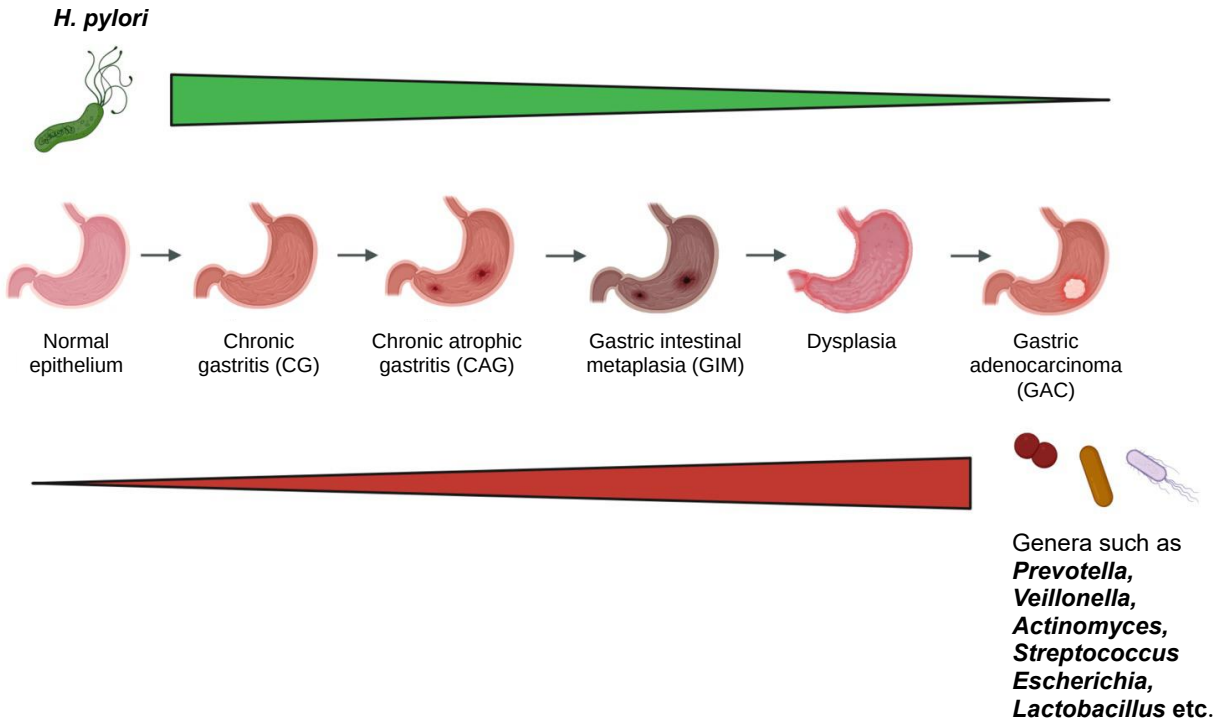

Figure 1.7. Alterations of the gastric mucosa during progression of GAC. It is currently hypothesised that during the early stages of carcinogenesis, *H. pylori* abundance is high. However, as GAC progresses, *H. pylori* is displaced and the gastric mucosa is dominated by non-*H. pylori* microbiota, including oral microbiota (Coker *et al*., 2018; Serrano *et al*., 2021). Figure created in Biorender.com.

Table 1.1. A comparison of studies investigating the effect of H. pylori on the gastric microbiome at various stages of carcinogenesis.

Author, year	Disease state and number of samples	Sequencing technique	Enriched bacteria (grouped by phyla, with examples of genera where applicable)	Key findings
Ferreira *et al*., 2018	54 (GAC), 81 (GC)	Gastroscopy or resection with 16S rRNA sequencing	**Bacteroidota** (e.g. *Prevotella*) **Proteobacteria** (e.g. *Neisseria, Helicobacter*) **Bacillota** (e.g. *Citrobacter, Clostridium, Streptococcus*) **Actinomycetota** (e.g. *Lactobacillus*) **Pseudomonata** (e.g. *Pseudomonas*)	Significant difference in microbiota between CG and GAC groups. *H. pylori* abundant in CG yet reduced in GAC. Bacillota and Actinomycetota significantly enriched in GAC**.**
Coker *et al*., 2018	21 (SG), 23 (AG), 17 (GIM), and 20 (GAC)	Gastroscopy with 16S rRNA sequencing	**Bacillota** (e.g. *Peptostreptococcus, Streptococcus, Slackia, Gemella*) **Bacteroidota** (e.g. *Prevotella*) **Fusobacteriota** (e.g. *Fusobacterium*)	No significant difference in gastric microbiota or diversity regardless of *H. pylori* status. However, the abundance of oral microbiota was enriched in GIM and GAC compared with CG.
Maldonado-Contreras *et al*., 2011	8 (GIM), 2 (AG)	Gastric biopsy with 16S gene microarray	**Actinomycetota** **Bacillota** (*H. pylori*-negative patients) **Pseudomonadota** **Spirochaetota** **Acidobacteriota** (*H. pylori*-positive patients)	*H. pylori* negatively correlated with Bacillota and Actinomycetota presence. Very limited study – patients taking antibiotics were not excluded.

Li *et al*., 2017	60 biopsy samples from 33 patients with *H. pylori* (CG, GIM, GAC) and *H. pylori*-negative control patients.	Gastric biopsy with Illumina MiSeq platform targeting 16S rDNA	**Pseudomonadota** **Bacteroidota** **Fusobacteriota** **Actinomycetota** (*H. pylori*-negative patients*)* **Eubacteria** (*H. pylori*-positive patients)	General decrease in microbial diversity observed in all *H. pylori*-positive patients.
Troncoso *et al*., 2020	155 (dyspepsia/ CG)	Gastric biopsy followed by MALDI-TOF	**Actinomycetota** (*H. pylori-negative* patients) **Bacillota** (e.g. *Streptococcus*)	No significant difference in genera such as *Neisseria, Lactobacillus, Staphylococcus,* or *Veillonella* regardless of *H. pylori* status. *H. pylori* absence associated with enriched Actinomycetota and streptococci.
Gantuya *et al*., 2019	11 (*H. pylori*-negative CG), 40 (*H. pylori*-positive CG), and 24 (healthy)	Gastric biopsy followed by 16S rRNA amplicon sequencing	**Bacillota** (e.g. *Streptococcus, Veilonella*) **Proteobacteria** (e.g. *Haemophilus*) **Spirochaetota** (e.g. *Treponema*) **Actinomycetota** (e.g. *Actinomyces*) **Bacteroidota** (e.g. *Prevotella*)	Results suggest that streptococci could be a risk factor for GAC, independent of *H. pylori* infection.
Wang *et al*., 2022	96 (CG, with or without *H. pylori* infection)	Gastric metagenomic shotgun sequencing of gastric swab samples	**Pseudomonadota** (e.g. *Pseudomonas*)	Pseudomonadota dominated both groups. No significant difference in overall microbial diversity between groups.

The reason behind these discrepancies remains unclear, but it is worth noting that both studies employed different sample preparation, sequencing techniques and downstream analyses pipelines which might influence findings (Allali *et al.,* 2017).

Whilst there is still a lack of conclusive evidence explaining the link between *H. pylori* presence and gastric disturbance during progression of GAC, several bacteria identified in *H. pylori* sequencing-based studies originate from the oral microbiome, as well as the gastrointestinal tract. The oral and gastric microbiota are anatomically connected through the oral-gut axis and although these microbiomes are usually distinct, oral bacteria are often detected at later stages of GAC progression. The reason behind this remains unclear, but is likely a result of *H. pylori* modulating the gastric microenvironment as previously discussed (Bakhti and Latifi-Navid, 2021). Additionally, oral species such as*, Streptococcus mitis*, *Streptococcus mutans, Ligilactobacillus salivarius* and *Actinomyces* have been observed to inhibit *H. pylori* growth and colonisation in vitro, potentially suggesting an opportunistic mechanism. This could explain the apparent reduction in *H. pylori* presence during the later stages of gastric carcinogenesis, outlined in Figure 1.7 (Ishihara *et al.,* 1997; Khosravi *et al.,* 2014).

As such, although *H. pylori* infection drives the initial inflammatory response and early stages of carcinogenesis, it is possible that non-*H. pylori* bacteria, such as oral and gastrointestinal species, might also play a key role in progression of GAC in tandem with *H. pylori*. For example, several oral bacteria, including members of the Bacillota phylum, secrete hydrogen peroxide, which is associated with chronic inflammation and

cancer development (Liu *et al.*, 2024). Additionally, bacteria such as *S. mitis, S. gordonii and S. sanguinis* can metabolise alcohol to acetyl aldehyde, which is associated with host cell damage and tumourigenesis (Pavlova *et al.,* 2013). Furthermore, bacteria such as fusobacteria and prevotella, which are often isolated from both the gastrointestinal and oral microbiome, are also associated with DNA damage, cell-cycle damage and tumour migration and have recently been identified as a risk factor for colorectal cancer (CRC) (Lo *et al.*, 2022; Zepeda-Rivera *et al.*, 2024).

1.9. Aims of this study

In summary, given that the precise role of *H. pylori* and the gastric microbiota in carcinogenesis remains controversial, the aims of this study are as follows. Firstly, using patient-derived human organoid monolayers as an infection model, we will identify whether primary gastric cells vacuolate following exposure to *H. pylori* VacA. Using multiplex imaging of ex vivo patient samples, we will visualise the abundance and spatial distribution of *H. pylori,* the gastric microbiota and mucins during the early, middle and late stages of carcinogenesis. Preliminary attempts will then be made to isolate bacteria from gastric histological tissue sections with laser capture microdissection and determine their identity using full-length 16S rRNA sequencing. Finally, a modified Gram stain will be validated as a cost-effective and rapid test for identification of any invasive bacteria within gastric histological tissue.

1.10 Study hypotheses

Based on the aims outlined above, the four key hypotheses of this thesis are as follows.

- *H. pylori* VacA will induce vacuolation in organoid monolayers, with only specific cell types exhibiting the vacuolation phenotype.
- A direct correlation exists between the presence of *H. pylori* and gastric microbiota in the context of pre-cancerous CG and GIM. However, in GAC, the gastric microbiota will dominate over *H. pylori*.
- Any non-*H. pylori* bacteria detected by RNAscope will predominantly consist of oral and gastrointestinal microorganisms.
- The modified Gram stain will effectively identify both Gram-positive and Gram-negative non-*H. pylori* bacteria and will provide improved contrast against surrounding gastric tissue, when compared with the traditional Gram stain.

Chapter 2: Materials and Methods

2.1. Bacterial strains and growth conditions

Bacterial strains used in this study are listed in Table 2.1; materials are listed in Table 2.2. Strains used for infection experiments were originally isolated from gastric biopsy or kindly gifted by the Robinson or Kuehne laboratory. *H. pylori* were routinely grown on blood agar (Oxoid) containing 8% defibrinated horse blood, Skirrow's selective supplement and 2.5 μg/mL amphotericin B. Skirrow's selective supplement (SSS) was prepared in house and contained 155 μg/mL polymyxin B sulphate (Biochemica), 6.3 mg/mL vancomycin (Sigma) and 3.2 mg/mL trimethoprim (suspended in 100% ethanol) (Thermo Fisher Scientific). Strains were incubated under microaerobic conditions with an atmosphere of 90% N_2, 5% O_2 and 5% CO_2. In the absence of an incubator, strains were grown in a candle jar in the presence of a CampyGen microaerobic sachet.

For infection experiments, 2-3 loops of *H. pylori* were streaked from frozen cryovial stocks onto blood agar and incubated for 72 h in aforementioned conditions. Colonies were then obtained from the edges of the bacterial lawn and streaked onto fresh blood agar plates for 24 h, this step was then also repeated for a further 24 h. This plate was used for experimental work whereby 2-3 loops of *H. pylori* were removed and used to inoculate 1 mL brain heart infusion (BHI) broth. 10 μL of the inoculum was removed and observed under a light microscope at 10 or 40x magnification to confirm *H. pylori* spiral conformation and flagellated movement. The remainder of the bacterial liquid culture absorbance was measured at an optical density (OD) of 600 nm with a spectrophotometer and adjusted to a desired multiplicity of infection (MOI).

Table 2.1. Bacterial strains used in this study

Organism	Strain	Genotype	Source
H. pylori	PMSS1	T4SS+/CagA+	Clinical Isolate
H. pylori	60190	Wild type, s1/m1	Dr Karen Robinson
H. pylori	60190	ΔVacA s1/m1	Dr Karen Robinson
H. pylori	60190	ΔCagA s1/m1	Dr Karen Robinson
H. pylori	Tx30a	Wild type s2/m2	Dr Karen Robinson
A. oris	Clinical isolate	Wild type	Dr Sarah Kuehne, Birmingham Dental Hospital

Table 2.2. Materials required for bacterial growth

Material	Manufacturer	Catalogue number
Blood agar base no. 2	Millipore	B1676
Defibrinated horse blood	EO Labs	DHB100
Brain heart infusion broth	Thermo Fisher	CM1135
CampyGen sachets	Oxoid	CN0025
Vancomycin	VWR	1205950010
Polymyxin B	VWR	A08900001
Trimethoprim	VWR	J6305306
Amphotericin B	VWR	12350000

In addition, in order to verify MOI, the adjusted bacteria were serially diluted onto blood agar plates and incubated for 48 h to obtain colony forming unit (CFU) counts.

2.2. Preparation of *H. pylori* lysates

H. pylori strains (wild type strain 60190 and strains 60190 ΔCagA, 60190 ΔVacA and Tx30a) were grown on blood agar plates for 48 h in microaerophilic conditions. For each strain, bacterial growth was removed with a sterile inoculating loop and added to 1 mL sterile distilled water in a 1.5 mL Eppendorf tube. Tubes were vigorously vortexed and incubated at room temperature for 20 min. Cells were removed by centrifugation at full speed for 5 min and the supernatant was transferred to a fresh sterile Eppendorf tube. The total protein concentration of each lysate was estimated using a Qubit Protein Assay Kit (Thermofisher) and adjusted with PBS to 1 mg/mL for each strain. Lysates were stored at -20°C until required.

2.3. Cell line culture and maintenance

AGS cells or Caco-2 cells when required were stored in cryovials containing Cell Recovery Freezing Medium (Gibco) in either liquid nitrogen or at -80°C. When required for experimental work, cryovials were rapidly thawed at 37°C and transferred to RPMI containing 10% FCS. Cells were centrifuged at 300 g for 5 min at 4°C. Cell pellets were resuspended in 1mL RPMI and FCS, prior to addition of complete medium (cRPMI) containing 10% FCS, 1% (v/v) L-glutamine and 1% (v/v) Penicillin-Streptomycin solution. Cells were transferred to a vented T-75 cell culture treated flask and incubated at 37 °C and 5% CO_2 for 2-3 days or until confluent. Once ~90-100% confluent. Cells

were passaged by rinsing once with PBS and adding 0.05% Trypsin (Gibco) for 5 min or until cells detached; cRPMI was then added to quench Trypsin and centrifuged as before. Cells were routinely passaged at a 1:8 dilution dependent on cell pellet size and passaged no more than 20 times.

2.4. Preparation of WNT and R-spondin-1 conditioned organoid medium

Both WNT3A-expressing L cells and R-spondin-1 expressing 293T cells were thawed from liquid nitrogen, resuspended in DMEM with high glucose, pyruvate and 1.25 μL Zeocin and seeded into a T-75 cell culture treated flask until confluent. Cells were then expanded and reseeded into T-150 flasks; this process was then repeated twice more. Cells were then dissociated for a final time and re-seeded into 150 mm^2 cell culture dishes in Zeocin-free medium. Cells were incubated for 6 days, before the medium was removed and vacuum filtered. Medium was aliquoted and stored at -20°C until required.

2.5. 3D organoid culture and maintenance

Human gastric organoids were kindly provided by Dr Claire Shannon-Lowe at the Institute of Cancer and Genomic Sciences, University of Birmingham and were derived from biopsy tissue obtained during a routine gastric endoscopy. All organoids used in this study demonstrated normal gastric morphology as identified by an independent pathologist. Organoid media used in this study are detailed in Tables 2.3, 2.4 and 2.5. Organoids were routinely stored in 0.5-1 mL Cell Recovery Freezing Medium in liquid nitrogen and were thawed when required. Cryovials containing 3D organoids were

removed from liquid nitrogen and briefly thawed at 37 °C on a hot block. Organoids were transferred to 9 mL AdDF medium (Table 2.3) before being centrifuged and the supernatant discarded. Matrigel (Corning) was used to resuspend the cell pellet, with required volume dependent on cell pellet size. Once resuspended in Matrigel, ~20-30 µL drops of Matrigel-suspended organoid cells were pipetted into a pre-warmed 24-well plate. After 30 seconds, the plate was inverted and the matrigel left to set at 37°C for ~10 min. 500 µL pre-warmed complete 3D organoid medium was added to each well and PBS added to the surrounding wells to maintain humidity. Small organoids began to form after 3 days, requiring fresh medium on day 5 and passaging on day 10.

2.6. 3D organoid passaging

Routine passages involved splitting the organoids in 1:2 or 1:4 ratio, dependent on original organoid number and whether organoids were also required for experimental work. Organoids suspended in Matrigel drops were disrupted and collected into a falcon tube, before centrifuging at 300 g for 5 min at 4°C. After centrifuging, a visible pellet and matrigel halo containing visible organoids were retained and 100 µL AdDF medium was added prior to mechanical disruption using an FCS-coated flamed-tip glass pipette. Depending on organoid number, 1-2 mL TrypLE (Gibco) containing 0.1% EDTA (Gibco) was added to the cell suspension and incubated for 10 min at 37°C, with further mechanical disruption after 5 min.

Following incubation, 1-2 mL AdDF medium with 10% FCS was added to inactivate the TrypLE with further glass pipetting to disrupt the organoids. Organoids were centrifuged once again and residual Matrigel layers and supernatant were discarded.

The pellet was washed by resuspending in AdDF medium, centrifuged again and resuspended in the required volume of matrigel. A 30 μL droplet was then added with a pipette to each well of a pre-warmed 24-well plate and inverted as before. After ~10 min, 500 μL pre-warmed complete 3D organoid medium was added to each well and PBS was added to the surrounding wells to maintain humidity. Following passaging, organoids were inspected with a light microscope and appeared as disrupted, single cells. After 3 days small organoids began to form and required passaging again after a further 7-10 days.

2.7. Preparation of 2D organoid monolayers

In order to establish 2D organoid monolayers on plates or transwell inserts at least 4+ wells of confluent and healthy 3D organoids were required. Healthy 3D organoids were defined as spherical, with clear lumens and no sign of budding or release of smaller cells. Transwell inserts or plates were pre-coated with 15 μg/cm^2 Bovine Collagen I (Corning). Coating density was calculated by multiplying surface area of well by coating density, then dividing by volume required per well. Dependent on well or transwell insert size, different volumes of collagen were required and were calculated as follows:

$$\text{Collagen concentration} = \frac{\text{(Plate or transwell insert area) x 15 } \mu\text{g/cm}^2}{\text{(Volume required per transwell insert or well)}}$$

This figure was then divided by the collagen stock concentration of 3.1mg/mL. The required volume of collagen stock was then prepared in a 1.5 mL Eppendorf tube by diluting collagen in tissue-culture grade 0.01 N HCL to the total volume required to coat

all wells. The diluted collagen solution was added to the required transwell inserts or wells and incubated for 1 hour at room temperature. The solution was removed and transwell inserts or wells were washed three times with PBS and air-dried. Plates were sealed with Parafilm and stored at 4°C for up to one week.

3D organoids were collected into a 1.5 mL Eppendorf and centrifuged. The supernatant was discarded, but the remaining pellet and Matrigel halo was preserved and used for processing. For generation of 2D organoid monolayers, wash buffers were prepared as detailed in Table 2.6. The cell pellet was resuspended in 1 mL wash buffer 1 using an FCS-coated flamed-tip glass pipette. After resuspending, a further 2 mL of wash buffer one containing PBS was added, and the solution was centrifuged. The supernatant was removed, and the remaining cell pellet was resuspended in 3 mL wash buffer 2 and placed on a 37°C hot block for 10 min to disrupt cells. An FCS-precoated glass pipette was rinsed in PBS to remove excess FCS and used to disrupt the organoids every 2 min during this time period. After 6-8 min, clumping was visibly reduced.

Wash buffer three was then added to the solution to inactivate the TrypLE, prior to gently pouring the solution into an FCS-precoated 50 mL falcon tube through a 70 µm mesh cell strainer to ensure single cells were collected. Cells were further centrifuged and resuspended in wash buffer 4, followed by a final centrifuge. Cells were then resuspended in 500 µL complete 2D medium and 10 µL of this suspension was quantified using a Countess II automated cell counter to determine cell number per mL. Using the calculated cell number, organoid monolayers were seeded at densities

of 3.5-7x10^5 cells/well in 6.5mm transwell inserts for further experiments, or 3-8x10^5 cells/well in 48 well plates passaging purposes. For 6.5 mm diameter transwell inserts, 200 µL complete medium was added apically and with 300 µL added basally. For 48 well plates, 400 µL was added on the apical surface of monolayers. Cells were incubated at 37°C with 5% CO_2 for 3-6 days, with monolayers visually monitored every day and medium changed every 2-3 days.

2.8. Disruption and passaging of 2D organoid monolayer

Confluent 2D organoid monolayers were washed twice with PBS, before adding 200-400 µL pre-warmed TrypLE for 8-10 min to disrupt the monolayer. Cells were monitored for rounding and detachment during this time using a light microscope and gentle agitation by tapping against the lab bench to ensure sufficient cell detachment. TrypLE was quenched by the addition of 2D complete medium and 10% FCS. Cells were then collected in a 1.5 mL Eppendorf tube and centrifuged. The supernatant was removed, and the small cell pellet was resuspended in 500 µL complete 2D medium. Cells were counted as described above and re-seeded onto fresh collagen-coated plates. 2D organoid growth was assessed daily using a light microscope passaged no more than three times in order to retain cell types and viability.

Table 2.3. Composition of AdDF organoid medium

Material	Manufacturer	Catalogue number	Final concentration
Advanced DMEM/F12	Thermo Fisher Scientific	12634010	1x
HEPES	Thermo Fisher Scientific	11550496	10 mM
GlutaMax	Gibco	35050061	2 mM
Rho-kinase inhibitor	Merck	Y0503-1MG	10 μM
Primocin	Invivogen	ANT-PM-5	1x
Penicillin-Streptomycin	Merck	P4333-20ML	1x

Table 2.4. Composition of complete 3D organoid medium

Material	Manufacturer	Catalogue number	Final concentration
AdDF medium	Prepared in laboratory	-	1x
Wnt 3A-conditoned medium	Prepared in laboratory	-	50% (v/v)
R-spondin-1-conditioned medium	Prepared in laboratory	-	10% (v/v)
Noggin-conditioned medium	Prepared in laboratory	-	10% (v/v)
B27 supplement	Thermo Fisher Scientific	17504044	1x
Nicotinamide	Merck	N0636	10 mM
A83 inhibitor	Merck	SML0788	1 μM
Rho-kinase inhibitor	Merck	Y0503-1MG	10 μM
Recombinant human EGF	Fisher	PHG0315	50 ng/mL
Primocin	Invivogen	ANT-PM-5	1x
Penicillin-Streptomycin	Merck	P4333-20ML	1x

Table 2.5. Composition of complete 2D organoid monolayer medium

Material	Manufacturer	Catalogue number	Final concentration
AdDF medium	Prepared in laboratory	-	1x
Wnt 3A-conditoned medium	Prepared in laboratory	-	50% (v/v)
R-spondin-1-conditioned medium	Prepared in laboratory	-	25% (v/v)
N2	Thermo Fisher Scientific	17502048	1x
NAD	Stem Cell Technologies	07154	10 mM
B27 supplement	Thermo Fisher Scientific	17504044	1x
Nicotinamide	Merck	N0636	10 mM
A83 inhibitor	Merck	SML0788	1 μM
Rho-kinase inhibitor	Merck	Y0503-1MG	7.5 μM
Recombinant human EGF	Gibco	PHG0315	20 ng/mL
Recombinant human Noggin	Peprotech	120-10C	150 ng/mL

Recombinant human FGF-10	Peprotech	100-26	150 ng/mL
Human Gastrin	Bio-Techne	3006	10 nM
Primocin	Invivogen	ANT-PM-5	1x

Table 2.6. Composition of wash buffers required for 2D organoid monolayer generation

Wash one	Wash two	Wash three	Wash four
3 mL PBS	3 mL TrypLE	10 mL AdDF medium	1 mL AdDF medium
0.5 mM EDTA	0.5 mM EDTA	10% foetal calf serum	10 μM Rho-kinase inhibitor
10 μM Rho-kinase inhibitor	10 μM Rho-kinase inhibitor	10 μM Rho-kinase inhibitor	

2.9. FITC-Dextran permeability assay

2D organoid monolayers, Caco-2 and AGS cells were grown to confluency on transwell inserts, as described above, over the course of 21 days. Caco-2 cells were used as a positive control for polarisation and transwells containing no cells were used as a negative control. At 7, 14 and 21 days, apical medium was removed from the transwell insert and replaced with relevant medium containing 4mg/mL 4kDa FITC-Dextran in PBS. Cells were then incubated for 3 h. After incubation, basal medium was removed and transferred to an opaque 96 well plate where fluorescence intensity was then measured using a Clariostar plate reader and plotted using Microsoft Excel.

2.10. Immunofluorescence imaging of 2D organoid monolayers and AGS cells

All immunofluorescence antibodies are detailed in Table 2.7. 2D organoid monolayers were grown to confluency on transwell inserts as described above. Monolayers were washed gently three times with warm PBS and fixed for 15 min in 4% formaldehyde in PBS at room temperature. Inserts were washed three times with PBS and blocked in 1x PBS, 3% BSA, 3% Goat Serum and 0.3% Triton X-100 for 2 h at room temperature. After blocking, inserts were washed three times with PBS and the relevant primary antibody diluted in the aforementioned blocking buffer was added overnight at 4 °C.

The following morning, the primary antibody was removed, and inserts were washed three times with PBS. The corresponding secondary antibody diluted in blocking buffer was added for one hour at room temperature. Inserts were washed with PBS a further three times, air-dried and carefully excised with a scalpel. The inserts were then mounted cell side up onto a glass slide in 4-8 µL VectaShield hard set mounting

medium with DAPI. A 1.5 thickness glass coverslip was added on top and was sealed with clear nail varnish or autoclave tape. Samples were stored in a light proof box at -20°C. Samples were then imaged using a Zeiss Axio Observer or LSM900 confocal microscope at 10, 20 and 63x magnification.

2.11. Neutral red uptake assay

AGS or 2D organoid cells were seeded in a collagen coated 96 well plate at a seeding density of $1.5x10^4$ for AGS cells and $3.5\text{-}7x10^5$ for 2D organoids. AGS cells and 2D organoids were washed three times with warm PBS, and 80 µL pre-warmed, relevant medium was added without antibiotics. 20 µL pre-diluted *H. pylori* lysates at a concentration of 200µg/mL or live *H. pylori* cells at an MOI of 50 were added to the cells overnight (~18 h) at 37°C and 5% CO_2. Relevant medium was added to the cell-only control wells. The following morning, cells were immediately imaged using a Zeiss Axio Observer microscope with phase contrast. Images were obtained and vacuolated cells per field of view were counted. An overall percentage of vacuolated cells per sample were calculated using Microsoft Excel. After imaging, the neutral red uptake assay was immediately carried out as described by Repetto *et al.,* (2008) at OD 540nm determined using a Clariostar 96 well plate reader.

Table 2.7. Antibody information for 2D organoid monolayer immunofluorescence imaging

Antibody	Catalogue number	Species reactivity	Host	Dilution	Clone ID
E-cadherin	24E10	Human	Rabbit	1:200	N/A
MUC5AC	MA1-19346	Human	Mouse	1:200	2-25LE
PGC	PA5-115746	Human	Rabbit	1:200	N/A
TROY	MA5-37871	Human	Rabbit	1:200	ARC2393
SST	MA5-17182	Human	Mouse	1:200	7G5

2.12. Optimisation of automated RNAscope pre-treatments and IHC antibody concentrations

All automated staining optimisation steps were kindly conducted by Ana Teodósio (Birmingham Tissue Analytics, University of Birmingham). RNAscope C1 and C2 probes against *H. pylori* and Eubacteria, respectively, were first tested on healthy colon tissue in a fluorescent fluorescent multiplex assay using an RNAscope LS Multiplex Fluorescent Reagent Kit (ACD; 322800) from following the standard protocol recommended for this platform. Both probes were diluted according to manufacturer instructions whereby the 50x C2 probe was diluted 1:50 in the pre-prepared C1 probe. Probes were then tested in combination with the RNAscope pre-treatment protocol provided by ACD without the addition of lysozyme to preserve tissue integrity. A positive and negative control probe section was used on every RNAscope run to validate and assess its quality and the sensitivity of the assay. The bacterial gene DapB (ACD; 312038) was used as negative control to confirm the absence of background noise and a cocktail of housekeeping genes Polr2A C1, PPIB C2 and UBC C3 (ACD; s320868) were used as positive controls to validate the detection of the signal and the tissue integrity.

All antibodies used in IHC steps were optimised with chromogenic DAB staining of healthy colon tissue. Antigen retrieval was tested using pH6 (Leica Bond TM Epitope Retrieval 1; AR9961) and pH9 (Leica Bond TM Epitope Retrieval; AR9640) buffers by heating to 100 °C for 20 min. Three different dilutions were tested for each antibody. Ideal staining pattern and intensity was assessed and approved by a pathologist, whereby slides were then used as reference throughout the validation process. All

antibodies were then tested for compliance with the RNAscope pre-treatment, to ensure stability after protease III digestion.

2.13. Automated FFPE tissue preparation

Tissue samples were collected from consenting patients at the Queen Elizabeth Hospital, Birmingham and prepared at the Human Biomaterial Resource Centre (HBRC), University of Birmingham, by fixing with formalin and embedding in paraffin (FFPE). 4 µm thick tissue sections were then prepared for eventual RNAscope, IHC and H&E staining using a Leica BOND RX Fully Automated Research Stainer. Prior to staining, sections were deparaffinised three times by incubating in xylene for 10 min, rehydrated with 100% ethanol and treated with hydrogen peroxide for a further 10 min. Sections were then rinsed in PBS and heated to 100°C in pH 6 target retrieval buffer for 20 min to facilitate induced epitope retrieval. Samples were then briefly added to 100% ethanol and dried at 60°C for 5 min. RNAScope protease III was then added to sections for 30 min at 40°C. Sections were then rinsed twice in RNAscope wash buffer.

2.14. Punch biopsy FFPE 5-plex RNAscope in situ hybridisation followed by automated IHC

The RNAscope multiplex fluorescent v2 assay was then performed according to the RNAscope LS Multiplex Fluorescent Assay. Briefly, C1 and C2 probes against *H. pylori* and Eubacteria were added to sections for 2 h, prior to amplification and labelling of probes with Opal fluorophores. Sections were then further washed in RNAscope wash buffer and the IHC protocol was immediately followed using a Leica Bond RX

Automated Research Stainer. Sections were heated in target retrieval buffer for 20 min, washed in RNAscope wash buffer and blocked in peroxide for 10 min at room temperature. Next, the first pre-diluted primary antibody in the desired staining sequence was added. Antibody information and incubation times for the automated assay are detailed in Table 2.8. Following incubation, sections were washed and incubated in Opal polymer HRP Mouse and Rabbit secondary antibody for 10 min. Sections were then washed, and pre-diluted Opal polymer was added to fluorescently label the antibody of interest. Opal fluorophore information and concentrations are also detailed in Table 2.8. Sections were then heated in relevant target retrieval buffer order to heat strip the previous antibody epitope, allowing for subsequent application and labelling of multiple primary antibodies in sequence by repeating the aforementioned protocol. After fluorescently labelling each antibody, sections were washed once again and counterstained with spectral DAPI (Akoya Biosciences) for 10 min. Sections were washed in distilled water, air dried and mounted with ProLong Diamond Antifade Mountant and 1.5. Whole slide scans of each tissue section were then obtained with a Vectra Polaris whole-slide scanner.

2.15. Optimisation of manual RNAscope pre-treatments and IHC antibody concentrations

Antibody concentrations and incubation times for FFPE were optimised by Ana Teodósio and tested for compliance with the manual staining assay by staining spare gastric CG and GIM FFPE punch biopsy tissue sections before continuing with the assay. RNAscope probes against *H. pylori* and Eubacteria were tested in vitro on

confluent AGS cells or 2D organoid monolayers grown on transwell inserts or chamber slides which were infected with *H. pylori* strain PMSS1 and *A. oris* at an MOI of 1:100.

2.16. Manual FFPE tissue preparation

Archived gastric tissue samples were collected from consenting patients at the Queen Elizabeth Hospital, Birmingham and prepared at the Human Biomaterial Resource Centre (HBRC), University of Birmingham, by fixing with formalin and embedding in paraffin (FFPE). 4 µm thick tissue sections were then kindly prepared for eventual staining by the HBRC and Dr Gary Reynolds (Institute of Cancer and Genomic Science, University of Birmingham). Prior to staining, all sections underwent manual deparaffinisation and rehydration, with a series of incubations for 5 min at room temperature in xylene in a fume hood, followed by incubating for 2 min in decreasing concentrations of ethanol from 100-50%.

Sections were then briefly washed in distilled water and RNAscope hydrogen peroxide was added for 10 min at room temperature. Sections were then rinsed in distilled water briefly before antigen retrieval was performed for 15 min at 20% power using microwave heat induced epitope retrieval (HIER). HIER was performed in a Simport staining jar filled with pre-heated RNAscope antigen retrieval buffer. Every 15-30 s, the jar was removed from the microwave and temperature was checked with a glass thermometer to prevent boiling and bubbling. Sections were then briefly added to 100% ethanol and dried at 60°C for 5 min, prior to addition of RNAScope protease III for 30 min at 40°C in a humidified box.

Table 2.8. Antibodies and probes used for automated RNAscope IHC assays.

Antibody/Probe	Catalogue number	Concentration	Opal fluorophore	Opal dilution
C1 *H. pylori*	542938	1x	520	1:1500
C2 Eubacteria	464468-C2	1:50	620	1:1500
MUC5AC	MA1-19346	1:200	570	1:150
MUC2	MA1-38215	1:200	480	1:150
E-cadherin	24E10	1:400	690	1:200

2.17. Manual FFPE RNAscope in situ hybridisation

Sections were washed twice in RNAscope wash buffer, prior to following the RNAscope multiplex Fluorescent v2 Assay according to manufacturer's instructions. Briefly, sections were incubated with C1 and C2 probes (Table 2.9) against *H. pylori* and Eubacteria for 2 h. Sections were washed twice more in RNAscope wash buffer and incubated overnight in 5 x sodium saline citrate (SSC) buffer at room temperature. On day two, sections were removed from SSC buffer and washed twice in RNAscope wash buffer, prior to continuing the v2 assay involving amplification and labelling of all RNAscope probes.

2.18. Manual 3-plex IHC following RNAscope probe amplification

Following successful labelling of RNAscope probes, sections were washed three times with warm PBS and blocked in 1x PBS, 3% BSA, 3% Goat Serum and 0.3% Triton X-100 for 1 hour at room temperature. After blocking, sections were washed three times with PBS and E-cadherin primary antibody diluted in blocking buffer was added overnight at 4 °C. The following morning, E-cadherin primary antibody was removed, and sections were washed three times with PBS prior to incubating in Alexa Fluor 594 diluted in blocking buffer for 2 h at room temperature (Table 2.9). Sections were washed with PBS a further three times, air-dried and mounted onto a glass slide in 4-8 µL VectaShield hard set mounting medium with DAPI. A 1.5 glass coverslip was added on top and was sealed with clear nail varnish or autoclave tape. Samples were stored in a light proof box at -20 °C. Sections were then imaged using a Mantra 2 Quantitative Pathology Workstation at 4x magnification and whole slide scans were then obtained with a Vectra Polaris whole-slide scanner.

Table 2.9. Antibodies and probes used for manual RNAscope 3-plex RNAscope and IHC assays

Antibody/Probe	Catalogue number	Concentration	Opal fluorophore	Opal dilution
C1 *H. pylori*	542931	1x	520	1:1500
C2 Eubacteria	464461-C2	1:50	570	1:1500
E-cadherin	24E10	1:400	N/A	N/A
Alexa Fluor 594	8889S	1:1000	N/A	N/A

Table 2.10. Antibodies used for sequential manual 3-plex IHC assays

Antibody/Probe	Catalogue number	Concentration	Opal fluorophore	Opal dilution
MUC5AC	MA1-19346	1:200	620	1:100
MUC2	MA1-38215	1:500	480	1:100
E-cadherin	24E10	1:400	690	1:100

2.19. Manual sequential 3-plex IHC

Consecutive were prepared as previously described, washed twice in TBST and placed inside Simport staining jars whereby microwave HIER was performed for 15 min at 20% power, using pre-heated AR6 antigen retrieval buffer. Sections were rinsed in TBST then sequentially labelled with antibodies against E-cadherin, MUC5AC and MUC2 following the Opal 7-colour IHC detection kit. All antibodies and Opals used in 3-plex IHC are detailed in Table 2.10. After rinsing twice in TBST followed by distilled water, sections were briefly air dried and mounted with ProLong Diamond Antifade Mountant and 1.5 thickness glass coverslips. As before, whole slide scans of each section were then obtained.

2.20. Qualitative image analysis

Raw. qptiff image files obtained following Vectra Polaris scanning were spectrally unmixed by importing and stamping in Phenochart Whole Slide Viewer (Akoya Biosciences), unmixed and exported in InForm software (Akoya Biosciences) and restitched as a BIGTIFF file using Visiopharm software (Visiopharm, Hørsholm, Denmark). Patient and disease state information were first omitted to ensure blinded analyses, and all images were then viewed by two independent researchers using Phenochart Whole Slide Viewer (Akoya Biosciences). Presence of each marker of interest (*H. pylori*, Eubacteria, E-cadherin, MUC5AC and MUC2) were scored whereby 1 = no/low staining intensity, 2 = medium staining intensity, 3 = high staining intensity. Invasion of Eubacteria was also qualitatively scored, whereby 0 = no invasion, 1 = sparse eubacterial invasion, 2 = moderate eubacterial cell invasion, 3 = high eubacterial cell invasion and 4 = dense eubacterial colonisation within patches.

2.21. Quantitative image analysis

Image analysis of BIGTIFF files was performed using the free and open source Qupath software (Version 0.4.3). For each slide scan, patient and disease state data were first omitted to ensure blinded analyses. Tissue regions were then annotated and defined as a region of interest (ROI). Tissue detection was then performed based on the average values of all channels using a simple pixel thresholder set to high quality. Each pixel thresholder was used to calculate tissue area (μm²), which was exported, and mean tissue area value was obtained. Pixel thresholders were then sequentially created for each individual OPAL channel, corresponding to *H. pylori*, Eubacteria, MUC5AC or MUC2. The thresholders were saved, and area annotation measurements (μm²) were obtained for each channel. For each whole slide scan, average percentage area coverage of each channel of interest was calculated by dividing individual channel area over total tissue area x 100. Data were exported from Excel to GraphPad Prism 9 (Version 9.5.1) for statistical analysis and presentation.

2.22. H&E staining of FFPE tissue

Gastric tissue sections underwent manual deparaffinisation by incubating in xylene for three 5-minute intervals in a fume hood. Sections were then incubated for 2 min each in in decreasing ethanol series from 100-50%, followed by three washes in distilled water. Staining was conducted using an H&E staining kit (abcam), according to manufacturer's instructions. Sections were then dehydrated with ethanol for 2 min each in increasing concentration from 50-100% and rinsed in distilled water. Sections were then cleared for 20 seconds in xylene and immediately mounted in ~50-70 μL DPX Mountant (Sigma-Aldrich) in a fume hood. Sections were air dried for 48 h and viewed

using a light microscope. Whole slide scans were obtained using a Zeiss Aperio Whole Slide Scanner.

2.23. Modified Gram stain for bacterial detection within FFPE tissue

Gastric tissue sections underwent manual deparaffinisation by baking at 60°C for one hour followed by incubating in xylene for three 5-minute intervals in a fume hood. Sections were then immediately incubated for 2 min in 100% ethanol, followed by 3 min in 95% ethanol and 3 min in distilled water. Distilled water was used for all rinsing steps. Sections were incubated in crystal violet solution for 2 min, rinsed and incubated in Gram's iodine for 5 min. Sections were rinsed and immediately decolourised with acetone for 10 sections, before dipping in distilled water immediately followed by incubation in Gram's safranin for a further 5 min. Following addition of stains, the sections were rinsed twice more and incubated in Gallego solution (distilled water, 0.05% formaldehyde, 0.01% acetic acid) for a further 5 min. Sections were then rinsed, and sequentially dipped 5 times in acetone, 0.05% picric-acid acetone, acetone-xylene and xylene in a fume hood, until the tissue appeared visibly yellow. Finally, sections were blotted dry and mounted in onto a glass microscope slide in DPX Mountant with a cover slip, in a fume hood. Sections were air dried for 48 h and viewed using a light microscope. Whole slide scans were also obtained using a Zeiss Aperio Whole Slide Scanner.

2.24. Laser-capture microdissection of FFPE tissue

GAC sections were H&E stained as described in 2.22 and immediately viewed using a Zeiss PALM MicroBeam laser capture microscope. Previous RNAscope slide scans of each tissue section of interest were used to locate regions of Eubacteria on the tissue. Eubacteria were then excised with the laser beam and transferred into a sterile 0.5 mL Eppendorf tube containing 200 μL DNA/RNA Shield (Zymo Research). CG and GIM punch biopsy tissue sections were manually lifted by a scalpel and transferred into 200 μL DNA/RNA Shield (Zymo Research) under sterile conditions in a cell culture hood.

2.25. DNA extraction and PCR amplification

Fresh punch biopsy tissue was obtained from the Queen Elizabeth Hospital, Birmingham and immediately stored in 200 μL DNA/RNA Shield (Zymo Research). The stored punch biopsy tissue, laser captured GAC tissue and scalpel lifted CG and GIM tissue were then prepared for DNA extraction by incubating at 55°C in Proteinase K and solid tissue buffer (blue) until clarified. Once clarified, DNA extraction was conducted according to manufacturer's instructions using a ZymoBIOMICS DNA extraction kit. 15 μL DNA from each sample was then eluted in nuclease free water and amplified by PCR using a Phusion High-Fidelity PCR Kit (Thermo Fisher) and 27F and 1429R 16S rRNA gene-targeting primers. Amplified DNA was analysed using agarose gel electrophoreses (AGE). Gels were prepared using 1% agarose in TRIS-EDTA buffer. A 1kb ladder (500bp-10kb) was used for DNA length estimation and a voltage of 120 V was applied for approximately 25 min to ensure accurate resolution of DNA. Amplified DNA was purified using a QIAquick PCR Purification Kit according

to manufacturer's instructions and 30 μL purified DNA was eluted in pre-warmed elution buffer. DNA concentration was quantified using a Qubit dsDNA HS kit and Qubit spectrophotometer. Purified and quantified amplicons were stored at -20°C prior to downstream analysis.

2.26. Nanopore amplicon sequencing

Purified amplicons were prepared for 16S sequencing following the Oxford Nanopore Technologies (ONT) Native Barcoding Kit 24 V14 protocol. Briefly, amplicons were end-prepped using NEB Next Ultra II End Repair/dA-tailing Module (NEB; E7546) and native barcodes (NB01-08) were ligated using NEB Blunt/TA Ligase Master Mix (NEB; M0367), pooled and ligated with sequencing adaptors using the NEBNext Quick Ligation Module (NEB; E6056). All clean-up steps used AMPure XP beads and a magnetic rack. A flow-cell with ~1600 remaining pores was primed with the addition of Flow Cell Flush and Flow Cell Tether, before 40 fmol of the final prepared library was added. The flow cell was connected to a GridION sequencer with MinKNOW software. Sequencing was set to 24 h, with each barcode detecting reads with a minimum and maximum of 1400 and 2000 base pairs, respectively. Once the sequencing run was completed, data were uploaded to the ONT EPI2ME portal and extracted as an html report and .csv file Microsoft Excel file. Relative genera abundance was calculated for each barcode, by dividing number of individual genera reads over total reads x 100. For downstream analyses, data were organised by removing *Helicobacter* genera which was a consistent and obvious contaminant across all samples. Unknown genera and any genera with reads of below 10 were also excluded for the purposes of data visualisation.

.

Chapter 3: Organoid models to study *Helicobacter pylori* VacA in vitro

3.1. Introduction

H. pylori infection of the gastric mucosa is difficult to model in vitro, primarily due to complex growth requirements and lack of a suitable host model. Since its discovery in the 1980s, several in vitro models have been developed to study *H. pylori* pathogenicity and carcinogenesis. The majority of early studies relied on animal models including mice, gerbils, and primates. Although animal models are useful for studying initial effects of *H. pylori* colonisation, they are inadequate for studying the long-term effects of chronic infection. Many animals artificially infected with *H. pylori* do not develop long-term pathologies outlined in Correa's cascade of carcinogenesis, such as CG, GIM, dysplasia and GAC (Taylor and Fox, 2012). Furthermore, *H. pylori* is not associated with clinical disease in animals. Small animal species such as rats and mice are ordinarily colonised with other *Helicobacter* species such as *H. hepaticus* (Taillieu *et al*., 2022).

Aside from animal models, cell lines have often been used to model *H. pylori* infection in vitro. Cell lines are more cost effective, easier to maintain and generally less expensive. Several cell lines have been used in *H. pylori* studies over the past thirty years, including gastric adenocarcinoma derived AGS and MKN-1, -7, -28, -74 (Taylor and Fox, 2012), cervical cancer HeLa (Cover *et al*., 1992), Chinese hamster ovary (CHO) (Löfling *et al*., 2008) and colon Caco-2 cell lines (Lytton *et al*., 2005). Although experiments using cell lines are generally reproducible, most cell lines used in these studies were derived from gastric tumours or did not originate from the stomach and were therefore not physiologically relevant for modelling the normal gastric mucosa, as they do not accurately reflect the in vivo environment of the human stomach. Cell

lines are also generally considered unsuitable for long-term infection studies as they cannot self-maintain over extended periods of time (Bartfeld *et al*., 2015; Takahashi *et al*., 1997). In recent years, patient-derived cell lines and gastric organoid models have emerged as an ideal model for studying *H. pylori* infection in vitro. Gastric organoids are self-sustaining, recapitulate the cellular architecture of the stomach and even share physiological features with the human stomach, such as mucus secretion (Bartfeld *et al*., 2015; Clevers, 2016). Modelling *H. pylori* infection with 3D organoids in vitro is difficult and requires microinjection of bacterial cultures. However, Boccellato *et al*. (2019), recently devised a method to derive and grow self-sustaining, mucin-producing 2D organoid monolayers from 3D gastric organoids.

H. pylori virulence factors cytoxin-gene associated A (CagA) and vacuolating cytotoxin-A (VacA) are virulence factors associated with carcinogenesis. CagA is injected into host cells via the Type IV secretion system and is associated with disruption of intercellular junctions and increased expression of pro-inflammatory cytokines, such as IL-8. Furthermore, CagA can enhance motility and elongation of host cells. VacA is a secreted virulence factor and induces a variety of phenotypic changes on cultured cells, such as apoptosis and disruption of intercellular junctions (Papini *et al*., 2001). A well-studied effect of VacA is the induction of prominent vacuoles on a variety of cell lines in culture, yet the mechanism behind this remains unclear. In addition, the effect of VacA allelic form has also been investigated, with Rhead *et al.* (2007) reporting that the s1/m1 form is more pathogenic than the s2/m2 form and might be an independent risk factor for gastric cancer. VacA and CagA have been observed to attenuate one

another, with CagA dampening vacuolating effects of VacA and VacA presence reducing cellular elongation induced by CagA. It is hypothesised that the antagonistic relationship between these two virulence factors could prevent host cellular stress, although this effect has not been investigated in depth (Argent *et al*., 2008).

Although many studies have indicated that VacA induces vacuolation of host cells, which might play a significant role in the early stages of gastric cancer development, the majority of these studies have been conducted on non-physiologically relevant cell lines and animal models (Papini *et al*., 2001; Winter *et al*., 2014). Therefore, the aims of the work presented in this chapter were to firstly generate and characterise reproducible and self-sustaining organoid monolayer models derived from 3D healthy gastric organoids. Polarisation of monolayers was compared with commonly used polarising and non-polarising cell lines, AGS and Caco-2 cells. These organoid models were then used in subsequent experiments to investigate whether exposure to both lysates and live cells of *H. pylori* strain Tx30a (s2/m2) and wild type strain 60190 (s1/m1) expressing VacA and, or CagA, resulted in vacuolation of cells within the monolayer. Overall, this results chapter aimed to validate organoid models as a *H. pylori* infection model and to determine the significance of VacA-induced phenotypic changes, such as vacuolation, during the early stages of *H. pylori* carcinogenesis.

3.2. Results

3.2.1. Effect of initial seeding density on organoid monolayer confluency

Initial studies were designed to determine the effect of initial seeding density on the formation of 2D organoid monolayers in three separate corpus organoid lines –

S278.602, S282.185 and S292.072. After ~5-7 days of growth in Matrigel, 3D organoids were collected, disrupted into single cells and reseeded onto collagen coated transwell inserts at seeding densities ranging from $2x10^5$ to $1x10^6$ cells per mL of complete 2D organoid culture medium. Cells were then incubated at 37 °C and 5% CO_2 with humidified conditions. Cell monolayer formation was monitored using phase-contrast microscopy at 24 h intervals, until 100% confluency was reached. In this instance, 100% confluency was defined as complete coverage of the transwell by organoid monolayers, with no visible holes or gaps between cells.

Although growth was observed in all three organoid lines, no clear correlation between initial seeding density and growth time was identified (Figure 3.1). In general, for S292.072 and S282.185, monolayer growth was enhanced with higher initial seeding densities, but this effect was not observed for S278.602. Whilst higher seeding densities were generally desirable for quicker monolayer growth, a larger volume of 3D organoids were required for seeding multiple transwell inserts. The requirement for high organoid numbers therefore became a bottleneck during these studies, as 3D organoids quickly became exhausted and new stocks were often required from liquid nitrogen or gastric biopsy. On average, growing new 3D organoids from stocks was a slow process and took around 7-9 days. Similarly, if seeded at a lower density, organoid monolayers also grew very slowly which further hindered experimental work. Therefore, in order to prevent either outcome, a middle-range initial seeding density of ~$4.5x10^6$ per mL was selected for future experiments. Confluency of monolayers were reached in ~5 days for organoid lines S282.185 and S278.602, or ~2 days for S292.072, which was suitable for minimising risk of a further growth bottleneck.

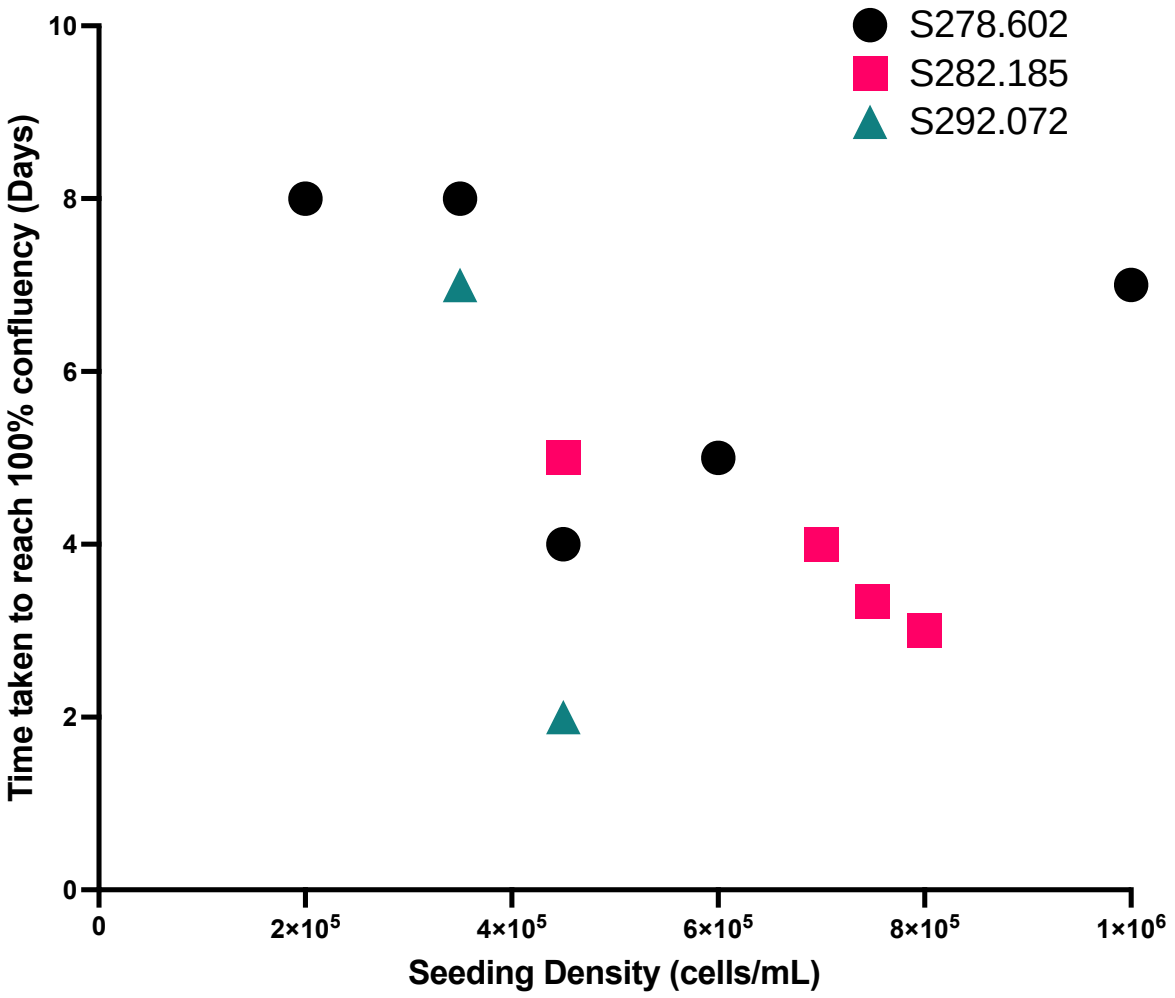

Figure 3.1. The effect of seeding density on time to reach 100% confluency for three independent patient-derived organoids. After 5-7 days of growth in complete 3D organoid cell culture medium, organoids were washed, disrupted into a single cell suspension and seeded at the required seeding density onto collagen-coated transparent PET transwell inserts. Cells were incubated at 37°C, 5% CO_2 and were visually inspected with a light microscope every 24 h following seeding until 100% confluency was reached. Data were obtained from multiple independent experiments using three separate patient-derived organoid lines.

3.2.2. Quantification of organoid monolayer polarisation

Once an approximation of initial cell seeding density was established for growth of organoid monolayers, monolayer polarisation and therefore tight junction integrity over 7, 14 and 21 days was measured using a FITC-dextran permeability assay. Three organoid monolayers were prepared from the S292.072 organoid line as previously described and seeded at a density of $1x10^5$ and $4.5x10^5$ per mL in 2D organoid culture medium with antibiotics and Primocin. Similarly, three transwells of both the Caco-2 and AGS cell lines were seeded at a density of $1x10^6$ and $2x10^6$ per mL in cRPMI medium, respectively. All cells were incubated at 37°C and 5% CO_2 with humidity for 7 days. At day 7, 14 and 21, transwells were removed from the incubator and the apical transwell surface was washed twice in PBS. The apical transwell surface was incubated with 4 mg/mL 4 kDa FITC-Dextran in PBS for 3 h at 37°C

After 3 h, liquid from the basal compartment of each transwell was transferred to a black 96-well plate and fluorescence intensity was measured in a micro plate reader (Figure 3.2). The extent of organoid monolayer and AGS cell permeability was compared with Caco-2 cells, which express tight junctional proteins such as E-cadherin and are well known to form polarised monolayers. At 7, 14 and 21 days, AGS cell permeability was significantly higher than Caco-2 cells, regardless of initial seeding density. Therefore, these data suggest that AGS cells do not polarise and form a monolayer, as the cells remained permeable to FITC-dextran throughout the assay, especially in comparison to Caco-2 cells and organoid monolayers.

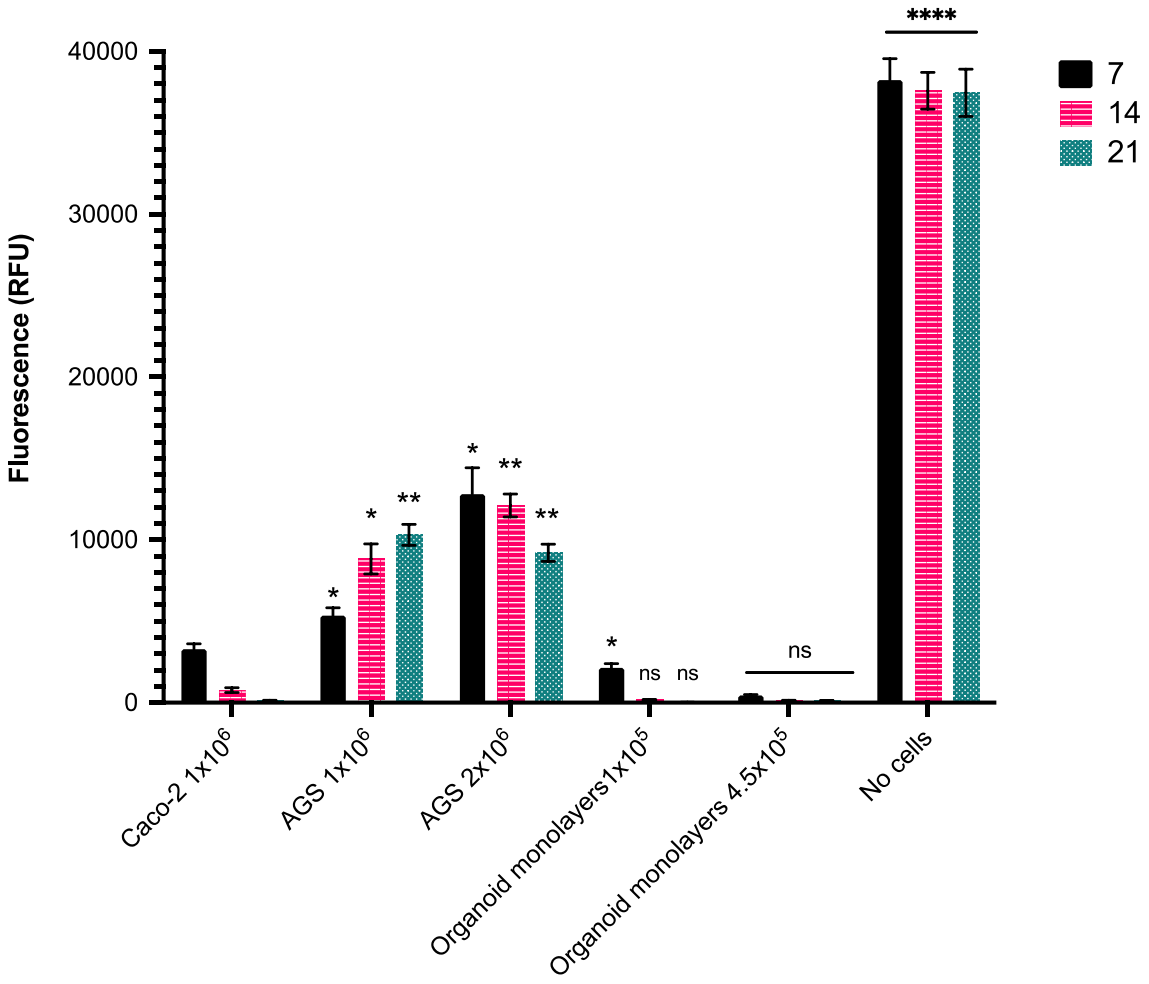

Figure 3.2. The effect of seeding density and cell type on permeability, over 7, 14 and 21 days. Caco-2 and AGS cells were grown to confluency in RPMI containing 10% FCS and penicillin-streptomycin solution (cRPMI); 3D organoids were grown for ~5-7 days in complete organoid culture media, disrupted into a single cell suspension and reseeded onto a transwell insert. At 7-, 14-, and 21-day intervals, all transwells were removed from the incubator and 4 mg/mL 4kDa FITC-Dextran in PBS was added to the apical surface of the transwell for 3 h at 37°C. After 3 h, the contents of the basal compartment of each transwell were transferred to a black 96-well plate and fluorescence intensity was measured in a micro plate reader. Values were obtained and transferred to Microsoft Excel and GraphPad Prism software. Data shown is mean ±SEM from three independent experiments; ns = non-significant, * = $p<0.05$ and ** = $p<0.01$ and **** = $p<0.0001$ relative to Caco-2 cell control, as determined by two-way ANOVA.

In contrast, although organoid monolayers seeded at a density of $1x10^4$ cells per mL were permeable to FITC-dextran at 7 days, at 14- and 21-days permeability was similar to polarising Caco-2 cells. These data therefore further suggest that 7 days is not adequate for complete polarisation of organoid monolayers seeded at a density of $1x10^4$ cells per mL. This corroborates with findings shown in Figure 3.1 where at least 8 days of growth was generally required for confluency. Organoid monolayers seeded at a density of $4.5x10^4$ cells per mL demonstrated no significant difference in permeability to Caco-2 cells at 7, 14 and 21 days, indicating that complete polarisation had occurred as negligible FITC-dextran was detected in the basal transwell compartment. Taken together, these data suggest that compared to organoid monolayers and Caco-2 cells, AGS cells are not a physiologically relevant model of the gastric mucosa as they did not form a monolayer and remained permeable throughout the assay. Although Caco-2 cells did polarise, they originate from the colon and are therefore unsuitable for further studies on *H. pylori* and the gastric microbiota.

3.2.3. Phenotyping organoid monolayers with immunofluorescence imaging

Previous studies suggested that organoid monolayers were able to polarise and were therefore a physiological relevant in vitro model to study bacterial infection (Boccellato *et al*., 2018; Caston *et al*., 2020). In order to confirm the physiological similarity of the organoid monolayers to human gastric mucosa and ensure presence of all relevant cell types, phenotyping of the monolayers was conducted using immunofluorescence imaging. Confluent organoid monolayers grown on transwells were prepared from the S292.072 organoid line as previously described. Monolayers were washed, fixed in 4% formaldehyde, and blocked for 90 min in blocking buffer. Monolayers were washed

and incubated overnight at 4 °C with primary antibodies against cell junction protein E-cadherin and, or health gastric mucin MUC5AC.

The following day, monolayers were washed and incubated for 1 h at room temperature with secondary antibodies Alexa Fluor 594 or 488. Finally, monolayers were washed, excised, and mounted in DAPI-containing mounting medium. Monolayers were viewed and images were captured using a confocal microscope. The monolayers stained positively for tight junction protein E-cadherin and MUC5AC on the apical cell surface, with no unspecific staining observed in any of the images obtained (Figure 3.3). E-cadherin staining was uniform across the monolayer, further suggesting that cell polarisation had occurred, as E-cadherin expression is highly associated polarity of cell monolayers and is often only expressed in fully polarised cells. MUC5AC expression was also uniform across the monolayer but appeared in patches which is likely due to random distribution of mucin secreting goblet cells, which was indicative of a healthy gastric epithelial layer.

Following successful antibody staining with antibodies against E-cadherin and MUC5AC, studies were repeated with primary antibodies against digestive enzyme pepsinogen C (PGC), corpus reserve stem cell marker $Troy^+$ (Troy), H^+ and K^+-ATPase proton pump (ATP4B) and somatostatin (SST) (Figure 3.4). The monolayers stained positively for each marker on the apical surface, with no non-specific staining observed in any of the images obtained. PGC and Troy expression was relatively uniform across the monolayer, appearing in patches likely due to random arrangement of cells within the monolayer.

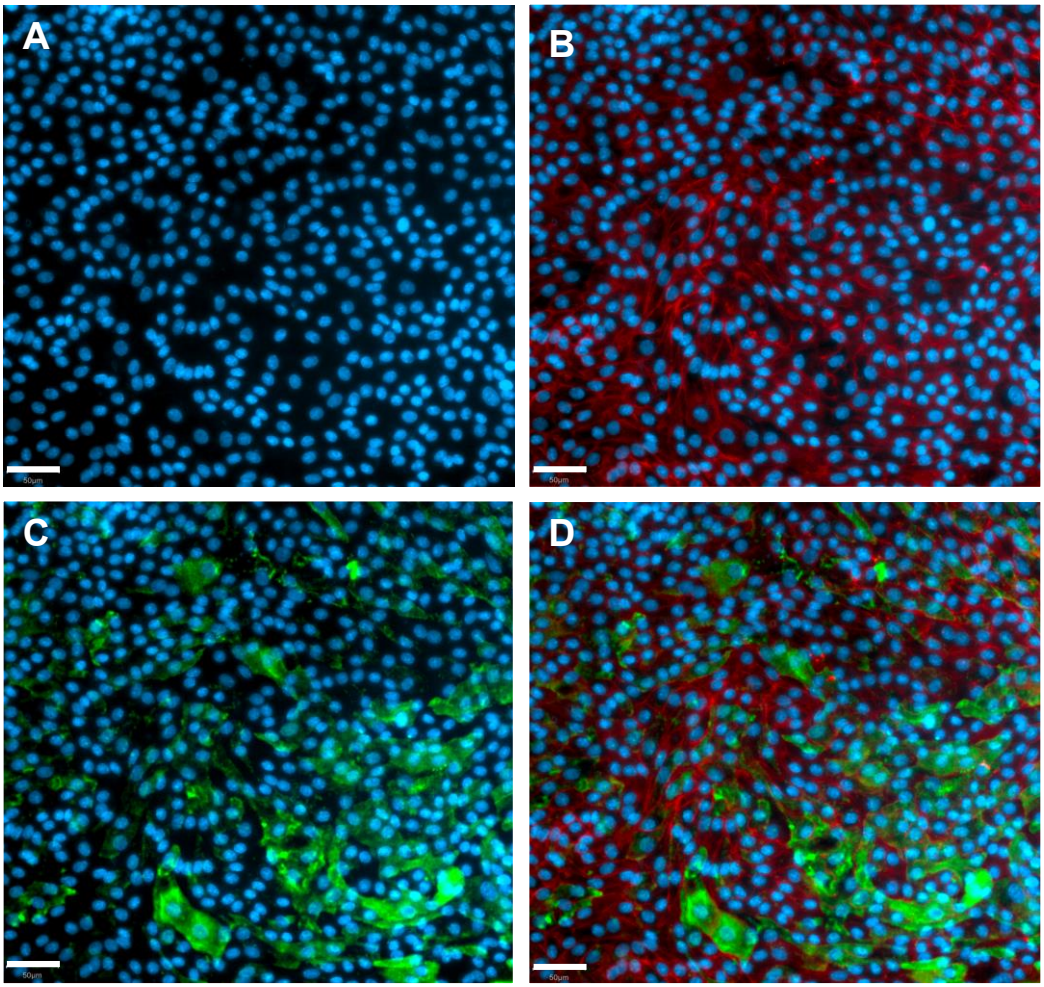

Figure 3.3. Immunofluorescence imaging of 2D organoid monolayers stained for E-cadherin, MUC5AC and DAPI. Confluent monolayers were prepared as described for Figure 3.1. Monolayers were and fixed in 4% formaldehyde before blocking in pre-prepared blocking buffer. Monolayers were then rinsed and incubated overnight with primary antibodies against E-cadherin and MUC5AC. The following day, primary antibodies were replaced with secondary antibodies Alexa Fluor 594 (red) and 488 (green) for 1 h. Monolayers were then washed, excised and mounted onto glass microscope slide in DAPI-containing hard set mounting medium. Slides were air dried and viewed using a confocal microscope. Images show DAPI (A), E-cadherin and DAPI (B), MUC5AC and DAPI (C) and an overlay of DAPI, E-cadherin and MUC5AC (D); Scale bar represents 50 μm.

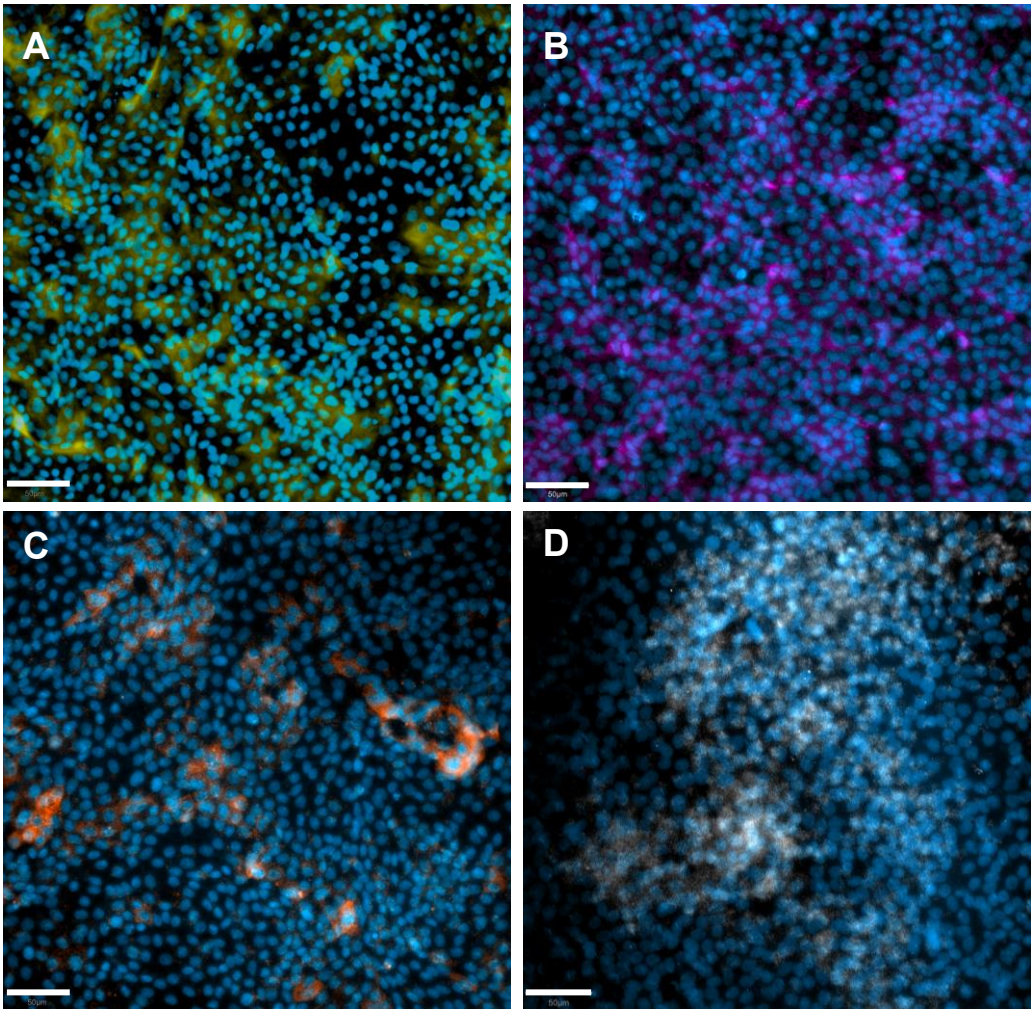

Figure 3.4. Immunofluorescence imaging of 2D organoid monolayers stained for PGC, Troy, ATP4B and SST. Confluent monolayers were prepared for staining as described for Figure 3.3. Monolayers were incubated overnight with primary antibodies against PGC, Troy, ATP4B and SST. The following day, primary antibodies were replaced by secondary antibodies Alexa Fluor 594 or 488 for 1 h. Monolayers were then washed, excised and mounted in DAPI-containing hard set mounting medium. Slides were air dried, before viewed using a confocal microscope. Images show PGC and DAPI (A), Troy and DAPI (B), ATP4B and DAPI (C) and SST and DAPI (D); Scale bar represents 50 μm.

ATP4B staining was sparser, generally surrounding no more than three cells at a time. SST staining was less uniform, with variation in staining pattern and intensity across the monolayer. Positive expression of PGC, Troy and ATP4B were expected, due to their defined roles in maintaining a healthy gastric mucosa in the healthy human stomach corpus. However, although staining intensity did appear lower, expression of SST was somewhat surprising as the organoids used in this work were corpus-derived, whereas SST is not usually identified within this region of the stomach.

3.2.4. Direct passaging of organoid monolayers without expansion of 3D organoids

Organoid monolayers were previously generated by dissociating 3D organoids into a single cell suspension and seeding onto a cell culture plate or transwell insert. Although reliable, this method was relatively slow as 3D organoids required at least ~5-7 days growth before they could be dissociated. Furthermore, once seeded as a monolayer, a further ~5 days of growth was usually required until a confluent monolayer could be obtained for further experimental work. The following study was therefore designed to establish whether organoid monolayers could be derived from already established confluent monolayers obtained from the S282.185 organoid line, thus removing the need for growing and dissociating 3D organoids and then re-seeding

3D organoids were therefore disrupted and seeded as previously described, into rat tail collagen-coated 48-well cell culture plates and incubated at 37 °C until confluency was reached. Once confluent, organoid monolayers were washed twice, disrupted with pre-warmed TrypLE and resuspended. Cells were counted with an automated cell

counter and 0.5 mL were used for seeding transwells for further experimental work whilst the remaining 0.5 mL were reseeded onto fresh rat tail collagen-coated 48-well cell culture plates and incubated at 37 °C until confluent. This process was repeated thrice more and monolayer growth was routinely monitored using a light microscope. After the fourth repeat, or passage, it was observed that organoid monolayers were not reaching confluency and began to grow in a spherical arrangement, rather than a monolayer (Figure 3.5)**.** This was an interesting observation and suggested that monolayers derived from for the S282.185 organoid line lost their ability to form confluent, healthy monolayers after 4 passages.

3.2.5. Effect of passage number on expression of stemness marker Troy in organoid monolayers

The reason for monolayers behaving in this way remains unclear. However, previous studies have suggested that primary or tissue derived cells generally have a lower passage limit as stem cells do not adhere well to cell culture plasticware and are lost during passaging (Gillooly *et al*., 2012; Piwocka *et al*., 2024). Therefore, in order to test this hypothesis, a further set of organoid monolayers were derived from 3D organoids and grown on a transwell, in order to excise and conduct immunofluorescence imaging of stem cell marker Troy, in addition to markers of healthy gastric mucosa, E-cadherin and MUC5AC. After four passages, organoid monolayers were again unable to form, and the spherical morphology was observed once more. As such, transwells were then washed and incubated overnight at 4 °C with primary antibodies against Troy, E-cadherin, or MUC5AC.

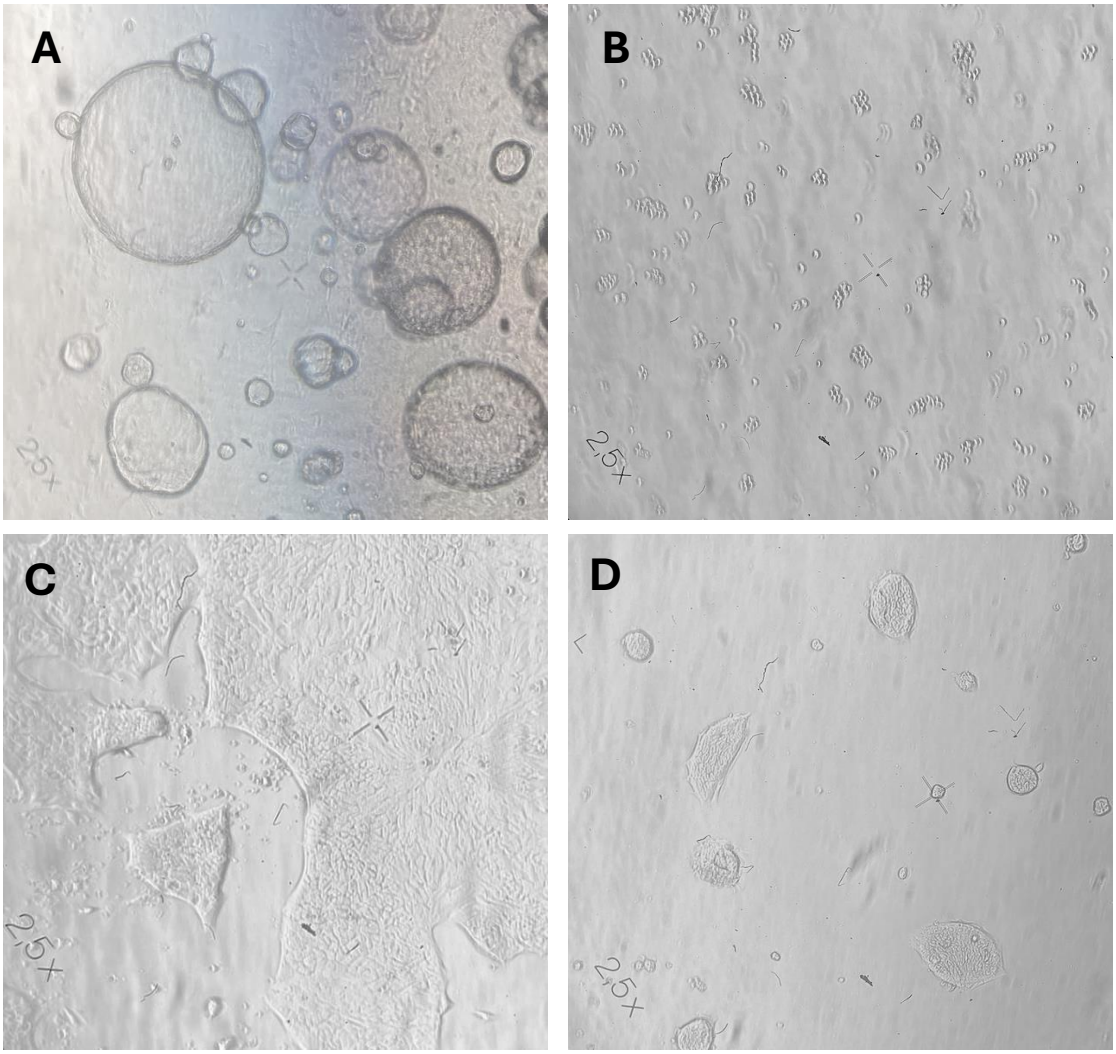

Figure 3.5. Development of 2D organoid monolayer from 3D organoids and subsequent change in growth characteristics. After ~5-7 days growth in 3D organoid media at 37 °C, organoids appeared transparent and spherical (A). Organoids were collected, disrupted and reseeded onto collagen coated 48 well plates (B). Monolayers began to form after approximately 3 days (C). Monolayers were routinely disrupted with TrypLE and passaged. After four passages, organoid monolayers stopped forming and appeared to grow in a spherical arrangement (D). Images were obtained at 2.5x magnification.

The following day, secondary antibody Alexa Fluor 594 or 488 was added for a further hour, before excising and mounting in DAPI-containing mounting media. Transwells were then viewed with a confocal microscope and antibody staining was compared with previous positive antibody staining from healthy confluent monolayer, derived directly from 3D organoids (Figure 3.6). Interestingly, although monolayers at passage four had not formed and appeared spherical, staining for E-cadherin and MUC5AC remained positive with visible intercellular junctions and uniform areas of mucin expression throughout the spherical cellular arrangement. The staining pattern for both E-cadherin and MUC5AC was somewhat similar for both the healthy monolayer and spherical shapes on the transwell. This suggests that E-cadherin and MUC5AC were not affected by a passage limit.

However, in comparison to the healthy monolayer, staining for Troy within the spherical arrangement was noticeably reduced and was not distributed throughout the cells. These data therefore indicate that after four passages, stem cell reserve marker Troy was lost or expression was altered, potentially because of the passaging process. Furthermore, due to this apparent loss of Troy, organoid monolayers do not retain the physiological architecture of a healthy gastric mucosa and begin to grow in an unusual pattern. Unfortunately, due to time constraints, this experiment was only conducted once and was limited by only using imaging techniques of three markers of interest. In order to investigate this phenomenon further, additional laboratory techniques such as qPCR or ELISA could be employed to confirm the apparent loss of stemness.

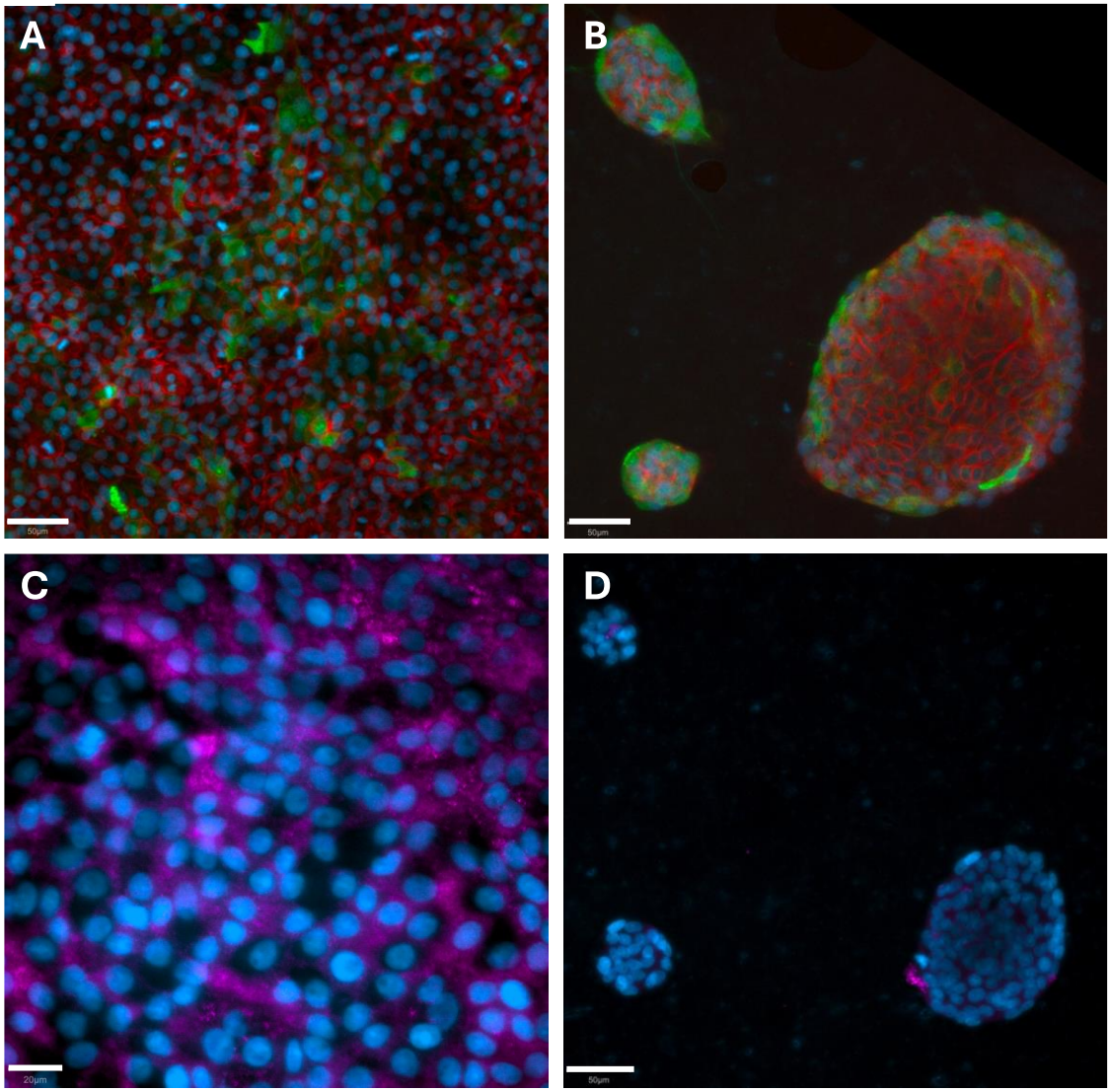

Figure 3.6. Comparison of healthy organoid monolayer derived directly from 3D organoids with 2D monolayer-derived organoid monolayers at passage 4. After 5-7 days of growth in complete 3D organoid cell culture medium, organoids were washed and disrupted into a single cell suspension, before seeding onto collagen coated transwell inserts. When confluent, monolayers were fixed, blocked, and incubated with primary antibodies against E-cadherin and MUC5AC (A) and Troy (C). Monolayers were then passaged thrice more and re-stained (B&D). Transwell inserts were then washed, excised and mounted in DAPI-containing hard set mounting medium. Scale bar represents 20μm (C) or 50μm (A, B&D).

3.2.6. Determination of the optimal *H. pylori* lysate concentration for vacuolation formation of the AGS cell line

Following successful development of an organoid monolayer, the following experiments aimed to determine whether vacuolation is physiologically relevant indicator of early infection during *H. pylori* pathogenesis and is also dependent on VacA allelic form. Before investigations were conducted on precious organoid monolayers or with live *H. pylori* cells, the following experiments assessed whether secreted *H. pylori* VacA induced vacuolation in the AGS cell line.

In order to first determine a suitable and reproducible concentration of *H. pylori* lysate for future vacuolation experiments, a dilution series was prepared for lysates of each *H. pylori* strain to be investigated and incubated with the AGS cell line. After growth on blood agar for 48 h, *H. pylori* strains (wild type 60190, 60190 ΔCagA, 60190 ΔVacA and Tx30a) were suspended in sterile water and mixed vigorously to promote lysis. Following removal of intact bacteria by centrifugation, the supernatant, or 'bacterial lysate' was adjusted to 1 mg/mL as a stock concentration. A doubling dilution series was prepared for each *H. pylori* lysate ranging from 3.125 to 200 µg/mL. Dilutions of each lysate were incubated at 37°C for 16 h with washed AGS cells that had been grown for 24 h in 96 well plates (Figure 3.7). The following day, vacuolation of the AGS cells were briefly confirmed using light microscopy prior to quantifying vacuolation with the neutral red assay described in Chapter 2. As expected, the untreated AGS cells showed minimal vacuolation and subsequent neutral red release throughout the assay. AGS cells treated with 60190 ΔVacA showed comparable vacuolation to the untreated cell with an optical density reading of approximately 0.2.

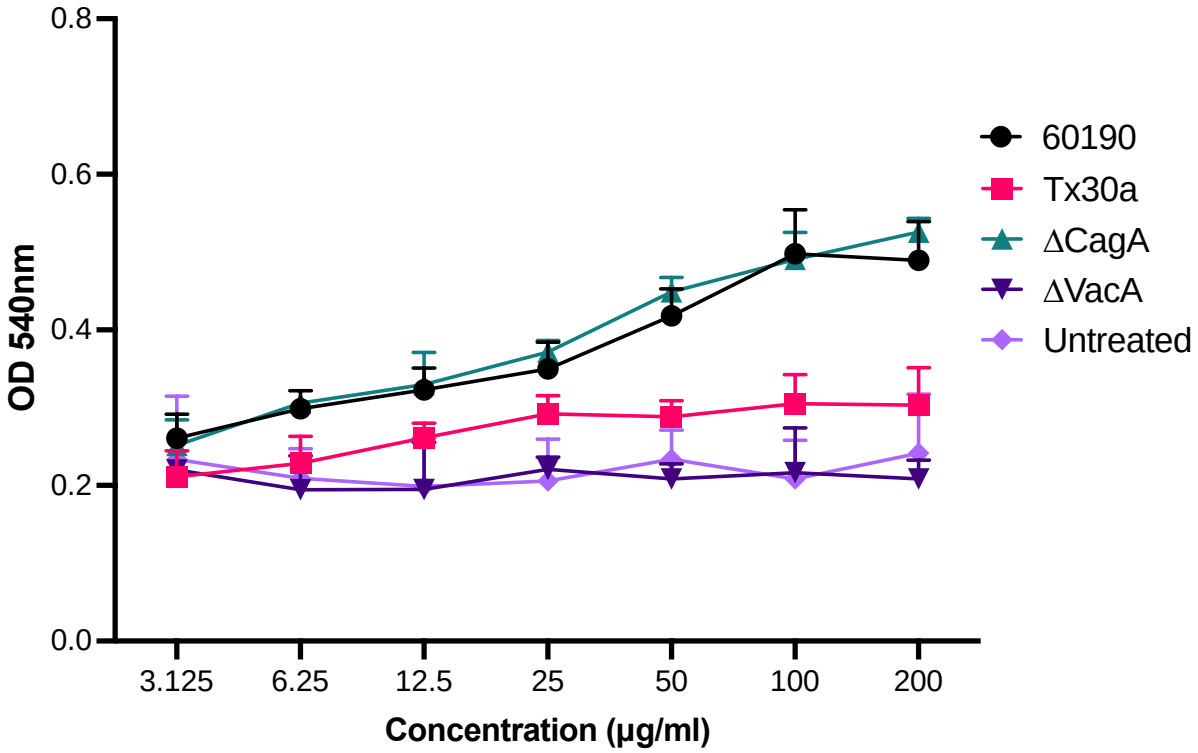

Figure 3.7. Vacuolation of the AGS cell line following treatment with serial dilutions of *H. pylori* lysate. After 48 h growth on blood agar *H. pylori* strains (wild type 60190, 60190 ΔCagA, 60190 ΔVacA ad Tx30a) were lysed in distilled water and adjusted 1 mg/mL. A doubling dilution series of each *H. pylori* lysate was prepared in cRPMI medium from 200 µg/mL to 3.125 µg/mL. AGS cells were incubated either with the culture medium, or with each concentration of the lysate at for 16 h. The cells were washed, before the neutral red assay was conducted and absorbance was measured at 540 nm in a plate reader. Values were obtained and transferred to Microsoft Excel and GraphPad Prism software. Data are presented as mean ± SEM.

At concentrations of 6.25 µg/mL or less, lysates of strains 60190 ΔVacA and Tx30a induced similar levels of vacuolation and subsequent neutral red dye release at an optical density of approximately 0.2. However, at a concentration of 12.5 µg/mL and above, regardless of concentration, lysates of strain Tx30a induced vacuolation and subsequent neutral red dye release at an optical density of approximately 0.3. In comparison, at a concentration of 6.25 µg/mL above, a positive correlation between concentration and neutral red dye release was quantified for lysates of strains 60190 and 60190 ΔCagA. At a concentration of 50 µg/mL, 100 µg/mL and 200 µg/mL, lysates of wildtype 60190 and 60190 ΔCagA released neutral red dye at an optical density of around 0.4 to 0.5 which was significantly higher than the other *H. pylori* lysates. Taken together, these data initially suggest that lysates of *H. pylori* wild type strain 60190 and 60190 ΔCagA significantly induce vacuolation of the AGS cell line at a concentration of 6.25 µg/mL or higher, with the highest neutral red release and therefore induction of vacuolation at a concentration of 100 µg/mL and 200 µg/mL. Whilst this experiment was useful for determining a suitable *H. pylori* lysate concentration for further vacuolation studies, vacuolation was briefly confirmed using light microscopy and relied on neutral red dye release as an indication. In further experiments, the use of light microscopy could be combined with improved imaging methods, such as higher resolution light microscopy in order to fully confirm host cell vacuolation.

3.2.7. Effect of a bacterial lysate of *H. pylori* wild type on vacuolation of AGS cells

The following experiment was designed to investigate whether the previously prepared lysates of *H. pylori*-induced vacuolation of the AGS cell line. Results from the previous experiment indicated that a lysate of *H. pylori* strain 60190 at a concentration of 200

µg/mL would be suitable to induce vacuolation of the AGS cell line. Therefore, pre-prepared wild type *H. pylori* 60190 lysate at a concentration of 200 µg/mL was incubated at 37°C for 16 h with washed AGS cells that had been grown for 24 h in 96 well plates. The extent of vacuolation was compared by phase contrast microscopy with untreated AGS cells (Figure 3.8). Minimal vacuolation was observed in the untreated control cells. In contrast, vacuoles were clearly visible in approximately 75% of the AGS cells following exposure to the *H. pylori* lysate. This indicated that *H. pylori* strain 60190 likely secretes VacA which indeed induces vacuolation.

3.2.8. Quantification of AGS cell vacuolation

After incubation with or without the bacterial lysate as described above, 12 phase-contrast images were obtained and saved for both treatment groups. For each image, the number of vacuolated cells and the total cell count were determined manually, and an average value of percentage vacuolated cells was obtained (Figure 3.9A). In the untreated control, 15-20% of AGS cells were vacuolated, whereas 70-75% of AGS cells treated with *H. pylori* 60190 lysate were vacuolated. This therefore indicated that *H. pylori* wild type strain 60190 was able to induce AGS cell vacuolation. Immediately after imaging, both the *H. pylori* lysate, and culture medium were removed from the AGS cells and neutral red assay was used to measure vacuolation on the underlying cells. AGS cells treated with *H. pylori* bacterial lysate released neutral red dye at an optical density of approximately 0.5, whereas untreated AGS also released a smaller volume of neutral dye, at an optical density of approximately 0.2 (Figure 3.9B).

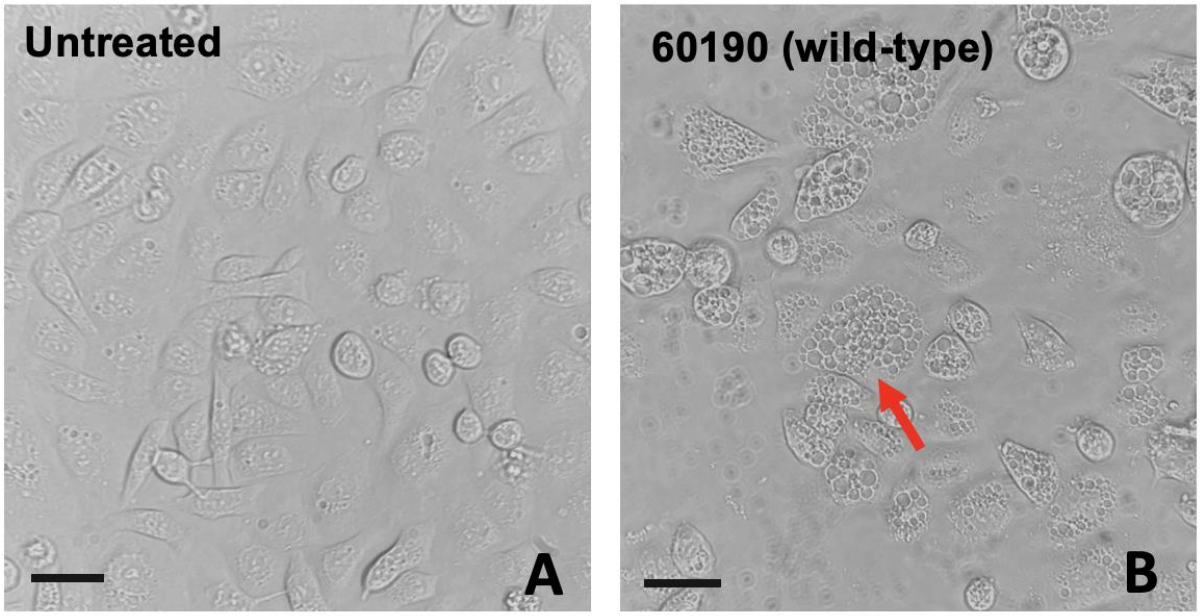

Figure 3.8. Effect of a bacterial lysate of *H. pylori* on vacuolation of AGS cells. Lysates o*f H. pylori* wild type stain 60190 at a concentration of 200 µg/mL were incubated overnight with AGS cells that had been grown for 24 h. Cells from three wells from each set were viewed using a Zeiss Axio Observer microscope with phase-contrast. Images were obtained at 40x magnification; the scale bar represents 25 µm. Vacuolated cells are indicated by red arrows. Similar observations were observed in multiple fields of view from three independent experiments.

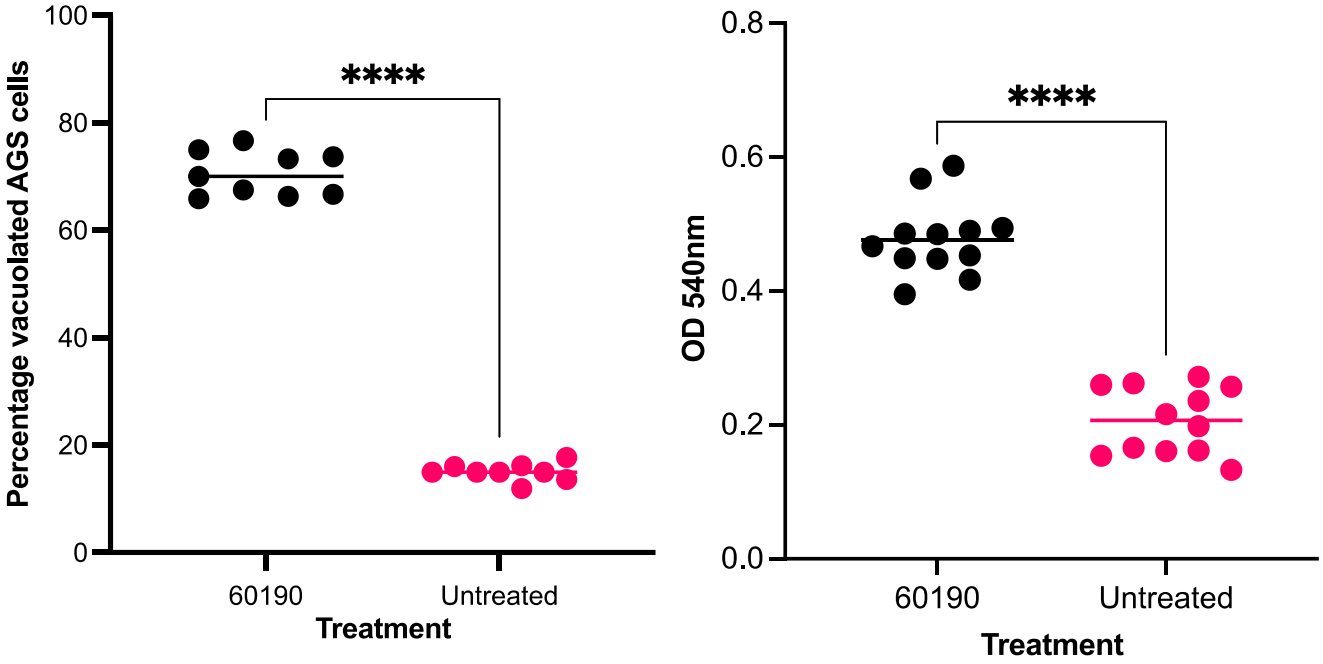

Figure 3.9A and Figure 3.9B. Quantification of AGS cell vacuolation induced by the *H. pylori* lysate. Lysates of *H. pylori* wild type strain 60190 were incubated with pre-prepared AGS cells overnight. Twelve images were then obtained for both treatment groups using a Zeiss Axio Observer with phase-contrast. For both 60190 and untreated AGS cells, the average percentage of vacuolated cells was calculated, and all media were then removed from the AGS cells. The neutral red uptake assay was conducted, and absorbance values read using a plate reader. Values were obtained and transferred to Microsoft Excel and GraphPad Prism software. Similar results were obtained from three independent experiments; **** $P<0.0001$ relative to untreated control, as determined by unpaired t-test.

These data therefore indicated that AGS cells treated with *H. pylori* 60190 lysates indeed formed vacuoles, in which neutral red dye can enter and subsequently be released following extraction with acidified ethanol. Interestingly, untreated AGS cells also appeared to contain naturally formed vacuoles or vacuole-like structures that absorbed less neutral red dye. Furthermore, although trends in vacuolation were similar when assessing vacuolation with both approaches, it is clear that results from the neutral red assay were variable. This suggests that although the neutral red assay provides an indication of vacuolation, this assay should be used in combination with manually counting vacuolated cells in order to improve experimental reliability.

3.2.9. Effect of mutation in *vacA* or *cagA* on AGS cell vacuolation

Previous studies confirmed that a soluble extract of *H. pylori* s1/m1 VacA expressing wild type strain 60190 induced vacuolation in the AGS cell line. Next, studies were repeated using bacterial extracts of 60190 knockout strains, 60190 ΔCagA and 60190 ΔVacA to determine whether the absence of these virulence factors influenced the vacuolating effect of *H. pylori* lysates. In addition, the effect of a different allelic form of VacA was investigated by repeating studies with lysates of the 'less pathogenic' strain Tx30a, which expresses the s2/m2 form of VacA but not CagA. The extent of AGS cell vacuolation was compared by phase contrast microscopy with untreated AGS cells (Figure 3.10). Minimal vacuolation was observed in the untreated (A) and 60190 ΔVacA treated cells (C). In contrast, vacuoles were clearly visible in approximately 75% of the AGS cells following exposure to lysates of both wild type strain 60190 (B) and 60190 ΔCagA (D). Smaller vacuoles were also visible in approximately 30% of AGS cells following exposure to lysates of strain Tx30a (E).

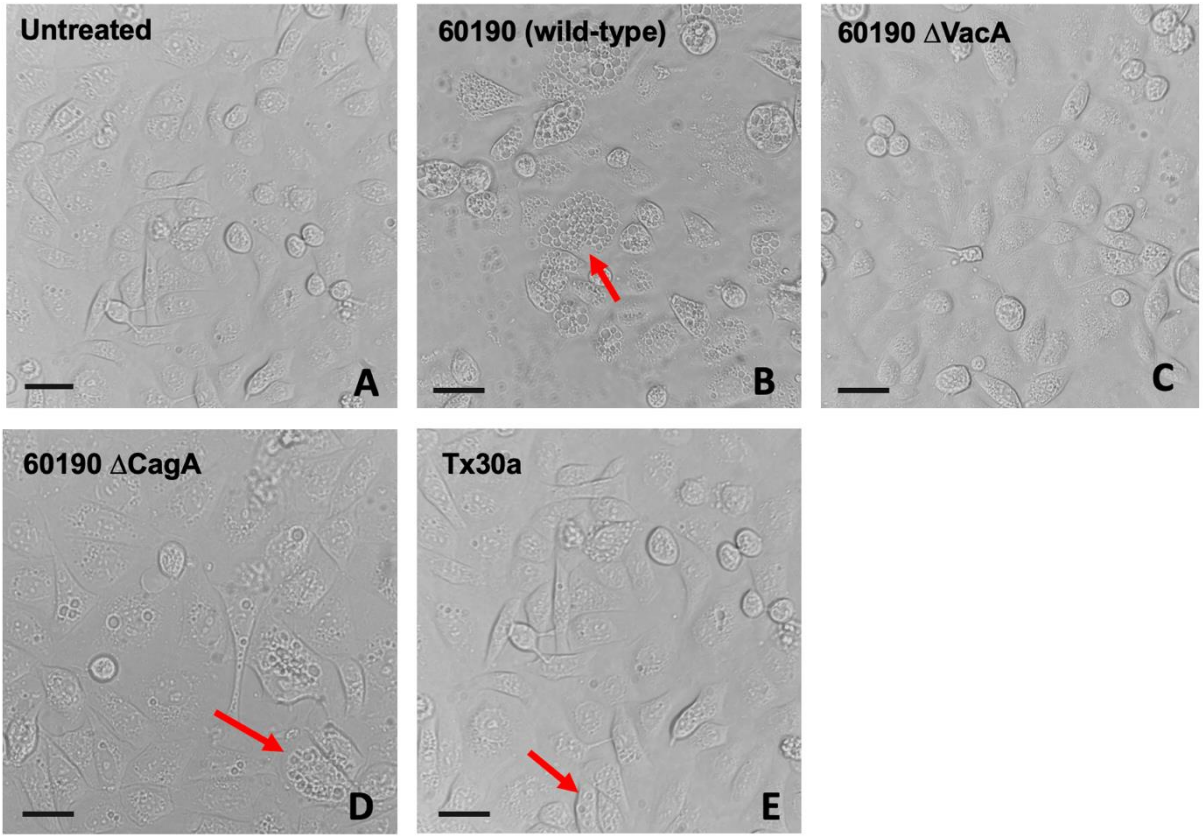

Figure 3.10. Effect of mutation in vacA or cagA on AGS cell vacuolation. Lysates of *H. pylori* strains 60190, 60190 ΔVacA, 60190 ΔCagA and Tx30a were prepared and incubated with AGS cells overnight. Cells from three wells from each set were viewed using a Zeiss Axio Observer microscope with phase-contrast. Images were obtained at 40x magnification; the scale bar represents 25μm. Vacuolated cells are indicated by red arrows. Similar observations were observed in multiple fields of view from three independent experiments.

These data therefore indicate that loss of CagA from strain 60190 does not impair vacuolating activity. In addition, induced vacuolation of AGS cells by *H. pylori* lysates appeared to rely on the presence of VacA, but the extent of vacuolation could be influenced by the VacA allelic form. Vacuole formation was then manually quantified, with the number of vacuolated cells in each group determined by inspection of the phase contrast images. In both the untreated control and AGS cells treated with lysates of 60190 ΔVacA, approximately 15-20% of AGS cells were vacuolated (Figure 3.11A). After treatment with lysates of 60190 ΔCagA, the percentage of vacuolated AGS cells were approximately 80%, whereas around ~70% of AGS cells treated with lysates of strain 60190 were vacuolated. In comparison, around 30% of AGS cells treated with lysates of Tx30a were vacuolated. These data indicate that loss of CagA from strain 60190 might enhance the vacuolating effect of the bacterial lysate. Furthermore, the allelic form of VacA appeared to affect percentage of vacuolated AGS cells, as significantly fewer cells treated with the Tx30a s2/m2 lysate were vacuolated in comparison with cells treated with 60190 s1/m1 lysates. Because the percentage vacuolation was similar between untreated AGS cells and cells treated with 60190 ΔVacA, this further indicates that VacA presence in *H. pylori* lysates is a requirement for AGS cell vacuolation.

The neutral red uptake assay was then used to quantify vacuolation (Figure 3.11B). AGS cells treated with lysates of 60190 and 60190 ΔCagA released neutral red dye at an optical density of approximately 0.5, whereas cells treated with Tx30a released less neutral red dye at an optical density of approximately 0.3. Similar absorbance readings were obtained for 60190 ΔVacA treated cells and the untreated control.

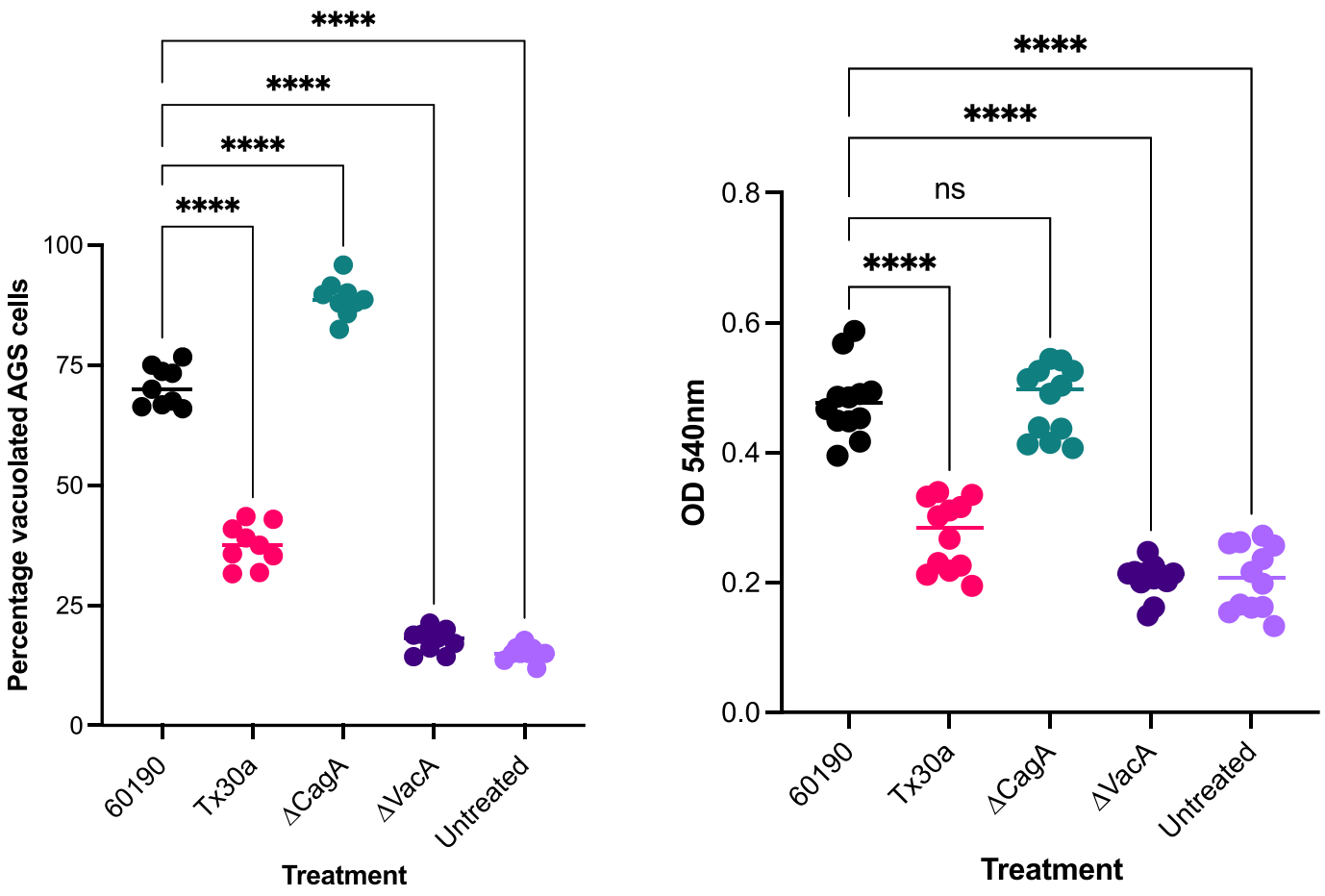

Figure 3.11A and Figure 3.11B. Quantification of AGS cell vacuolation induced by the mutant *H. pylori* lysates. Lysates of *H. pylori* strains wild type 60190, 60190 ΔVacA, 60190 ΔCagA and Tx30a were incubated with AGS cells overnight and vacuolation was quantified by phase-contrast microscopy and the neutral red assay. Values were obtained and transferred to Microsoft Excel and GraphPad Prism software. Similar results were obtained from three independent experiments; **** P<0.0001, ns P>0.005 relative to lysates of strain 60190 as determined by one-way ANOVA.

Data trends were similar for Figures 3.9A and 3.9B, further suggesting that percentage vacuolation quantification, in combination with a neutral red uptake assay, are useful methods for assessing vacuolation of AGS cells after treatment with *H. pylori* lysate. However, in contrast to manual quantification by inspection of phase contrast images, there was no significant difference in neutral red uptake between strains 60190 and 60190 ΔCagA, suggesting that removal of CagA might not enhance vacuolating activity of the bacterial lysate as previously suggested.

3.2.10. Effect of *H. pylori* co-culture on vacuolation of AGS cells

Initial experiments determined that bacterial lysates of *Helicobacter pylori* strain 60190 induce vacuolation in AGS cells. Subsequent experiments followed similar protocols as previously described but instead aimed to determine whether live *H. pylori* strain 60190 in a co-culture system also induced vacuolation. After growth on blood agar for 24 h, the bacteria were washed twice in 1 mL sterile brain heart infusion broth (BHI) and resuspended in 1mL antibiotic-free RPMI cell culture medium. 100 μL resuspended bacteria were incubated at 37°C for 16 h with washed AGS cells that had been grown for 24 h in 96 well plates, at a multiplicity of infection (MOI) of 50. After visual inspection, a low level of background vacuolation (~20%) was observed in the uninfected control cells, whereas approximately 80% of cells infected with *H. pylori* strain 60190 were vacuolated (Figure 3.12). This indicated that as expected, live *H. pylori* wild type strain 60190, in addition to its lysate induced vacuolation in the AGS cell line.

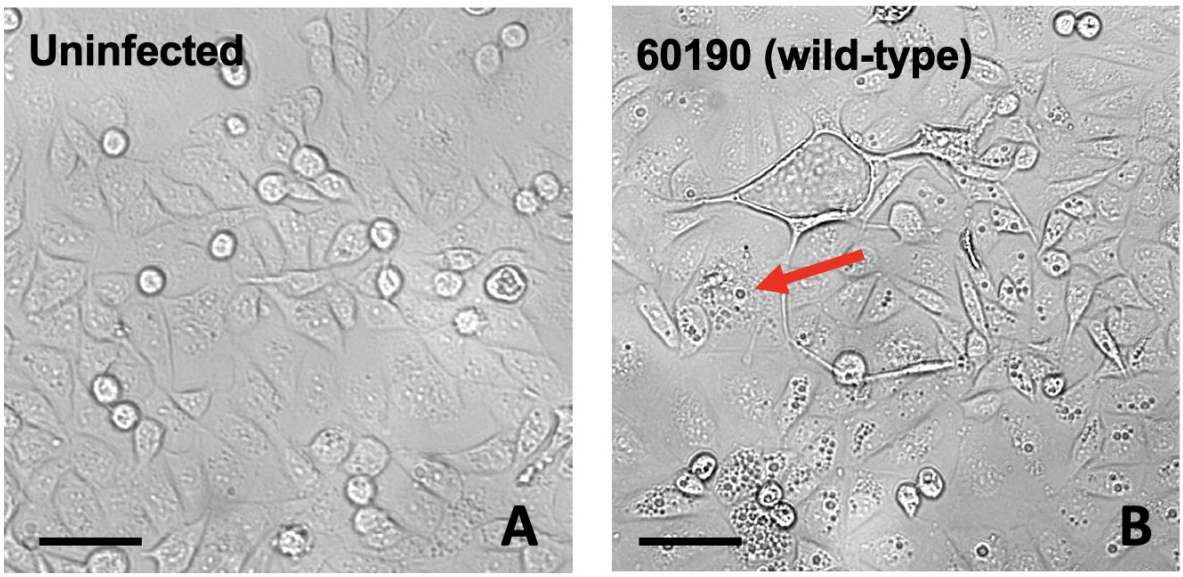

Figure 3.12. Effect of *H. pylori* co-culture on vacuolation of AGS cells. After 24 h growth of *H. pylori* wild type strain 60190 on blood agar, bacteria were resuspended, washed and resuspended in sterile RPMI with 10% FCS. AGS cells that had been grown for 24 h in 96 well plates were washed with PBS and incubated either with the culture medium, or with RPMI containing live *H. pylori* at an MOI of 50. Cells from three wells from each set were viewed using a Zeiss Axio Observer microscope with phase-contrast. Images were obtained at 40x magnification; the scale bar represents 50μm. Vacuolated cells are indicated by red arrows. Similar observations were observed in multiple fields of view from three independent experiments.

3.2.11. Quantification of co-culture induced AGS cell vacuolation

As previously described, the neutral red assay in combination with phase contrast microscopy was then used to quantify AGS cell vacuolation but was modified for infection with live *H. pylori* strain 60190. First, manual quantification was performed by counting vacuolated cells. In the uninfected control, approximately 20% of AGS cells were vacuolated, whereas ~80% of AGS cells infected with live cultures of *H. pylori* wild type strain 60190 were vacuolated (Figure 3.13A). Interestingly, although trends were similar, the actual number of vacuolated AGS cells were higher after infection with live *H. pylori* cells, in comparison to treatment with bacterial lysates. For example, *H. pylori* 60190 infected cells released neutral red dye to give an optical density of 0.4. However, untreated AGS cells released a smaller amount of neutral red dye, at an optical density of approximately 0.2 (Figure 3.13B). Although trends in vacuolation were similar after treatment with bacterial lysate and infection with live bacteria, it is clear that results from cultures with live bacteria are more variable.

3.2.12. Effect of mutation in *vacA* or *cagA* on co-culture induced AGS cell vacuolation

Previous studies determined secreted VacA from *H. pylori* lysates induced vacuolation of AGS cells, in addition to the effect of live *H. pylori* strain 60190 in a co-culture system. The following experiments combined previous experiments and thus determine the effect of VacA allelic form and CagA expression in a *H. pylori* co-culture induced AGS cell vacuolation. *H. pylori* strain 60190 ΔVacA, 60190 ΔCagA, 60190 and Tx30a were prepared and added to AGS cells, whereby the extent of AGS cell vacuolation was compared by phase contrast microscopy with uninfected AGS cells (Figure 3.14).

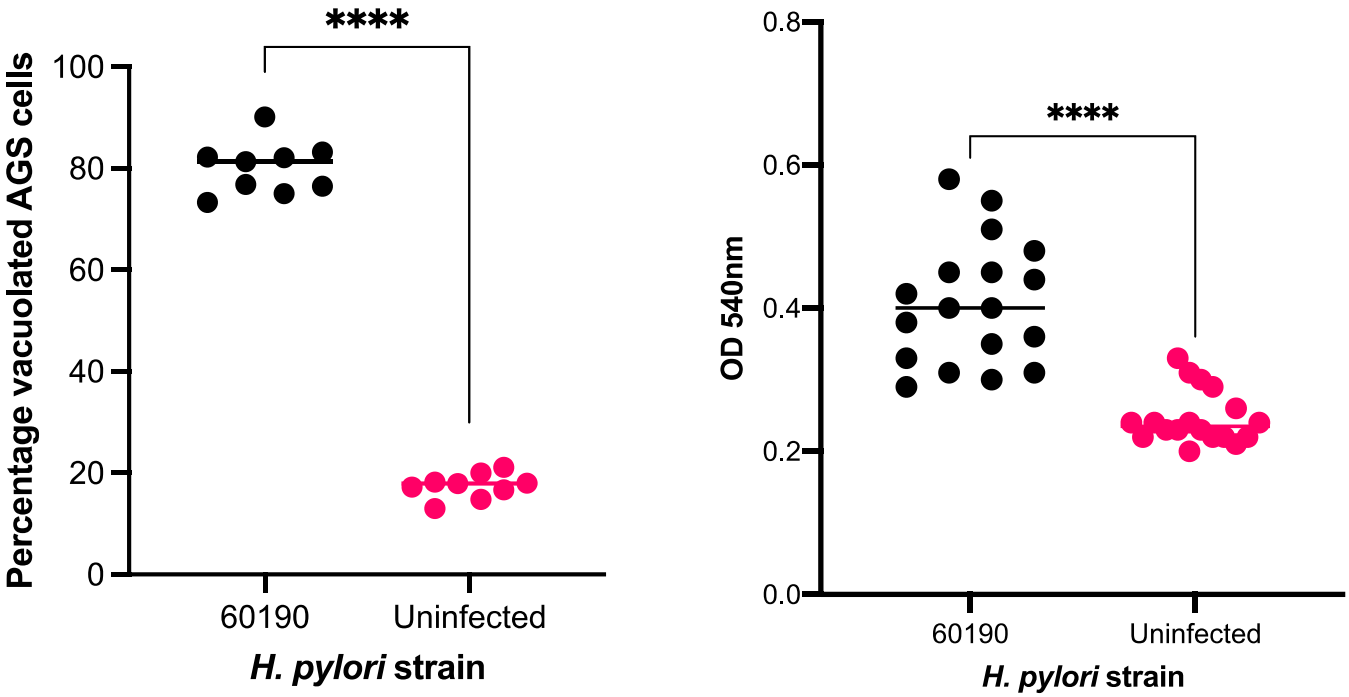

Figure 3.13A and Figure 3.13B. Quantification of AGS cell vacuolation induced by *H. pylori* co-culture. AGS cells that had been grown for 24 h in 96 well plates were washed with PBS and incubated either with the culture medium, or with RPMI containing live *H. pylori* wild type strain 60190 at an MOI of 50. Cells from three wells from each set were viewed using a Zeiss Axio Observer microscope with phase-contrast. Percentage vacuolation and quantification using the neutral red assay was performed as described for Figure 2A and Figure 2B. Similar results were obtained from three independent experiments; **** $P<0.0001$ relative to uninfected control, as determined by unpaired t-test.

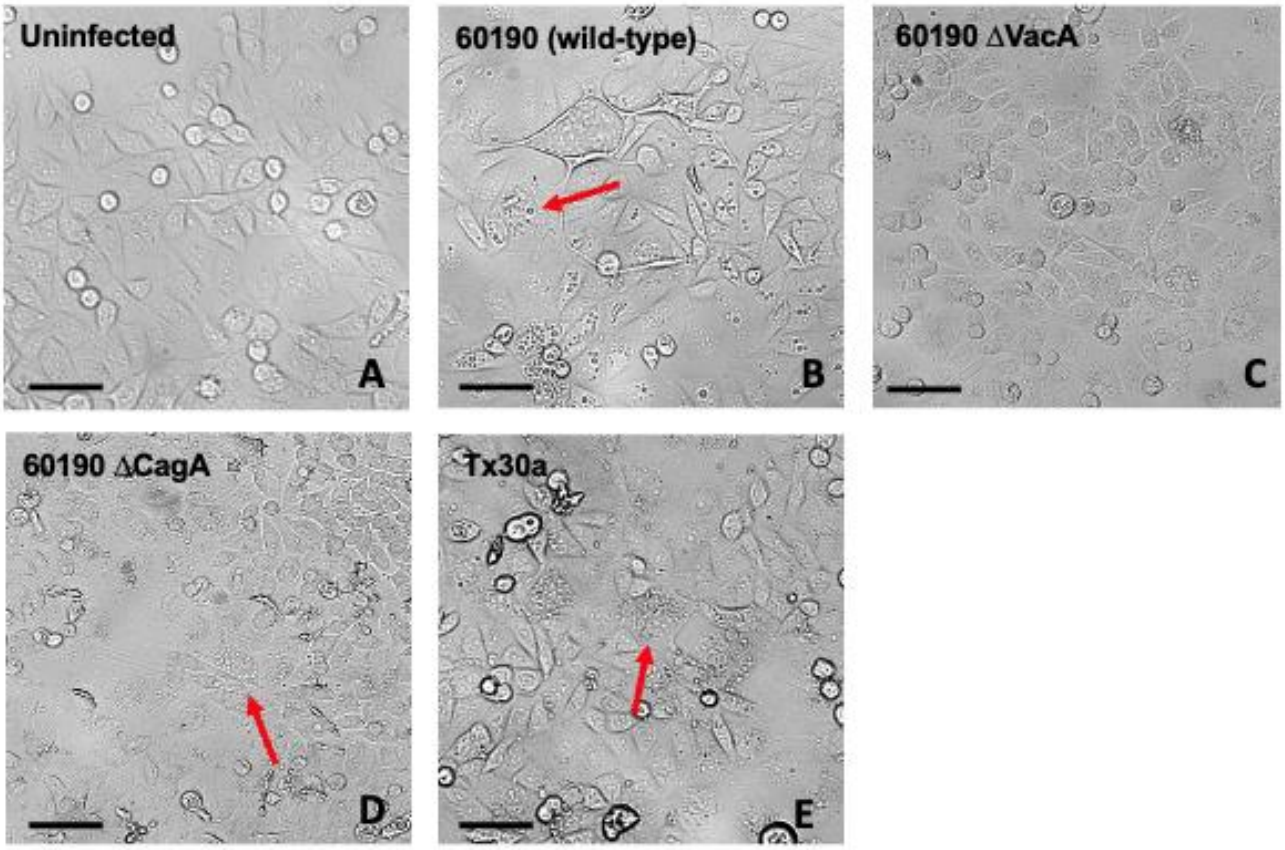

Figure 3.14. Effect of mutation in vacA or cagA on co-culture induced AGS cell vacuolation. Live *H. pylori* strains 60190, 60190 ΔVacA, 60190 ΔCagA and Tx30a were incubated with AGS cells overnight. The following morning, cells from three wells from each set were viewed using a Zeiss Axio Observer microscope with phase-contrast. Images were obtained at 40x magnification; the scale bar represents 50μm. Vacuolated cells are indicated by red arrows; similar observations were observed in multiple fields of view from three independent experiments.

Minimal vacuolation was observed in the uninfected cells (A). No vacuolation was observed in 60190 ΔVacA treated cells (C), but ~70% vacuolated cells were observed in 60190 and 60190 CagA treated cells (B&D) and smaller vacuoles were also visible in approximately 20% of AGS cells following exposure to lysates of strain Tx30a. These data demonstrate that vacuolation of AGS cells can be induced to a similar extent, both by bacterial lysates of, and live *H. pylori* strains in a co-culture system. After imaging, vacuole formation was manually quantified. In both the uninfected control and AGS cells infected with 60190 ΔVacA, approximately 15-20% of AGS cells were vacuolated (Figure 3.15A). The percentage of vacuolated AGS cells was ~80%, ~70% and ~60% following infection with 60190 ΔCagA, wild type 60190 and Tx30a respectively. Taken together, these data indicate that loss of CagA from strain 60190 might enhance the vacuolating effect of *H. pylori,* a phenomenon observed with both co-culture and bacterial lysate induced vacuolation assays. Furthermore, whilst Tx30 induced significantly lower vacuolation in both bacterial lysate and co-culture systems, results were more variable when infecting with live *H. pylori*.

Next, the neutral red uptake assay was also used to quantify vacuolation (Figure 3.15B). AGS cells infected with 60190, 60190 ΔCagA and Tx30a all released neutral red dye at an optical density of approximately 0.5. Similar absorbance readings of approximately 0.3 were obtained for 60190 ΔVacA infected cells and the uninfected control. This was an interesting result, indicating that 60190 and 60190 ΔCagA are potent inducers of vacuolation, in comparison to Tx30a. However, overall results for all strains were more varied when infecting AGS cells with live *H. pylori*, in comparison to bacterial lysate treatment.

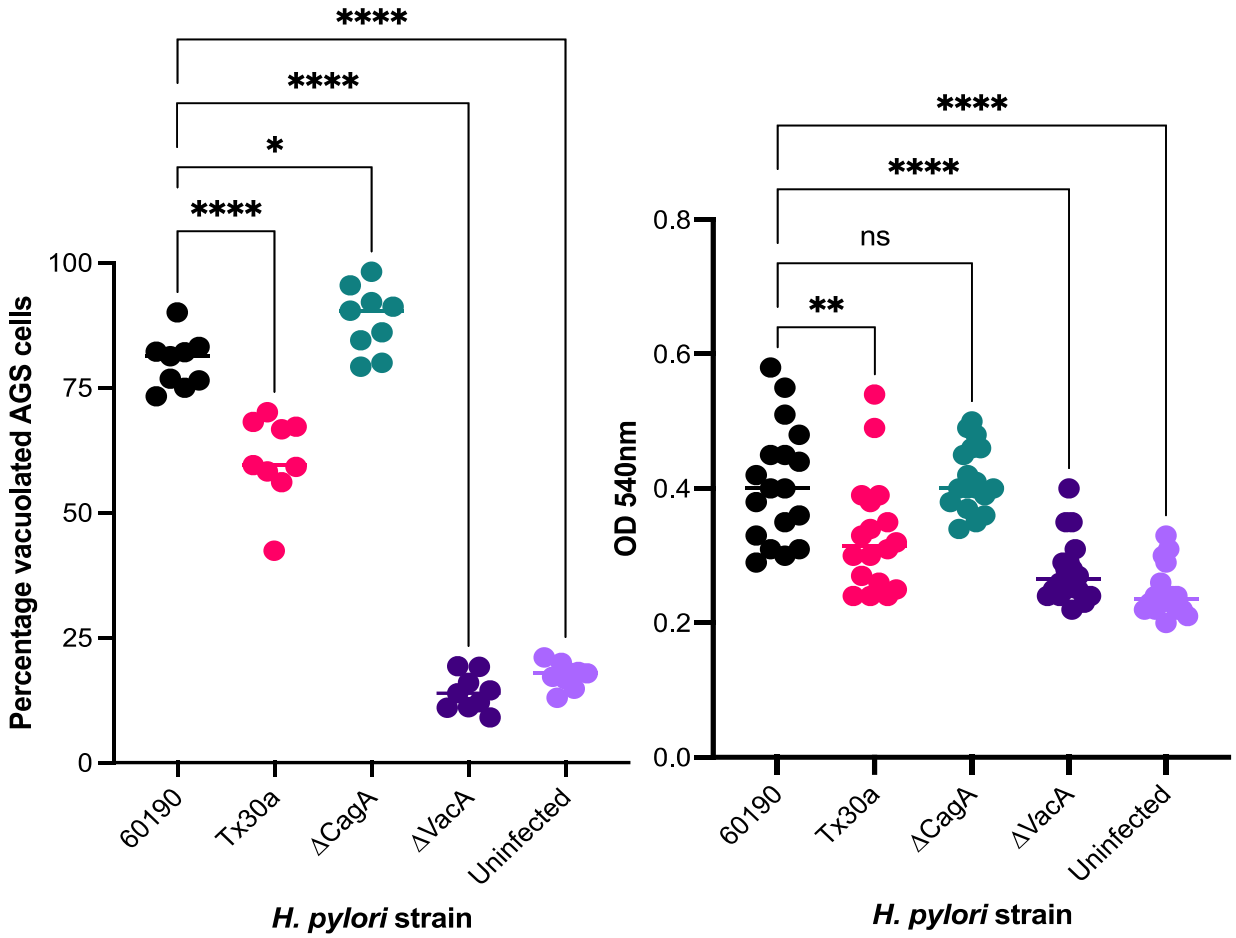

Figure 3.15A and Figure 3.15B. Quantification of AGS cell vacuolation induced by the mutant *H. pylori* strains in a co-culture system. AGS cells were incubated overnight with live *H. pylori* strains wild type 60190, 60190 ΔVacA, 60190 ΔCagA and Tx30a. The neutral red assay in combination with phase-contrast microscopy was then used to quantify vacuolation. Values were obtained and transferred to Microsoft Excel and GraphPad Prism software. Similar results were obtained from three independent experiments; **** P<0.0001, ns P>0.005 relative to strain 60190 as determined by one-way ANOVA.

3.2.13. Effect of a bacterial lysate of *H. pylori* on vacuolation of organoid monolayers

Initial experiments indicated that both bacterial lysates and live cultures of *H. pylori* induce extensive vacuolation in the AGS cell line due to the presence of secreted VacA. The following experiments therefore aimed to determine whether bacterial lysates of *H. pylori* strains also induced vacuolation of 2D organoid monolayers. Previously prepared *H. pylori* bacterial lysates adjusted to a protein concentration of 200 μg/mL were incubated for 16 h with washed, confluent organoid monolayers that had been grown for 3-5 days, or until confluent, in 96 well plates. The extent of vacuolation was compared by phase contrast microscopy with untreated organoid monolayers (Figure 3.16). Minimal vacuolation was observed in both the untreated and treated organoid monolayer. This indicated that whilst secreted compounds of *H. pylori* induce prominent vacuolation of the AGS cell line, this phenotype was not observed when repeating this experiment with organoid monolayers.

3.2.14. Quantification of *H. pylori* lysate induced organoid monolayer vacuolation

The neutral red assay in combination with phase contrast microscopy, as also outlined for AGS experiments was used to quantify vacuolation of organoid monolayers following treatment with *H. pylori* bacterial lysates. Manual quantification was first completed by visually assessing monolayers for vacuolation. As cells within a monolayer were difficult and labour intensive to count individually, a qualitative vacuolation scoring system was instead utilised, whereby 1 = 0-20%, 2 = 20-40%, 3 = 40-60%, 4 = 60-80% and 5 = 80-100% vacuolated cells per 12 fields of view.

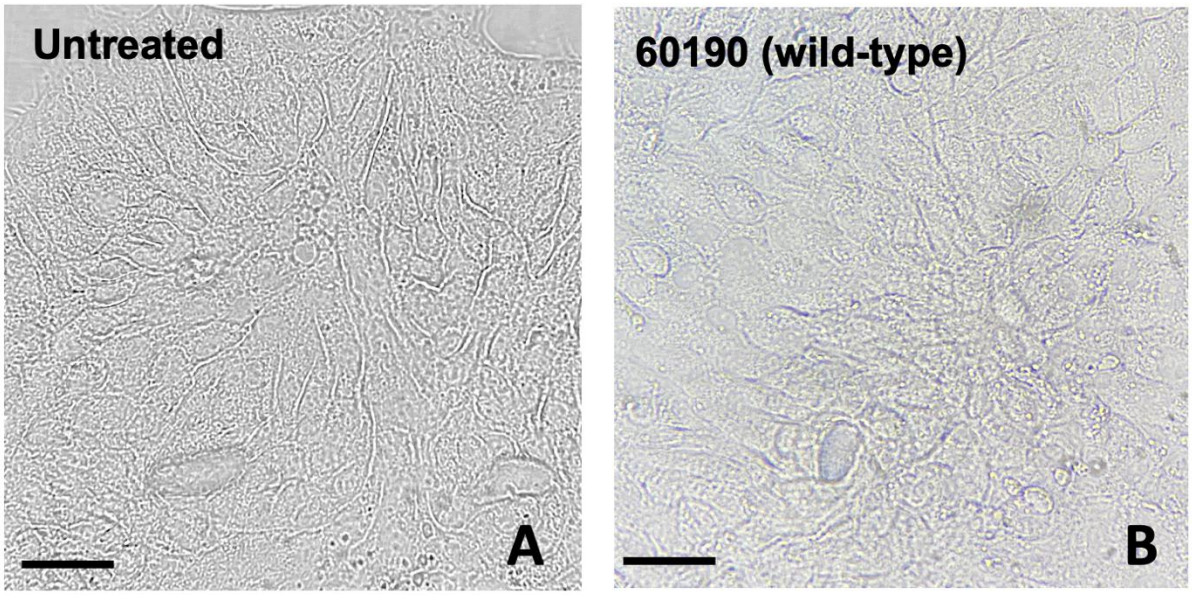

Figure 3.16. Effect of a bacterial lysate of *H. pylori* on vacuolation of confluent 2D organoid monolayers. Lysates of *H. pylori* wildtype strain 60190 were prepared and incubated with confluent 2D organoid monolayers that had been grown for 3-6 days in collagen-coated 96 well plates for 16 h. Cells from three wells from each set were viewed using a Zeiss Axio Observer microscope with bright field. Images were obtained at 40x magnification; the scale bar represents 25 μm. Vacuolated cells are indicated by red arrows. Similar observations were observed in multiple fields of view from three independent experiments.

It was observed that vacuolation was similar between the two groups with a mean vacuolation score of 1.33 and 1.44 respectively, for strain 60190-treated monolayers and the untreated control (Figure 3.17A). The neutral red uptake assay was then used to further quantify vacuolation, whereby both treated and untreated organoid monolayers released neutral red dye at an optical density of 0.3, with no statistically significant difference between treatment groups (Figure 3.17B). These data indicated that although the AGS cell line vacuolated following treatment with *H. pylori* bacterial lysates, similar phenotypes were not observed when studies were repeated on organoid monolayers. These data therefore suggest that the apical surface of 2D organoid monolayers likely do not respond to *H. pylori* VacA.

3.2.15. Effect of mutation in *vacA* or *cagA* on organoid monolayer vacuolation

Previous vacuolation studies using the AGS cell line demonstrated the significance of virulence factors VacA and CagA in both *H. pylori* bacterial lysate and co-culture induced vacuolation. The effect of these virulence factors on vacuolation of organoid monolayers were then assessed by repeating AGS cell line vacuolation studies using bacterial lysates of knock-out *H. pylori* strains, 60190 ΔVacA and 60190 ΔCag 60190 in addition to 60190 and Tx30a. The extent of organoid monolayer vacuolation was compared by bright field microscopy (Figure 3.18). During visual inspection, minimal vacuolation was observed in either of the treated and untreated and organoid monolayers, further suggesting that organoid monolayers likely do not respond to secreted compounds of *H. pylori*, such as VacA.

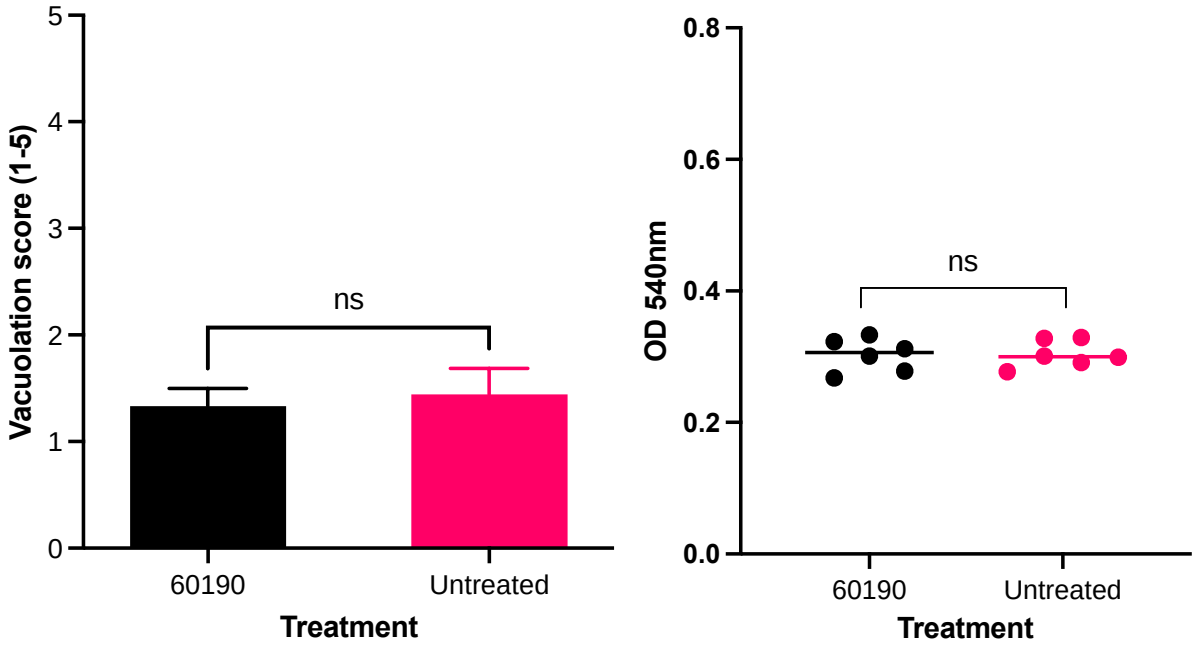

Figure 3.17A and Figure 3.17B. Quantification of organoid monolayer cell vacuolation induced by the *H. pylori* lysate. Lysate of *H. pylori* wildtype strain 60190 were prepared and incubated overnight with organoid monolayers. Nine images were then obtained for both treatment groups using a Zeiss Axio Observer with phase-contrast. For each image, vacuolation was scored whereby 1 = 0-20%, 2 = 20-40%, 3 = 40-60%, 4 = 60-80% and 5 = 80-100% vacuolated cells. *H. pylori* lysate, and culture media were removed from the monolayer. Monolayers were then washed before the neutral red assay was conducted and absorbance was then measured at 540 nm in a plate reader. Data were analysed with Microsoft Excel and GraphPad Prism software. Similar results were obtained from three independent experiments; ns = non-significant relative to untreated control, as determined by an unpaired t-test.

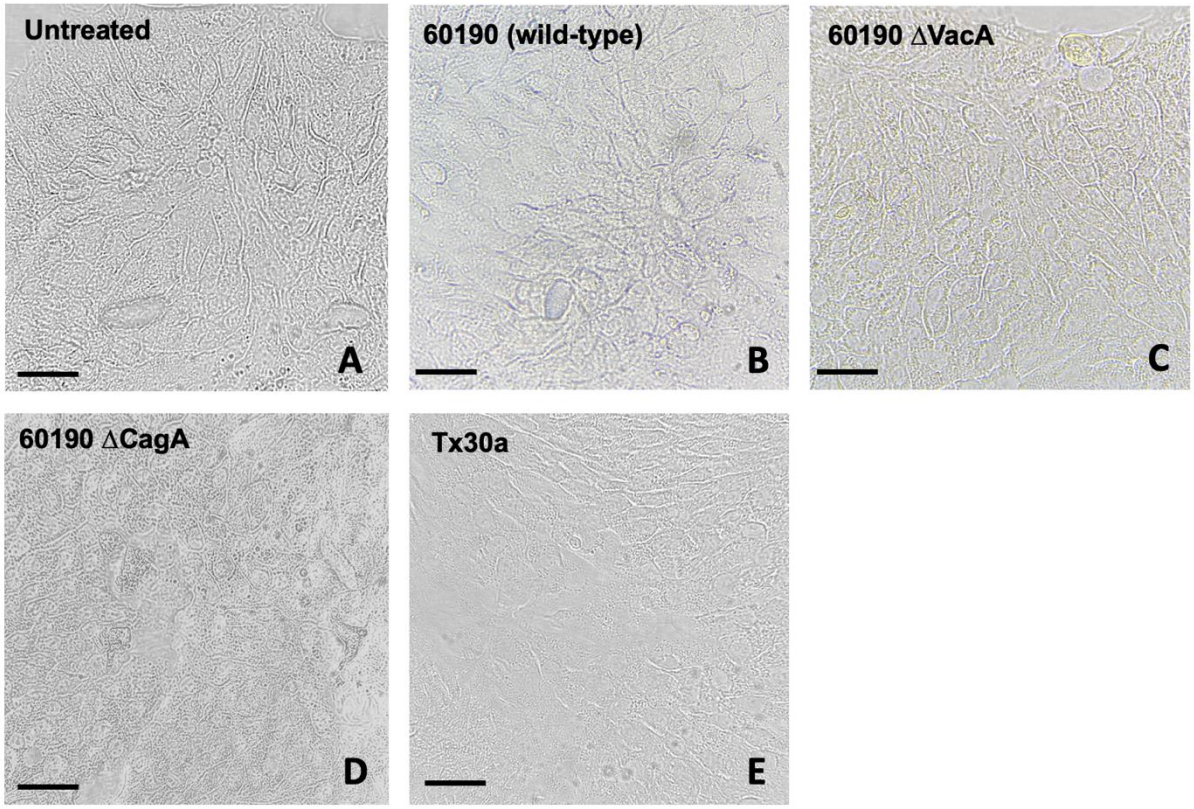

Figure 3.18. Effect of mutation in vacA or cagA on organoid monolayer vacuolation. Organoid monolayers and *H. pylori* lysates of strains 60190, 60190 ΔVacA, 60190 ΔCagA and Tx30a were incubated with one another overnight. Organoid monolayers from three wells from each set were viewed using a Zeiss Axio Observer microscope with phase-contrast. Images were obtained at 40x magnification. The scale bar represents 25μm. Similar observations were observed in multiple fields of view from three independent experiments.

Nonetheless, any changes in cellular morphology can be difficult to observe using within the organoid monolayer using light microscopy alone due to the presence of multiple, irregular-shaped cell types and the apical mucus layer.

Following imaging, vacuole formation was manually quantified with a qualitative scoring system as described for Figure 3.19A. Vacuolation scores were similar between treatment groups, with a score of 1.33, 1.44, 1.89, 1.44 and 1.44 obtained for 60190, 60190 ΔVacA, 60190 CagA, Tx30a and the non-treated control, respectively (Figure 3.19A). For all treatment groups, vacuolation scores correlated to approximately 15-20% vacuolated cells per field of view. Whilst a scoring system provided an easier approach to score vacuolation of cells within a monolayer, this method relies on visual assessment and is therefore subjective and should therefore be used with caution.

To further investigate vacuolation of organoid monolayers the neutral red uptake assay was again used to quantify vacuolation. Organoid monolayers treated with bacterial lysates of 60190, 60190 ΔVacA, 60190 ΔCagA, Tx30a all released neutral red dye at an optical density of approximately 0.3 (Figure 3.19B). Taken together, these data suggest that not only do organoid monolayers not respond to secreted compounds of *H. pylori*, but also that loss of VacA and CagA does not impact vacuolating activity of the bacterial lysate on the organoid monolayers, despite inducing prominent phenotypic changes in the AGS cell line.

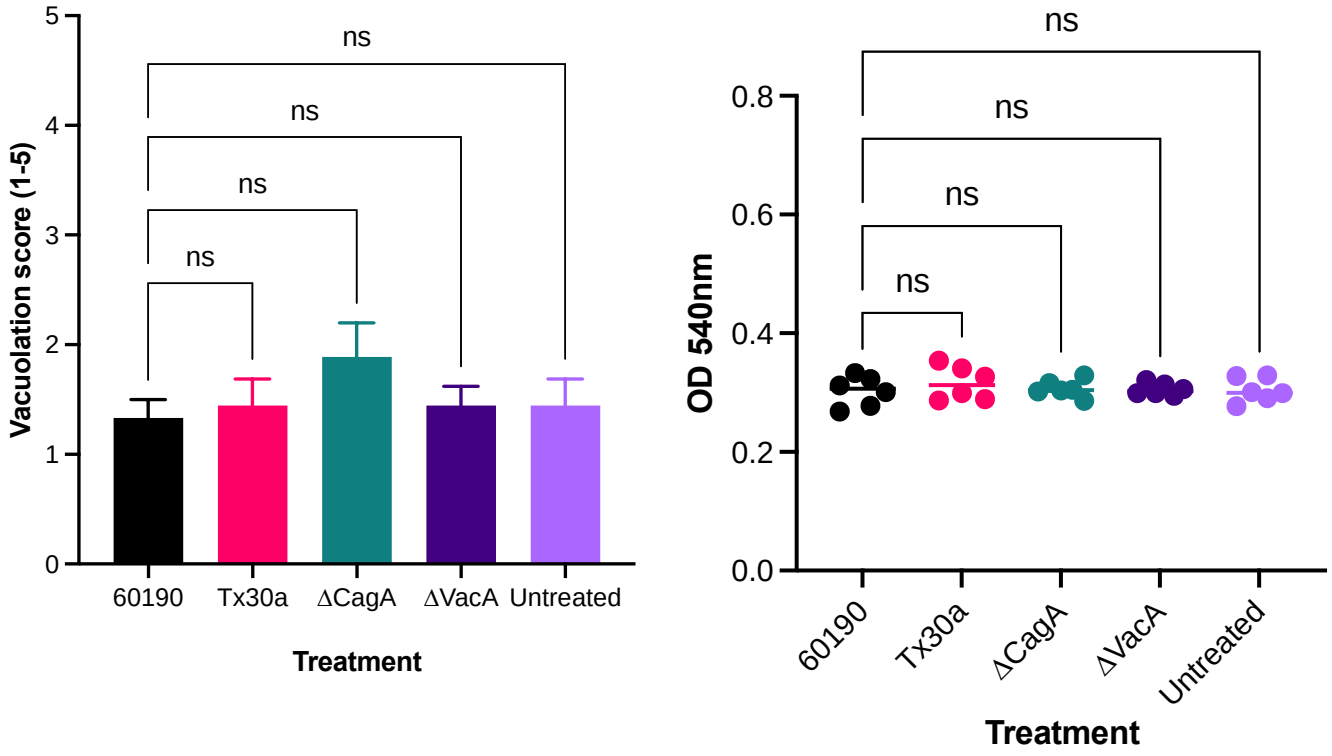

Figure 3.19A and Figure 3.19B. Quantification of organoid monolayer cell vacuolation induced by the *H. pylori* lysate. *H. pylori* lysates were incubated with confluent organoid monolayers overnight. Nine images were then obtained for both treatment groups using a Zeiss Axio Observer with phase-contrast. For each image, vacuolation was scored whereby 1 = 0-20%, 2 = 20-40%, 3 = 40-60%, 4 = 60-80% and 5 = 80-100% vacuolated cells. *H. pylori* lysate, and culture media were removed from the monolayer. Monolayers were then washed before the neutral red assay was conducted and absorbance was then measured in a plate reader. Data were analysed with Microsoft Excel and GraphPad Prism software. Similar results were obtained from three independent experiments; ns = non-significant relative to untreated control, as determined by an unpaired t-test.

3.2.16. Effect of *H. pylori* co-culture on vacuolation of organoid monolayers

Previous experiments revealed that organoid monolayers did not respond to incubation with bacterial lysates of *H. pylori* wild type strain 60190. This might have been due to the presence of MUC5AC on the apical surface of the monolayer acting as an insoluble barrier. Experiments were therefore repeated with live *H. pylori* cells, instead of the bacterial lysate. This was to investigate whether the apical mucus layer did indeed prevent lysates of *H. pylori* from interacting with the monolayer surface and whether motile live *H. pylori* cells would penetrate through the mucus layer due to their flagella. *H. pylori* strain 60190 was grown as described for infection of the AGS cell line were resuspended in 1 mL sterile 2D organoid monolayer medium containing no Primocin or antibiotics. Resuspended bacteria (100 μL) at an MOI of 50 were incubated at 37°C for 16 h with washed organoid monolayers cells that had been grown for 3-5 days, or until confluent, in 96 well plates. As before, organoids were then visually inspected for formation of vacuole formation (Figure 3.20).

Following visual inspection, no vacuolation was observed in either the infected, or uninfected control monolayers. However, a potential alternative phenotype was observed, whereby loosened intercellular junctions appeared in the infected monolayers that were not visible on the uninfected control monolayers (Figure 3.20). However, this was a difficult observation to comment on based on light microscopy images alone and this effect was not investigated further during this experiment. These data further indicate that both live *H. pylori* strain 60190 and its lysate induce vacuolation in the AGS cell line but not in organoid monolayers. Furthermore, these

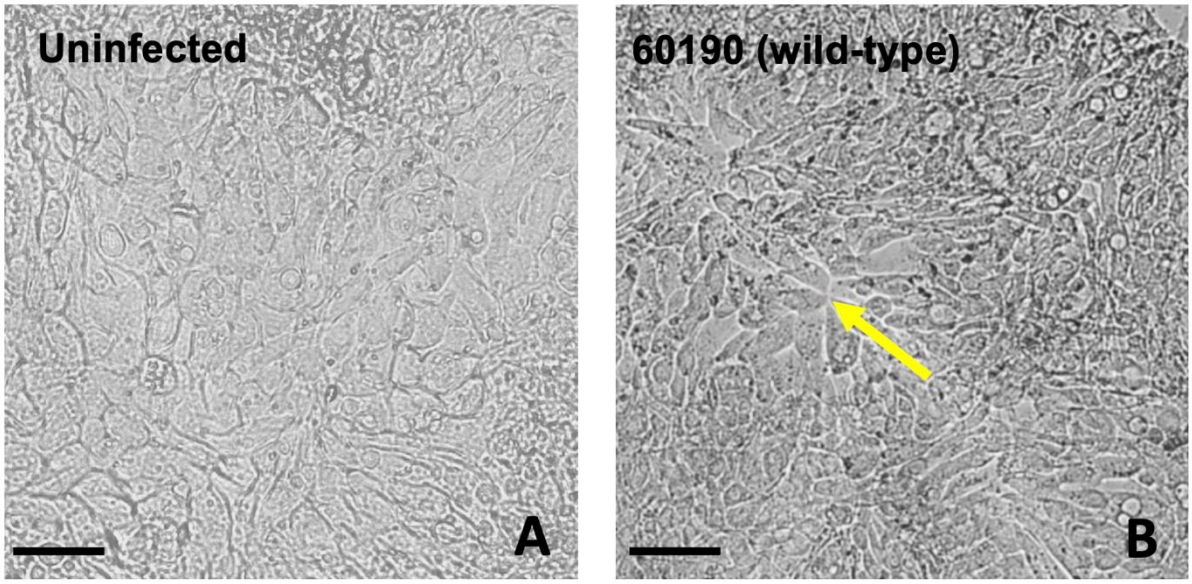

Figure 3.20. Effect of *H. pylori* co-culture on vacuolation of organoid monolayer. Live *H. pylori* strain 60190 was prepared and incubated with confluent monolayers overnight at an MOI of 50. Cells from three wells from each set were viewed using a Zeiss Axio Observer microscope with phase-contrast. Images were obtained at 40x magnification; the scale bar represents 25 μm. Possible interupted intercellular junctions are indicated by yellow arrows. Similar observations were observed in multiple fields of view from three independent experiments.

data also suggest that although infection with strain 60190 did not induce vacuolation, this strain could instead induce other phenotypic changes to host cells, specifically intercellular junctions.

3.2.17. Quantification of co-culture induced organoid monolayer vacuolation

As also described for previous experiments, phase contrast microscopy followed by the neutral red assay was used to score and quantify monolayer vacuolation. Monolayers were first scored for vacuolation, both the 60190-infected and uninfected control received a score of 2, corresponding to 20-40% cells within the monolayer vacuolated per field of view (Figure 3.21A). Next, the neutral red assay was used, as described for Figure 3.18B. Similar results were also obtained for the uninfected and 60190 infected monolayers, with an optical density of 0.3. (Figure 3.21B). This further suggested that vacuolation of organoid monolayers did not occur following exposure to live *H. pylori* wildtype strain 60910.

3.2.18. Effect of mutation in *vacA* or *cagA* on co-culture organoid monolayer vacuolation.

Previous experiments suggested that organoid monolayers do not respond to *H. pylori* VacA within bacterial lysates. Furthermore, despite organoid monolayers not vacuolating following infection with s1/m1 expressing strain 60190, studies were repeated in a co-culture system with additional live strains of *H. pylori* strains 60190, 60190 ΔVacA and 60190 ΔCag and Tx30a.

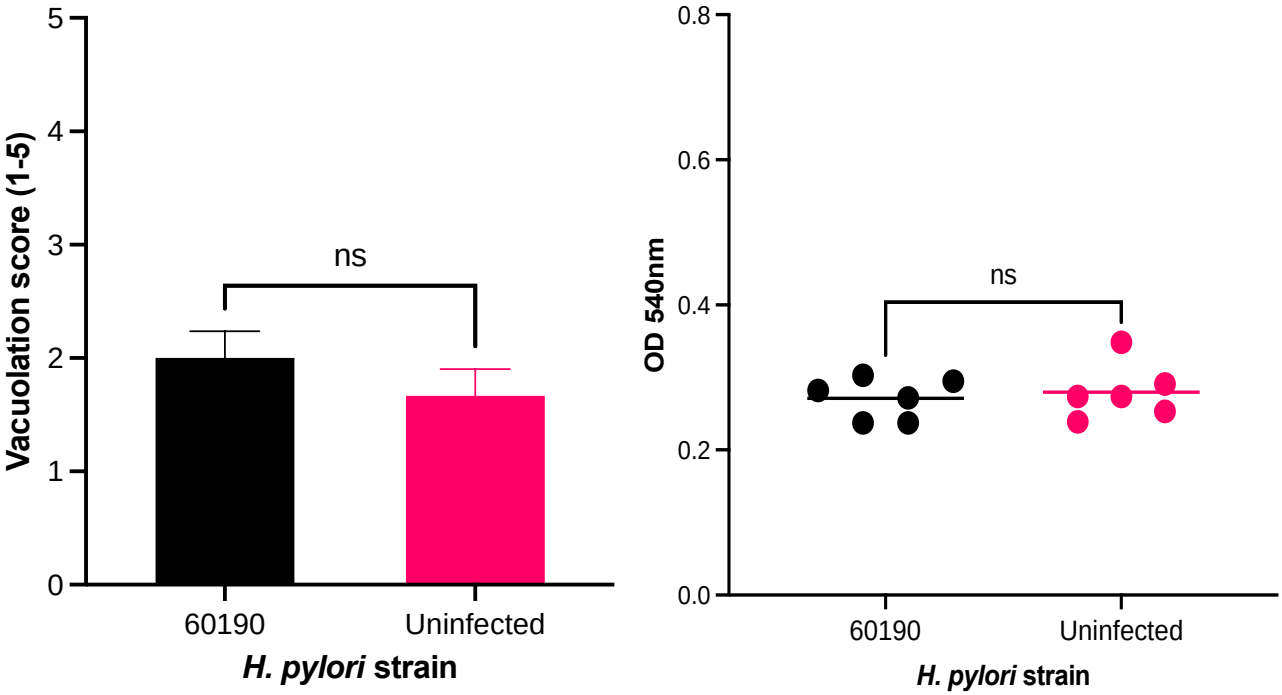

Figure 3.21A and Figure 3.21B. Quantification of organoid monolayer cell vacuolation induced by *H. pylori* co-culture. Live *H. pylori* strain 60190 was prepared and incubated with organoid monolayers overnight. Nine images were then obtained for both treatment groups using a Zeiss Axio Observer with phase-contrast. For each image, vacuolation was scored whereby 1 = 0-20%, 2 = 20-40%, 3 = 40-60%, 4 = 60-80% and 5 = 80-100% vacuolated cells. *H. pylori* lysate, and culture media were removed from the monolayer. Monolayers were then washed before the neutral red assay was conducted. Absorbance was then measured at 540 nm in a plate reader. Values were obtained and transferred to Microsoft Excel and GraphPad Prism software. Similar results were obtained from three independent experiments; ns = non-significant relative to untreated control, as determined by unpaired t-test.

Following infection for 16 h, infected organoid monolayers were visually assessed using bright field microscopy (Figure 3.22). Minimal vacuolation was again observed following infection with any of the *H. pylori* strains, with monolayers appearing visually identical to the uninfected control. These data therefore further indicate that cells within organoid monolayers do not vacuolate following either treatment or infection with lysates of, or live *H. pylori* cells. Furthermore, the absence of CagA and VacA allelic form does not influence vacuolation of organoid monolayers.

Interestingly, following infection with wild-type strain 60190, organoid monolayers appeared to exhibit slight alterations to intercellular junctions, which appeared wider than usual (indicated by yellow arrow). Conversely, cells within monolayers infected with 60190 ΔVacA and Tx30a appeared slightly elongated (indicated by blue box). Following initial observations using light microscopy, the extent of vacuolation of organoid monolayers following infection with live *H. pylori* cells was then quantified. A qualitative vacuolation score was given, whereby monolayers infected with strains 60190, 60190 ΔVacA, 60190 CagA, Tx30a scored 2, 2.1, 2, and 1.78, respectively, with the uninfected control scoring 1.7 (Figure 3.23A). For all infection groups, the vacuolation scores correlated to approximately 20-40% vacuolated cells per field of view and no differences in vacuolation were observed between the groups using this scoring method. The neutral red uptake assay was then used to further quantify vacuolation. Organoid monolayers infected with strains 60190, 60190 ΔVacA, 60190 ΔCagA, Tx30 all released neutral red dye at an optical density of approximately 0.3, with no significant differences between groups (Figure 3.23B).

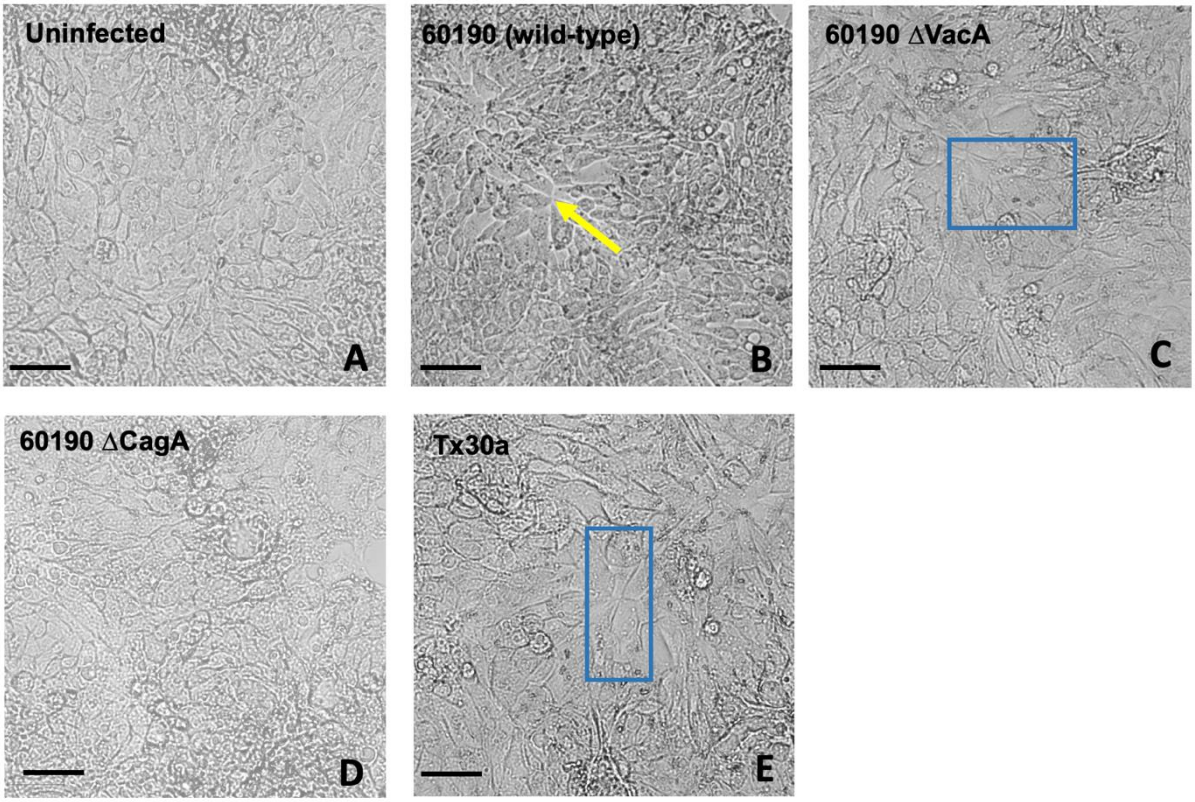

Figure 3.22. Effect of mutation in vacA or cagA on organoid monolayer vacuolation, induced by *H. pylori* co-culture. Organoid monolayers were incubated overnight with live *H. pylori* strains 60190, 60190 ΔVacA, 60190 ΔCagA and Tx30a. Cells from three wells from each infection group were viewed using a Zeiss Axio Observer microscope with phase-contrast. Images were obtained at 40x magnification; the scale bar represents 25 μm. Yellow arrow indicates intercellular gaps, blue boxes indicate slight cellular elongation. Similar observations were observed in multiple fields of view from three independent experiments.

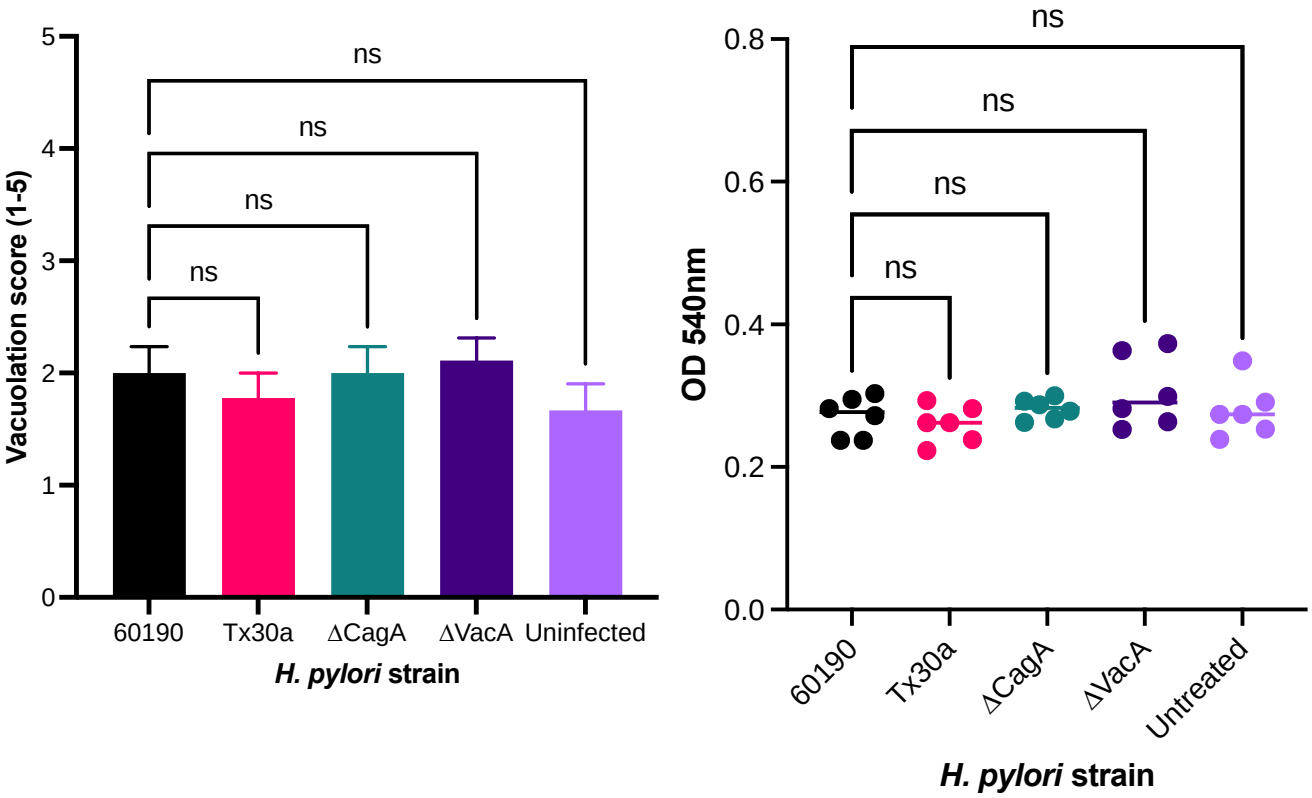

Figure 3.23A and Figure 3.23B. Quantification of organoid monolayer cell vacuolation induced the mutant *H. pylori* strains in a co-culture system.
Live *H. pylori* strains were incubated with organoid monolayers overnight. Nine images were then obtained for both treatment groups using a Zeiss Axio Observer with phase-contrast. For each image, vacuolation was scored whereby 1 = 0-20%, 2 = 20-40%, 3 = 40-60%, 4 = 60-80% and 5 = 80-100% vacuolated cells. *H. pylori* cells, and culture media were removed from the monolayer. Monolayers were washed and the neutral red assay was conducted. Absorbance was then measured at 540 nm in a plate reader. Values were obtained and transferred to Microsoft Excel and GraphPad Prism software. Similar results were obtained from three independent experiments; ns = non-significant relative to untreated control, as determined by unpaired t-test.

Although no differences were observed, results for all strains were more varied when infecting monolayers with live *H. pylori*, in comparison to bacterial lysate treatment. This effect was also observed following co-culture experiments with AGS cells and live *H. pylori*, suggesting that experiments using live bacterial cells might be more reliable in comparison to *H. pylori* lysates, as virulence factors have not been lost which could influence biological variation and therefore experimental outcome.

To conclude, when taken together, these data suggest that treatment of organoid monolayers with bacterial lysates is not a suitable method to investigate *H. pylori*-induced vacuolation. The apical surface of organoid monolayers is decorated with mucin which likely acts as an insoluble barrier. Additionally, lysates of *H. pylori* lack necessary virulence factors to overcome this barrier, such as flagella and are therefore unlikely to penetrate and reach the organoid monolayer. However, when studies were repeated using live *H. pylori* strains, vacuolation was still not observed. This was a surprising result and suggests that the apical surface of these organoid monolayers do not vacuolate following exposure to VacA even in the presence of additional virulence factors expressed by live *H. pylori* cells such as CagA.

3.3. Discussion

3.3.1. Generation of organoid monolayers from 3D organoids

Initial results presented in this chapter demonstrated that three individual 3D gastric patient-derived organoid lines could be successfully dissociated into a single cell suspension and re-seeded onto a transwell insert, following methods described by Boccellato *et al*., 2019. At the same initial seeding density of $4.5x10^5$, all three organoid

lines required different incubation times to reach 100% confluency, which appeared as a complete sheet of cells across the transwell surface. All organoid lines used in this experiment were incubated in the same environmental conditions and growth medium. These results therefore suggest that each patient-derived organoid line likely shows variation in growth characteristics because of biological variation. Inter-patient heterogeneity is a concern when using organoid models and is likely due to genetic or epigenetic differences between the patient donors (Mohammadi *et al*., 2021). Although the three patients were male and of a similar age, no information was provided about their medication at the time of donation, or lifestyle factors such as diet and weight which can influence signalling factors and host-cellular responses.

3.3.2. Polarisation of organoid monolayers

Due to difficulties in growing and maintaining multiple organoid lines at a given time, permeability could only be assessed and quantified for the S292.072 organoid line.

Polarisation is an important feature of eukaryotic cells and involves the formation of an asymmetric cell surface, which divides the plasma membrane into an apical and basolateral surface. Polarisation involves reorganisation of the cell cytoskeleton and ensures that cells within the monolayer form a barrier, preventing leakage and promoting correct ion transportation (van Beest *et al*., 2006). Caco-2 cells are widely used to model the intestinal mucosa, as they express E-cadherin and form a polarised monolayer (Schreider *et al*., 2002). When seeded with an appropriate initial seeding density, the S292.072 was able to form a comparable polarised monolayer to Caco-2 cells and maintained its barrier function over 21 days. This result agreed with data published by Boccellato *et al*., (2019), who were the first to demonstrate the ability of

gastric organoid monolayers to self-maintain over extended periods of time. Results of this experiment further emphasised that the AGS cell line is not suitable or physiologically relevant for studying the gastric mucosa in vitro. AGS cells do not express tight-junction protein E-cadherin and did not form a polarised monolayer during the assay (Schreider *et al*., 2002).

Additionally, the FITC-dextran permeability assay is a macromolecular tracer assay, which relies on incubating monolayers with a water-soluble, fluorescently labelled polysaccharide for three hours. Although the assay is cost-effective and relatively easy to conduct, questions remain over whether the FITC-dextran itself interferes with cell junctions or damages cells, resulting in a loss of barrier integrity. Moreover, a significant drawback of this assay is that cells cannot be used for further experiments afterwards (Bednarek, 2022). In future work involving organoid monolayers, a non-invasive transepithelial electrical resistance (TEER) assay could instead be conducted, whereby an electrode is placed in both the apical and basal transwell compartment to measure continuous electrical resistance across the monolayer (Srinivasan *et al*., 2015). This method would ensure that monolayers are not damaged, disrupted and discarded during the assay.

3.3.3. Phenotyping of organoid monolayers

Immunofluorescence imaging successfully revealed that the S292.072 organoid monolayer expressed several markers associated with the healthy gastric mucosa. Whilst several protocols currently exist for generating patient-derived gastric organoids from biopsy tissue or single cell digests, the majority of these studies do not employ

methods to fully characterise and visually phenotype the organoids. Additionally, although 3D organoids are regularly characterised, very little literature exists on the characterisation of organoid monolayers. The staining panel detailed in this results chapter was selected based on a study by Bartfeld *et al*., 2014, which was one of the first studies reporting the use of gastric organoids to study *H. pylori* infection in vitro. Bartfeld *et al*., (2014) used histological staining combined with qPCR to assess mRNA expression of healthy gastric markers including E-cadherin, MUC5AC, PGC, TROY, SST and ATP4B. Expression of these markers were also observed in our organoid line, when using immunofluorescence imaging. Negative primary antibody only and non-antibody controls were included in this experiment, ensuring no non-specific staining was observed.

Interestingly, as expected for corpus-derived organoids, our organoid monolayer also expressed the parietal cell marker ATP4B, despite Bartfeld *et al*. (2014) reporting that their corpus derived gastric organoids did not express this. Whilst this was an interesting observation as our organoid line appeared to express markers of a healthy gastric mucosa, staining for intestinal markers which should not be present in our organoid monolayer was not conducted and could strengthen future data by acting as an additional negative control. This was an additional control conducted by Bartfeld *et al*., who also stained gastric organoids for intestinal markers MUC2, CDX and CDX2 which were not expressed and thus strengthened the likelihood that positive staining was due to true expression and not nonspecific staining. In future work, it could be worthwhile to also stain other tissue types which are known expressors of the markers, in order to further reduce the likelihood of false-positive staining. A weakness of this

experiment was that staining for each marker was conducted using different monolayers on different days. Although monolayers were consistently derived from the S292.072 organoid line, monolayers were selected for staining only when they were deemed 100% confluent by visual assessment. Due to limited organoid numbers, the FITC-dextran assay was not conducted, and it is therefore possible that cells within the monolayers were not fully polarised which could affect marker expression.

3.3.4. Effect of *H. pylori* VacA on the AGS cell line

Once organoid monolayers were successfully developed and phenotyped, they could be used for further experiments. In this chapter, we investigated whether the apical surface of organoid monolayers vacuolated following exposure to *H. pylori* VacA. Organoids are limited in numbers and expansion or development of monolayers within the laboratory is a slow and laborious process. As such, the effect of secreted VacA was first tested using lysates of *H. pylori* with the AGS cell line. AGS cells treated with both lysates and infected with live cells of pathogenic wild type *H. pylori* s1/m1 strain 60190 exhibited prominent vacuolation when compared to cells treated or infected with 60190 ∆VacA or *H. pylori*-free cell culture medium. Interestingly, strain 60190 ∆CagA induced vacuolation, but at a slightly higher level of compared to 60190. Although this is likely a coincidence, Argent at al., 2008 also observed that *H. pylori cagA* knockout strains induced increased vacuolation when compared with the wild type, suggesting antagonistic activity between VacA and CagA. As also expected due to the presence of the 'less pathogenic' s2/m2 form of VacA, strain Tx30a induced significantly less vacuolation in our AGS cell line compared to the wild type (Atherton *et al*., 1995b; Caston *et al*., 2020). Overall, this experiment was vital for confirming the VacA status

of each *H. pylori* strain in the laboratory before further experimentation could be conducted on precious organoid monolayers. Whilst this experiment confirmed VacA status of the strains and mutants in preparation for future work, it is worth noting that vacuolation was only observed in the AGS cell line and did not investigate other cell types. As such, in future work involving the effects of various *H. pylori* VacA allelic forms on additional gastric epithelial cell lines such as MKN7 could also be conducted. Finally, this experiment was only conducted using one *H. pylori* lysate concentration or multiplicity of infection. Initial data indicated that 200 μg/mL *H. pylori* lysate induced high levels of vacuolation for the 60190 and 60190 ΔCagA strains, whilst increasing lysate concentration of Tx30a had no effect on vacuolation. During initial preparation of the *H. pylori* lysates, total protein concentration was measured, rather than VacA concentration. As such, it might be possible that Tx30a secretes lower amounts of VacA, and a higher concentration of lysate would have been more appropriate to artificially stimulate vacuolation. Additionally, only one MOI of 50 was selected based on previous *H. pylori* infection studies, where a range of 20-200 is commonly used. Similarly, if this experiment were to be repeated a range of MOIs should be prepared to investigate whether vacuolation is proportional to number of live *H. pylori* cells.

Although AGS cells did indeed vacuolate following exposure to *H. pylori* lysates and live cells, it is worth noting that there are many translational limitations of using AGS cells to model *H. pylori* infection of the gastric mucosa in vitro, which might have influenced the cellular response to VacA. For example, AGS cells are derived from the stomach of a patient with GAC and are therefore not genetically ‘healthy’. AGS cells typically have chromosomal instability and mutations in the *TP53* gene, which affects

cell cycle, apoptosis and downstream signalling pathway (Ashktorab et al., 2003). As such, it is possible that these genetic alterations promote survival of the AGS cells under stress, such as infection, resulting in accumulation of vacuoles as a stress or survival response, rather than due to VacA-induced vacuolation. Furthermore, many cancer cells such as AGS cells have disrupted endocytic and vesicular trafficking pathways, in addition to enhanced sensitivity to toxins, potentially resulting in them becoming more susceptible to vacuolation (Palframan *et al.,* 2012, Lakoduk *et al*., 2021). Therefore, it is possible that the vacuolation observed in AGS cells in this study, as well as in previous studies, is primarily a consequence of the genetic characteristics of these cells rather than a direct effect of *H. pylori* VacA.

3.3.5. Effect of *H. pylori* VacA on organoid monolayers

Organoid monolayers did not vacuolate following treatment with lysates of our *H. pylori* strains. However, this result was not surprising as vacuolation is rarely reported in vivo. For example, although Winter *et al*. (2014) observed extensive vacuolation of AGS and RK-13 cells in vitro following treatment with bacterial extracts of *H. pylori* strain SS1, when mice were treated with the same strains in vivo, no vacuolation was observed in subsequent histological sections. Furthermore, routine biopsy and H&E staining is routinely used for grading of disease severity in patients with *H. pylori*-associated CG, GIM and GAC, considering glandular atrophy, infiltration of immune cells and *de novo* expression of goblet cells (Dixon *et al*., 1994). However, vacuolation of the gastric mucosa is rarely documented by clinicians or pathologists, or within pathology reports, suggesting that this phenomenon may not actually occur in human stomach mucosa under physiological conditions. This raises the possibility that vacuolation induced by

H. pylori VacA in traditional cell culture models may be an artifact of the artificial in vitro environment rather than a genuine biological response. Given that organoid monolayers more closely mimic the in vivo gastric mucosa, the absence of vacuolation observed in this study likely provides a more physiologically relevant representation of VacA-induced effects compared to previous studies using conventional cell lines.

Another factor that may have influenced the vacuolation observed in AGS cells, but not in organoid monolayers, is the pH of the surrounding cell culture media. Several studies have shown that VacA activity is enhanced by acidic or basic environments, as this promotes membrane binding, pore formation, and intracellular trafficking (Atherton *et al.,* 2001). As shown in this results chapter, the organoid monolayers contained cells which express the proton pump, ATP4B, which likely regulates local pH and lowers the pH of the monolayer apical surface. In contrast, the AGS cells do not express a functional proton pump and therefore lack the ability to regulate local pH as effectively as organoid monolayers or native gastric cells. As such, it is possible that the lack of proton pump makes the AGS cells more susceptible to VacA-induced vacuolation in culture conditions. This further suggests that in addition to defects within AGS cells, any vacuolation observed in AGS cells could be artifact of the medium, such as pH, rather than as a result of VacA activity.

Finally, it is plausible that absence of vacuolation observed in organoid monolayers is a result of cells within the monolayer not expressing receptors for VacA. Interestingly, as of 2024, only one study has used organoid monolayers to study VacA, whereby Caston *et al.,* (2020) reported that apical surface of monolayers did not vacuolate

following treatment with purified VacA. In addition to vacuolation, they also reported an absence of VacA receptors on the apical surface, yet an abundance on the basolateral surface. Although this study did not directly measure vacuolation, it provided evidence to suggest that the apical surface of organoid monolayers may lack the ability to respond to stimulation by VacA, due to the absence of available receptors. Taken together, there are several explanations for the lack of vacuolation observed in this study. However, it is likely that vacuolation is not a physiological in vivo phenotype and could instead be result of the cell genetic characteristics or culture environment, such as media pH, rather than a direct result of *H. pylori* VacA.

3.4. Summary

In conclusion, this chapter demonstrated that despite inter-patient variability, 3D patient-derived gastric organoids were successfully grown as a 2D monolayer following a previously established protocol described by Boccellato *et al*. 2019. Organoid monolayers were successfully phenotyped by staining for known gastric cell types and mucins using immunofluorescence imaging and assessed for polarisation using a tracer assay. Despite the gastric AGS cell line vacuolating following exposure to different allelic forms of *H. pylori* VacA, this phenotype was not observed in organoid monolayers. Although VacA is commonly associated with vacuolation of cell lines in vitro, results presented in this chapter raise questions over the relevancy of vacuolation in vitro during the early stages of carcinogenesis and whether vacuolation is in fact an artifact of in vitro cell culture.

Chapter 4: Multiplex imaging techniques to reveal the spatial distribution of *Helicobacter pylori* and the gastric microbiota during carcinogenesis

4.1. Introduction

Previous results described in Chapter 3 demonstrated that patient-derived gastric organoids are a useful tool for modelling early *H. pylori* infection in vitro and investigating the role of virulence factor VacA in the early stages of gastric carcinogenesis. However, in addition to the effect of virulence factors, it is currently understood that *H. pylori*-induced carcinogenesis is a multifactorial process which also involves non-*H. pylori* gastric microbiota, 'Eubacteria'. As such, the following work will focus on the interaction between *H. pylori* and the gastric microbiota during Correa's cascade of carcinogenesis, using archived ex vivo patient gastric histological sections and multiplex spatial imaging techniques.

The global prevalence of *H. pylori* infection is 50-70%, yet it is defined by the WHO as a group 1 carcinogen and is associated with approximately 70% of global GAC cases (Correa and Houghton, 2007). Development of GAC is a stepwise process following initial infection with *H. pylori*, resulting in histopathological changes to the gastric mucosa outlined in Correa's cascade of carcinogenesis. *H. pylori* first triggers chronic gastritis (CG), which can lead to gastric intestinal metaplasia (GIM), dysplasia and finally GAC (Correa, 2004). Several in vitro studies have indicated that *H. pylori* virulence factors, such as VacA, CagA and HtrA play a role in carcinogenesis and are associated with severe disease outcomes. However, studies have also shown that *H. pylori* knock-out strains without these virulence factors are still capable of causing GAC globally, suggesting involvement of another mechanism independent of virulence factors during carcinogenesis (Safaralizadeh *et al*., 2017; Saruuljavkhlan *et al*., 2023).

For many years, it was hypothesised that the stomach was a sterile environment, uninhabited by microbiota due to its hostile environmental condition. In the last twenty years, multiple studies have profiled the human gastric microbiota in health and disease, using a variety of techniques including 16S rRNA and metagenomic sequencing (Eun *et al*., 2014). It is now recognised that the stomach supports a diverse bacterial community with hundreds of species, which are impacted by disease state and *H. pylori* presence (Coker *et al*., 2018; Zhang *et al*., 2023).

During Correa's cascade of carcinogenesis, aside from histopathological alterations, a shift in microbiota community structure of the gastric microbiota has been observed following *H. pylori* infection through to the development of CG, GIM and GAC. The current hypothesis is that following initial infection with *H. pylori*, it remains the dominant bacterial species in CG with very few other microorganisms present; however, as carcinogenesis progresses, other bacterial species displace *H. pylori*. Whilst several sequencing studies have observed this phenomenon, there remains much debate behind the reason for this shift in microbial diversity.

Although sequencing studies have proved useful in providing an indication of relative abundance and showing that the gastric microbiota are more diverse than first thought, there are still many discrepancies between studies. These discrepancies are usually because of sample contamination, resulting in false-positive results and therefore overestimation of genera within the microbiome of interest (Salter *et al*., 2014). Furthermore, sequencing studies do not provide spatial resolution or contextual information regarding bacterial localisation or specific interactions between bacteria

and the host. In recent years, spatial biology has gained popularity and is a powerful tool in combination with traditional methods, for determining whether location and arrangement of biomarkers, such as bacteria contribute to pathogenesis and treatment outcomes (Kulasinghe *et al*., 2023). Finally, several questions remain regarding the relationship between *H. pylori* and the gastric microbiota and whether the gastric microbiota play a causative or correlative role in the development of GAC. Whilst sequencing studies provide information regarding relative bacterial abundance and genera present during these stages, the interaction between *H. pylori* and the microbiota during the early stages of GAC, to our knowledge, has not been studied using imaging techniques.

As such, the aims of the work presented in this chapter were to identify the presence and determine the spatial distribution of *H. pylori*, gastric microbiota and gastric mucins during the early, middle and late stages of GAC. High resolution RNAscope in situ hybridisation in combination with IHC was used to fluorescently label *H. pylori*, all non-*H. pylori* bacteria 'Eubacteria', healthy-associated and GIM-associated mucins MUC5AC and MUC2 respectively, in addition to E-cadherin within archived patient biopsy tissue sections. Whole slide scans were obtained for all patients and were qualitatively and quantitatively analysed for coverage of each marker of interest. The distribution and localisation of both *H. pylori* and Eubacteria were then visually assessed and analysed. In summary, this results chapter aimed to investigate the abundance and spatial relationship between *H. pylori* and the gastric microbiota during CG, GIM and GAC and to determine whether Eubacteria play a pivotal role in the early stages of *H. pylori*-associated carcinogenesis.

4.2. Results

4.2.1. Automated 3- and 5-plex RNAscope IHC staining panels to fluorescently label CG and GIM tissue

Initial studies were designed to visualise the presence, spatial distribution and localisation of *H. pylori*, Eubacteria and mucins during chronic gastritis (CG) and gastric intestinal metaplasia (GIM). RNAscope ISH probes were used to fluorescently detect *H. pylori* and Eubacterial 16S ribosomal rRNA, whereas key gastric markers, E-cadherin, MUC5AC and MUC2 were labelled using IHC; ISH and IHC staining protocols were kindly optimised by Ana Teodósio at Birmingham Tissue Analytics (BTA). Staining was conducted on archived 4 μm thickness patient formalin-fixed paraffin-embedded gastric corpus punch biopsy tissue sections which were retrieved from the Human Biomaterials Research Centre (HBRC). Clinical pathology reports confirmed that the patients were *H. pylori*-positive CG (n=9) or GIM (n=10) and *H. pylori*-negative CG (n=6) or GIM (n=7).

In the first instance, RNAscope probes in combination with E-cadherin only were tested on archived *H. pylori*-positive CG and GIM tissue sections in a '3-plex' assay, to ensure specifity of the probes and antibody. As the Eubacteria is specific to the generic 16S rRNA sequence of all bacteria, *H. pylori* bind both the highly specific *H. pylori* and generic Eubacteria probe (Figure 4.1). Once 3-plex staining was successfully conducted, a '5-plex' staining panel was devised, including the RNAscope probes, directly followed by sequential addition of antibodies against E-cadherin, MUC5AC and MUC2. For the automated 5-plex assay all protocol steps were conducted in an

automated research stainer. Whole slide scans were then acquired for each tissue section at 40x magnification using a Vectra Polaris whole slide scanner (Figure 4.2). All CG and GIM *H. pylori*-positive sections stained positively for *H. pylori*, Eubacteria, MUC5AC and E-cadherin, whereas as expected, MUC2 staining was only observed in GIM sections. As also expected, *H. pylori* was not observed in *H. pylori* negative sections. MUC5AC staining was generally localised to the glands or tissue surfaces, whereas GIM MUC2 staining was not as evenly distributed across the sample and localised to the glandular regions which are likely rich in goblet cells. In *H. pylori* positive sections, *H. pylori* staining appeared most prominent in the glands, whereas Eubacterial staining was more distributed across the tissue sections and often observed within the lamina propria. Additionally, initial qualitative observations revealed a possible correlation between *H. pylori* and Eubacteria presence. This experiment demonstrated that automated staining is a reliable and useful method for fluorescently labelling bacteria and mucins in tissue sections.

4.2.2. A manual 3-plex RNAscope IHC panel to identify *H. pylori,* Eubacteria and E-cadherin in GAC and NAT tissue

Previous results showed that CG and GIM punch biopsy sections could be successfully stained for bacteria and mucins using an automated 3-plex or 5-plex RNAscope and IHC staining protocol. The following experiment aimed to manually stain GAC (n=3) and normal tissue adjacent to tumour (NAT) (n=3) gastrectomy tissue sections from three individual patients using similar methods described for Figure 4.2. However, rather than using an automated research stainer, this technique was modified for manual staining on the laboratory bench.

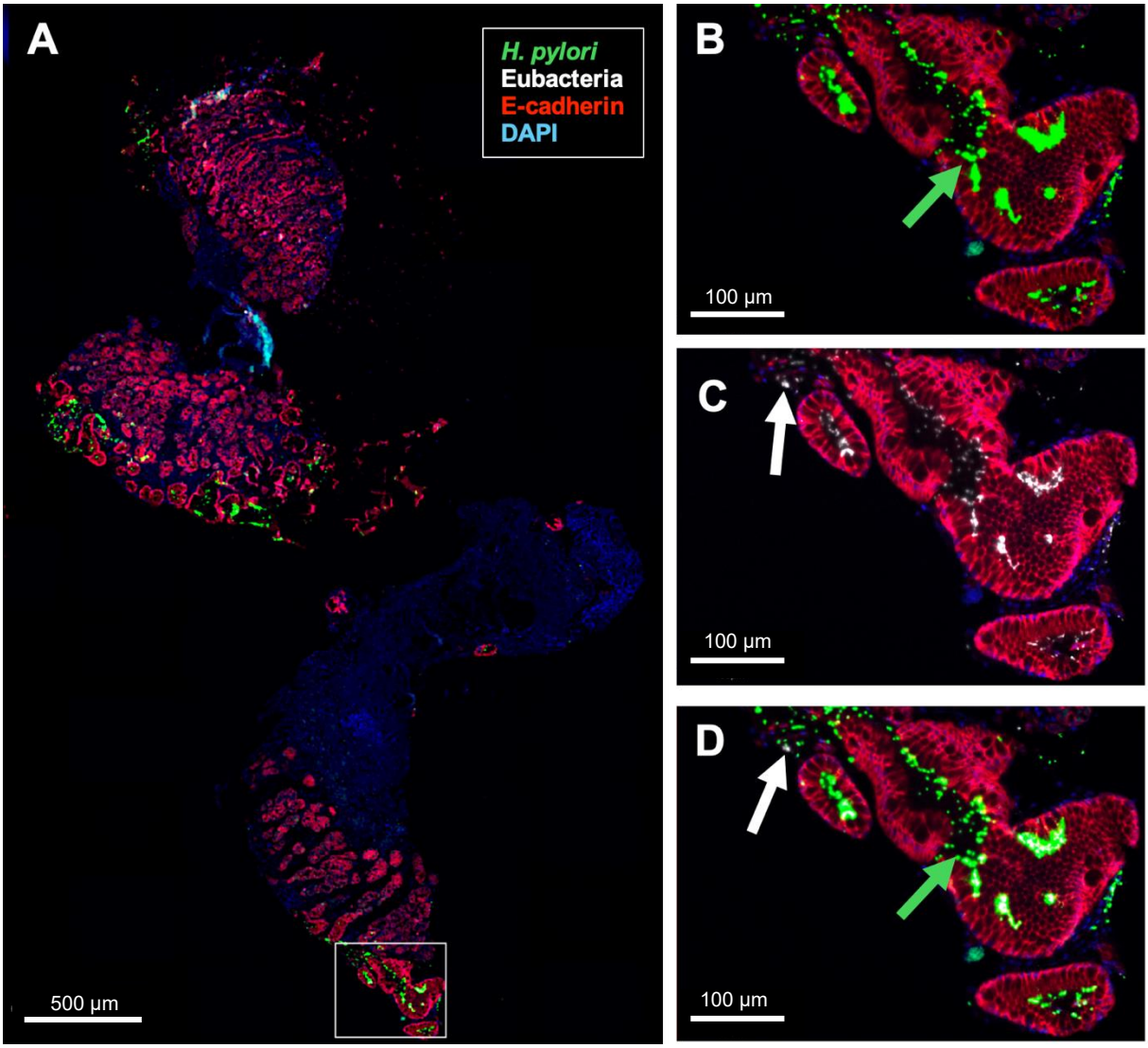

Figure 4.1. Representative image of automated 3-plex panel showing *H. pylori*, Eubacteria and E-cadherin in a *H. pylori*-positive GIM patient. Archived formalin-fixed paraffin-embedded gastric corpus tissue sections were retrieved from the Human Biomaterials Research Centre (HBRC). Sections were fluorescently labelled using a 3-plex panel with RNAscope probes against *H. pylori* (green), Eubacteria (white), E-cadherin (red) and counterstained with DAPI (blue). Panel A shows whole slide scan image; panels B, C and D show *H. pylori* channel only; Eubacteria channel only; and *H. pylori* and Eubacteria channels only, respectively. Scale bar represents 500 µm (A) or 100 µm (B-D).

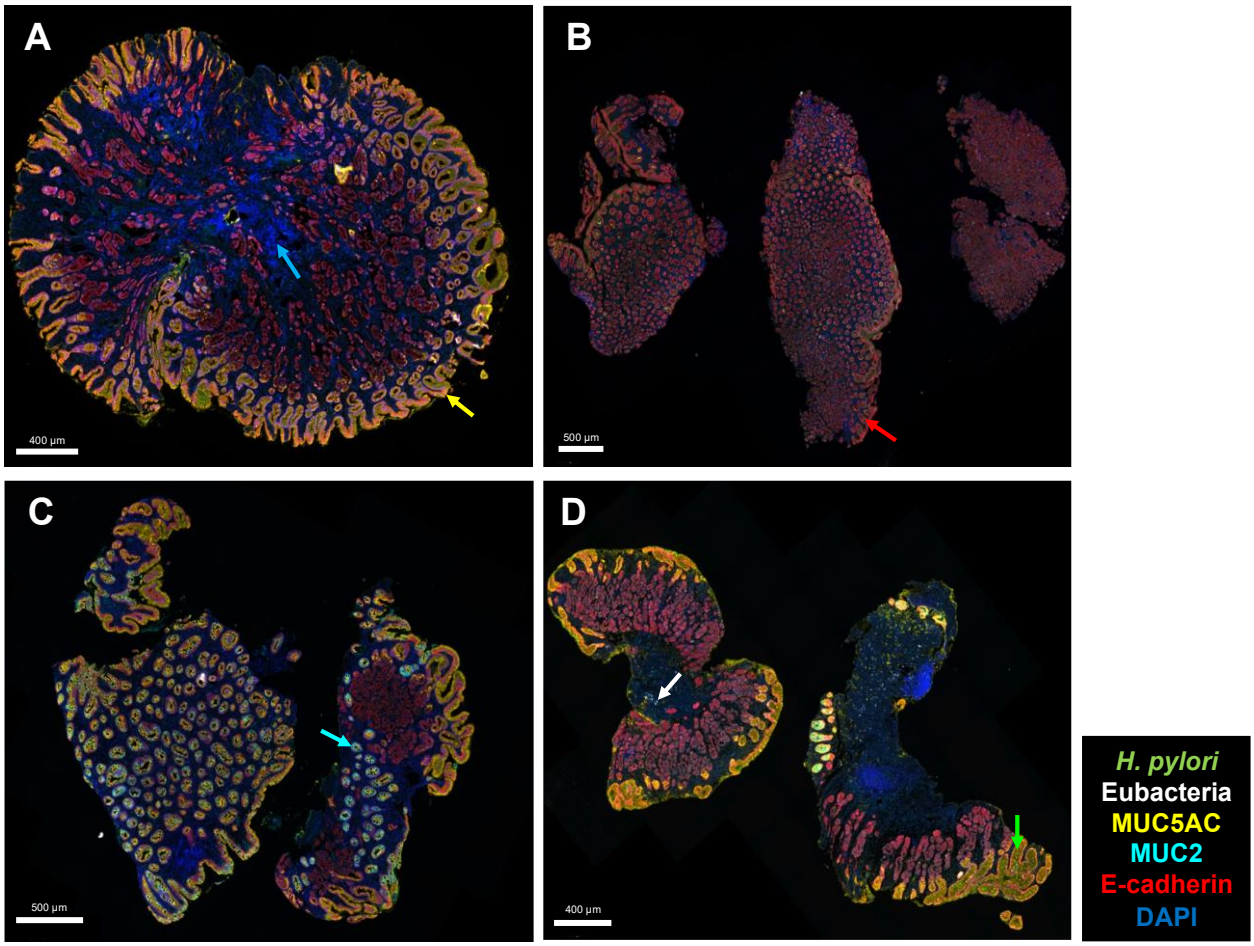

Figure 4.2. Representative whole slide scans of automated 5-plex panel showing *H. pylori*-positive and negative CG and GIM patients. Archived formalin-fixed paraffin-embedded gastric corpus tissue sections were retrieved from the HBRC. Sections were fluorescently labelled using a 5-plex panel with RNAscope probes against *H. pylori* (green), Eubacteria (white), E-cadherin (red), MUC5AC (yellow), MUC2 (turquoise) and counterstained with DAPI (blue). Images were spectrally unmixed and viewed using QuPath software. Representative images show *H. pylori*-positive CG (B) or GIM (D) and *H. pylori*-negative CG (A) or GIM (C); scale bar represents 400 or 500 µm.

Before conducting the manual staining assay, RNAscope probes against *H. pylori* and Eubacteria were tested in vitro using infected organoid mucosoid monolayers; all antibodies were previously optimised by Ana Teodósio. As before, sections were also tested for tissue integrity following pre-treatment protocols. One of the major modifications in the manual staining protocol was the use of a microwave oven, rather than automated stainer for Heat Induced Epitope Retrieval (HIER). Although automated 5-plex staining successfully labelled *H. pylori* and Eubacteria using RNAscope probes in addition to fluorescently labelling antibodies against MUC5AC, MUC2 and E-cadherin, this was not possible using the manual staining method. This was likely due to the use of a microwave oven for HIER steps, as RNAscope probes to detect bacteria were continually lost and uniform antibody staining across the tissue section was difficult to obtain. To rectify this issue and ensure consistent staining of each section, the staining was divided into two sets of 3-plex experiments using consecutive tissue sections.

The first 3-plex panel aimed to label only *H. pylori* and Eubacteria using RNAscope probes and E-cadherin with a primary and secondary antibody. In brief, gastrectomy tissue from three patients was manually deparaffinised and rehydrated prior to adding RNAScope probes against *H. pylori* and Eubacteria. Following successful addition of RNAscope probes, sections were blocked and incubated over night with E-cadherin antibody. The following day, the sections were washed and incubated with secondary antibody Alexa Fluor 594, counterstained with DAPI and mounted. Whole slide scans were then acquired for each section using a Vectra Polaris^{TM} whole slide scanner (Figure 4.3). For GAC sections, E-cadherin staining was uniform across all three

patients, whereas *H. pylori* staining was negligible, with minimal staining observed even within glandular regions. Eubacterial staining showed variation between the three patients, with one patient harbouring a dense region of colonisation, whereas the other two patients showed more sparse, uniform distribution of Eubacteria across the whole tissue section. Staining of NAT sections showed a similar trend, with uniform E-cadherin staining. Interestingly, the matched NAT section to the densely Eubacterial colonised GAC section showed a similar staining pattern with a dense region of colonisation, whereas Eubacterial staining of the other two NAT sections were also similar to their matched GAC section with sparse, evenly distributed bacterial colonisation. Finally, across all three NAT sections, small regions of *H. pylori* were observed located within glandular regions. Due to the large size of gastrectomy tissue sections in comparison to punch biopsy sections described for Figures 4.1 and 4.2, uniform staining as observed for E-cadherin and Eubacteria was relatively easy to observe whereas it was difficult to fully observe the extent of *H. pylori* staining without magnifying regions of each whole slide scan.

4.2.3. A manual 3-plex IHC panel for sequential identification of MUC5AC, MUC2 and E-cadherin in GAC and NAT tissue

Consecutive tissue sections were then used to manually stain GAC and NAT gastrectomy sections by fluorescently labelling antibodies against MUC5AC, MUC2 and E-cadherin in a 3-plex panel. (Figure 4.4). Tissue sections were prepared as previously described and sequentially labelled with antibodies against MUC5AC, MUC2 and E-cadherin, counterstaining with DAPI and mounted. Between each antibody incubation step, sections underwent HIER using a microwave oven. As also

expected, and also observed for Figure 4.3, E-cadherin staining was relatively uniform across all GAC and NAT sections, localised to glandular regions. Within NAT sections, MUC5AC staining was generally localised to glandular or epithelial surface regions, whereas within GAC sections, staining intensity and arrangement was relatively sparse. This is likely due to an increased presence of glandular regions with a defined structure in NAT sections, in comparison to GAC tissue which is often associated with damaged gastric glands. In NAT sections, MUC2 staining was generally localised to goblet cell regions found within the gastric glands, whereas in GAC sections, MUC2 did not appear localised to glandular regions and was higher in abundance. Antibodies within NAT tissue sections appeared visually like CG or GIM sections presented in Figure 4.2, likely owing to similarities in histological features. GAC tissue sections were visually different when compared to CG, GIM and NAT sections, likely owing to phenotypic changes associated with tumours such as cellular overcrowding and loss of tissue architecture.

4.2.4. Quantification of MUC5AC, MUC2 and E-cadherin across CG, GIM, NAT and GAC tissue

Once whole slide scans were obtained for all CG, GIM, NAT and GAC sections, each section was visually assessed for staining and image quality, they were spectrally unmixed and re-named without patient or pathology details for blinded, downstream image analysis using QuPath software. For each image, pixel thresholders were used to detect area covered by the channel corresponding to MUC5AC, MUC2 and E-cadherin. There was no significant difference in MUC5AC coverage across any of the CG, GIM, NAT and GAC tissue sections (Figure 4.5A).

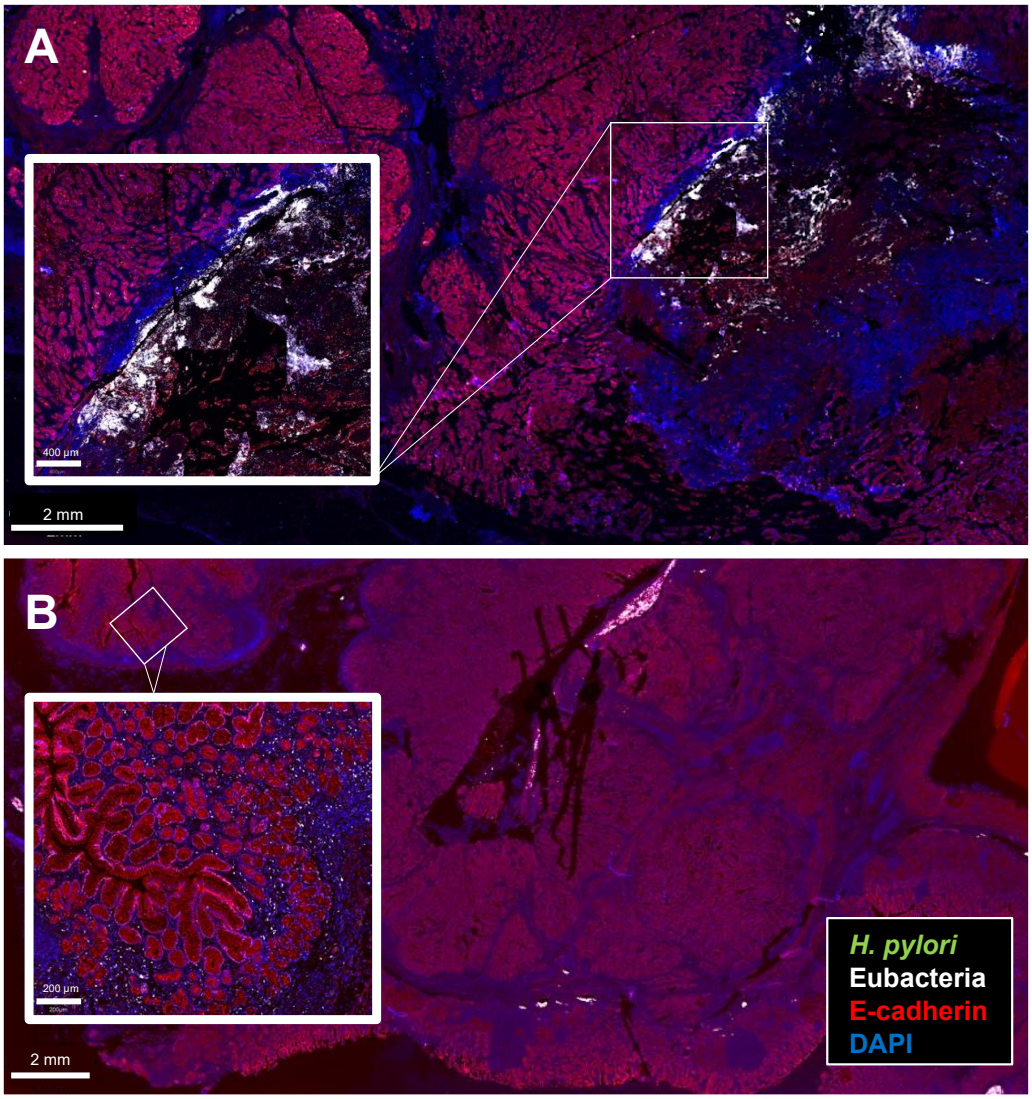

Figure 4.3. Representative whole slide scan image of manual 3-plex panel RNAscope probe and E-cadherin labelled GAC and NAT tissue sections. Gastrectomy tissue from three patients was obtained from the Queen Elizabeth Hospital Birmingham (QEHB) and stained with a 3-plex panel using RNAScope probes against *H. pylori* (green) and Eubacteria (white) followed by an antibody against E-cadherin (red). Sections were counterstained with DAPI and whole-slide scans were obtained. Images were viewed using QuPath software. Images show GAC section (A) and matching NAT (B) from one patient, white inset boxes show regions of Eubacterial staining; scale bar represents 2 mm.

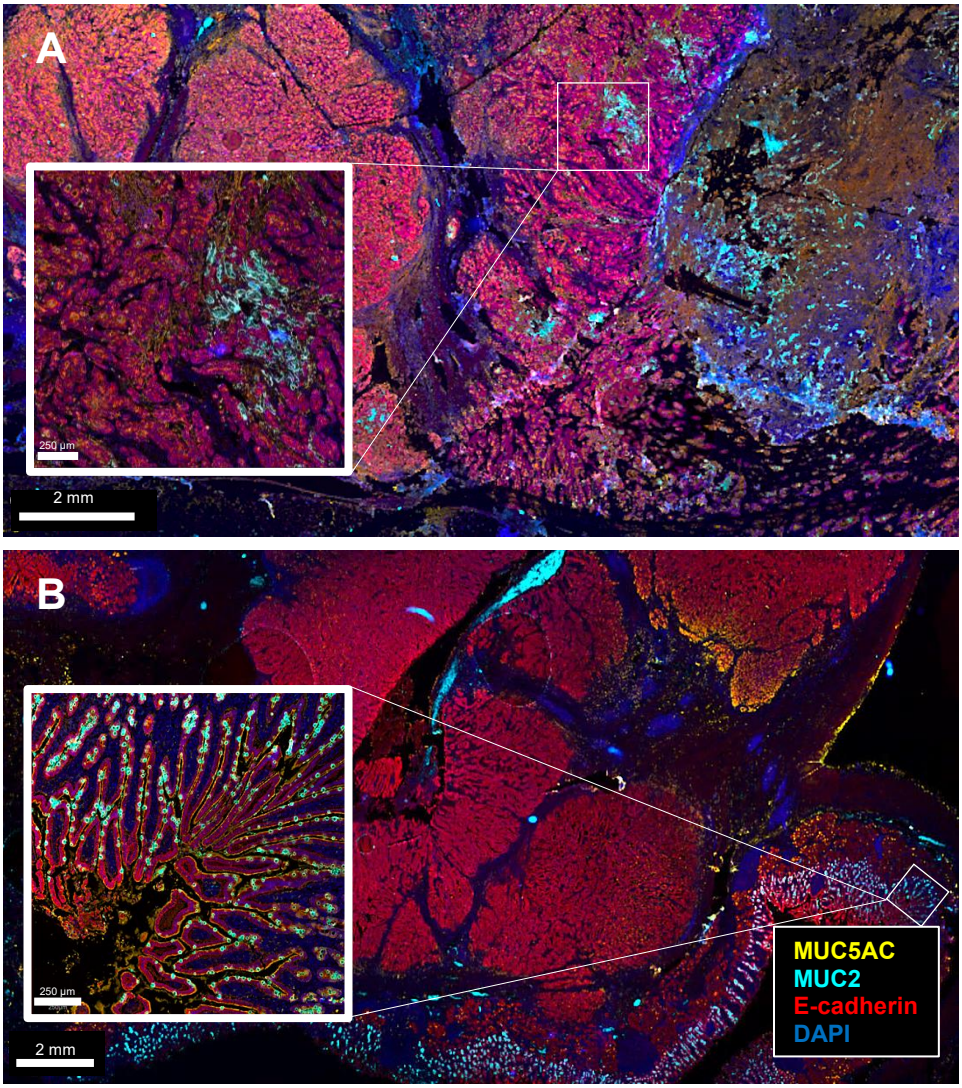

Figure 4.4. Representative whole slide scan image of manual 3-plex panel IHC labelled GAC and NAT tissue sections. Gastrectomy tissue from three patients was obtained from the Queen Elizabeth Hospital Birmingham (QEHB) and stained with a 3-plex panel using antibodies targeting MUC5AC (yellow), MUC2 (Turquoise) and E-cadherin (red). Sections were counterstained with DAPI and whole-slide scans were obtained. Images were viewed using QuPath software. Images show GAC section (A) and matching NAT (B) from one patient, white inset boxes show regions containing goblet cells expressing MUC2; scale bar represents 2 mm.

Although these data therefore suggest that presence of *H. pylori* or disease status does not impact MUC5AC coverage, it appeared that there was a slight increase in MUC5AC coverage from CG to GIM which was also heightened by presence of *H. pylori*. However, this result was not significant, which might be due to the relatively small sample size and variation observed within each patient.

As expected, MUC2 coverage was negligible in CG patients regardless of *H. pylori* status, whereas coverage was significantly higher in both *H. pylori* positive and negative GIM patients (Figure 4.5B). MUC2 expression is a histological indicator of GIM, due to the presence of intestinal goblet cells and was therefore expected within these patients. Although MUC2 coverage was heightened in GIM patients, these data also demonstrate the degree of variation between individual patients as MUC2 coverage ranged from approximately 2-25%. As also expected, MUC2 coverage was heightened in both NAT and GAC sections. This is likely due to the fact that these patients will have experienced some degree of GIM prior to a GAC diagnosis. There was no significant difference in MUC2 coverage between NAT and GAC sections, which was an expected result due to the likelihood of NAT and GAC sharing histological features due to tissue obtained within close proximity during gastrectomy.

No significant difference in E-cadherin coverage was observed between CG patients, regardless of *H. pylori* status. In addition, no significant difference was observed between NAT and GAC sections (Figure 4.6). Interestingly, E-cadherin coverage was significantly higher in NAT and GAC tissue compared with CG and GIM, although the reason behind this remains unclear and was not explored further.

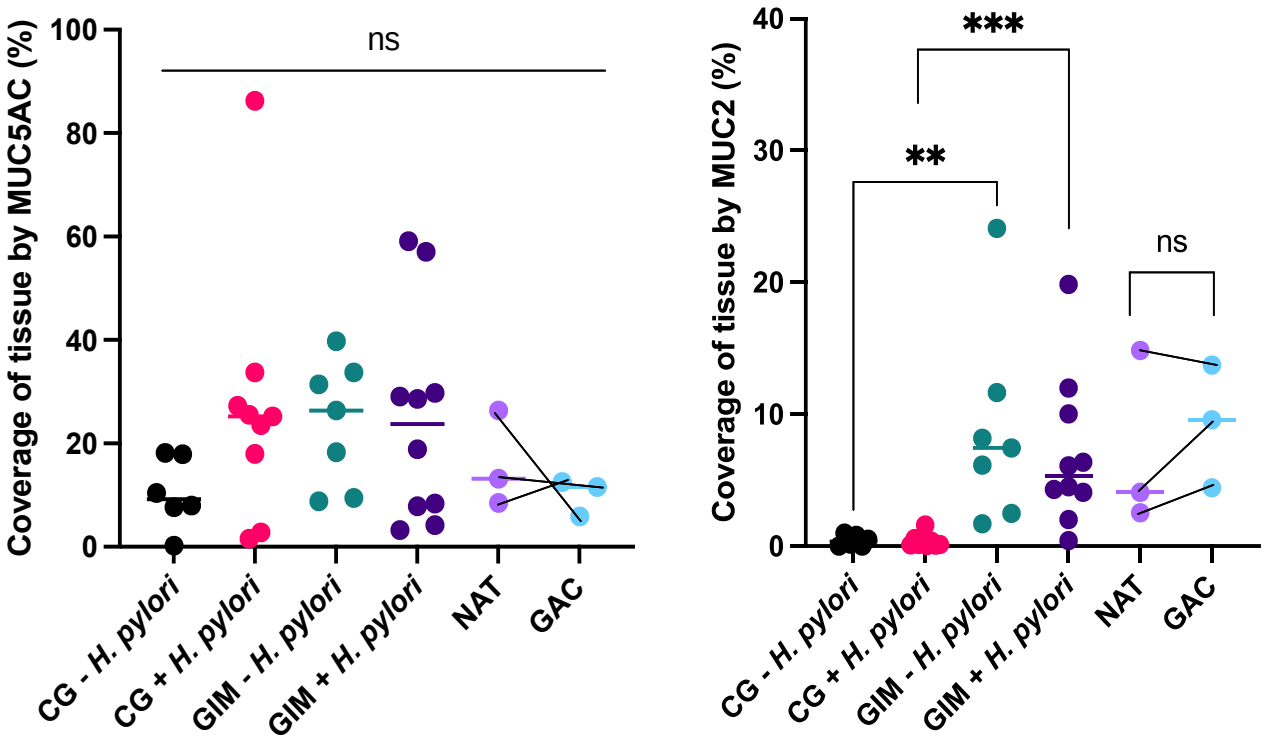

Figure 4.5A and Figure 4.5B. Quantification of MUC5AC and MUC2 coverage in CG, GIM, GAC and NAT sections. CG, GIM, GAC and NAT tissue sections were fluorescently labelled with RNAscope probes against *H. pylori,* Eubacteria, MUC5AC, MUC2 and E-cadherin. Clinical pathology reports confirmed that the patients were *H. pylori*-positive CG (n=9) or GIM (n=10), *H. pylori*-negative CG (n=6) or GIM (n=7) and GAC (n=3) or healthy tissue adjacent to tumour (NAT) (n=3). Whole slide scans were obtained of each tissue section, spectrally unmixed and analysed using QuPath software. For each marker of interest, percentage area coverage of tissue was calculated using a pixel thresholder. Data were exported from Excel to GraphPad Prism 9 (Version 9.5.1). A Mann-Whitney test was used for statistical analysis, whereby ** $P \leq 0.01$, *** $P \leq 0.001$ and ns indicates non-significant. Data are presented as median ± SEM, for each group.

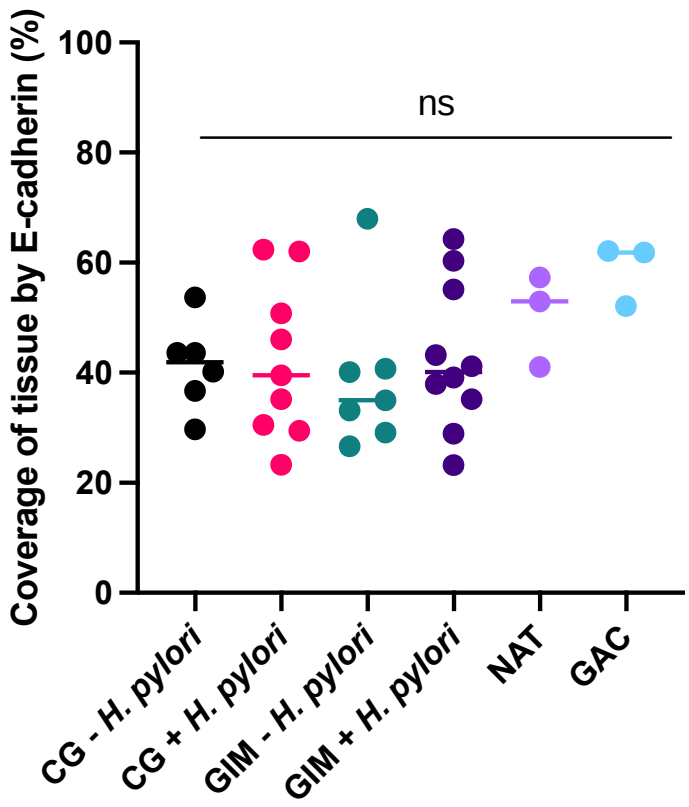

Figure 4.6. Quantification of E-cadherin coverage in CG, GIM, GAC and NAT sections. CG, GIM, GAC and NAT tissue sections were fluorescently labelled with RNAscope probes against *H. pylori,* Eubacteria, MUC5AC, MUC2 and E-cadherin. Clinical pathology reports confirmed that the patients were *H. pylori*-positive CG (n=9) or GIM (n=10), *H. pylori*-negative CG (n=6) or GIM (n=7) and GAC (n=3) or healthy tissue adjacent to tumour (NAT) (n=3). Whole slide scans were obtained of each tissue section, spectrally unmixed and analysed using QuPath software. For E-cadherin. percentage area coverage of tissue was calculated using a pixel thresholder. Data were exported from Excel to GraphPad Prism 9 (Version 9.5.1). A Mann-Whitney test was used for statistical analysis, whereby ns indicates non-significant. Data are presented as median ± SEM, for each group.

4.2.5. Distribution of *H. pylori* and Eubacteria within CG, GIM, NAT and GAC tissue

Colonisation of tissue by *H. pylori* and Eubacteria across CG, GIM, NAT and GAC sections were also blindly quantified using the channels corresponding to *H. pylori* and Eubacteria. To account for *H. pylori* double-staining and detection in both the *H. pylori* and Eubacteria channels, absolute Eubacteria area was determined by excluding any bacteria which had also been detected with the *H. pylori* probe.

As expected, *H. pylori* coverage was significantly higher in the CG and GIM *H. pylori* positive sections, compared with CG and GIM *H. pylori*-negative sections (Figure 4.7A). Although not statistically significant, *H. pylori* colonisation appeared to be higher in NAT sections compared with GAC. This result was expected as previous sequencing studies have suggested that *H. pylori* colonisation is reduced in GAC compared with 'healthy' tissue. As also observed for quantification of mucin coverage, there was much variation in regions of tissue covered by *H. pylori* between each patient, further highlighting the potential issue of interpatient variability and small sample size in this experiment. Interestingly, for both CG and GIM patients, Eubacteria presence was significantly heightened in the presence of *H. pylori* (Figure 4.7B). Conversely, Eubacteria presence was significantly reduced in the absence of *H. pylori* infection. This was an interesting result, which contrasts with the current dogma that *H. pylori* and Eubacteria presence is usually mutually exclusive during CG and GIM. Additionally, although there was no significant difference in Eubacterial presence between NAT and GAC sections, areas of tissue covered by Eubacteria were notably higher in GAC. Taken together, these data indicate that despite sequencing studies

suggesting otherwise, infection with *H. pylori* might indeed correlate with increased numbers of Eubacteria during CG and GIM. Conversely, in agreement with sequencing studies, although non-significant, these data suggest that Eubacterial presence is higher in GAC.

4.2.6. Localisation of Eubacterial invasion in CG, GIM, GAC and NAT tissue

Once total area coverage of each marker of interest had been quantified and a correlation between *H. pylori* and Eubacteria presence had been established, the spatial distribution and localisation of these bacteria were determined by visual assessment. Two independent researchers viewed each CG, GIM, GAC and NAT whole slide scan using Phenochart whole slide viewer or QuPath software. Location of *H. pylori* was first investigated, whereby it was noted that within the majority of *H. pylori*-positive CG and GIM patient sections, *H. pylori* was localised to the glands (Figure 4.8 A-E and Figure 4.9 B-E).

In Figure 4.9 A, a rare incidence of *H. pylori* presence outside of the glands and within the lamina propria was observed. As expected, *H. pylori*-negative CG and GIM sections showed little to no staining for *H. pylori* (Figure 4.8 F and Figure 4.9 F). Very little *H. pylori* staining was observed in any of the GAC sections (Figure 4.10 A-E), whereas although *H. pylori* presence remained generally low in NAT sections, some localisation of *H. pylori* within glandular structures was observed (Figure 4.10 D). Once *H. pylori* was located within each whole slide scan, the location and distribution of Eubacteria was then visually studied.

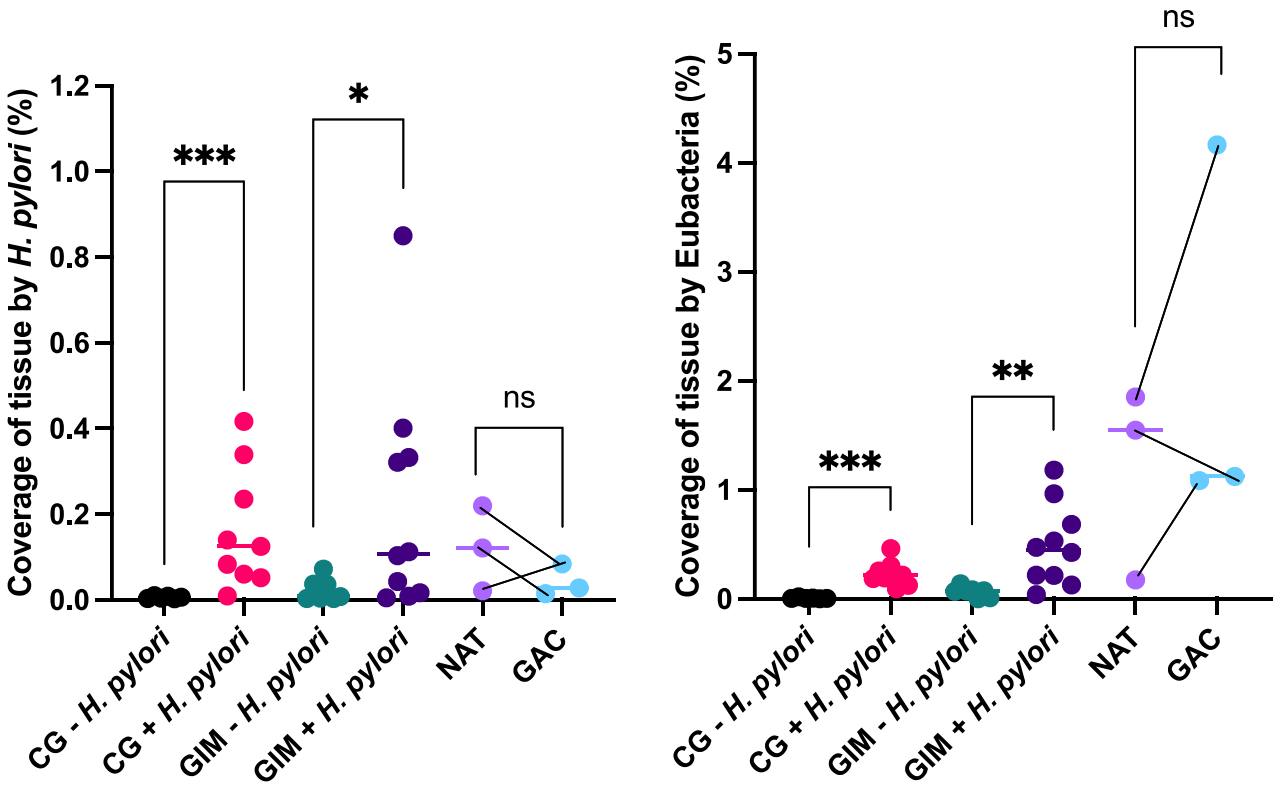

Figure 4.7A and Figure 4.7B. Quantification *H. pylori* and Eubacteria coverage in CG, GIM, GAC and NAT sections. CG, GIM, GAC and NAT tissue sections were fluorescently labelled with RNAscope probes against *H. pylori,* Eubacteria, MUC5AC, MUC2 and E-cadherin. Clinical pathology reports confirmed that the patients were *H. pylori*-positive CG (n=9) or GIM (n=10), *H. pylori*-negative CG (n=6) or GIM (n=7) and GAC (n=3) or healthy tissue adjacent to tumour (NAT) (n=3). Whole slide scans were obtained of each tissue section, spectrally unmixed and analysed using QuPath software. For *H. pylori* and Eubacteria percentage area coverage of tissue was calculated using a pixel thresholder. Data were exported from Excel to GraphPad Prism 9 (Version 9.5.1). A Mann-Whitney test was used for statistical analysis, whereby * $P \leq 0.05$, ** $P \leq 0.01$, ***$P \leq 0.001$ and ns indicates non-significant. Data are presented as median ± SEM, for each group.

Low Eubacterial numbers were observed in *H. pylori*-negative CG and GIM sections. However, *H. pylori*-positive CG and GIM sections generally showed a significantly higher density of Eubacteria in comparison to *H. pylori* negative sections, whereby Eubacteria were generally located within the lamina propria and appeared to be 'invading' deep into the gastric tissue (Figure 4.8 A-E and Figure 4.9 A-E). In GAC sections, Eubacteria appeared either evenly distributed across the tissue in two GAC patients (Figure 4.10 C&E) or as dense regions of colonisation in one GAC patient (Figure 4.9 A). It was also observed that Eubacterial distribution and subsequent invasion increased progressively from CG to GIM and GAC. Increased Eubacterial density and invasion was also observed in GAC compared with their matched NAT sections and also appeared similar in distribution (Figure 4.10 B, D & F).

4.2.7. Scoring of Eubacterial invasion in CG, GIM, GAC and NAT tissue

Following blinded visual assessment of whole slide scans for Eubacterial distribution, a qualitative scoring system was devised to Eubacterial invasion across each CG, GIM, GAC and NAT whole slide scan (Figure 4.11). Scoring was blindly conducted by two independent researchers, who had no knowledge of patient details or disease status, whereby 0 = no invasion, 1 = sparse invasion, 2 = moderate invasion (patches of bacteria across sample), 3 = high invasion (multiple clear regions of bacterial invasion across sample) and 4 = dense colonisation of bacteria (large regions of sample colonised). In agreement with initial visual assessment, *H. pylori*-negative CG and GIM sections scored relatively low for Eubacterial invasion. Conversely and also in agreement with initial visual assessment, for CG *H. pylori*-positive patients, several scored 1, 2 or 3, aside from one patient who scored 0. Scoring was also similar for

GIM *H. pylori* patients, with scores ranging from 1-3 for invasion, aside from one patient who also scored 0. Interestingly, Eubacterial invasion was generally higher in *H. pylori*-positive GIM patients compared with CG, correlating with data presented in Figure 4.7B which highlights an increase in Eubacteria from CG to GIM. Overall, although there was clear interpatient variability, *H. pylori*-positive CG and GIM sections scored statistically significantly higher for invasion than *H. pylori*-negative sections.

Taken together, these data suggest that Eubacterial presence and invasion into the lamina propria is correlated with presence of *H. pylori.* GAC and NAT tissue sections were then scored for Eubacterial invasion, whereby each NAT section showed high interpatient variability, scoring 0, 1 and 3 respectively. As expected, Eubacterial invasion was higher in GAC sections, with each section scoring 3, 3 and 4 respectively. These data therefore suggest that Eubacterial distribution and invasion into the lamina propria is elevated in GAC and NAT tissue. This was an expected result, as previous sequencing studies have highlighted an increase in microbial numbers and diversity in GAC tissue. Following visual assessment and qualitative scoring, these data suggest that not only is *H. pylori* presence associated with increased Eubacterial colonisation, but also subsequent Eubacterial invasion into the lamina propria during the early stages of gastric carcinogenesis. In contrast, although small numbers of sparsely distributed Eubacteria were observed in *H. pylori*-negative CG and GIM sections, minimal colonisation and invasion into the lamina propria was observed.

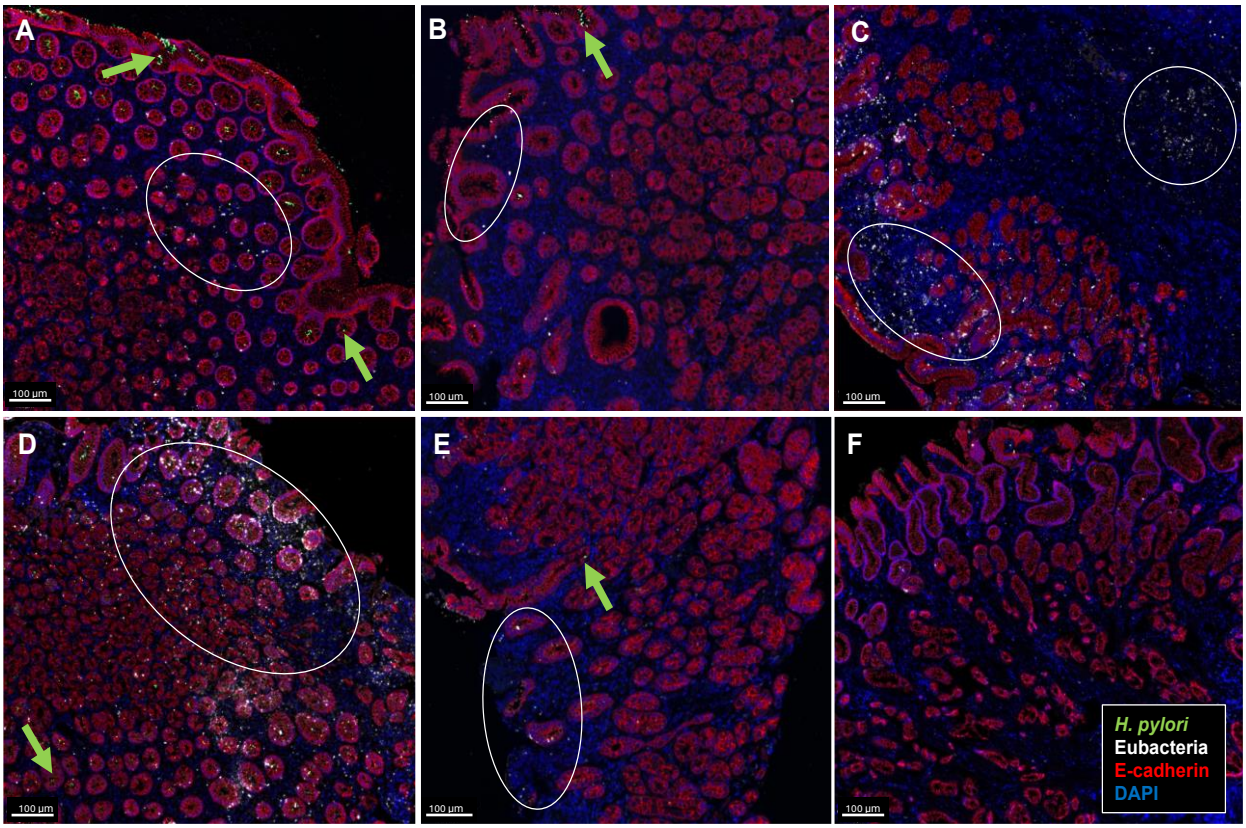

Figure 4.8. Representative images of Eubacterial invasion in *H. pylori*-positive CG tissue. Automated 5-plex RNAscope and IHC staining was conducted to fluorescently label *H. pylori*, Eubacteria, E-cadherin, MUC5AC and MUC2 in *H. pylori*-positive punch biopsy CG tissue sections (n=9). Images were viewed using QuPath. Images show Eubacterial invasion five representative CG *H. pylori* positive sections (A-E) and a representative image of *H. pylori*-negative CG section (F). Eubacterial invasion is indicated by white oval and *H. pylori* is indicated by green arrow. For visualisation purposes, only channels for *H. pylori* (green), Eubacteria (white) and E-cadherin (red) are turned on); Scale bar represents 100 µm.

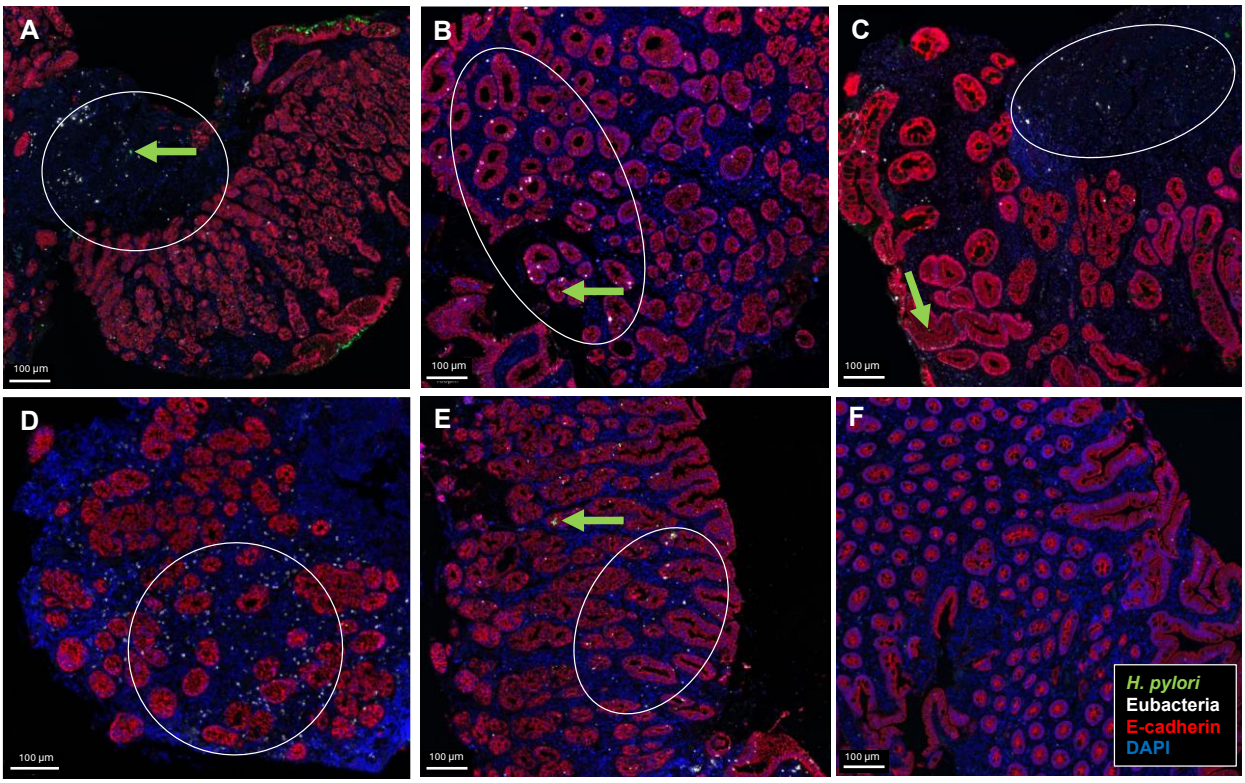

Figure 4.9. Representative images of Eubacterial invasion in *H. pylori*-positive GIM tissue. Automated 5-plex RNAscope and IHC staining was conducted to fluorescently label *H. pylori*, Eubacteria, E-cadherin, MUC5AC and MUC2 in *H. pylori*-positive punch biopsy GIM tissue sections (n=10). Images were viewed using QuPath. Images show Eubacterial invasion five representative *H. pylori*-positive GIM sections (A-E) and a representative image of *H. pylori*-negative GIM section (F). Eubacterial invasion is indicated by white oval and *H. pylori* is indicated by green arrow. For visualisation purposes, only channels for *H. pylori* (green), Eubacteria (white) and E-cadherin (red) are turned on); Scale bar represents 100 µm.

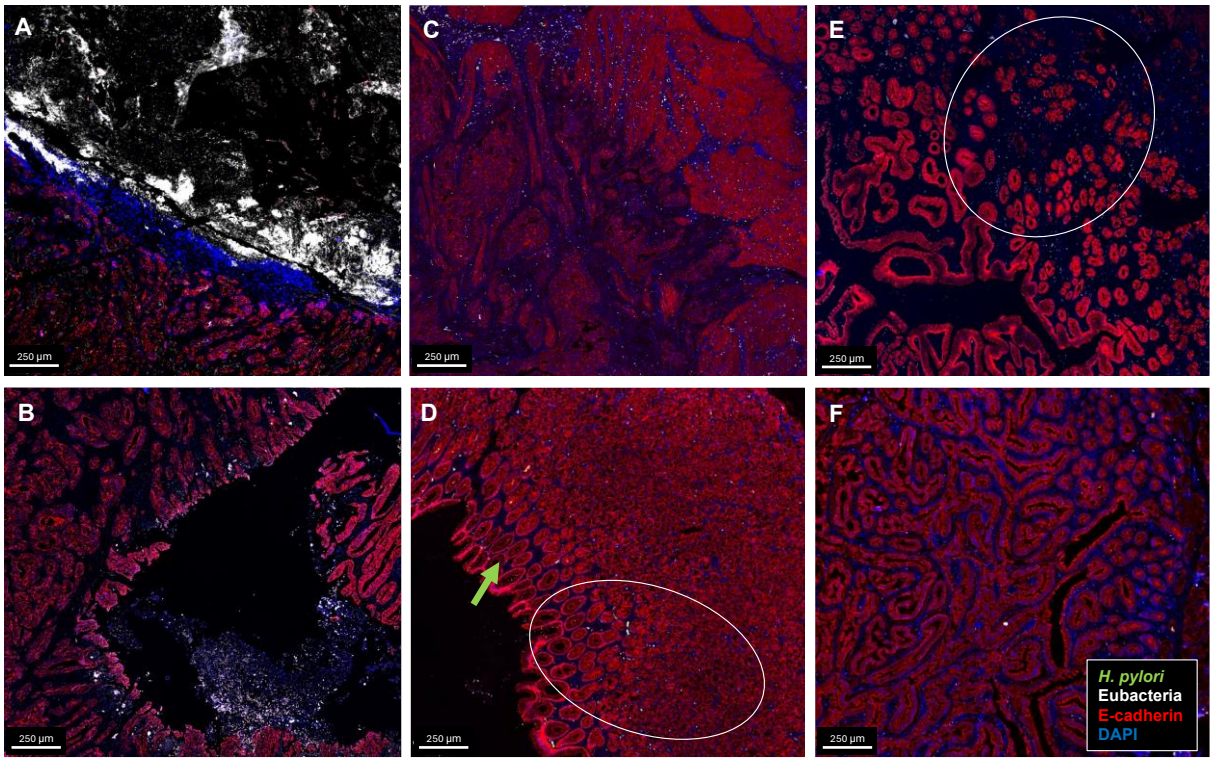

Figure 4.10. Representative images of Eubacterial invasion in GAC and NAT tissue. Manual 3-plex RNAscope and IHC staining was conducted to fluorescently label *H. pylori*, Eubacteria and E-cadherin in gastrectomy tissue (n=3). Images were viewed using QuPath. Images show Eubacterial invasion in matched GAC and NAT patient sections; GAC sections (A, C, E) and matched NAT sections (B, D, E). Patient 1 = A-B, patient 2 = C-D and patient 3 = E-F. Eubacterial invasion is indicated by white oval and *H. pylori* is indicated by green arrow. Scale bar represents 250 μm.

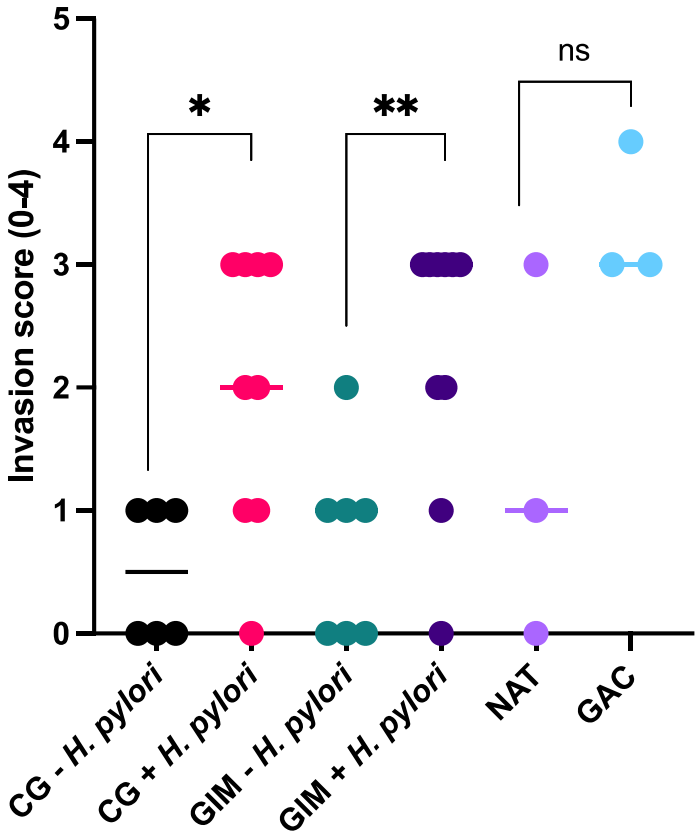

Figure 4.11. Qualitative scoring of Eubacterial invasion in CG, GIM, GAC and NAT tissue. Automated 5-plex (CG and GIM) or manual 3-plex (GAC and NAT) staining was conducted to fluorescently label *H. pylori*, Eubacteria, E-cadherin, MUC5AC and MUC2. Clinical pathology reports confirmed that the patients were *H. pylori*-positive CG (n=9) or GIM (n=10), *H. pylori*-negative CG (n=6) or GIM (n=7) and GAC (n=3) or healthy tissue adjacent to tumour (NAT) (n=3). Images were viewed using QuPath software and Eubacterial invasion was qualitatively scored by two independent researchers, whereby 0 = no invasion, 1 = sparse invasion, 2 = moderate invasion (patches of bacteria across sample), 3 = high invasion (multiple clear regions of bacterial invasion across sample) and 4 = dense colonisation of bacteria (large regions of sample colonised). A Mann-Whitney test was used for statistical analysis, whereby * $P \leq 0.05$, ** $P \leq 0.01$ and ns indicates non-significant.

4.3 Discussion

4.3.1. 3 and 5-plex automated staining panels to identify *H. pylori*, Eubacteria and mucins in CG and GIM tissue

Results presented in this chapter demonstrated that archived CG and GIM punch biopsy sections could be successfully prepared for multiplex RNAscope staining immediately followed by IHC using an automated research stainer. Whilst RNAscope has been successfully combined with immunostaining in previous studies, the majority of previous experiments only included fluorescent labelling of one or two antibodies in combination with RNAscope probes (Ball *et al*., 2023). In the current project, both 3-plex and 5-plex multiplex immunofluorescence panels (mIF) successfully labelled *H. pylori* and Eubacteria in addition to three antibodies of interest, without loss of tissue integrity or staining uniformity. Aside from technical expertise and rigid optimisation steps conducted by Ana Teodósio, successful staining can also be attributed to the use of an automated research stainer. Although high running and maintenance costs are associated with these staining machines, automated staining facilitates faster, reproducible and uniform staining of multiple sections in a given protocol. Additionally, other factors that often affect staining uniformity can be easily controlled and monitored, such as HIER temperature, reagent and antibody volume and incubation times (Đorđević *et al*., 2021).

4.3.2. Manual 3-plex staining panels to identify *H. pylori*, Eubacteria and mucins in GAC and NAT tissue

A manual laboratory-based protocol was devised to repeat the aforementioned experiment using gastrectomy GAC and NAT tissue sections. The automated approach

was used as a guideline when devising the manual protocol and shared several similarities including staining order, incubation times and antibody concentrations. A major difference between the automated and manual assays was that for manual staining all staining was conducted on the laboratory bench without the use of automated technology. Incubation steps were conducted in a humidified plastic box within a dry incubator and HIER steps required heating antigen retrieval buffers to just below boiling in a microwave oven. Whilst this was a cost-effective way of staining several sections at once, it required several quality control steps to ensure tissue integrity and staining uniformity that were difficult to control compared with an automated research stainer (Đorđević *et al*., 2021). It was initially hoped that the full automated protocol (RNAscope probes immediately followed by IHC) could be directly repeated using a manual approach, but due to several difficulties this experiment was divided into two parts. Following successful labelling of bacteria with RNAscope probes, which were briefly confirmed with confocal microscopy, it was found that the subsequent HIER steps involved in the IHC component of the protocol were either drastically reducing brightness or stripping RNAscope probes completely from the tissue. This is a common problem, as microwave ovens are difficult to control temperature and do not dissipate heat as well as an automated research stainer and often result in hot and cold areas across the tissue, causing uneven antigen retrieval or superheating (Kumar *et al.,* 2016). Alternative HIER options include using a water bath, which was found to be inconvenient due to the time taken to reach and maintain temperature, or the use of a pressure cooker, which was not available for this work (Krenacs *et al*., 2010). As such, in order to avoid exposing RNAscope probes to excessive heat, probes targeting *H. pylori* in combination with overnight E-cadherin

antibody staining were used to identify bacteria in GAC and NAT, whilst a consecutive section was used to label antibodies against MUC5AC, MUC2 and E-cadherin.

4.3.3. Expression and localisation of MUC5AC, MUC2 and E-cadherin in CG, GIM, GAC and NAT tissue

Whilst tissue coverage by MUC5AC varied between patients, these data suggest that MUC5AC expression is relatively stable across each stage of gastric carcinogenesis. This finding was expected based on literature searches, as although MUC5AC is highly associated with the healthy gastric mucosa, it has also been found in gastric tumours and expression is often maintained in GIM (Reis *et al*., 1999; Rico *et al*., 2021). Additionally, although non-significant, coverage of CG and GIM tissues by MUC5AC was slightly elevated in *H. pylori*-positive sections. Although this was not investigated further, this correlates with previous studies which observed *H. pylori*-induced upregulation of MUC5AC and subsequent deposition of Lewis antibodies for adhesion purposes (Gonciarz *et al*., 2019). Owing to the presence of mucin-secreting goblet cells as a result of the intestinal phenotype in GIM, MUC2 coverage was markedly elevated in GIM sections compared with CG. This was a vital finding which further confirmed antibody staining specifity and disease status between the patient groups. Interestingly, MUC2 coverage was also elevated in GAC and NAT tissue sections, likely indicative of NAT tissue not being truly 'healthy', as it is directly adjacent to tumour (Aran *et al*., 2017). This finding therefore indicates that NAT tissue might be more histologically similar to GIM tissue than healthy tissue and that this tissue type should be used with caution when described as 'healthy' in future studies. MUC2 expression was markedly elevated in GAC tissue, which provided further confirmation of the disease state of

these patients. Furthermore, *de novo* MUC2 expression is highly correlated with poorer prognosis and tumour severity, indicating that these patients represented the most 'severe' stage of carcinogenesis (Wakatsuki *et al*., 2008). The precise role of MUC2 in GAC remains unclear, but is currently hypothesised that overexpression of mucin, such as MUC2, serves as a protective barrier which limits exposure to bacteria and dampens the inflammatory response (Van der Sluis *et al.*, 2006). Interestingly, a recent study also identified a direct link between mucin expression and bacterial diversity in GAC. High MUC2 expression was associated with a depletion of *Streptococcus* species, but an increase of *Lactobacillus* and *Neisseria* species. Samples with high MUC2 expression also exhibited an upregulation of the sucrose degradation IV (sucrose phosphorylase) pathway, suggesting a reliance of mucins as a bacterial food source in GAC (Oosterlinck *et al.*, 2023).

In addition to mucins, E-cadherin was selected as a marker for intercellular junctions, allowing visualisation of tissue architecture and glandular regions. No significant differences or differences of note were observed between patient groups and specific interactions between bacteria and E-cadherin were not investigated directly in this study. However, the interaction between *H. pylori* and E-cadherin has frequently been investigated, with a recent study suggesting that *H. pylori* virulence factor HtrA facilitates E-cadherin shedding and subsequent impairment of barrier function in an organoid model (Murata-Kamiya *et al.*, 2007). Furthermore, *H. pylori* CagA is also highly associated with impaired cellular polarisation, as CagA injection into the host cell inhibits the association of E-cadherin with β-catenin, resulting in intracellular accumulation of cytoplasmic and nuclear catenin (Murata-Kamiya *et al*., 2007).

4.3.4. Expression and localisation of *H. pylori* and Eubacteria in CG, GIM, GAC and NAT tissue

In agreement with previous studies suggesting that *H. pylori* establish colonies deep within the gastric glands using mouse models, this study also demonstrated *H. pylori* exclusively colonised the gastric glands in human CG and GIM tissue (Fung *et al*., 2019). This finding was expected, as it has recently been established that *H. pylori* within the gastric environment occupy specific 'microniches', with some populations of *H. pylori* occupying the superficial gastric mucus, whilst the majority embed within deep regions of the gastric glands. Although the reason behind the formation of these microniches remains unclear, there are several mechanisms which could explain the distribution and arrangement of *H. pylori* during carcinogenesis.

The presence of *H. pylori* deep within the gastric glands is likely attributed to *H. pylori* flagella-driven motility and secretion of urease enabling deep colonisation and protection against the harsh gastric environment (Celli *et al*., 2009). In addition, the distribution of *H. pylori* within gastric tissue is also attributed to chemotaxis in response to urea, bicarbonate or sodium chloride which are secreted by gastric epithelial and parietal cells. Parietal cells originate from gastric stem cells and are often found at the base of the gastric gland, where *H. pylori* was also identified in this study *(Mizote et al*., 1997). MUC5AC expression is highly expressed in gastric glands and is composed glycans which are also bound and utilised by *H. pylori* as an attachment site for subsequent proteolytic degradation of the gastric mucin (Celli *et al*., 2009; Mahdavi *et al*., 2002). The Lewis-B antigen is a tetrasaccharide also found within MUC5AC and

serves as a binding site for several *H. pylori* adhesins, facilitating adherence and colonisation throughout the gastric glands (Gonciarz *et al*., 2019; Löfling *et al*., 2008).

Quantification of tissue coverage area by *H. pylori* confirmed visual observations and provided a numerical value for bacterial presence. Interestingly, *H. pylori* coverage was relatively high in NAT tissue compared with *H. pylori* negative CG and GIM sections. This is likely indicative of NAT tissue not being truly 'healthy', as it is adjacent to tumour as previously discussed. *H. pylori* coverage was also higher than expected in GAC sections, as previous sequencing data has shown that *H. pylori* abundance decreases during the final stages of carcinogenesis. However, it is possible that small numbers of *H. pylori* were easily identified in these sections due to the high specifity and high amplification of the probe targeting *H. pylori* ribosomal rRNA. Quantification of *H. pylori* coverage across each tissue section revealed high inter-patient variability, which is likely due to patients within the *H. pylori* positive groups all at varying stages of carcinogenesis, whilst some were also prescribed PPIs or taking additional medications which were not documented (Appendix A). Although these patients were not taking antibiotics, other drugs such as metformin, antidepressants and laxatives have been shown to alter the gastric microbiota which might contribute to observed variation (Weersma *et al*., 2020). Furthermore, no information was provided on patient lifestyle factors such as diet, exercise or smoking.

A major observation was a significant correlation between Eubacteria presence and with *H. pylori* infection in CG and GIM. This was a significant finding as it contrasts with the current dogma that the microbiota of *H. pylori* negative individuals is unique and

enriched (Noto and Peek, 2017). Although interpatient variability was lower than for *H. pylori*, this can also be attributed to the patient health, diet and lifestyle factors. Furthermore, Eubacteria coverage increased from CG, through to GIM and GAC, which suggests that *H. pylori*-induced histological changes occurring later in Correa's cascade might provide more favourable conditions for Eubacteria.

De novo expression of MUC2 is associated with both GIM and GAC, serving as a protective barrier or bacterial food source (Oosterlinck *et al*., 2023; Van der Sluis *et al*., 2006). As such, it is possible that the enrichment of Eubacteria during GIM and GAC observed in our data is also a result of MUC2 overexpression and that there is a direct correlation between MUC2 availability and bacterial colonisation. Additionally, during CG parietal cells are often lost as a result of *H. pylori*-induced atrophy, resulting in reduced stomach acid production and neutralisation of local pH (Dixon *et al*., 1996). It is hypothesised that this rise in pH results in a shift in microbial diversity, with increased colonisation of phyla such as Bacillota or Bacteroidota, an effect commonly observed in inflammatory bowel disease (IBD) (Walker *et al*., 2005). Several sequencing studies which have documented a gradual increase in bacterial phyla abundance and diversity during gastric carcinogenesis, with Bacillota, Bacteroidota and some Fusobacteriota often enriched in GAC (Png *et al*., 2022). Although this shift in microbial diversity remains unclear, it is likely a multifactorial process involving host factors such as mucin expression, inflammation and alterations in tissue architecture and pH (Eun *et al*., 2014).

Whilst the identification of non-*H. pylori* Eubacteria was a striking observation, it is also worth noting that some species might not have been detected by the 16S rRNA probe, resulting in an element of bacterial under-reporting in this study. Although the Eubacteria 16S rRNA probe was designed to target conserved regions of the 16S rRNA, some bacterial groups possess highly divergent 16S sequences, which might not be recognised by standard probes or primers. For example, previous studies have reported that Eubacteria-specific probes often miss certain phyla, such as Planctomycetes and Verrucomicrobia (Daims *et al.* 1999). In addition, successful rRNA labelling of Eubacteria relies on good quality and readily available cellular ribosome content and any bacteria possessing poor quality rRNA or target sites hindered by rRNA-rRNA interactions might not be easily targeted by a 16S rRNA probe (Behrens *et al.,* 2003). Finally, bacterial cell wall permeability can influence 16S rRNA probe binding. For example, Gram-positive bacteria such as streptococci and staphylococci possess a thick outer cell wall, which requires permeabilisation, usually with lysozyme, before the 16S rRNA probe is applied (Rocha *et al.,* 2018). In this study, lysozyme was not used due to the detrimental effect on tissue quality and as such, it is possible that certain Gram-positive bacteria were not readily targeted by the 16S rRNA probe due to their cell wall not becoming permeabilised. Nonetheless, although permeability is frequently reported as an issue in more traditional FISH approaches, the use of brighter Opal fluorophores (containing fluorescein-tyramide) in this study in combination with horseradish peroxidase likely resolved this problem, as the tyramide-HRP system reportedly increases bacterial signal intensity up to 20-fold compared with more traditional fluorophore-based approaches (Schonhuber *et al.,* 1997).

4.3.5. Invasion of Eubacteria into the lamina propria in CG, GIM, GAC and NAT tissue

Following quantitative analysis, it was revealed by visual assessment that Eubacteria invade deep into the lamina propria whilst *H. pylori* exclusively colonised the gastric glands in CG and GIM tissue. This was a highly interesting finding, as in addition to demonstrating a correlation between *H. pylori* and Eubacteria presence, these data also suggest that Eubacterial invasion might play a key role in the early stages of carcinogenesis. Bacterial invasion is associated with multiple diseases of the gastrointestinal tract including as colitis, IBD and Chron's disease, causing damage to the epithelial architecture by triggering inflammatory responses (Linares *et al*., 2021). However, invasion of Eubacteria in gastric carcinogenesis is rarely studied, as development of GAC is often attributed to *H. pylori* virulence or host factors. Interestingly, although this was rarely observed in our data and the significance still remains unclear, *H. pylori* invasion into the lamina propria and translocation into lymph tissue has been reported in a previous study (Ito *et al*., 2008).

There are several plausible explanations for the presence of Eubacteria within the lamina propria. Firstly, it is possible that these invading Eubacteria have entered on their own accord, using virulence factors such as flagella to aid motility. Although this mechanism is frequently observed with invasive bacterial genera such as *Salmonella* and *Shigella*, these bacteria are not commonly associated with the gastric microbiota, so this explanation is unlikely (Khoramian-Falsafi *et al*., 1990; Wortel *et al.*, 2022). Secondly, it is possible that these Eubacteria are gastric commensals and have colonised regions of connective tissue within the lamina propria. However, this

explanation is also highly unlikely as the lamina propria is rich in blood vessels and phagocytic immune cells, which would be a hostile environment for most commensal bacteria (Pennelli *et al.*, 2020).

Given that *H. pylori* presence significantly correlated with invasion of Eubacteria into the lamina propria, which is rarely observed in gastric tissue, it is likely that *H. pylori* cells act as a 'gatekeeper' and facilitates entry of Eubacteria through the gastric glands. Recently, Sharafutdinov *et al*. (2024) reported that *H. pylori* strains encoding the trimeric form of HtrA are associated with higher risk of GAC development. In addition to HtrA, *H. pylori* CagA and VacA are also associated with disruption of intercellular junctions and loss of polarity in gastric epithelial cells in vitro (Argent *et al.,* 2008; Murata-Kamiya *et al.,* 2007). As such, it is plausible that data presented in this results chapter demonstrates a later stage of this mechanism, whereby *H. pylori* has disrupted intercellular junctions, which facilitated the entry of Eubacteria through the intercellular junctions and into the lamina propria. Aside from direct damage to intercellular junctions, the effect of several *H. pylori* virulence factors induces inflammation of the gastric mucosa during carcinogenesis. Chronic inflammation eventually results in overexpression of pro-inflammatory cytokines, such as TNF-α and IL1-β, production of neutrophil reactive oxide species (ROS) and anti-oxidative enzymes, which all contribute to glandular atrophy and erosion (Yisireyili *et al.*, 2020). Damage to the gastric mucosa results in a loss of tissue architecture and cellular polarity, resulting in a 'leaky' barrier to bacterial infection. As previously mentioned, bacterial invasion as a result of chronic inflammation is a mechanism involved in several gastrointestinal diseases, such as IBD (Sartor, 2008). Although invasion is not frequently reported in

gastric pathologies, our data suggests that Eubacterial invasion could be secondary phenomenon, which occurred as a result of gastric mucosal damage initially induced by *H. pylori* infection.

The work presented in this results chapter was recently published in the journal Helicobacter (Giddings *et al.,* 2025; Appendix B). In addition to these results, this paper included analysis of additional patient samples and the application of the modified Gram stain, detailed in chapter 6, for validation of RNAscope data.

4.4. Summary

In summary, data presented in this chapter demonstrated that RNAscope ISH combined with IHC is a reliable method for fluorescently labelling both bacterial 16S ribosomal rRNA and antibodies in archived gastric FFPE tissue sections. Although the use of an automated stainer is desirable for optimal staining conditions and reproducibility, a manual staining method can be successfully employed for repeating experiments on the laboratory bench. Results described in this chapter revealed that whilst MUC5AC and E-cadherin expression was relatively stable across Correa's cascade of carcinogenesis, MUC2 expression was elevated in GIM and GAC compared with CG. Interestingly, a correlation between *H. pylori* and Eubacteria presence was also observed in CG and GIM, where it was also observed that Eubacteria 'invade' the lamina propria. The mechanism behind this remains unclear but is possible that Eubacterial invasion is facilitated by the direct action of *H. pylori* loosening intercellular junctions.

Chapter 5: Optimisation of techniques to identify invasive bacteria within gastric histological tissue samples

5.1. Introduction

The use of RNAscope in situ hybridisation (ISH) technology detailed in chapter 4 revealed a significant correlation between *H. pylori* presence and non-*H. pylori* bacterial invasion of the lamina propria throughout the early, middle and late stages of gastric carcinogenesis. Although this technique was a powerful tool for detecting and studying the spatial distribution of non-*H. pylori* bacteria within gastric tissue samples, the identity of these invasive bacteria remained unknown. As such, the following work aimed to optimise methods for isolation of bacteria from gastric histological tissue samples, which could then be identified using full-length 16S ribosomal rRNA gene sequencing and validated with further multiplex imaging approaches.

Although ISH is a popular technique to identify bacterial distribution and abundance within a given histological sample, common ISH probes, such as 'EUB338' target all bacteria in a given sample and do not differentiate between bacterial phyla, genera or species (Okada *et al*., 2022). Despite advances in ISH technology and the increasing availability of highly specific probes against specific bacterial 16S rRNA sequences, many ISH probes still require meticulous design and are expensive. Therefore, ISH remains unsuitable for identification of multiple bacteria and is more suited to small-scale studies which only aim to identify a few bacteria at a time (Kalhor *et al*., 2023) Therefore, the current gold standard for high-throughput bacterial identification is 16S rRNA gene sequencing, which is a culture-free approach that sequences and maps bacterial rRNA sequences against a standardised database (Durazzi *et al*., 2021). Although several sample types can be sequenced, studies are usually conducted on blood, saliva, fresh, or fresh-frozen biopsy tissue for optimal results (Kool *et al*., 2023).

However, the invasive non-*H. pylori* bacteria identified in chapter 4 were embedded in gastric FFPE tissues sections and first required removal before DNA extraction and sequencing could be conducted. As such, in selected samples with high invasion scores, regions of tissue containing invasive bacteria were first removed from the section using laser capture microdissection (LCM). LCM is a powerful technique which uses a laser beam for excision of regions of interest (ROI) from histological tissue. The ROIs can then be used for a variety of downstream analyses, such as mass-spectrometry, 16S rRNA sequencing and metagenomics (Herrera *et al*., 2020; Tsai *et al*., 2023; Wang *et al*., 2010). LCM has been reported in a variety of microbiome studies, with a relatively recent study detailing LCM for removal of mucus-associated bacteria in proximal human colon specimens, followed by successful DNA amplification and 16S rRNA sequencing (Chassaing and Gewirtz, 2018).

Given the promising application of LCM followed by 16S rRNA sequencing in published literature, the first aim of this work was to optimise these methods for isolation of invasive non-*H. pylori* bacteria from gastric FFPE tissue sections outlined in chapter 4. Briefly, consecutive gastric tissue sections were obtained from selected patients with high bacterial invasion observed in chapter 4. Tissue regions containing invasive bacteria were removed from each sample by LCM or manually lifted with a scalpel. The second aim of this work was to characterise the composition of these bacteria using full-length 16S rRNA sequencing, whereby DNA was extracted, and amplicons were sequenced using a full-length nanopore 16S rRNA sequencing protocol and compared against a standardised 16S rRNA database. In addition, punch biopsy

samples collected from one patient with *H. pylori*-positive CG and one patient with *H. pylori*-negative GIM were also sequenced in parallel.

As discussed, although 16S rRNA sequencing provides an identity for bacteria within a given sample, it does not provide information regarding bacterial location or distribution. As such, in addition to bacterial identification, information provided from 16S rRNA sequencing data will also be used to guide the design of specific, custom ACD BIO RNAscope probes against genera or phyla of interest. A proposed workflow for this is outlined in Figure 5.1. By using 16S rRNA sequencing data to guide genus-specific probe design, the presence and location of these bacteria can be confirmed in further consecutive sections of CG, GIM and GAC FFPE tissue. This is a unique approach which, to the best of our knowledge, has not been reported for the identification of bacteria within histological patient tissue samples. However, this method has been reported for viral studies, whereby next generation sequencing (NGS) was used to guide ISH probe design ('NGS-ISH') for detection of viral mRNA in a variety of host samples (Resende *et al*., 2019).

In summary, the presence of non-*H. pylori* bacteria during early stages of carcinogenesis are often overlooked, yet they likely play a pivotal role in driving inflammation and carcinogenesis. As such, identification and characterisation of key invasive bacteria by 16S rRNA sequencing followed by ISH could provide a basis for translation into novel interventions for preventing, diagnosing and surveying patients who are at risk of developing GAC.

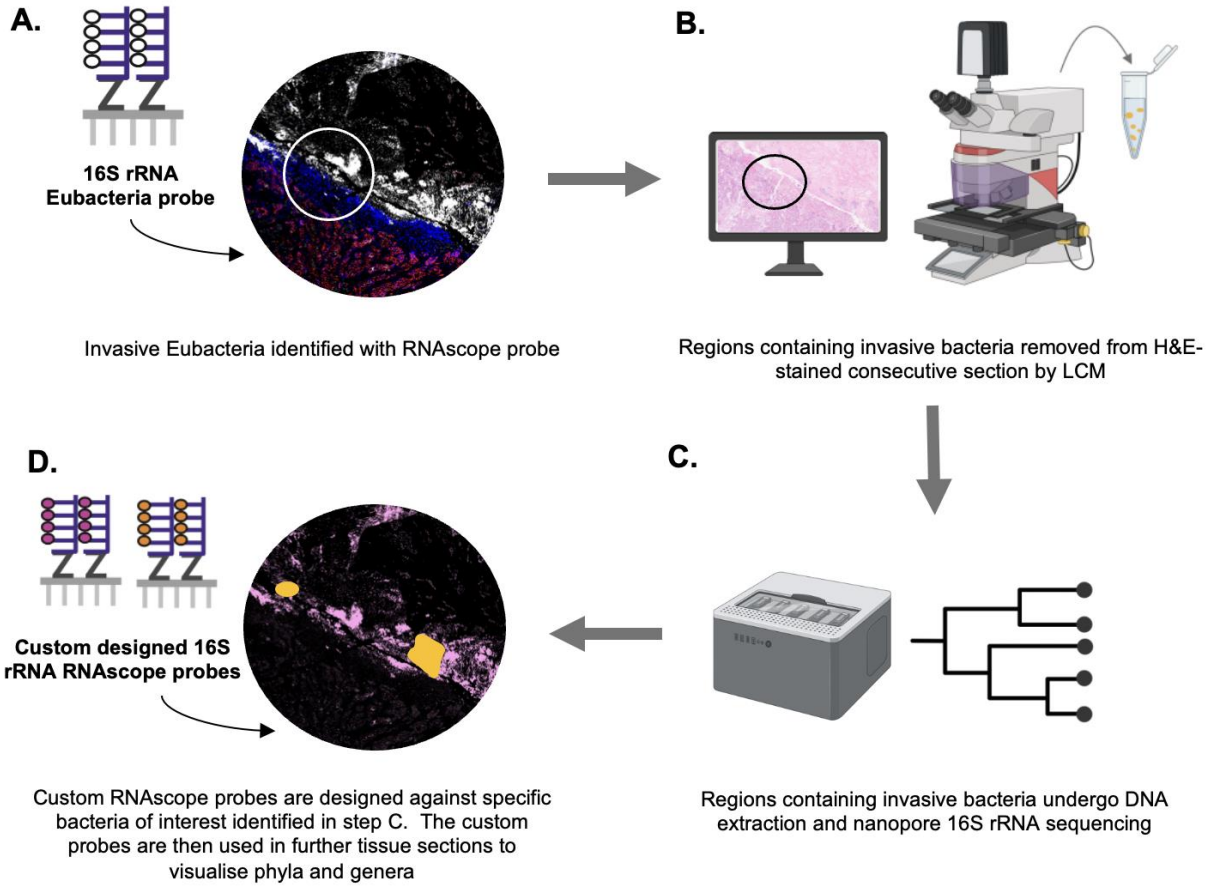

Figure 5.1. A proposed workflow for phyla and genera bacterial identification with custom RNAscope probes. In chapter 4, invasive non-*H. pylori* bacteria were identified with an RNAscope probe against all bacteria 'Eubacteria' (A). Consecutive sections will be obtained from patients with high invasion scores and H&E stained. Tissue areas containing known bacterial invasion will then be excised by LCM (B). DNA will be extracted and amplified from excised tissue using 16S rRNA sequencing (C). Custom designed RNAscope probes will then be designed by ACD Bio to target the 16S rRNA sequences of specific bacteria identified by sequencing (D).

5.2. Results

5.2.1 Laser capture microdissection as a tool to excise regions of bacterial invasion histological tissue

In chapter 4, a GAC sample with a high bacterial invasion score of 4 containing regions with high microbial density was identified and chosen for the first attempt at LCM and subsequent identification of invasive bacteria. Prior to conducting LCM, a consecutive tissue section was first stained with H&E for visualisation of tissue architecture. This section was then viewed using LCM and compared with the previous RNAscope-labelled reference image. In order to limit contamination during LCM, the microscope was thoroughly wiped with 70% ethanol and a sterile open Eppendorf containing DNA/RNA shield was placed on the microscope stage to capture any airborne contaminants. Approximate areas of tissue with known non-*H. pylori* bacterial invasion (LCM GAC^+) in addition to bacteria-free regions (LCM GAC^-) were measured and excised by laser beam into an Eppendorf containing DNA/RNA shield and stored until required. Presence of extracted and fragmented tissue section inside the Eppendorf was confirmed by visual assessment under a light microscope.

Once LCM was successfully conducted on GAC tissue, studies were repeated using consecutive sections of archived punch biopsy GIM or CG FFPE blocks with known *H. pylori* infection from chapter 4 (2 GIM, 1 CG). Each section was H&E stained and viewed using the LCM. Although some areas of bacterial invasion were located and measured, the fragments of tissue were very small and not easily excised and transferred into an Eppendorf. Upon visual inspection, it was observed that the Eppendorf contained negligible extracted tissue (LCM GIM or CG). In order to rectify

this issue and try to obtain CG and GIM tissue for downstream analyses, a further consecutive section was obtained, deparaffinised and rehydrated. Under sterile conditions in a cell culture flow hood, the whole section of rehydrated tissue was lifted off the glass slide using a sterile scalpel, transferred into an Eppendorf containing DNA/RNA shield and stored until required (Lifted GIM or CG).

5.2.2. Quantification of extracted DNA

In addition to laser capture micro-dissected or scalpel-lifted tissue, gastric CG (*H. pylori* -positive) and GIM (*H. pylori*-negative) fresh tissue samples were obtained during gastric punch biopsy from the Queen Elizabeth Hospital, Birmingham and stored in DNA/RNA shield in an Eppendorf. Once all samples of interest were obtained, the Eppendorfs containing fresh, laser capture micro-dissected or scalpel-lifted tissue were briefly centrifuged and digested in Proteinase K. DNA was then extracted into nuclease-free Eppendorfs under sterile conditions in a PCR hood, which was thoroughly cleaned with bleach solution prior to starting the procedure. DNA was then eluted in pre-warmed elution buffer and prepared for 16S rRNA PCR using 16S primers c27f and 1492r. PCR amplification cycles were optimised prior, whereby 35 cycles were used for all FFPE tissue, and 30 cycles were used for biopsy tissue (data not shown).

H. pylori strain SS1 DNA and nuclease-free water were also prepared and used as positive and negative controls, respectively (Figure 5.2). As expected, bands were visible for the two biopsy tissue samples, lifted GIM and CG samples and LCM GAC^{+}. Interestingly, a band was also visible for LCM GAC^{-}, which could be indicative of contamination or bacterial cells which were not detected using RNAscope. Almost no

bands were detected for the LCM CG and GIM samples, which was expected due to difficulties during the procedure and very low sample biomass. Finally, the use of positive and negative controls demonstrated that amplification was successful with minimal contamination. Once DNA presence and size was confirmed, the remaining amplicons were purified and eluted. For each sample, DNA concentration was quantified and compared with approximate tissue area (Table 5.1). As expected, the areas of LCM GIM and CG tissue were minimal, and DNA concentration was too low to quantify as DNA concentration less than 0.5 ng/μL for the three sections. However, lifted GIM and CG consecutive sections of the same samples provided a larger tissue area which yielded higher DNA concentrations, with 3.5 ng ng/μL for the CG sample and 14.3 and 11.5 ng/μL for the GIM samples. LCM GAC^+ and LCM GAC^- regions were relatively small areas in comparison to the scalpel-lifted tissue, yet DNA concentration was 14.2 and 19.7 ng/μL respectively. Interestingly, DNA concentration was higher for the LCM GAC^- sample, which was expected to have a lower concentration due to minimal bacterial invasion observed with RNAscope.

Additionally, although the two biopsy tissue samples were not weighed, DNA concentration was 14.9 and 11.3 ng/μL for the CG *H. pylori*-positive and GIM *H. pylori*-negative samples, respectively. Overall, these were vital steps in confirming that PCR amplification of gastric histological and biopsy tissue samples were free from contamination and provided enough DNA for downstream 16S rRNA sequencing.

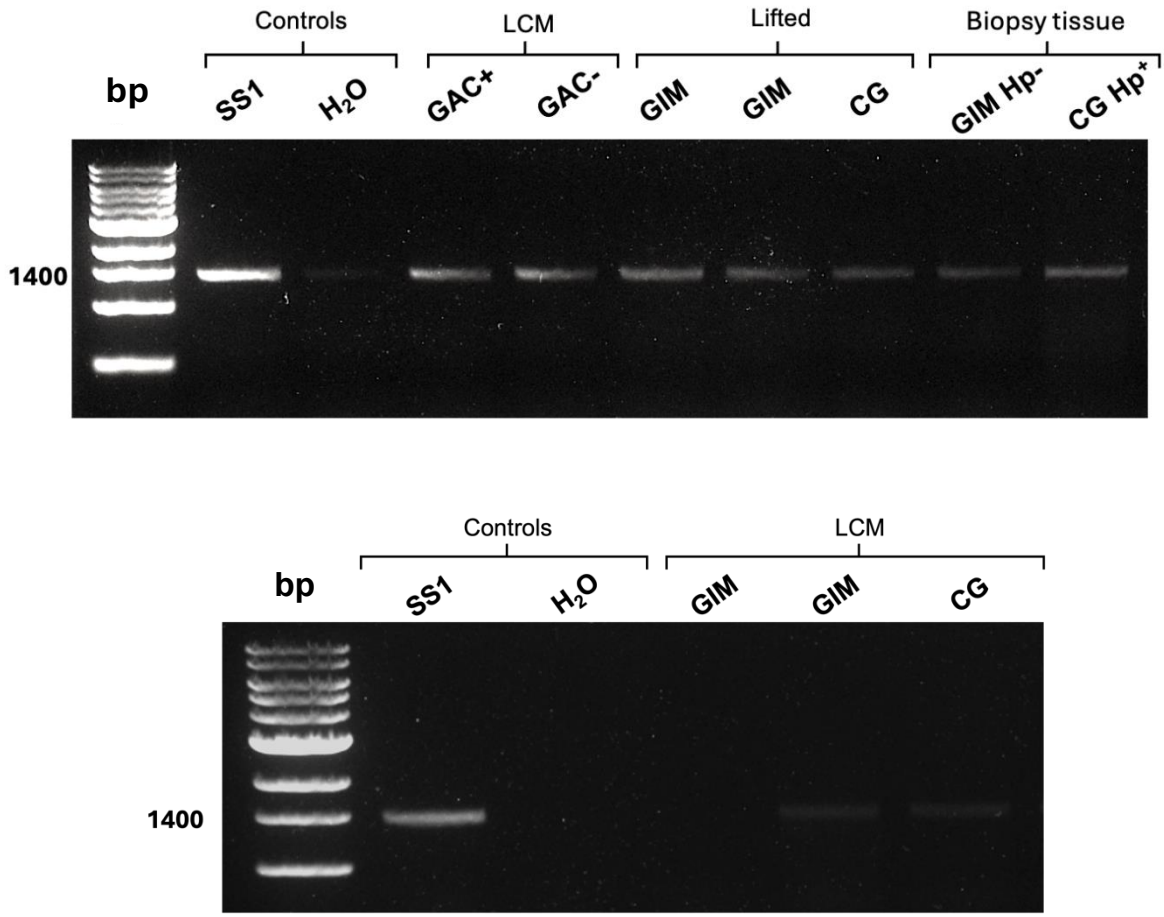

Figure 5.2. Agarose gel electrophoresis (1% agarose) showing PCR products of 16S rRNA full-length gene amplification. FFPE tissue was removed from a microscope slide either by LCM or by sterile removal with a scalpel. Fresh gastric tissue was obtained during routine punch biopsy. All tissue samples underwent DNA extraction and PCR amplification using full-length 16S primers c27f and 1429r. PCR products were visualised by electrophoresis. A 1kb ladder was used and the band for 1400 bp is annotated, corresponding to expected PCR amplicon size. Positive control was *H. pylori* SS1 DNA and negative control was sterile DNase free water.

	LCM		Tissue		Lifted			LCM		
Sample	**GAC+**	**GAC-**	**CG Hp$^+$**	**GIM Hp-**	**CG**	**GIM**	**GIM**	**CG**	**GIM**	**GIM**
Concentration (ng/μL)	14.2	19.7	14.9	11.3	3.5	14.3	11.5	<0.5	<0.5	<0.5
Approximate tissue area (mm^2)	0.79	0.91	N/A	N/A	24.2	5.5	5.11	0.18	0.15	0.1

Table 5.1. Individual sample tissue area and subsequent concentration of amplified and purified DNA. FFPE tissue was removed from a microscope slide either by LCM or by sterile removal with a scalpel; fresh gastric tissue was obtained during routine punch biopsy. FFPE tissue areas were estimated by measuring regions from a consecutive section on QuPath software. DNA was extracted from all tissue samples, amplified by PCR and then purified. DNA was eluted in pre-warmed elution buffer; 1 μL was immediately quantified using a Qubit spectrophotometer.

5.2.3. Full length 16S rRNA sequencing

Once extracted DNA was successfully purified and quantified, amplicons were prepared for full length 16S rRNA sequencing using the Oxford Nanopore Technologies Native Barcoding Kit 24 V14 protocol. Raw data were then aligned with the SILVA 138.2 database. In this study, two sequencing runs were conducted due to issues with the GRID sequencer during the first run, whereby the computer crashed four hours into the programme producing low sequence reads for each sample (data not shown). As such, all data presented in this chapter are from the second successful sequencing run which was completed over 24 hours.

During data analyses, it was observed that *Helicobacter* genera were a consistent contaminant throughout all samples including the barcoded 'negative' control with a relative abundance of ~99% across all of the samples (Figure 5.3) This was unexpected and a concern, as aside from *H. pylori* presence in the 'negative' barcoded controls, the GIM sample was also clinically *H. pylori*-negative and unlikely to have a high relative abundance of *Helicobacter* genera. Furthermore, the raw basecalled data indicated that the second highest relative abundance across all samples were unknown genera. The reason behind this remains unclear but is likely due to the SILVA 138.2 database not recognising these sequences, possibly indicating bacterial evolutionary divergence which were not recognised by the database

In order to rectify this issue, the data were adjusted (organised), whereby *Helicobacter* and unknown reads were discarded from each sample and any genera with reads below 10 were also discounted as these were likely contaminants.

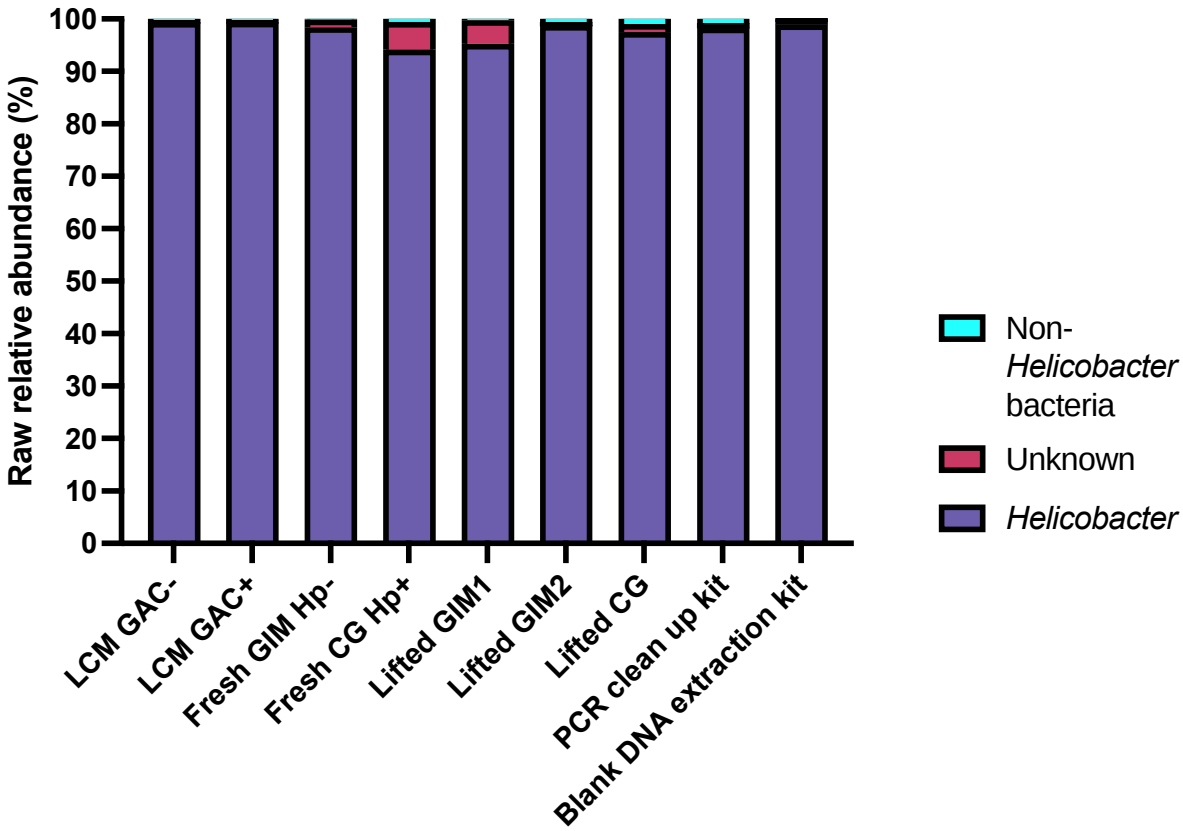

Figure 5.3. Raw full length nanopore sequencing data showing relative abundance of genera. DNA was extracted and amplified from FFPE and fresh tissue samples, as previously described. Amplicons were prepared for 16S rRNA nanopore sequencing. Minimum and maximum read lengths were 1200 and 2000 base pairs, respectively. Blank DNA extraction and PCR clean up kit eluate were also sequenced to check for contamination. Per sample, relative abundance of each genus was calculated by dividing individual genus reads over total reads x 100.

The resulting dataset therefore presented non-*Helicobacter* bacteria per sample which were also unlikely to be contaminants. The LCM GAC$^-$ sample was a region of GAC tissue which contained no obvious bacterial invasion as identified by RNAscope. Interestingly, sequencing data suggested that excluding *Helicobacter,* this region had a relative abundance of 70% *Acinetobacter* and approximately 30% *Pseudomonas* genera, with negligible other bacterial genera identified. Conversely, the LCM GAC$^+$ sample, which was high in Bacteria according to RNAscope data, had a relative abundance of approximately 80% *Acinetobacter*, ~10% *Pseudomonas* and a small percentage of *Streptococcus*, in addition to low numbers of opportunistic genera, including *Burkholderia* and *Staphylococcus* (Figure 5.4). Taken together, although this dataset must be used with caution due to exclusion of *Helicobacter* and unknown reads, these data indicate that regions of Bacterial colonisation which were previously identified using RNAscope are indeed diverse and composed of multiple genera.

For the lifted *H. pylori* positive GIM and CG samples, non-*Helicobacter* bacteria mostly comprised *Ralstonia* and *Acinetobacter* (Figure 5.5A). This was a surprising finding, as *Ralstonia* presence is not often associated with gastric pathologies and could be a contaminant found within the paraffin or the scalpel. Nonetheless, these data also indicated that *H. pylori*-positive GIM samples showed more bacterial diversity in comparison to the *H. pylori*-positive CG sample. Furthermore, the GIM samples contained genera associated with pathologies of the oral cavity including *Pseudomonas, Burkholderia, Fusobacterium, Veillonella* and *Streptococcus,* whereas the CG sample contained less virulent genera such as *Lactococcus*. An additional observation was the presence of gastrointestinal and oral microbiota in the GIM

samples, further suggesting that the gastric microbiome alters during the transition from CG to GIM.

Overall, as expected, the CG *H. pylori*-positive and GIM-*H. pylori* negative biopsy tissue samples were rich in bacteria in comparison to histological tissue sections (Figure 5.5B). The *H. pylori*-positive CG sample showed higher bacterial diversity compared with the *H. pylori*-negative GIM sample and contained several genera of interest, including *Veillonella, Streptococcus, Pseudomonas, Burkholderia* and *Fusobacterium.* Interestingly, these findings corroborate with data presented in Chapter 4, which suggest that *H. pylori* presence is associated with an enrichment and invasion of non-*Helicobacter* bacteria. Another key observation was the presence of *Acinetobacter* and *Pseudomonas*, which were higher in the*. pylori*-negative GIM sample. Given that these genera were also identified in the LCM GAC tissue samples, it is plausible that these genera are associated with the final stages of Correa's cascade of carcinogenesis.

5.3. Discussion

5.3.1. Laser capture microdissection for removal of gastric FFPE tissue

Previous findings outlined in chapter 4 identified significant presence of invasive non-*H. pylori* bacteria within the lamina propria of gastric FFPE tissue sections. Methods described in this chapter then aimed to confirm the identity of these bacteria with 16S rRNA sequencing, by first excising regions of bacterial invasion from selected patients.

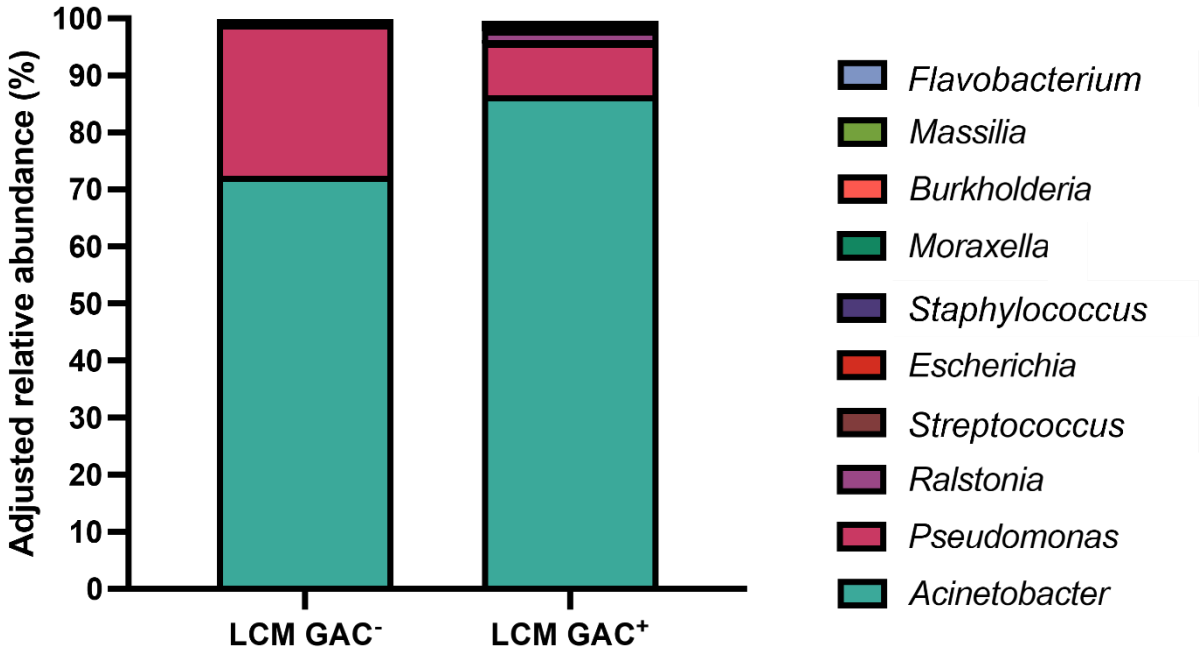

Figure 5.4. Adjusted full-length nanopore sequencing data showing relative abundance of non-*Helicobacter* genera in LCM FFPE GAC patient tissue section. Regions no obvious colonisation (GAC^-) and clear bacterial invasion (GAC^+) were removed from gastric FFPE tissue sections using LCM and transferred into an Eppendorf containing DNA/RNA shield. DNA was then extracted, amplified and prepared for Nanopore sequencing. *Helicobacter* and unknown genera were excluded due to contamination and genera with reads <10 were also excluded. Relative abundance of the remaining genera was calculated by dividing individual reads over total reads x 100.

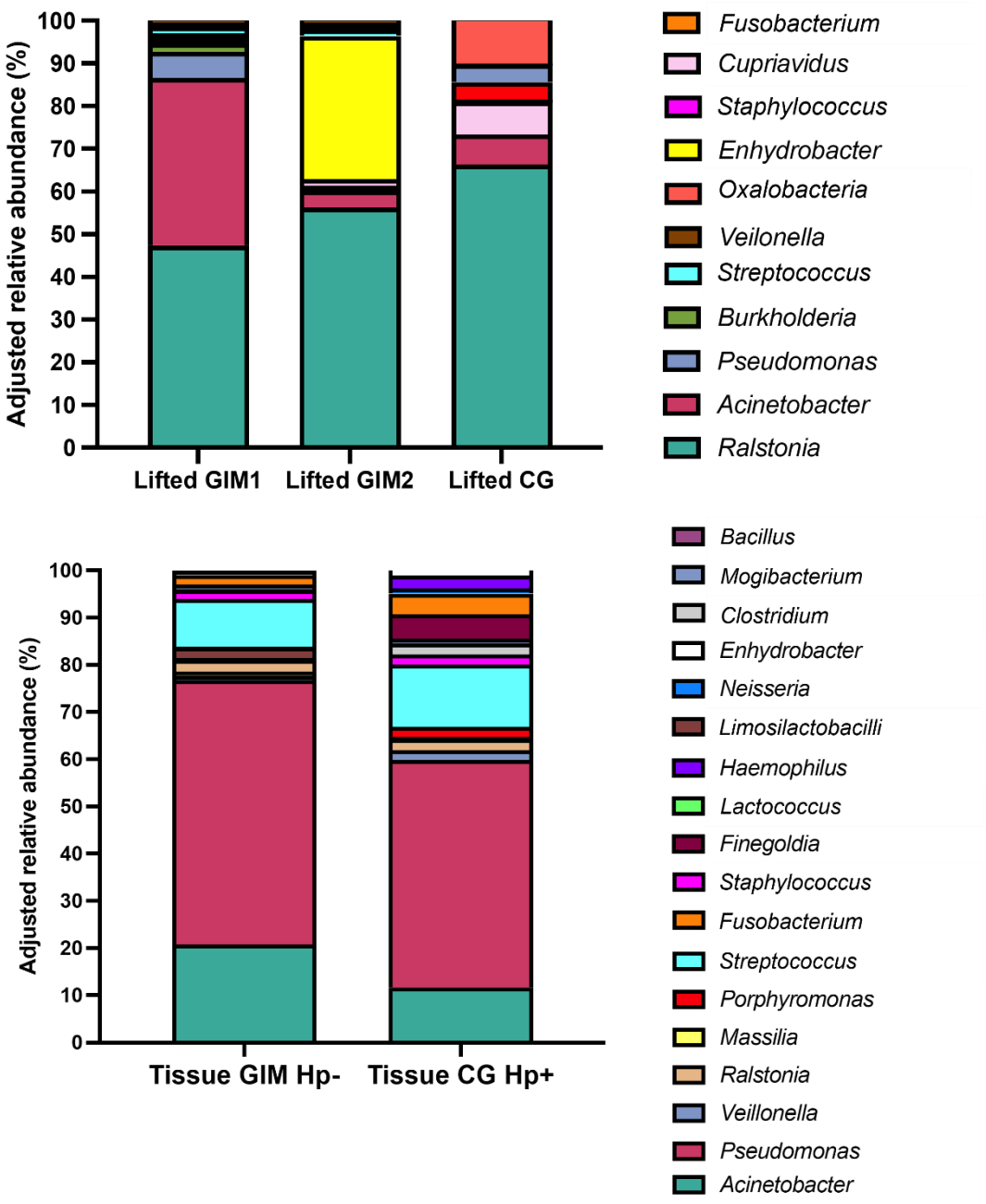

Figure 5.5A and Figure 5.5B. Adjusted full-length nanopore sequencing data showing relative abundance of non-*Helicobacter* genera in lifted FFPE tissue sections and biopsy tissue. Regions of clear bacterial invasion in CG and GIM FFPE tissue as previously identified using RNAscope were removed using by manually lifting with a scalpel under sterile conditions. Each sample was transferred into an Eppendorf containing DNA/RNA shield. DNA was then extracted, amplified and prepared for Nanopore sequencing. *Helicobacter* and unknown genera were excluded due to contamination, genera with reads <10 were also excluded. Relative abundance of the remaining genera was calculated by dividing individual reads over total reads x 100.

Using consecutive tissue sections of the selected patients, regions containing invasive bacteria as previously indicated by RNAscope were removed by LCM from the glass slide and homogenised, prior to DNA extraction and 16S rRNA sequencing. In this study, although LCM was successful for removal of selected areas within gastrectomy-derived GAC tissue, the LCM was unable to remove smaller areas from punch biopsy tissue. In order to rectify this issue, the whole tissue sample was later lifted from additional sections by manual removal with a scalpel in a flow hood. As the whole sample was removed, rather than small, selected regions, this approach yielded far more material in comparison to LCM. Interestingly, a similar observation was reported by Jeroch *et al*., 2023 who also compared LCM with scalpel removal and noted that larger sample correlated with increased DNA yield. Taken together, these data suggest that although LCM shows promise for excision of interesting material from histological samples, its reliability varies in proportion to tissue area. As such, when designing further experiments with LCM, it is important to consider the biopsy and tissue type to ensure enough sample is available for accurate removal of tissue regions.

5.3.2. DNA extraction of gastric FFPE and fresh tissue

Once selected regions of tissue from GAC, CG and GIM FFPE patient samples were successfully obtained, DNA were extracted and amplified from each sample. A standard ZymoBIOMICS DNA extraction kit was used for all extraction steps, despite frequent reports that DNA extraction of FFPE tissue can be difficult. Several studies have reported that formalin often induces irreversible cross-linking effects on DNA during fixation steps, rendering some samples unsuitable for successful DNA extraction (Singh *et al*., 2020). Additionally, studies have reported that most resultant

DNA extracted from FFPE tissue is usually low quality, yield and often contaminated by reagents used during tissue preparation (Gilbert *et al*., 2007).

Although DNA was successfully extracted from the samples detailed in this chapter and visualised on a gel, the DNA bands were generally dim in comparison with the positive control. In addition, the punch tissue which was unsuccessfully removed by LCM had very dim bands, despite Qubit quantification suggesting negligible DNA content. Taken together, although these initial observations suggest that DNA was successfully extracted from each sample with the standard kit, DNA was of low quality and contamination was possibly an issue.

Unfortunately, contamination during the FFPE process is difficult to avoid due to the multitude of steps involved, such as tissue resection, transportation, processing, fixing and paraffin-embedding (Carll *et al*., 2022). Nonetheless, several steps were taken to mitigate contamination, such as the use of a PCR hood and 70% ethanol, it is likely that contamination arose during the LCM procedure or within the original paraffin embedding process itself. As such, given that FFPE tissue is notoriously difficult to extract DNA from, future studies should instead use a specialised FFPE DNA extraction kit in order to produce a much higher yield and quality of DNA. The majority of FFPE DNA extraction kits contain ‘clean-up’ steps which reverse the impact of damage obtained during the FFPE process, such as removal of excess paraffin, cross-linking, airborne contaminants and excess calcium content (Sarnecka *et al*., 2019).

5.3.3. Full-length 16S rRNA sequencing of CG, GIM and GAC FFPE tissue

Once raw data was obtained from the GRID sequencer and extracted to Microsoft Excel, the first major observation was that reads for every sample, including 'negative' DNA extraction and PCR clean-up kit controls, were dominated by *Helicobacter* genera in both sequencing runs (Figure 5.3). Although *Helicobacter* presence was expected in the lifted CG and GIM samples as these were *H. pylori*-positive, it was hypothesised that their relative abundance would be relatively low. Furthermore, given that negligible *Helicobacter* were detected by RNAscope in the GAC sample, a relative abundance of ~99% was surprising.

During the first sequencing run, amplicon preparation was conducted in a cell-culture flow hood which had been cleaned with UV and 70% ethanol. However, subsequent sequencing data for every sample, including the negative controls, were dominated by *Helicobacter* for all samples (data now shown). Despite measures taken to ensure sterility and cleanliness, it was initially hypothesised that contamination arose, as cultures of *H. pylori* were previously routinely prepared in the same flow hood within the laboratory. In addition, it was also hypothesised that contamination by *H. pylori* arose as a result of amplicon carryover during preparation of the PCR positive control *H. pylori* SS1 DNA amplicon. Therefore, in order to rectify these issues, new amplicons were prepared for a second sequencing run in a HEPA-filtered PCR hood, whereby filtered air and UV sterilisation prevented cross-contamination between samples and contamination from the air flow was unlikely. In addition, every sample was individually and separately prepared for PCR amplification with UV sterilisation between each. The *H. pylori* SS1 DNA was also prepared last to negate the possibility of amplicon

carryover. Unfortunately, regardless of stringent measures in place to limit contamination for a second time, contamination by *Helicobacter* genera was still apparent in every sample.

Additionally, ~99% *Helicobacter* genera were detected in a blank DNA extraction and PCR clean-up kit eluate. The reason for this is unclear but given that contamination occurred within kits and regardless of where amplicons were prepared, it is possible that *Helicobacter* contamination arose due to cross-contamination of laboratory items, such as pipettes or laboratory coats used in steps before PCR amplification. As such, in the future, further steps should be taken to minimise contamination risk, such as wearing a clean laboratory coat, conducting all work in a specialised PCR room and by not using pipettes or other laboratory items which are also used for other work.

Furthermore, a major cause of contamination in this study is likely due to low-sample biomass. This phenomenon is frequently reported, whereby high biomass samples such as faeces or soil contain a high abundance of 'real' bacteria within the sample, which dominates any sequencing reads introduced by contaminants. In contrast, ultra-low biomass samples are easily overwhelmed and dominated by contaminating sequences (de Steenhuijsen Piters and Bogaert, 2020). Ideally, sequencing the original biopsy tissue immediately after removal from the patient would have provided more sample volume and therefore higher biomass, likely minimising the likelihood of contaminants overwhelming the sample. However, given that histological tissue sections were instead used for this study, methods were selected to cleanse the data by removing all *Helicobacter* genera and any sequencing reads <10 which likely rose

from external contamination and were also present in the 'negative' controls. Currently, there is no gold standard for controlling or removal of contaminating 16S rRNA sequencing reads and techniques to filter these vary between studies. For example, commonly used approaches include application of abundance filters, removal of obvious contaminants and removal of sequences found in negative controls in a variety of published 16S rRNA sequencing studies (Bittinger *et al*., 2014; Glassing *et al*., 2016; Willner *et al*., 2012). As such, the decision to remove all *Helicobacter* genera and any sequencing reads <10 were selected following extensive literature searches.

5.3.4. Genera of interest in GAC, CG and GIM FFPE tissue

Despite the exclusion of *Helicobacter* reads, several other non-*H. pylori* genera of interest were identified by 16S rRNA sequencing. For the two regions of GAC tissue extracted by LCM (GAC^+ and GAC^-) the highest reads were obtained from *Acinetobacter*, *Pseudomonas* and *Streptococcus*. Although *Pseudomonas* is not associated with the normal gastric mucosa and is occasionally identified as a kit contaminant, there is some evidence for its role in carcinogenesis. For example, a recent study observed an inverse correlation between *H. pylori* and *Pseudomonas* infection in CG patients, suggesting that *Pseudomonas* might play a role independent of *H. pylori* in the later stages of gastric carcinogenesis (Kachuei *et al*., 2020; Salter *et al*., 2014). In addition, *Pseudomonas* is often associated with hospital-acquired infection and has been shown to translocate from the gastrointestinal tract into the bloodstream in critically unwell individuals and cancer patients (Markou and Apidianakis, 2014). As such, although *Pseudomonas* is not typically associated with

the gastric microbiota, its presence in a cancer biopsy sample is certainly not unexpected.

In addition, *Acinetobacter* were identified in both GAC samples. Although not frequently isolated from the gastric microbiota, *Acinetobacter* is emerging as a multi-drug resistant (MDR) genus and is often associated with infection or immunocompromised individuals. As such, its presence within a GAC sample could be as a result of the patient being immunocompromised or more susceptible to infection. Interestingly, a 2021 study revealed that the human gastrointestinal tract acts as a reservoir for several *Acinetobacter* species, which is elevated in response to inflammation during onset of inflammatory bowel diseases such as colitis and IBD (Fu *et al*., 2024; Rathinavelu *et al*., 2003). Taken together, it is possible that a similar effect is observed during gastric carcinogenesis, whereby *Acinetobacter* abundance increases in response to mucosal inflammation induced by *H. pylori.*

For the lifted *H. pylori*-positive GIM and CG tissue, 16S rRNA sequencing identified several genera which were not present in the GAC tissue. For example, *Ralstonia* and *Acinetobacter* were the most abundant genera. As discussed, *Acinetobacter* presence could indeed be a result of inflammation. However, it is worth noting that *Ralstonia* is a common contaminant of laboratory kits, such as DNA extraction kits and is also frequently isolated from paraffin embedded tissue (Lam *et al*., 2021; Salter *et al*., 2014). As such, although a high abundance of *Ralstonia* was identified across the three lifted FFPE samples, its presence is likely a result of contamination during the paraffin-embedding process. In contrast to GAC tissue, *Pseudomonas* abundance was far

lower for the lifted *H. pylori*-positive GIM and CG FFPE tissue. As discussed, although *Pseudomonas* is often associated with infection of immunocompromised individuals and is rarely isolated from CG and GIM patients.

Interestingly, although every sample was clinically *H. pylori*-positive, the two lifted GIM samples generally showed greater microbial diversity compared with the lifted CG sample. Within the two GIM patient samples, aside from *Acinetobacter* and *Ralstonia*, a number of bacterial genera associated with the gastrointestinal tract and oral cavity were also enriched, including bacteria often associated with the oral cavity or gastrointestinal tract, such as streptococci, staphylococci and fusobacteria. This was an interesting observation which correlated with data presented in chapter 4, suggesting that bacterial abundance and diversity increases from CG to GIM.

5.3.5. Genera of interest in *H. pylori*-positive CG biopsy tissue

Greater microbial sequence diversity was found for both the *H. pylori*-positive CG and *H. pylori*-negative GIM biopsy tissue samples in comparison to LCM or lifted FFPE tissue (Figure 5.4A and 5.4B). This was expected, given the higher sample biomass and therefore reduced likelihood of contaminating sequencing reads overwhelming the sequencing data, as previously discussed (de Steenhuijsen Piters and Bogaert, 2020). Interestingly, the *H. pylori* positive CG tissue sample showed greater microbial diversity in comparison with GIM *H. pylori*-negative sample further suggesting that *H. pylori* presence is associated with microbial enrichment, irrespective of disease state. Bacterial genera of interest detected in the CG patient included oral bacteria such as *Veillonella, Streptococcus, Porphyromonas* and *Fusobacterium*. This was an

interesting finding, which correlated with sequencing data for the lifted *H. pylori*-positive CG and GIM tissue sections. Taken together, given that oral bacteria were identified in both FFPE and biopsy CG and GIM tissue, it is plausible that these bacteria play a role in driving inflammation or carcinogenesis. Although more patient samples are required to determine the presence of oral bacteria within CG and GIM samples, it is possible that the invasive bacteria identified in chapter 4 are indeed composed of oral bacterial species which have arrived in, colonised and invaded the gastric mucosa (Bakhti and Latifi-Navid, 2021).

In addition to oral bacteria, genera associated with the gastrointestinal tract such as *Clostridium*, were also identified in the *H. pylori* positive CG sample. *Clostridium* is not commonly isolated from the gastric mucosa and is usually associated with the colon. However, proton-pump inhibitor (PPIs) and antibiotic therapy can also increase the risk of *Clostridium* infection (Patil and Blankenship, 2013). Although no information was provided about the patient's medication history, it is possible that PPI and antibiotic use also influenced the bacterial genera identified from this patient.

5.3.6. Genera of interest in *H. pylori*-negative GIM biopsy tissue

Acinetobacter, Pseudomonas, Ralstonia and *Streptococcus* were all detected in the biopsy *H. pylori*-negative GIM sample, possibly suggesting as role for these genera in gastric carcinogenesis, independent of *H. pylori* infection. Interestingly, *Acinetobacter* and *Pseudomonas* in particular were elevated in the GIM sample compared with CG. Given that a high abundance of these genera was also identified in GAC, it is plausible that they are highly adapted to surviving with inflammatory environments such as the

later stages of carcinogenesis. However, it is worth noting that although this patient was clinically *H. pylori*-negative at the time of biopsy, no information was provided on previous *H. pylori* infection which could have influenced downstream presence of these bacteria.

In comparison with the *H. pylori*-positive CG patient, microbial diversity was generally lower with far fewer genera detected. Although abundances were low, oral genera such as *Streptococcus, Porphyromonas* and *Fusobacterium* were detected, which further suggests that either this patient was previously diagnosed with *H. pylori,* or that oral bacteria are associated with carcinogenesis irrespective of *H. pylori* infection. In contrast, elevated *Limosilactobacillus* and *Lactococcus* were also identified, suggesting an inverse relationship with *H. pylori* infection. The presence of these genera are typically associated 'normal', non-inflamed gastric mucosa and therefore correlate with the *H. pylori* status of this patient. Furthermore, *Lactococcus* have been shown to alleviate *H. pylori*-induced inflammation in vitro, which might also suggest a protective role for these genera within this patient sample (Chen *et al*., 2019).

Although 16S rRNA sequencing identified particular genera of interest in CG, GIM and GAC, the direct link between *H. pylori* and non-*H. pylori* bacteria presence were investigated using these data due to contamination issues resulting in exclusion of *Helicobacter* genera. Furthermore, whilst a potential increase in microbial diversity from CG to GIM was observed using this approach, no 'true negative', such as an *H. pylori*-negative normal adjacent to tumour (NAT) or healthy biopsy tissue was sequenced. It therefore remains uncertain whether bacterial identified in these data

were present as a result of *H. pylori* infection or were commensals of the gastric mucosa and exist regardless of *H. pylori* presence.

5.4. 16S rRNA sequencing data as basis for RNAscope probe design

16S rRNA sequencing was first conducted to provide an identity for invasive non-*H. pylori* bacteria outlined in chapter 4 and most importantly, to provide a basis for further RNAscope custom probe design for visualisation of specific phyla and genera in gastric histological samples. Given that *Acinetobacter* and *Streptococcus* were consistently identified across the samples and evidence exists for their role in gastric carcinogenesis, custom RNAscope probes were therefore designed against the 16S rRNA sequences of these bacteria (Fu *et al*., 2024; Rathinavelu *et al*., 2003). Although *Pseudomonas* was also identified, probes were not designed for this bacterium as it is a commonly reported sequencing contaminant, and few studies have reported its association with GAC. Unfortunately, due to time constraints this work was not completed as part of the project but will be pursued in future studies within the laboratory.

5.5. Summary

In summary, data presented in this chapter demonstrated that although LCM was a promising tool for isolation of regions from FFPE tissue sections, it was more suitable for larger tissue samples with greater surface area. Furthermore, although DNA was successfully extracted from gastric FFPE tissue, these samples were low-biomass and

overwhelmed by microbial contamination. As such, future studies using this technique could benefit from a specialised FFPE DNA extraction kit or high-biomass, fresh biopsy samples. Nonetheless, despite the technical issues presented in this chapter, preliminary results confirmed the identity of several non-*H. pylori* bacteria associated with gastric carcinogenesis that were previously identified using RNAscope probes. Given that *Streptococcus* and *Acinetobacter* were identified consistently in CG, GIM and GAC samples, future studies will use custom designed RNAscope probes against the 16S rRNA sequences of these bacteria to validate and identify their presence in further tissue sections.

Chapter 6: A tool for rapid histological detection of *Helicobacter pylori* and other gastric bacteria in precancer and cancer

6.1. Introduction

Previous findings outlined in chapter 4 identified a significant correlation between *H. pylori* and non-*H. pylori* bacterial invasion during early, middle and late stages of gastric carcinogenesis. Results presented in chapter 5 then optimised methods to identify these invasive bacteria using 16S rRNA sequencing of gastric FFPE tissue, whereby despite technical issues, sequences of several genera such as *Streptococcus* and *Acinetobacter* were enriched in GAC and *H. pylori*-positive CG and GIM patient samples. Taken together, these results contrast the current dogma that the gastric microbiota is enriched in *H. pylori*-negative individuals and also propose a causative role for non-*H. pylori* bacteria in carcinogenesis. Despite routine identification of *H. pylori* using histological tools, no suitable method has been validated for rapid detection of invasive bacteria in gastric histological sections.

Currently, patients presenting with symptoms of CG and GIM are routinely screened for *H. pylori* infection and treated, if necessary. Common symptoms indicative of infection include nausea, acid reflux, heartburn, abdominal pain and bloating (Kavitt *et al*., 2019). Patients who are diagnosed with *H. pylori* infection are treated with a combination of antibiotics and proton pump inhibitors (PPIs). Given that GIM is clinically termed ‘the point of no return’, antibiotics do not provide a benefit. Instead, patients who are at high risk of developing GAC also receive routine endoscopic and histological surveillance following *H. pylori* eradication (García-Morales *et al*., 2023; Lee and Kim, 2015). Currently, surveillance only monitors progression of GAC by identifying further histological changes to the gastric mucosa, as there is a lack of evidence on current biomarkers (Banks *et al*., 2019). Therefore, a biomarker for GAC

is urgently required for patient stratification and for identifying at-risk patients where further intervention is required.

Invasive bacteria identified in this study could serve as a novel biomarker for GAC. However, further work is required to determine whether invasive bacteria increase the risk of patients progressing from CG or GIM to GAC. Whilst non-*H. pylori* bacteria were successfully identified by RNAscope in situ hybridisation (ISH), it is an expensive and laborious technique which is not applicable to large scale studies (Kalhor *et al*., 2023). Therefore, a rapid and cost-effective method for routine identification of non-*H. pylori* bacteria within clinical biopsy samples is preferable. This could be used in the first instance to easily identify and monitor patients with invasive bacteria for progression to GAC. It could then be integrated as part of routine clinical care to identify patients that require further intervention, such as antibiotic treatment to clear invasive bacteria, thereby reducing the risk of progression to GAC.

H. pylori are commonly identified in gastric endoscopic biopsy sections by Haematoxylin and Eosin (H&E) staining, which is analysed by a pathologist (Batts *et al*., 2013). H&E is a principal stain used in routine histology and is composed of both an acidic and basic dye, which stain acidic and basic compartments of a given tissue section. As such, it provides an overview of tissue microanatomy, immune cell presence or distribution and inflammation (Fischer *et al*., 2008). H&E has excellent sensitivity for *H. pylori* cells and they are easy to identify, as a pink or red spiral-shaped organism within the gastric glands (Lee and Kim, 2015). Additional histological stains are also used for identification of *H. pylori* and include Giemsa, Gimenez and Warthin-

Starry stain. Although in comparison to H&E, these stains are less favoured due to low sensitivity and high likelihood of false-positive or false-negative staining (Yadav and Sagar, 2022). Whilst several stains exist for detection of *H. pylori* specifically, other bacteria are not readily identified with these stains due to lack of contrast between the bacteria and the tissue.

A common laboratory technique for identification of bacteria is the Gram stain, which differentiates bacteria into Gram-positive or Gram-negative, based on the structural properties of their cell walls (Gram, 1884). The Gram stain usually involves collecting a sample on a sterile swab and smearing it onto a glass microscope slide and is not routinely conducted on histological biopsy samples. However, several attempts have been made over the last 100 years to modify the Gram stain to reveal the complexity of bacterial infections in mammalian tissue samples, often involving an additional counter stain to differentiate between tissue and bacteria. One of the first modifications was by Brown and Brenn (1931), followed by Brown and Hopps (1973) who developed a widely used variation involving an additional fixative step and addition of a yellow Tartrazine counterstain to label tissue. In recent years, Becerra *et al.* (2016) described a further variation of the modified Gram stain and highlighted its potential use in clinical diagnosis of skin infections. Whilst these modifications have allowed for detection of bacteria within paraffin-embedded biopsy tissue, there remains discrepancies between studies and loss of Gram-negative staining is frequently reported (Engbaek *et al.,* 1979).

Although H&E and Giemsa stains are commonly reported for preliminary detection of *H. pylori* within gastric biopsy tissue, to our knowledge, no studies exist which also include the Gram stain for this purpose. Given that Gram stains should clearly differentiate between Gram-positive and negative bacteria, we hypothesised that with slight modifications, the Brown and Hopps Gram stain could be implemented for identification of both *H. pylori* and invasive non-*H. pylori* bacteria in gastric FFPE tissue sections. In addition to bacterial identification, the modified Gram stain should also provide information about bacterial distribution, abundance and diversity within a given sample. Although it is widely reported that the gastric microbiota alters during carcinogenesis, no studies have investigated a correlation between bacterial distribution, morphology, diversity and GAC risk. As such, the modified Gram stain is a promising tool for preliminary stratification of patients at risk of GAC and will further our understanding of the significance of non-*H. pylori* bacteria during carcinogenesis.

Therefore, the aims of the work presented in this chapter were to first validate a reliable and rapid detection method for identification of *H. pylori* and non-*H. pylori* bacteria in gastric histological tissue sections. Consecutive tissue sections were obtained from selected patients with a high abundance of *H. pylori* and non-*H. pylori* bacteria (as identified in chapter 4). Sections were then stained with the modified Gram stain and Gram-positive and negative bacteria were visualised with a light microscope. The modified Gram stain was also compared against H&E staining and previous RNAscope images. In addition, the suitability of the modified Gram stain as a future stratification tool was then assessed by repeating staining on additional CG and GIM sections with varying bacterial invasion scores and bacterial abundance.

6.2. Results

6.2.1. Comparison of conventional Gram stain with modified Gram stain for identifying bacteria within gastric tissue

In the first instance, the traditional Gram staining method without modification was assessed and compared with the modified Gram staining method to confirm the requirement for a yellow counterstain when using this technique to identify bacteria within gastric FFPE tissue sections. An archived *H. pylori*-positive GIM patient with high bacterial invasion, as previously identified using RNAscope labelling, was selected and two further consecutive 4 μM thickness tissue sections were obtained from the patient block. Both tissue sections were deparaffinised and rehydrated, with the first tissue section stained using the traditional Gram staining method (Figure 6.1A). The second tissue section was stained with the traditional Gram staining approach, with the addition of Gallego solution fixative and 0.1% picric acid-acetone, which gave the tissue sample a yellow colour (Figure 6.2A). Each tissue section was cleared in xylene, mounted in DPX mountant and visually assessed using a light microscope and whole slide-scanner and compared with the previous RNAscope-labelled section to identify regions containing bacteria.

Using the traditional Gram staining method, the whole tissue section turned pink with little contrast between histological features (Figure 6.1A). Furthermore, regions of tissue containing bacteria were viewed at 100x magnification with oil immersion, yet bacteria were not visible against the pink background of the tissue (Figure 6.1B, C and D). In contrast, the tissue section stained with the modified Gram stain was yellow in

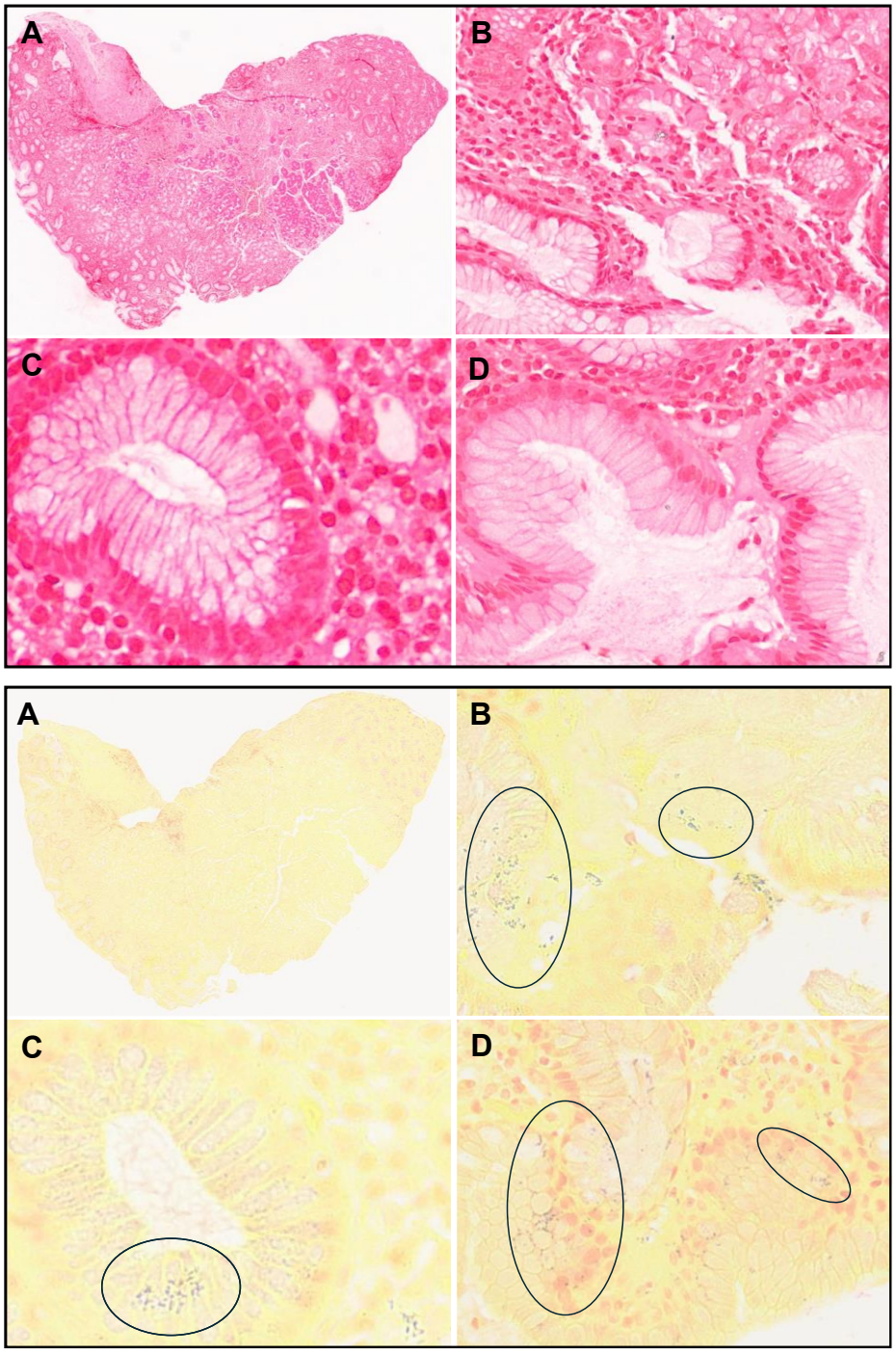

Figure 6.1 and Figure 6.2. Comparison of Gram stain with modified Gram stain for identification of bacteria in GIM tissue. Archived consecutive sections of GIM FFPE tissue were deparaffinised and stained with the traditional Gram stain (Figure 6.1) or the modified Gram stain (Figure 6.2). Sections were viewed at 4x magnification with a light microscope and staining was compared (Figure 6.1A and Figure 6.2A). Regions of each section containing bacteria were then viewed at 100x magnification with oil immersion to visualise bacterial morphology (Figure 6.1 A, B and C and Figure 6.2 A, B and C). Black ovals indicate regions of tissue with bacterial cells present.

appearance (Figure 6.2A). Histological features, such as glands and lamina propria were more visible compared with the traditional Gram-staining approach. The same regions containing bacteria were magnified and the presence of Gram-positive cocci and diplococci were identified throughout the gastric glands and within lamina propria (Figure 6.2B, C and D). These preliminary data therefore suggest that the modified Gram staining method, in comparison with traditional Gram staining methods, was more suitable for staining FFPE tissue given that the picric-acid acetone counterstain provides contrast between the purple Gram-positive bacterial cells and yellow gastric tissue.

6.2.2. Modified Gram stain for identifying non-*H. pylori* bacteria within high-biomass gastric tissue

Given the promising application of the modified Gram stain for gastric FFPE tissue, we next sought to stain the GAC tissue sample, in which we found the highest microbial biomass with RNAscope (Chapter 4, Figure 4.3) and a number of different bacteria, as revealed by 16S rRNA sequencing data (Chapter 5, Figure 5.4). A consecutive tissue section was obtained from the GAC patient block and was deparaffinised, rehydrated and stained using the modified Gram stain. The section was cleared in xylene, mounted in DPX and viewed using a light microscope. Using the RNAscope image as reference (Figure 6.3A and Figure 6.3E), we also found multiple bacterial cells in the same location using the modified Gram stain (Figure 6.3B and Figure 6.3F). Furthermore, the modified Gram stain revealed a variety of bacterial morphologies including Gram-positive cocci and diplococci (Figure 6.3C) and Gram-positive spindle-shaped cells (Figure 6.3D). These correlated with the bacterial regions identified using

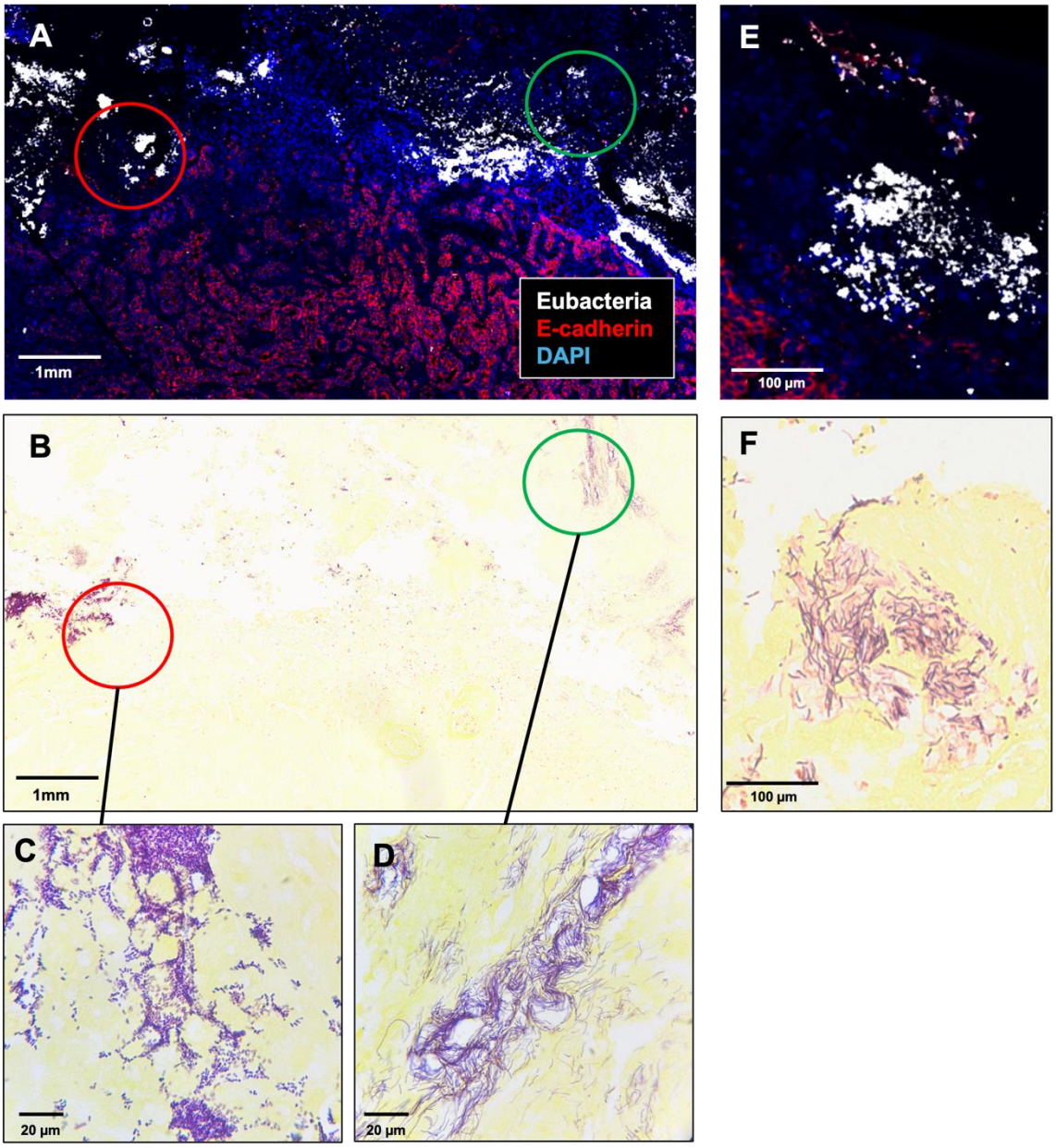

Figure 6.3. RNAscope compared with modified Gram stain for rapid detection of Gram-positive and Gram-negative bacteria in GAC tissue. Gastrectomy tissue from a GAC patient was obtained from the Queen Elizabeth Hospital Birmingham (QEHB) and was stained with a 3-plex panel using RNAScope probes against *H. pylori* (green) and Eubacteria (white) followed by an antibody against E-cadherin (red). Sections were counterstained with DAPI and whole-slide scans were obtained (A&E). A consecutive section of the same tissue sample was also stained using the modified Gram stain and visualised at 4x using a light microscope (B). Microniches containing different Gram-positive (C and D) and Gram-negative or Gram-variable (F) bacterial morphologies were visible at 100x using a light microscope with oil immersion. Matched regions from each section are shown in A&B and E&F.

RNAscope. Interestingly, in a different region on the same sample, both Gram-positive and Gram-negative (or Gram-variable) spindle and rod-shaped bacteria were also observed (Figure 6.3F). These observations also correlated with preliminary sequencing data presented in chapter 5, whereby a high number of Gram-positive and negative genera sequences, such as *Acinetobacter, Pseudomonas* and *Streptococcus* were identified. A further observation was that bacteria were stained more vividly in the GAC section (Figure 6.3B) in comparison with bacteria in the GIM section (Figure 6.2). This suggests that although the Gram stain does successfully stain bacteria within gastric FFPE tissue, staining might be dependent on bacterial biomass, with dense regions of bacteria staining more vividly than sparsely distributed bacterial cells.

5.2.3. Comparison of H&E with modified Gram stain for identification of *H. pylori*

Once it was established that the modified Gram stain was a promising tool for rapid identification of Gram-positive and Gram-negative bacteria within gastric FFPE tissue, it was hypothesised that the same method could be used to identify *H. pylori*. To test this, a high biomass *H. pylori*-positive CG patient from chapter 4 was selected, and a consecutive section obtained. The first section was stained with H&E (Figure 6.4A), which is the current gold-standard for histological identification of *H. pylori.* The second section was stained using the modified Gram stain (Figure 6.4B). Both sections were then compared with the previously labelled RNAscope reference image (Figure 6.4C). H&E staining is the current gold standard for diagnosing *H. pylori* infection and histopathological assessment of inflammation and expression of inflammatory markers in patients at risk of GAC. Therefore, as expected, *H. pylori* was highly visible when

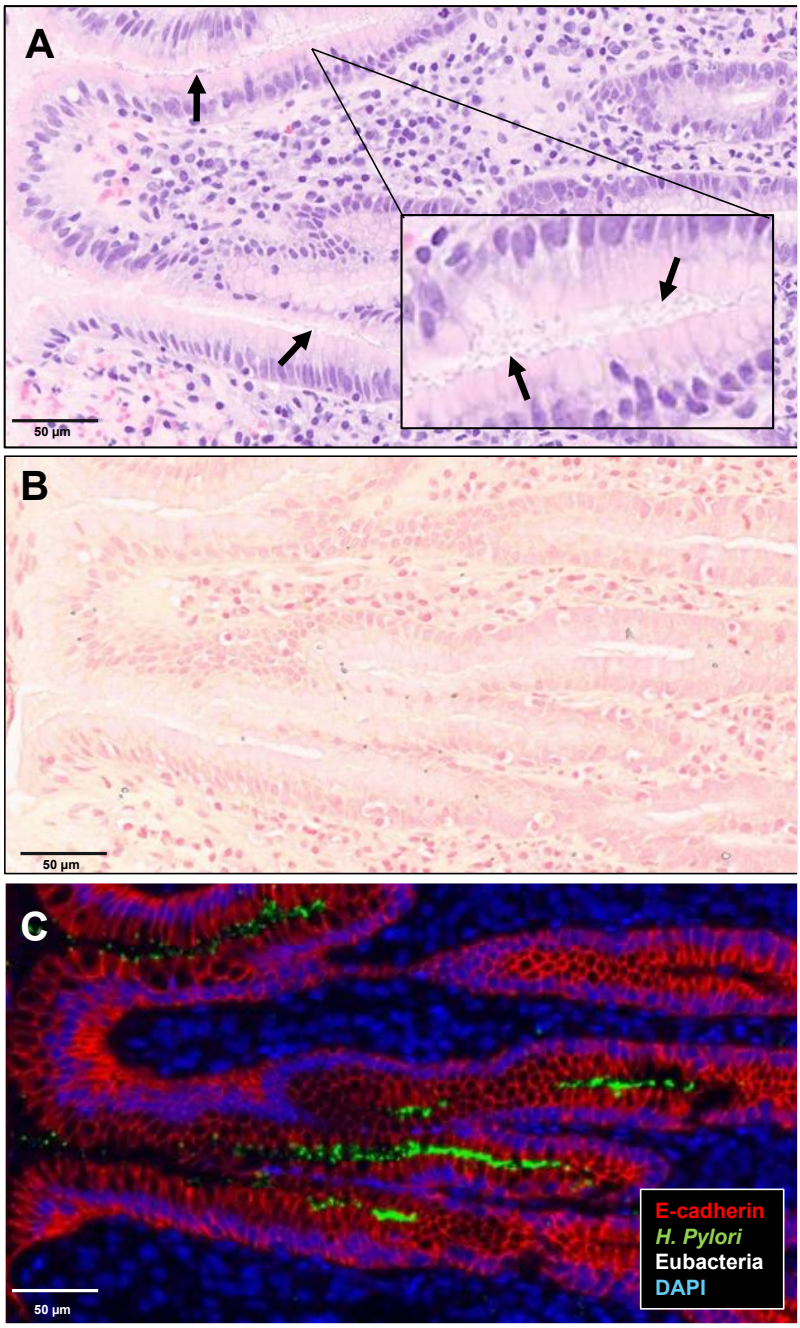

Figure 6.4. H&E compared with modified Gram stain for rapid detection of *H. pylori*. Three punch biopsy FFPE sections from an archived *H. pylori*-positive CG patient were obtained from the HBRC, deparaffinised and rehydrated. The first section was stained by H&E (A) and the second was stained with the modified Gram stain (B). Both were viewed at 100x magnification by light microscopy with oil immersion. The third section was labelled with a 3-plex panel using RNAScope probes against *H. pylori* (green) and Eubacteria (white) followed by an antibody against E-cadherin (red) (C). Sections were counterstained with DAPI and whole-slide scans was obtained and used as a reference image for bacterial localisation.

stained with H&E and appeared as small cocci or spiral-shaped clusters primarily within the gastric glands (Figure 6.4A). The distribution and location of *H. pylori* within the gastric glands matched observations previously made with RNAscope (Figure 6.4C). However, *H. pylori* were difficult to detect with the modified Gram stain, even though location within the section as the same (Figure 6.4B). Furthermore, in this sample, the modified Gram stain did not readily stain the gastric tissue yellow, resulting in further lack of contrast between any bacteria and the gastric tissue. The reason for this is unclear but is likely due to an error made when conducting the modified Gram stain, such as incomplete removal of stains during washing or incomplete counterstaining. In conclusion, although H&E and RNAscope readily identified the presence of *H. pylori*, it is not suitable for detection of non-*H. pylori* bacteria.

6.2.4. H&E for detection and differentiation of non-*H. pylori* bacteria within high-biomass tissue

As expected, *H. pylori* were readily detected by H&E and were clearly visible within the gastric glands. However, although H&E is routinely used for detection of *H. pylori*, few studies detail the application of H&E for identification of non-*H. pylori* bacteria. We therefore sought to investigate whether H&E readily stains and differentiates between a variety of bacterial morphologies and phyla in an additional high-biomass sample. Given that proton-pump inhibitors are generally associated with increased bacterial diversity, a *H. pylori*-negative GIM who was prescribed Rabeprazole from chapter 4 was selected and further sections were obtained by the HBRC. Each section was deparaffinised, rehydrated and prepared for staining, whereby the first section was labelled with an RNAscope probe against all bacteria ‘Eubacteria’ (Figure 6.5A), the

second section was labelled with phylum-specific RNAscope probes against Actinomycetota and Bacillota (Figure 6.5B) and the third section was stained with H&E (Figure 6.5C). RNAscope revealed regions of tissue high in Eubacteria (Figure 6.5A). By repeating studies with Phyla-specific probes, it was revealed that the dense region of Eubacteria was largely composed of Actinomycetota and Bacillota (Figure 6.5B). Regions which stained highly for Eubacteria, but did not stain for Actinomycetota or Bacillota were therefore indicative of other bacterial phyla such as Bacteroidota. A consecutive section was then stained with H&E to visualise morphology of these identified bacteria. Interestingly, although the spiral-shaped confirmation *H. pylori* was readily identified by H&E, precise morphology of non-*H. pylori* bacteria such as Actinomycetota and Bacillota were difficult to identify by H&E, most likely due to the high density of bacteria within this cluster.

Unfortunately, the modified Gram stain was not conducted for this patient but would have likely provided better contrast between bacteria and tissue, in addition to readily differentiating between Gram-positive and negative bacteria. Taken together, findings presented in Figure 6.5 suggest that although H&E is not routinely used for identification of non-*H. pylori* bacteria, regions of high bacterial biomass can be identified using this stain. However, H&E did not differentiate between Gram-positive and negative bacteria and did not provide contrast between bacteria and gastric tissue or mucin and therefore may be limited to detecting bacteria within the mucus layer, rather than bacteria that are associated with the glands or gastric lamina propria. In conclusion, this further confirms that the modified Gram stain is more appropriate for routine identification of non-*H. pylori* bacteria within gastric histological tissue.

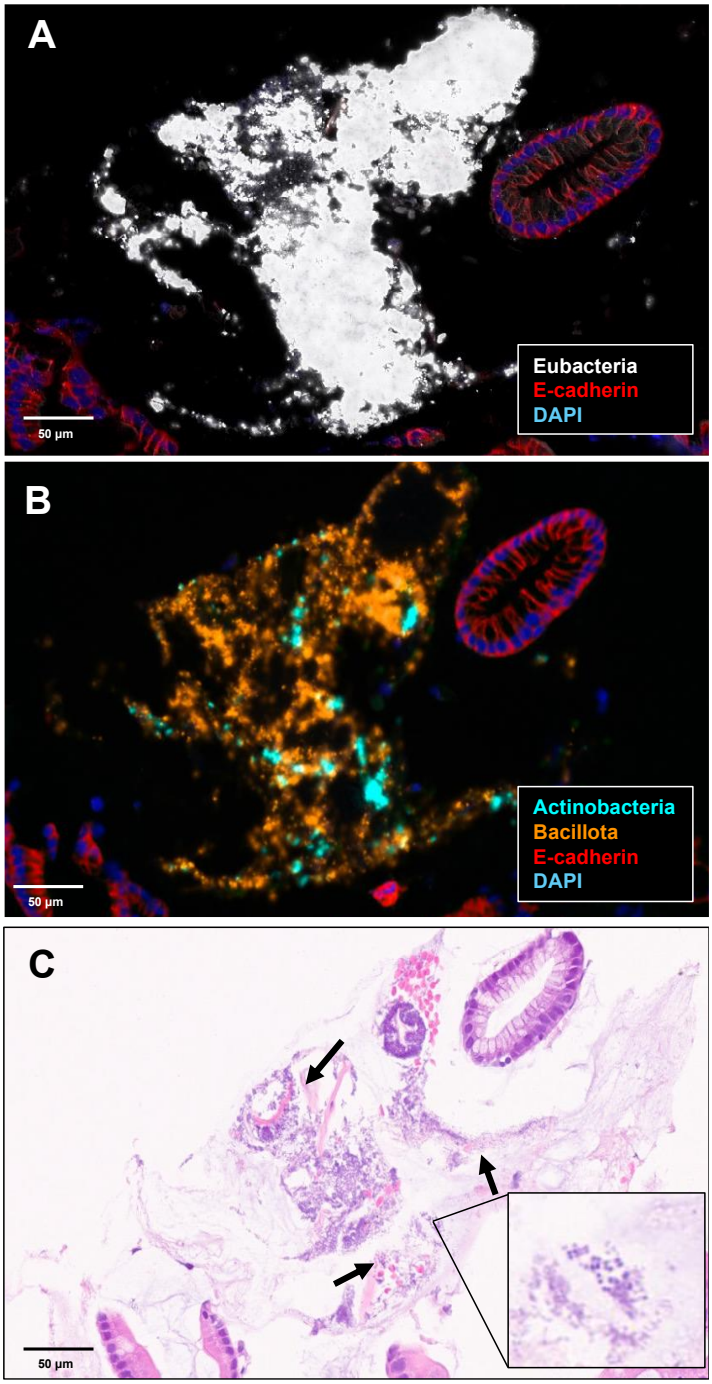

Figure 6.5. Phyla-specific RNAscope compared with H&E for differentiation between bacterial morphology. Three punch biopsy FFPE sections from an archived *H. pylori*-negative GIM patient were obtained from the HBRC, deparaffinised and rehydrated. The first section was labelled with an RNAScope probe against Eubacteria (white) followed by an antibody against E-cadherin (red) (A). The second section was also labelled with E-cadherin (red) and an RNAScope probe against Actinomycetota (turquoise) and Bacillota (orange) (B). Sections were counterstained with DAPI and whole-slide scans were obtained and used as a reference image for bacterial localisation. The third section was stained with H&E and was visualised at 100x magnification by light microscopy with oil immersion (C).

5.2.5. The modified Gram stain as a stratification tool for patients at risk of developing GAC

Despite difficulty identifying *H. pylori* with the modified Gram stain and non-*H. pylori* bacteria not easily detected by H&E, it was clear that non-*H. pylori* bacteria could be successfully and rapidly identified using the modified Gram stain. Additionally, although Gram-positive non-*H. pylori* bacteria were identified in the GIM patient, the bacteria stained more vividly in the higher biomass GAC patient. Therefore, given the possible effect of bacterial biomass on staining reliability, it was important to test this stain on additional patient samples with varied bacterial biomass. As the overall aim of this study was to validate the modified Gram stain as a patient surveillance tool, by repeating studies on patients at different stages of carcinogenesis, a potential correlation between non-*H. pylori* bacteria and disease state could be identified.

Eight further sections of *H. pylori*-positive CG (n=4) and GIM (n=4) FFPE sections were obtained from the HBRC, deparaffinised, rehydrated and stained using the modified Gram stain. Each section was visually assessed using a light microscope with oil immersion and any tissue regions containing Gram-positive and negative bacteria were identified. Interestingly, a general trend was observed whereby far more bacteria were identified in *H. pylori*-positive GIM patients compared with the CG patients (Figure 6.6). This was a key finding, which further suggests that presence of non-*H. pylori* bacteria might indeed correlate with disease state.

However, despite the GIM patients generally having higher bacterial abundance, there was also clear inter-patient variability in terms of bacterial biomass and abundance,

even within groups. For example, differences in bacterial location and morphology were observed for the GIM patients. In patients A and B (Figures 6.6A and B) several Gram-positive cocci and rods were visible surrounding the gastric glands, with some sparse bacterial cells distributed in the lamina propria. In patient C, a dense region of Gram-positive cocci was found primarily on top of or surrounding gastric glands, whereas few were within the lamina propria (Figure 6.6C). In contrast, in patient D, Gram-positive bacteria were low in abundance and were sparsely distributed across the tissue (Figure 6.6D).

Taken together, these observations showed that bacterial abundance and distribution varied between patients. Inter-patient variation is expected but could also be associated with disease severity or timescale. For example, although the four aforementioned patients were clinically classified as GIM, no information was provided about severity or how long they ago were diagnosed. As such, although data presented in this figure is preliminary, it is possible that higher bacterial biomass also correlates with disease timescale and severity, in addition to risk of developing GAC. By conducting the modified Gram stain on further patient samples, we have shown a correlation between disease state and non-*H. pylori* bacteria presence, which further proposes a role for these bacteria in driving carcinogenesis. Furthermore, we have also shown that the modified Gram stain provides information on bacterial abundance, morphology and diversity, which could be used for stratification of patients at risk of GAC.

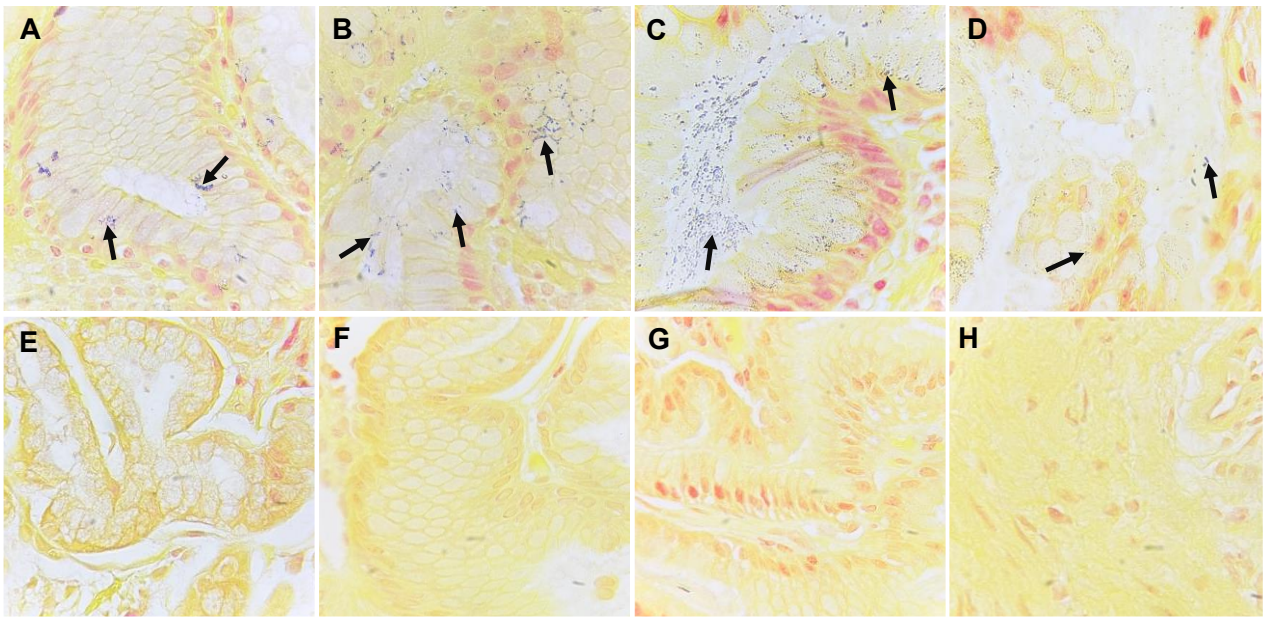

Figure 6.6. Modified Gram stain for stratification of *H. pylori*-positive GIM and CG patients. Archived consecutive sections of *H. pylori*-positive GIM (A-D) and CG (E-H) FFPE tissue were obtained from the HBRC, deparaffinised, rehydrated and stained using the modified Gram stain. Sections were viewed at 100x magnification using light microscopy with oil immersion and images were obtained with an iPhone (scale bar unavailable). Black arrows indicate Gram-positive bacteria.

6.3. Discussion

6.3.1. A modified Gram stain for detection of bacteria in histological tissue sections

Initial results presented in this chapter demonstrated that a conventional Gram stain was unsuitable for use with FFPE tissue sections due to the tissue architecture retaining the purple and red dyes used within the assay. This was an expected issue and prompted our use of a modified Gram stain approach, which provides improved contrast between the tissue architecture and bacteria. The modified Gram stain readily stained Gram-positive bacteria purple which contrasted with the yellow tissue, showing promise for rapid and reliable identification of various bacteria within histological tissue samples. Furthermore, in contrast to RNAscope, this method also provided visual assessment of bacterial diversity, whereby multiple morphologies of coccoid, rod and spindle-shaped bacteria were observed.

Although the modified Gram successfully identified several non-*H. pylori* bacterial morphologies within a variety of histological samples in comparison with H&E, bacterial biomass had a significant effect on visibility. Bacteria within punch biopsy CG and GIM samples, which contain fewer bacteria than the GAC sample were difficult and tedious to identify using light microscopy. In contrast, the GAC patient stained vividly for both Gram-positive, negative and variable bacteria, suggesting that the modified Gram stain works best on samples with higher bacterial biomass. Interestingly, this effect was also documented by Stagg *et al*., (2024), who evaluated the modified Gram stain for diagnosis of skin infections. It was reported that although the modified Gram stain for skin FFPE tissue highly was specific, it lacked sensitivity, and a negative result did not

necessarily exclude the likelihood of infection. However, difficulty identifying bacteria with the modified Gram stain could also be a result of staining issues, rather than low sample biomass. For example, difficulty staining Gram-negative bacteria such as *H. pylori* is a commonly reported issue when conducting the modified Gram stain on paraffin-embedded tissue. The reason for this is unclear, but is often attributed to their thin cell walls, which retain far less dye in comparison to Gram-positive bacterial cell walls (Becerra *et al.,* 2016; Claus, 1992). In addition, staining might also be dependent on the choice of dyes used in the assay. For example, although safranin is routinely used for detection of Gram-positive bacteria in smears, fuchsin is a brighter dye that is less likely to be rinsed away with ethanol (Claus, 1992). Additionally, it is possible that a longer incubation time is required for staining of Gram-negative bacteria within gastric glands, due to the presence of gastric mucin preventing penetration of the stain (Engbaek *et al*., 1979).

6.3.2 Implementation of the modified Gram stain as a diagnostic or surveillance tool for patients at risk of GAC

Although data presented in this results chapter highlighted the potential application of the modified Gram stain in routine histology, a critical next step is to assess its true clinical utility by sharing these findings and consulting with pathologists. While bacteria were readily observed using this technique, given that this method is not currently routinely used in histology, it is essential to first determine whether pathologists can also reliably identify bacteria stained with this method. This validation is necessary to confirm that any observations are genuine and not artifacts, such as contamination, and because pathologists would be the end-users of this technique in clinical practice.

Furthermore, whilst data presented in this chapter highlight the promising application of the modified Gram stain in a clinical setting, the sample size was small, and both staining and imaging was only conducted by one researcher, which could have introduced bias. Therefore, it is important to expand the sample size and invite other researchers and pathologists to validate this technique. To further assess the clinical utility of the modified Gram stain in histology in clinical practice, within a pathology laboratory, an additional tissue section could be obtained from any patient tissue blocks that are already undergoing sectioning and H&E staining. This additional tissue section could then be relatively easily stained with the modified Gram stain technique and assessed by a pathologist for presence of bacterial cells and differentiation between Gram-positive and Gram-negative bacteria. Additionally, by comparing the stained samples to established diagnostic methods, such as H&E and Giemsa staining, pathologists could determine the reliability and specificity of this technique, ultimately assessing its potential for routine use in clinical histopathology.

Nonetheless, data presented in this thesis have shown that non-*H. pylori* bacteria invade the gastric lamina propria during carcinogenesis and that presence of these bacteria also correlate with disease state. Furthermore, these bacteria were also identified in pre-cancer and cancer tissue, further suggesting that they play a role in carcinogenesis. Although several studies, including ours, have suggested a potential role for non-*H. pylori* bacteria in GAC development, no study has yet determined whether bacterial invasion during pre-cancerous GIM directly correlates with risk of developing GAC (Ferreira *et al*., 2018; Fu *et al*., 2024; Png *et al*., 2022). Currently, patients diagnosed with severe gastric atrophy (GA) or GIM receive three-yearly endoscopic surveillance for identification of further histological changes. However,

biomarkers are not currently included in surveillance due to lack of evidence and as such, only alterations to mucosal architecture and histology are recorded (Banks *et al*., 2019). Nonetheless, increasing evidence is emerging which proposes a role for non-*H. pylori* bacteria in carcinogenesis and given that the modified Gram stain detailed in this thesis shows promise as a cost-effective bacterial identification tool, which in the long-term, could be implemented in the future as a screening tool for GIM patients at risk of GAC.

Once the reliability of this technique is confirmed in larger-scale studies, there is therefore potential for use of the modified Gram stain alongside H&E following gastric endoscopy. For example, GIM patients who are currently monitored every three years, could also be assessed for presence and invasion by non-*H. pylori* bacteria, in addition to histological changes indicative of GAC progression, such as atrophy (Correa, 2004; Lee *et al.*, 2018). This approach would be a relatively cost-effective and easy approach to document any potential correlations between presence of non-*H. pylori* bacteria and progression of carcinogenesis. In addition, the modified Gram stain could be used to stratify patients into either high or low risk for developing GAC, according to high or low microbial biomass and diversity, whereby the bacteria serve as a biomarker.

Given that bacteria are associated with several pathologies, the modified Gram stain could also be applied to other cancers which also rely on histological inspection or sequencing, such as colorectal cancer (CRC), liver cancer and breast cancer (Lo *et al*., 2022; Yusuf *et al*., 2023). Furthermore, it also shows promise as a validation tool in targeted bacterial cancer therapy, where it could be used to identity whether bacteria

have successfully penetrated tumours (Liang *et al*., 2022). In addition, given that bacteria have also been reported to affect the efficacy of chemotherapeutic drugs, the modified Gram stain could be used to correlate bacterial biomass and abundance with chemotherapy response in cancer patients (Lehouritis *et al*., 2015). Finally, as shown in this chapter, the modified Gram stain is an easy and cost-effective tool for validating data from other experiments, such as 16S rRNA sequencing. As such, the modified Gram stain could become commonplace in microbiome and or immunology laboratories as an inexpensive and rapid stain for validation of previous imaging and sequencing-based findings.

6.4. Summary

Data presented in this chapter demonstrated that a modified Gram stain is a promising tool for the rapid identification of non-*H. pylori* bacteria in gastric histological sections and components of this chapter were recently published in the journal Helicobacter (Giddings *et al.,* 2025; Appendix B). Although further optimisation is required for successful staining of Gram-negative bacteria such as *H. pylori*, this technique readily identified many other bacteria in a variety of gastric histological samples in comparison with H&E. Given that non-*H. pylori* bacteria might also drive gastric carcinogenesis and therefore act as a potential biomarker, the modified Gram stain could be implemented as a rapid diagnostic or surveillance tool for patients at risk of GAC. Using this tool, patients could be routinely screened for non-*H. pylori* bacteria and stratified for risk of GAC according to bacterial diversity, biomass and invasion. Furthermore, the modified Gram stain could be used to dictate treatment options in the early stages of carcinogenesis, such as eradication of both *H. pylori* and non-*H. pylori* bacteria.

Chapter 7: Final Discussion

7.1. Introduction

Despite *H. pylori* infection remaining the strongest risk factor for GAC, the precise mechanism behind carcinogenesis remains unclear. However, it is currently hypothesised to be a multifactorial process, involving genetic and environmental risk factors, *H. pylori* virulence factors and the gastric microbiota. Results presented in chapter 3 of this thesis indicated that although patient-derived organoid monolayers were a useful tool for modelling the gastric mucosa in vitro, they did not vacuolate following exposure to *H. pylori* VacA. Results presented in chapter 4 then indicated that *H. pylori* infection significantly correlated with invasion of non-*H. pylori* bacteria into the lamina propria throughout several stages of carcinogenesis. A preliminary method for isolation and identification of bacteria from gastric histological tissue was detailed in chapter 5, whereby several genera of interest were identified in both histological and biopsy tissue. Finally, given that findings presented in this thesis indicated a role for invasive non-*H. pylori* bacteria in driving carcinogenesis, a proposed, rapid histological test for routine bacterial identification and surveillance is detailed in chapter 6.

7.2. Relevance of *H. pylori*-induced vacuolation during infection

Organoid monolayers did not vacuolate following infection or treatment with *H. pylori* VacA, despite prominent vacuoles appearing within the AGS cell line following the same protocol. Although vacuolation is frequently reported in vitro, this effect has rarely been observed in vivo and is not currently a histological feature of *H. pylori* infection used during diagnosis (Lee and Kim, 2015). There are several plausible explanations for the absence of vacuolation. Firstly, it is possible that the absence of vacuolation

was a result of differences in cell culture media used for AGS cells and organoid monolayers. The AGS cells were maintained with complete RPMI medium, which is commonly used for the growth and maintenance of various cell lines and has been used in previously published vacuolation studies (Foegeding *et al*., 2019; Garner and Cover, 1996). In contrast, the organoid monolayers were derived and maintained using a mostly homemade conditioned medium, containing a cocktail of human growth factors. It is therefore possible that components within the organoid medium provided a protective response to VacA.

For example, noggin has been shown to prevent autophagy and reduce autophagic vacuole formation within the pancreas during pancreatitis (Cao *et al*., 2013). Furthermore, VacA-induced vacuole formation of HeLa cells were inhibited by an antibody against EGF receptors, suggesting that availability and subsequent binding molecules to EGF receptors could play a preventative role during vacuolation (Seto *et al*., 1998). In addition, VacA activity is enhanced in low-pH conditions (Bernard *et al*., 1995). Although media pH was not routinely measured during this study, it is possible that the media used for routine maintenance of AGS cells and organoids differed in pH, which impacted the downstream vacuolating activity of VacA. Whilst this theory is unlikely, as both media contained buffers and coloured pH indicators, this could be easily tested in a future study by comparing vacuolation of AGS cells and organoid monolayers in different cell culture media or at different pH.

It is also possible that organoid monolayers did not vacuolate following exposure to VacA due to the absence of VacA receptors on the organoid apical cell surface. In

contrast, several VacA receptors are located on the AGS cell surface, such as receptor protein tyrosine phosphatase (RPTP) α and β, epidermal growth factor receptor (EGFR) and fibronectin (FN) (Pachathundikandi *et al*., 2013; Tegtmeyer *et al.*, 2009). Few studies have detailed the presence of these receptors within human-derived organoids or monolayers. In fact, only one study has investigated the interaction of purified VacA with organoid monolayers, where it was reported that VacA did not bind to the apical monolayer surface. However, this study also reported that VacA preferentially bound to the basolateral surface of organoid monolayers, suggesting an availability of VacA receptors on the basolateral surface, which are not expressed apically (Caston *et al*., 2020).

This suggests that vacuolation could be a result of *H. pylori* VacA interacting with the basolateral membrane, which harbours VacA receptors. Given that cells within the gastric mucosa are polarised, *H. pylori* is usually found within mucin secreted from the apical cell surface and rarely comes into contact with the basolateral surface. However, a proposed mechanism for induction of vacuolation is outlined in Figure 7.1, where it is possible that *H. pylori* infection induces inflammation resulting in interrupted intercellular junctions and cellular depolarisation. In turn, this might facilitate direct passage of secreted VacA to the to the basolateral cell surface where it can bind to available VacA receptors and induce vacuolation. As such, it is possible that although vacuolation is frequently observed in vitro due to the availability of VacA receptors on several commonly used cell lines, vacuolation in vivo is a phenotype that only occurs following a period of chronic inflammation and subsequent availability of VacA receptors.

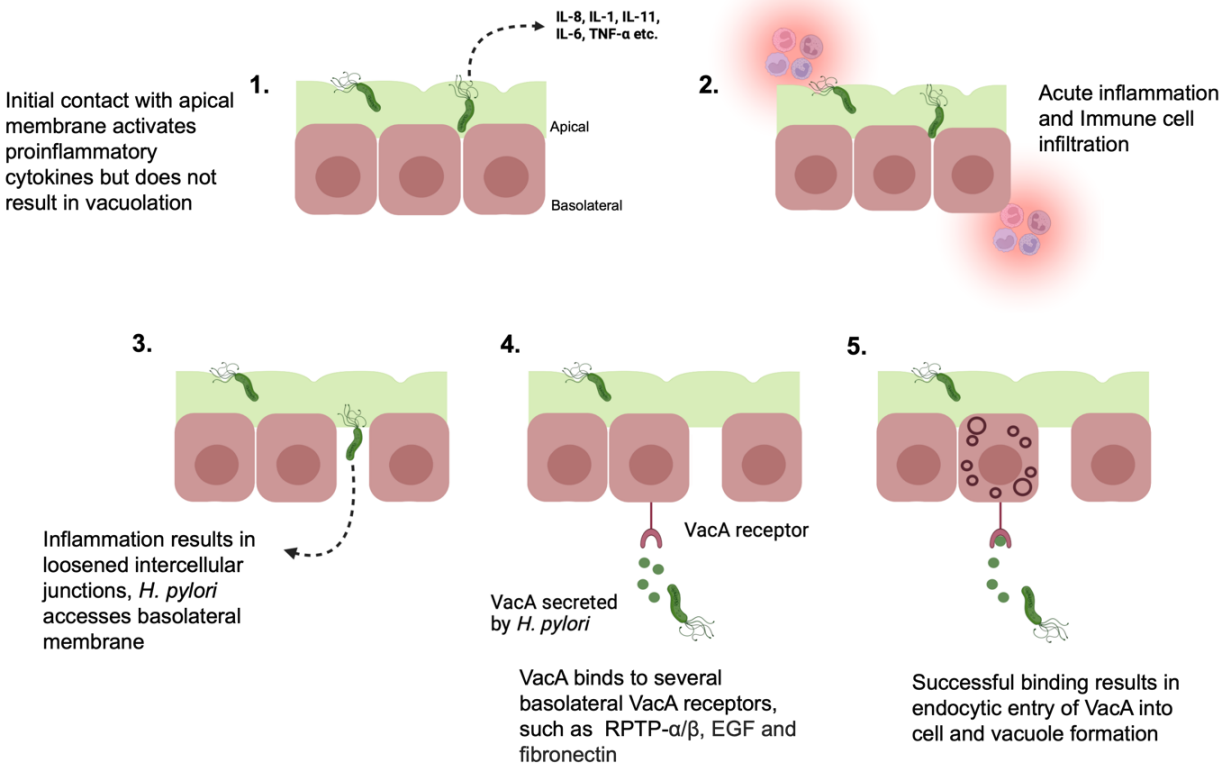

Figure 7.1. Proposed mechanism of *H. pylori* VacA-induced vacuolation in vivo. *H. pylori* is usually found within the gastric mucin on the apical surface of the gastric epithelium, whereby infection results in release of pro-inflammatory cytokines. Inflammation results in cellular damage, depolarisation of the gastric epithelium and loosening of intercellular junctions. *H. pylori* secrete VacA, which passages through the loosened intercellular junctions and binds to VacA receptors within the basolateral membrane. Successful binding of VacA results in vacuolation of the gastric epithelial cell. Figure created in Biorender.com.

7.3. *H. pylori* and the gastric microbiota in gastric carcinogenesis

The precise relationship between *H. pylori* and the gastric microbiota remains unclear, but it is widely understood that when present, *H. pylori* dominate the gastric microbiota and reduce the abundance and diversity of other bacteria. However, this remains a controversial hypothesis, as this dogma is primarily supported by bacterial sequencing techniques. These techniques are prone to sample cross-contamination and amplicon carryover, often resulting in a dominance and an over-estimation of certain bacteria (Durazzi *et al*., 2021; Glassing *et al*., 2016; Salter *et al*., 2014).

In comparison with sequencing-based data, in situ hybridisation (ISH) is a targeted approach for visualising bacterial abundance, location and distribution within a histological tissue sample. Given that ISH is a highly specific approach, sample cross-contamination is unlikely. Therefore, by using RNAscope ISH to visualise all non-*H. pylori* bacteria alongside *H. pylori*, a 'snapshot in time' could be obtained of all bacteria within a given sample, reducing the likelihood of bacterial dominance and over-estimation. Interestingly, in *H. pylori*-positive CG and GIM tissue, RNAscope ISH combined with IHC revealed a significant correlation between *H. pylori* and the gastric microbiota, contrasting the current dogma that *H. pylori* reduce abundance of non-*H. pylori* bacteria. In contrast, very few non-*H. pylori* bacteria were identified in *H. pylori*-negative CG and GIM tissue. Taken together, these observations provided evidence, which suggest that *H. pylori* presence directly facilitates the colonisation and survival of other bacteria within the gastric mucosa, given that the opposite effect was observed when *H. pylori* was absent. As an RNAscope probe against all bacteria was used, the identity of non-*H. pylori* bacteria remained unknown. However, given that compelling

evidence has emerged which proposes a role for several oral bacteria such as fusobacteria, klebsiella and streptococci in IBD (Elzayat *et al*., 2023), colorectal cancer (CRC) (Lo *et al*., 2022; Zepeda-Rivera *et al*., 2024), gastric atrophy and GAC (Fu *et al*., 2024a), it is plausible that non-*H. pylori* bacteria identified in this study were also oral pathogens. Although the oral cavity and gastrointestinal tract are distinct from one another, they are connected by the oral-gut axis and share a similar mucosal pH of around 7.1-7.5 (Baliga *et al*., 2013; Yamamura *et al*., 2023). Therefore, the ability of oral bacteria to survive and colonise the gastrointestinal tract is unsurprising.

In contrast, the pH of the stomach is approximately 1.3-3.5, which is unsuitable for growth of most bacteria (Bravo *et al*., 2018). As such, superficial gastric mucins MUC5AC, MUC1 and gland mucin MUC6 are secreted to protect host cells from stomach acid (Babu *et al.,* 2006). Although gastric mucins generally facilitate the growth of many bacteria, *H. pylori* is widely known to modulate the gastric microenvironment in several ways during chronic inflammation, resulting in changes such as elevated pH. For example, it secretes urase which lowers gastric pH and also induces chronic inflammation and gastric atrophy resulting in a loss of acid-secreting parietal cells (Athmann *et al*., 2000; Murakami *et al*., 2013). Therefore, the increase in pH as a result of *H. pylori* infection likely supports the colonisation and survival of multiple bacteria, such as oral bacteria, which have arrived from the oral cavity. In addition, gastrointestinal bacteria might have arrived in the stomach because of small intestinal bacterial overgrowth (SIBO) and then utilise the elevated stomach pH for survival. Furthermore, the loss of parietal cells during gastric atrophy (GA) could also explain why a higher abundance of non-*H. pylori* bacteria were observed in GIM

compared with CG in this study. In CG, gastric glands and therefore acid-secreting parietal cells are usually present, whereas during GIM, gastric atrophy has likely occurred, resulting in increased local pH which is favoured by non-*H. pylori* bacteria (Correa, 2004, Murakami *et al*., 2013).

In this study, *de novo* MUC2 expression was identified in GIM and CG patients, which also correlated with an observed increase in non-*H. pylori* bacteria. MUC2 is highly expressed in the gastrointestinal tract and is thought to provide a glycan nutrient source for a variety of gastrointestinal phyla, such as Acinomycetota and Bacteroidota (Yao *et al*., 2021). Given that a correlation was observed between non-*H. pylori* bacteria and MUC2, it is therefore possible that elevated expression of MUC2 provided availability of glycan nutrient sources, which were utilised by oral or gastrointestinal non-*H. pylori* bacteria to promote their survival and colonisation. In addition, the pH of MUC2 is approximately 6.1-7.5, which as previously discussed, could also promote the colonisation and survival of non-*H. pylori* bacteria, such as oral or gastrointestinal species (Yamamura *et al*., 2023).

Although MUC2 likely promotes survival of many bacteria, its primary role is protection of the gastrointestinal tract against pathogenic bacteria, whereby *de novo* expression also occurs as a result of bacterial stimulation or inflammation (Van der Sluis *et al*., 2006). Following initial infection, MUC2 overexpression has been shown to inhibit in vitro adhesion and colonisation of bacteria such as *Escherichia coli* to epithelial cells (Bergstrom *et al*., 2010; Johansson *et al*., 2008). Given that MUC2 was elevated in both *H. pylori*-negative and positive individuals with GIM, there are several distinct

explanations for this. In *H. pylori*-negative individuals, MUC2 secretion is likely a result of *de novo* goblet cell expression, which occurs during progression of GAC (Conze *et al*., 2010). However, in *H. pylori*-positive individuals, in addition to mutations, it is also possible that MUC2 expression is a result of *H. pylori* and non-*H. pylori* bacteria triggering a feedback loop. A proposed mechanism for this is shown in Figure 7.2, whereby infection with *H. pylori* modulates the local gastric pH, resulting in colonisation by non-*H. pylori* bacteria. In response to bacterial infection and tissue damage, MUC2 is secreted by goblet cells. MUC2 provides a glycan nutrient source, promoting the growth colonisation of several gastrointestinal bacteria and maintenance of elevated pH. This results in further colonisation and survival of multiple non-*H. pylori* bacteria, including oral and gastrointestinal genera. Persistent bacterial infection then maintains MUC2 secretion in this feedback loop.

In conclusion, given discrepancies between studies, the precise relationship between *H. pylori* and the gastric microbiota remains unclear. However, by using a targeted approach such as ISH, a correlative link was identified in *H. pylori*-positive CG and GIM patients. Although the identity of these bacteria remained unknown at this stage, deduced from compelling evidence and published literature, these bacteria were likely opportunistic bacteria which arrived from the oral cavity along the oral-gut axis or were gastrointestinal bacteria, which have entered the distal stomach as a result of SIBO and favour elevated pH and mucin availability. Furthermore, irrespective of *H. pylori* presence, non-*H. pylori* bacteria also correlated with elevated MUC2 levels in GAC patients, further suggesting that elevated pH and mucin availability facilitates survival and colonisation of non-*H. pylori* bacteria during carcinogenesis.

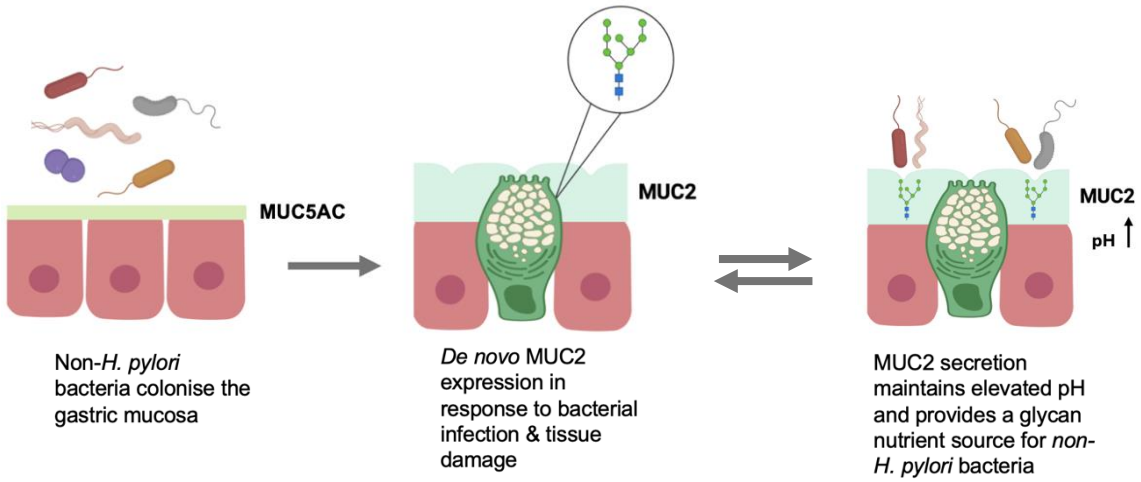

Figure 7.2. Proposed mechanism of de novo MUC2 secretion following infection by *H. pylori* and non-*H. pylori* bacteria. Following initial *H. pylori* infection, local pH is raised due to urease production and gland atrophy, resulting in colonisation of oral and gastrointestinal non-*H. pylori* bacteria. In response to bacterial infection and tissue damage, *de novo* expression of MUC2-secreting goblet cells occurs and replaces MUC5AC. MUC2 secretion maintains elevated pH and also provides glycan nutrient source for non-*H. pylori* bacteria, promoting their survival and colonisation. MUC2 expression is therefore maintained because of chronic infection by non-*H. pylori* bacteria.

7.4. Non-*H. pylori* bacteria invade the lamina propria during gastric carcinogenesis

In addition to a correlative relationship between *H. pylori* and the gastric microbiota, RNAscope also revealed significant invasion of these non-*H. pylori* bacteria into the gastric lamina propria during CG, GIM and GAC. This was an important observation, which to our knowledge, has not previously been reported in gastric cancer studies. However, invasion of bacteria into the lamina propria is frequently reported in gastrointestinal studies, involving IBD such as Chron's disease and colitis (Sekido *et al*., 2020). These patients often have impaired epithelial barrier function as a result of chronic inflammation, which facilitates entry of bacteria into the sub-epithelial layers of the intestines, resulting in colonisation of the lamina propria, activation of immune cells and a heightened inflammatory response, which further drives inflammation and exacerbates symptoms (Dheer *et al*., 2019). In addition, an increased abundance of mucosal-associated phyla, such as Bacillota and Fusobacteriota are often reported in these patients compared with healthy controls (Bibiloni *et al*., 2006).

Given that the lamina propria is generally rich in immune cells, it is unclear why bacteria invade this region of the tissue. However, it is plausible that some bacteria invade in an effort to 'hide' within immune cells and avoid clearance. For example, Gamma Pseudomonadota were found to be enriched within $CD14^{+}$ lamina propria macrophages from patients with Crohn's disease (Sekido *et al*., 2020). In addition, it is also possible that some invasive bacteria 'hijack' and utilise immune cells for translocation purposes. This effect well-studied in vitro for bacterial cancer therapy, but it was recently reported that dendritic cells facilitated entry of gastrointestinal bacteria,

such as Enterobacteriaceae, into secondary lymphoid organs of a murine model, which further suggests that this type of mechanism is involved in later stages of IBD (Choi *et al*., 2023). As also described for Figure 7.1, it is widely understood that *H. pylori* infection directly results in release of pro-inflammatory cytokines and chronic inflammation (Blaser *et al*., 1995). This results in depolarisation and increased permeability of the gastric epithelia causing the barrier to become ‘leaky, which is a similar effect observed in IBD (Amieva *et al*., 2003). However, *H. pylori* secreted virulence factor HtrA is also capable of cleaving E-cadherin, resulting in depolarisation of the gastric epithelia and disruption of intercellular junctions (Hoy *et al*., 2010). In fact, a similar effect has recently been studied in vitro using organoid models, where it was reported that HtrA cleavage of E-cadherin results in enhanced translocation of *H. pylori* and CagA across the monolayer (Canadas-Ortega *et al*., 2024). Furthermore, a single nucleotide polymorphism (SNP) within HtrA has been identified in several *H. pylori* strains associated with GAC, where it was reported as a potential biomarker for the later stages of carcinogenesis (Sharafutdinov *et al*., 2023). As such, although more work must be conducted to assess the function of HtrA in promoting invasion of non-*H. pylori* bacteria, it is possible that bacterial invasion observed in this study was a result of a combination of HtrA-mediated E-cadherin cleavage and chronic inflammation.

A proposed mechanism for bacterial invasion in carcinogenesis is therefore outlined in Figure 7.3, which suggests that *H. pylori* infection results in cleavage of E-cadherin, leading to invasion of opportunistic non-*H. pylori* bacteria through the gastric glands and into the surrounding lamina propria.

.

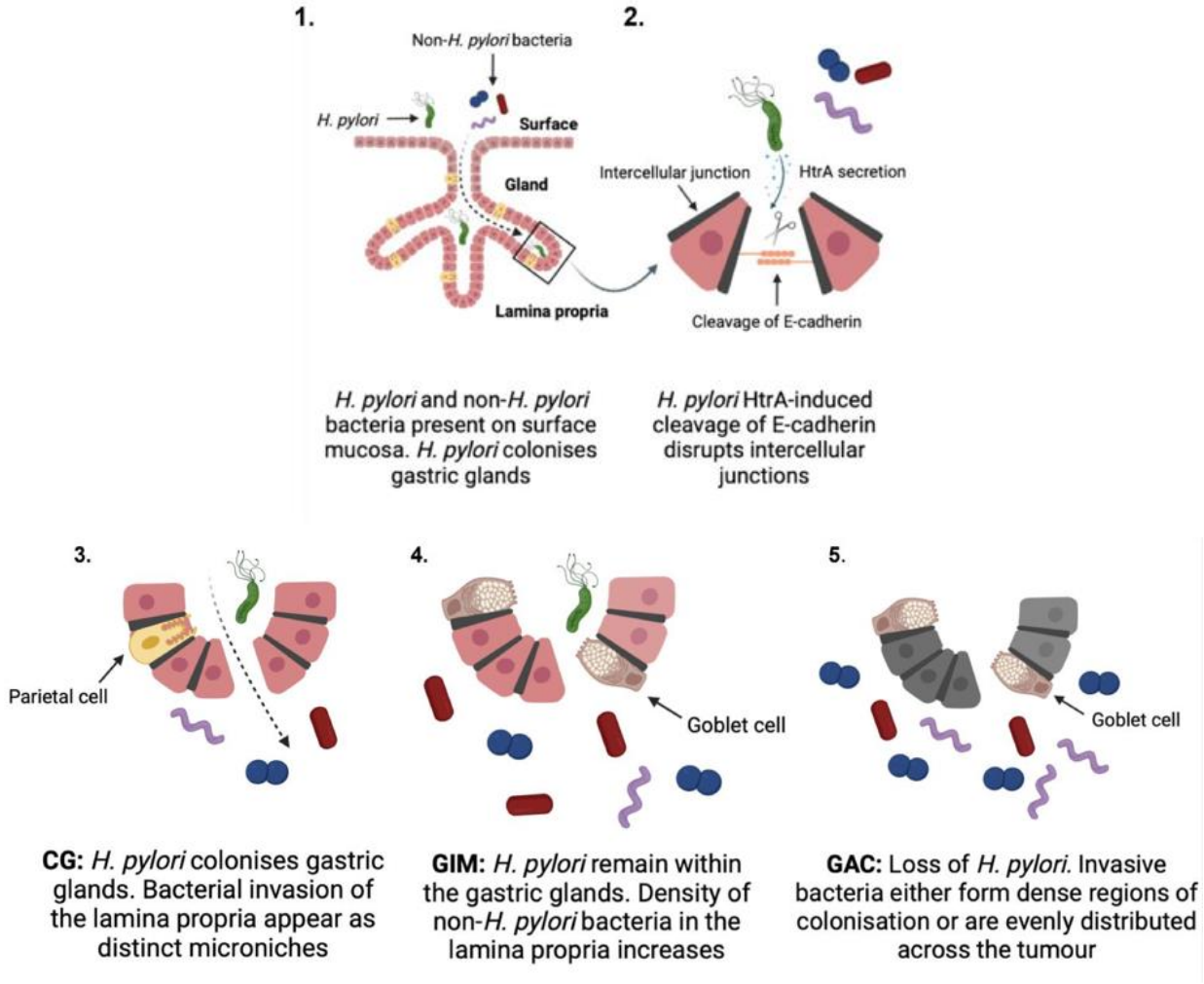

Figure 7.3. Illustrative model proposing *H. pylori*-induced bacterial invasion to the gastric lamina propria. Stage 1-5 are 1) Non-*H. pylori* bacteria and *H. pylori* within the gastric surface and gland, respectively. 2) *H. pylori* secrete HtrA, which cleaves tight junction protein E-cadherin, causing loss of polarisation and disrupted intercellular junctions. 3) Non-*H. pylori* bacteria translocate and 'invade' through the gland and disrupted intercellular junctions in CG. 4) Non-*H. pylori* bacteria further colonise the lamina propria in GIM. 5) In GAC, invasive bacteria increase in numbers and colonise dense regions or evenly across the tumour. Figure created in Biorender.com.

As also discussed in section 7.3 of this chapter, the loss of acid-secreting parietal cells and *de novo* secretion of mucins, such as MUC2, likely modulate the gastric pH which supports the growth and colonisation of opportunistic invasive non-*H. pylori* bacteria within the gastric tissue. In turn, these bacteria then further drive carcinogenesis by producing a variety of species-specific virulence factors, which damages the host tissue in several ways, such as inducing cytokine release, cellular proliferation, production of free radicals, mutations, DNA damage and tumorigenesis (Lo *et al*., 2022; Matozaki *et al*., 1992; Schulz *et al*., 2019).

7.5. Identity of non-*H. pylori* bacteria involved in gastric carcinogenesis

Once the relationship between *H. pylori* and the gastric microbiota was established, methods were conducted to deduce the identity of non-*H. pylori* bacteria involved in carcinogenesis. Whilst several technical difficulties arose in preparation, resulting in contamination and exclusion of *Helicobacter* and unknown genera from the dataset, 16S rRNA gene sequencing revealed certain non-*H. pylori* genera which were present in CG, GIM and GAC samples.

Acinetobacter was the most abundant genus, particularly for GAC and GIM FFPE tissue. This was surprising, as although *Acinetobacter* is emerging as a multidrug resistant genus and is associated with severe hospital acquired infections, it is only occasionally reported in gastric sequencing studies, in comparison with other bacterial phyla such as Bacteroidota or Bacillota (Ibrahim *et al*., 2021). Furthermore, *Acinetobacter* is often isolated from a variety of environmental samples, such as soil

and water, and is frequently identified in FFPE tissue, suggesting that this genus is a common contaminant (Borgognone *et al*., 2021).

Acinetobacter express a limited array of 'traditional' virulence factors, such as adhesins. However, many species express a multitude of secretion systems which are associated with disease initiation, including Type I, Type II, Type IV and Type 6; in addition to outer membrane OmpA protein (Morris *et al.,* 2019). In addition, they are also protected by an exopolysaccharide capsule which facilitates survival in harsh environments such as the stomach and prevents clearance by immune cells. Additionally, capsular expression can also be enhanced following exposure to antibiotics, which could also be a mechanism employed by *Acinetobacter* in response to stomach acid (Geisinger and Isberg, 2015). Interestingly, *Acinetobacter baumanii* in particular also secrete phospholipase C and D enzymes, with phospholipase D in particular associated with epithelial cell invasion and bacteraemia (Jacobs *et al.*, 2010). Given that *Acinetobacter* are therefore well adapted to surviving harsh conditions, evading the immune response and invading tissue, it is plausible that invasive non-*H. pylori* bacteria identified with RNAscope could indeed include some species of *Acinetobacter.*

Interestingly, although *Acinetobacter* is not currently correlated with gastric carcinogenesis, two key studies from the early 2000s reported similarities in pathogenicity between *H. pylori* and *Acinetobacter lwoffii.* Ofori-Darko *et al*. (2000) reported that *A. lwoffii* produces an OmpA-like protein, which directly stimulated gastrin and IL-8 gene expression, epithelial cell proliferation and inflammation in a mouse

stomach. Similarly, Rathinavelu *et al*. (2003) showed that *A. lwoffii* infection increased T and B cell numbers and parietal cell expression in a mouse infection model, which resulted in mucous gland metaplasia. Although these studies proposed a similarity between *H. pylori* and *Acinetobacter,* there is a distinct lack of published literature or evidence which further investigates or implicates *Acinetobacter* in driving gastric carcinogenesis specifically.

In addition, the modified Gram stain proved difficult to visualise Gram-negative bacteria. As such, given that *Acinetobacter* are primarily Gram-negative, they were not clearly identified using the modified Gram stain. However, *Acinetobacter* can sometimes be Gram-variable and appear as bacillus or coccoid-shaped cells (Bazzi *et al*., 2017). Although no bacteria of this description were identified in CG or GIM tissue, several unknown Gram-positive and negative bacteria were observed in the GAC tissue. Taken together, data presented in this thesis suggest that although *Acinetobacter* was identified by 16S rRNA sequencing, the modified Gram stain was inconclusive, and this bacterium is rarely associated with gastric carcinogenesis.

In addition to *Acinetobacter, Pseudomonas* were also identified from FPPE and biopsy tissue by 16S rRNA sequencing. Although this was an interesting observation, it also shares similarities with *Acinetobacter* as it is associated with hospital acquired infections and laboratory contamination (Markou and Apidianakis, 2014). *Pseudomonas* express a multitude of virulence factors which drive host cell invasion and pathogenesis, including flagella outer membrane lipopolysaccharide (LPS) and proteases, which are capable of degrading connective tissues such as fibronectin and

elastin (Garcia et al., 2018; Jurado-Martín et al., 2021). In addition, *Pseudomonas* have been observed to invade mucin-secreting goblet cells in the respiratory tract via its Type VI secretion system. This is then followed by further damage using its Type III secretion system, resulting in goblet cell death, expulsion of mucin and rupture of the surrounding epithelia, which facilitates bacterial translocation across the epithelial membrane (Swart *et al.*, 2023). Taken together, it is clear whilst *Pseudomonas* are highly pathogenic, they also express a variety of invasion-associated virulence factors, which could indeed facilitate invasion of the gastric lamina propria in particular patients at various stages of gastric carcinogenesis.

However, to our knowledge, no study has reported *Pseudomonas* presence in GIM, and one study has detailed its association with gastritis, independent of *H. pylori* (Kachuei *et al.*, 2020). In contrast, *Pseudomonas* frequently infects immunocompromised individuals, such as cancer patients. In fact, a recent study analysed 727 gastric tissues with RNA sequencing and identified an enrichment of *Pseudomonas aeruginosa* within gastric tumour tissue (Ai *et al.*, 2023). *Pseudomonas* is a Gram-negative rod which was not identified in CG and GIM tissue by the modified Gram stain, further suggesting it does might not play a role in the early stages of carcinogenesis. However, Gram-negative bacteria were identified in the GAC tissue, which could be indicative of this bacterium. Taken together, although *Pseudomonas* unlikely plays a role in the early stages of carcinogenesis, compelling evidence suggests that its abundance increases in GAC. As such, whilst *Pseudomonas* presence in CG and GIM tissue was likely a result of contamination, its presence in

our GAC tissue is not unexpected and could be a result of this bacterium taking advantage of an inflamed and altered tissue microenvironment.

Taken together, precise roles for *Acinetobacter* and *Pseudomonas* in carcinogenesis are yet to be determined. Although they are rarely detected in gastric 16S rRNA sequencing studies, they are usually identified in addition to common laboratory contaminants such as *Sphingomonas, Curvibacter* and *Rhizobium* (Liu *et al*., 2021). As such, although identification of *Acinetobacter* and *Pseudomonas* was a relatively novel finding, as these genera are not often correlated with gastric carcinogenesis in comparison with other well-reported phyla. Nonetheless, given that they were identified in both FFPE and gastric biopsy tissue, further work could be conducted to repeat 16S rRNA sequencing on further patient samples, taking care to minimise contamination risk.

Aside from *Acinetobacter*, *Pseudomonas* and potential contaminants such as *Ralstonia*, several Bacillota were also identified in CG, GIM and GAC tissue. In addition, modified Gram staining of GIM and GAC also revealed significant presence of Gram-positive cocci, which were highly indicative of Bacillota such as streptococci and staphylococci. As discussed in section 7.3 of this chapter, it is highly likely that invasive non-*H. pylori* bacteria were composed of oral or gastrointestinal microbiota which have arrived from the oral-gut axis or due to SIBO. As such, a particular genus of interest identified by 16S rRNA sequencing was *Streptococcus.* In comparison to *Acinetobacter* and *Psuedomonas, Streptococcus* are frequently identified by 16S rRNA in healthy and unhealthy gastric tissue (Zi *et al*., 2022). In addition, an enrichment of

streptococci in gastric cancer tissue has also been reported, suggesting a potential role for this genus at all stages of gastric carcinogenesis (Qi *et al*., 2019).

Although streptococci are found within the healthy gastric microbiota, it is also likely that many pathogens, including streptococci, originated from the oral cavity by means of the previously discussed oral-gut axis (Yamazaki, 2023). Several studies have identified an interaction between *H. pylori* and oral streptococci and several species have been reported to inhibit *H. pylori* growth in vitro. For example, *Streptococcus mutans* and *Streptococcus salivarius* inhibit growth of *H. pylori* in vitro, likely by producing acid or hydrogen peroxide (Ishihara *et al*., 1997). Similarly, *Streptococcus mitis* induces a morphological change in *H. pylori*, whereby cells convert from spiral-shaped to coccoid, resulting in a reduction in growth and cellular metabolism (Khosravi *et al*., 2014a).

Interestingly, other oral species, such as *Actinomyces naeslundii*, *Actinomyces oris, Actinomyces israelli* and *Prevotella nigrescens* also inhibit growth of *H. pylori* (Ishihara *et al*., 1997 and preliminary work in the Rossiter lab). Additionally, RNAscope data presented in this thesis generally revealed a higher abundance of non-*H. pylori* bacteria compared with *H. pylori*. Therefore, it is possible that this is a result of non-*H. pylori* bacteria inhibiting or reducing *H. pylori* growth, in addition to invading the lamina propria and driving carcinogenesis. As such, future studies could identify which oral bacterial species inhibit *H. pylori* growth and then correlate these findings with 16S rRNA sequencing or metagenomics of healthy and unhealthy gastric tissue to assess whether *H. pylori*-inhibiting bacteria also play a role in GAC development.

Although several studies have elucidated a relationship between streptococci and *H. pylori*, streptococci are also reported in *H. pylori*-negative patients with CG, GIM or GAC (Gantuya *et al*., 2019; Khosravi *et al*., 2014). A particular species of interest, is *Streptococcus anginosus* which is frequently isolated from GAC tissue and enriched in several stages of carcinogenesis as revealed by RNA sequencing (Coker *et al*., 2018). Furthermore, a recent murine infection study using germ-free and normal mice also reported that *S. anginosus* promoted gastric inflammation, atrophy and tumorigenesis following 3, 6, 9 and 12-month infection with *H. pylori* strain SS1 (Fu *et al*., 2024a). In addition, at regular intervals, gastric biopsies were obtained and stained with H&E or labelled with ISH probes. It was then revealed that significant *S. anginosus* colonisation of the basal and lamina propria area occurred at each interval (Fu *et al*., 2024a). Interestingly, this finding correlated with novel data presented in this thesis, whereby unidentified non-*H. pylori* bacteria were consistently found within the lamina propria of gastric tissue. Taken together, although this study was conducted on mice, these are exciting findings which further propose a causative role for streptococci in carcinogenesis and also agree with novel RNAscope data presented in this thesis.

In conclusion, although further work must be conducted to confirm the identity of the invasive non-*H. pylori* bacteria identified in this thesis, it is likely that several are oral or gastrointestinal bacteria. As previously discussed, oral bacteria are associated with several gastrointestinal diseases, including IBD and colitis (Elzayat *et al*., 2023). Although these diseases are distinct from GAC, they share several similarities including expression of MUC2, loss of cellular polarity and infiltration of invasive bacteria and immune cells (Dheer *et al*., 2019). Streptococci are frequently isolated

from gastric and gastrointestinal samples and are also highly adapted to surviving and colonising harsh environments. For example, *S. salivarus* has an arginine deaminase system (ADS) which convert arginine into ammonia to raise local pH. Additionally, streptococci are often described as 'pioneer colonisers' as they express a variety of fimbriae, AgI/II family binding proteins and adhesins to aid adherence to mucosal surfaces a (Moschioni *et al*., 2010). Taken together, it is clear that streptococci are highly capable of invading, colonising and avoiding immune-mediated responses throughout the body. Although the gastric microbiota is likely composed of several genera, several published studies, in addition to 16S rRNA gene sequencing findings and modified Gram staining presented in this thesis, suggest that streptococci might be inherently involved in driving gastric carcinogenesis in addition to *H. pylori*.

7.6. Surveillance of non-*H. pylori* bacteria in patients at risk of GAC

In the United Kingdom, patients with CG diagnosed with *H. pylori* infection are treated with a combination therapy of Amoxicillin, Clarithromycin and Omeprazole in addition to proton-pump inhibitors (PPIs) (Black *et al*., 2022). However, for patients with extensive gastric atrophy (GA) or GIM, antibiotic treatment provides minimal benefit as the gastric mucosa is usually irreversibly damaged. Instead, patients are referred for a diagnostic endoscopy and grading of atrophy, whereby patients with low atrophy and low risk of GAC require no further action. In contrast, patients with severe mucosal damage and elevated risk of GAC are monitored every three years by endoscopic surveillance (Banks *et al*., 2019). Surveillance involves visual identification of any changes to the gastric mucosa, in addition to biopsy for H&E staining and

histopathological analysis to grade inflammation and identify whether reinfection with *H. pylori* has occurred (Lee and Kim, 2015).

Currently, non-*H. pylori* bacteria are not routinely identified during surveillance, as H&E lacks sensitivity for detection of bacteria within the lamina propria and deeper gastric tissue. Therefore, whilst H&E readily identifies *H. pylori* within gastric glands, potentially pathogenic and carcinogenic non-*H. pylori* are overlooked, despite compelling evidence proposing a role in driving carcinogenesis (Fu *et al*., 2024b; Gantuya *et al*., 2019; Zi *et al*., 2022). Furthermore, although many species are potentially involved in carcinogenesis, a direct correlation between presence of non-*H. pylori* bacteria and risk of GAC is yet to be established. As such, the modified Gram stain detailed in chapter 6 shows promise as a tool for investigating this further. The modified Gram stain is a cost-effective and rapid technique, which provides powerful insight into bacterial abundance, distribution and diversity of non-*H. pylori* bacteria in a given sample and could easily be included as a histopathological tool alongside H&E. As such, in order to determine whether non-*H. pylori* bacteria indeed correlate with increased risk of GAC, the modified Gram stain could be included as a clinical test alongside H&E in the current three-yearly surveillance of patients at high risk of GAC (Banks *et al*., 2019). Patients at risk of GAC could therefore be stratified according to histological changes, indicating progression of carcinogenesis, alongside reinfection with *H. pylori* and invasion of non-*H. pylori* bacteria. By including the modified Gram stain in routine surveillance of several patients, a potential correlation between non-*H. pylori* bacteria and progression of carcinogenesis will be reported, which would provide further evidence for the role of non-*H. pylori* bacteria in development of GAC.

In addition, no GAC biomarkers are currently used in the UK due to lack of available evidence, despite other countries such as the USA including pepsinogen II and gastrin-17 as biomarkers for chronic *H. pylori* infection and GAC progression (Loong *et al*., 2017; UK NSC, 2021). As discussed above, although further work is required to first determine a correlation between non-*H. pylori* bacteria and risk of GAC, depending on the outcome of further studies, it is possible that non-*H. pylori* bacteria could also be included as a biomarker for GAC. As such, in addition to surveillance, the modified Gram stain could also be utilised as a biomarker screening tool for patients at risk of GAC, such as those with CG, AG and GIM. Given that the modified Gram stain also provides information about bacterial abundance, diversity and distribution, it could also be used to guide treatment options involving antibiotics to prevent over-prescribing and ensure patients are given relevant antibiotics. For example, following endoscopic examination, biopsy tissue could be obtained and stained with the modified Gram stain in order to evaluate proportions of Gram-positive or negative bacteria within the tissue. Based on results from the modified Gram stain, patients could then be prescribed antibiotics only according to which types of bacteria are present. Therefore, a patient with high proportions of Gram-positive bacteria could be prescribed Gram-positive-targeting antibiotics (Aksoy and Unal, 2008).

Taken together, further work must be conducted to determine the significance of non-*H. pylori* bacteria in carcinogenesis before they can be included as a biomarker. As bacterial identification is expensive and laborious, the modified Gram stain provides an alternative, cost-effective solution which could be easily implemented in a pathology clinic or research laboratory.

7.7. Future Work

In addition to *H. pylori* VacA, the gastric microbiota was also investigated in this thesis whereby invasive non-*H. pylori* bacteria were identified by RNAscope in chapter 4. In addition, it was hypothesised that this was a direct result of *H. pylori* HtrA cleaving intercellular junctions and facilitating bacterial entry. Given that Figure 7.3 is relatively speculative, this hypothesis could be modelled in vitro using the organoid monolayer system outlined in chapter 3. For example, using a relatively simple bacterial translocation assay, potentially invasive non-*H. pylori* bacteria, such as streptococci could be cultured on the apical surface of monolayers alongside *H. pylori* with or without HtrA. After a given time period, any bacteria that have passed through the monolayer and arrived at the basolateral compartment could be serially diluted and cultured on agar. This experiment would determine whether *H. pylori* with or without HtrA are indeed capable of loosening intercellular junctions and facilitating the translocation of other bacteria through the monolayer.

Although some non-*H. pylori* genera of interest were identified by laser-capture microdissection (LCM) and 16S rRNA sequencing in chapter 5, FFPE tissue was of low biomass and prone to bacterial contamination. As such, although LCM was an interesting method for bacterial isolation, it was better suited to samples with larger tissue area. Therefore, a relationship between *H. pylori* and non-*H. pylori* bacteria could be determined by 16S rRNA sequencing biopsy tissue from patients with or without *H. pylori* infection at different stages of carcinogenesis, ensuring contamination risk is minimised. Additionally, normal adjacent to tumour (NAT) tissue should also be sequenced as it represents ‘normal’ gastric tissue without pathology indicative of

carcinogenesis. As also discussed in chapter 5, although bacteria such as streptococci and *Acinetobacter* were identified as potential bacteria of interest, future studies could then confirm the identity of these invasive bacteria in consecutive sections of the original patients, using highly sensitive, custom-designed RNAscope phyla and genera probes to target these bacteria.

Furthermore, given that invasive non-*H. pylori* bacteria were identified within the lamina propria of gastric tissue, it is important to understand potential mechanisms by which these bacteria further drive carcinogenesis and whether inflammation is involved. As such, further high throughput hyperplex imaging methods, such as COMET^{TM} by Lunaphore, could also be incorporated which facilitate identification of up to 40 immune markers in a given slide, in addition to RNAscope probes against particular bacteria (Rivest *et al*., 2023). This would provide visual insight into which immune pathways are upregulated by non-*H. pylori* bacteria and whether immune cell infiltration is involved at different stages of carcinogenesis. Additionally, once particular involved with carcinogenesis are confirmed, the role of specific virulence factors, such as adhesin proteins or capsule polysaccharides in bacterial invasion could be interrogated further using advanced molecular microbiology methods, such as transposon directed insertion site sequencing (TRADIS). Finally, as already discussed, the modified Gram stain detailed in chapter 6 was a valuable tool for rapid detection of non-*H. pylori* bacteria in gastric FFPE tissue, reducing the requirement for expensive tools such as bacterial sequencing and IS*H.* Therefore, in combination with H&E, the modified Gram stain is a promising tool that could be implemented in many future studies to fully elucidate a causative relationship between non-*H. pylori* bacteria and risk of GAC.

References

Aguilar, C., Alves da Silva, M., Saraiva, M., Neyazi, M., Olsson, I.A.S., Bartfeld, S., 2021. Organoids as host models for infection biology – a review of methods. Exp Mol Med 53, 1471–1482.

Ahmed, N., 2005. 23 years of the discovery of *Helicobacter pylori*: Is the debate over? Ann Clin Microbiol Antimicrob 4, 17.

Ai, B., Mei, Y., Liang, D., Wang, T., Cai, *H.*, Yu, D., 2023a. Uncovering the special microbiota associated with occurrence and progression of gastric cancer by using RNA-sequencing. Sci Rep 13, 5722.

Ai, W., Li, *H.*, Song, N., Li, L., Chen, *H.*, 2013. Optimal method to stimulate cytokine production and its use in immunotoxicity assessment. International Journal of Environmental Research and Public Health. 4, 29.

Aksoy, D.Y., Unal, S., 2008. New antimicrobial agents for the treatment of Gram-positive bacterial infections. Clinical Microbiology and Infection 14, 411–420.

Allali, I., Arnold, J.W., Roach, J., Cadenas, M.B., Butz, N., Hassan, *H.*M., Koci, M., Ballou, A., Mendoza, M., Ali, R., Azcarate-Peril, M.A., 2017. A comparison of sequencing platforms and bioinformatics pipelines for compositional analysis of the gut microbiome. BMC Microbiology 17, 194.

Allison, M, Bergman T, Gerszten, E. 1999. Further Studies on Fecal Parasites in Antiquity, *American Journal of Clinical Pathology*, Volume 112, Issue 5, Pages 605–609.

Alseekh, S., Fernie, A.R., 2018. Metabolomics 20 years on: what have we learned and what hurdles remain? The Plant Journal 94, 933–942.

Altobelli, A., Bauer, M., Velez, K., Cover, T.L., Müller, A., 2019. *Helicobacter pylori* VacA Targets Myeloid Cells in the Gastric Lamina Propria To Promote Peripherally Induced Regulatory T-Cell Differentiation and Persistent Infection. mBio 10, e00261-19.

Amgalan, B., Day, C.-P., Przytycka, T.M., 2023. Exploring tumor-normal cross-talk with TranNet: Role of the environment in tumor progression. PLOS Computational Biology 19, e1011472.

Amieva, M.R., El-Omar, E.M., 2008. Host-bacterial interactions in *Helicobacter pylori* infection. Gastroenterology 134, 306–323.

Amieva, M.R., Salama, N.R., Tompkins, L.S., Falkow, S., 2002. *Helicobacter pylori* enter and survive within multivesicular vacuoles of epithelial cells. Cell Microbiol 4, 677–690.

Amieva, M.R., Vogelmann, R., Covacci, A., Tompkins, L.S., Nelson, W.J., Falkow, S., 2003a. Disruption of the epithelial apical-junctional complex by *Helicobacter pylori* CagA. Science 300, 1430–1434.

Andersson, A.F., Lindberg, M., Jakobsson, *H.*, Bäckhed, F., Nyrén, P., Engstrand, L., 2008. Comparative Analysis of Human Gut Microbiota by Barcoded Pyrosequencing. PLOS ONE 3, e2836.

Ansari, S., Yamaoka, Y., 2017. *Helicobacter pylori* BabA in adaptation for gastric colonization. World J Gastroenterol 23, 4158–4169.

Apostolos, A.J., Chordia, M.D., Kolli, S.*H.*, Dalesandro, B.E., Rutkowski, M.R., Pires, M.M., 2022. Real-time non-invasive fluorescence imaging of gut commensal bacteria to detect dynamic changes in the microbiome of live mice. Cell Chemical Biology 29, 1721-1728.e5.

Aran, D., Camarda, R., Odegaard, J., Paik, *H.*, Oskotsky, B., Krings, G., Goga, A., Sirota, M., Butte, A.J., 2017. Comprehensive analysis of normal adjacent to tumor transcriptomes. Nat Commun 8, 1077.

Ardenne, M., Reitnauer, P.G., 1975. [Demonstration of tumor inhibiting properties of a strongly immunostimulating low-molecular weight substance. Comparative studies with ifosfamide on the immuno-labile DS carcinosarcoma. Stimulation of the autoimmune activity for approx. 20 days by BA 1, a N-(2-cyanoethylene)-urea. Novel prophylactic possibilities]. Arzneimittelforschung 25, 1369–1379.

Argent, R.*H.*, Thomas, R.J., Letley, D.P., Rittig, M.G., Hardie, K.R., Atherton, J.C., 2008. Functional association between the *Helicobacter pylori* virulence factors VacA and CagA. J Med Microbiol 57, 145–150.

Arnold, M., Park, J.Y., Camargo, M.C., Lunet, N., Forman, D., Soerjomataram, I., 2020. Is gastric cancer becoming a rare disease? A global assessment of predicted incidence trends to 2035. Gut 69, 823–829.

Asonuma, S., Imatani, A., Asano, N., Oikawa, T., Konishi, *H.*, Iijima, K., Koike, T., Ohara, S., Shimosegawa, T., 2009. *Helicobacter pylori* induces gastric mucosal intestinal metaplasia through the inhibition of interleukin-4-mediated HMG box protein Sox2 expression. American Journal of Physiology-Gastrointestinal and Liver Physiology 297, G312–G322.

Ashktorab, H., Ahmed, A., Littleton, G. 2003. p53 and p14 Increase Sensitivity of Gastric Cells to *H. Pylori*-Induced Apoptosis. *Dig Dis Sci* **48**, 1284–1291. https://doi.org/10.1023/A:1024198807619

Ates, G., Vanhaecke, T., Rogiers, V., Rodrigues, R.M., 2017. Assaying Cellular Viability Using the Neutral Red Uptake Assay, in: Gilbert, D.F., Friedrich, O. (Eds.), Cell Viability Assays: Methods and Protocols, Methods in Molecular Biology. Springer, New York, NY, pp. 19–26.

Atherton, J.C., Cao, P., Peek, R.M., Tummuru, M.K., Blaser, M.J., Cover, T.L., 1995a. Mosaicism in vacuolating cytotoxin alleles of *Helicobacter pylori*. Association of specific vacA types with cytotoxin production and peptic ulceration. J Biol Chem 270, 17771–17777.

Atherton J.C., Cover TL, Papini E, et al. 2009. Vacuolating Cytotoxin. In: Mobley HLT, Mendz GL, Hazell SL, editors. Helicobacter pylori: Physiology and Genetics. Washington (DC): ASM Press. Chapter 9.

Athmann, C., Zeng, N., Kang, T., Marcus, E.A., Scott, D.R., Rektorschek, M., Buhmann, A., Melchers, K., Sachs, G., 2000. Local pH elevation mediated by the intrabacterial urease of *Helicobacter pylori* cocultured with gastric cells. J Clin Invest 106, 339–347.

Aumpan, N., Mahachai, V., Vilaichone, R., 2022. Management of *Helicobacter pylori* infection. JGH Open 7, 3–15.

Aumpan, N., Vilaichone, R.-K., Nunanan, P., Chonprasertsuk, S., Siramolpiwat, S., Bhanthumkomol, P., Pornthisarn, B., Uchida, T., Vilaichone, V., Wongcha-Um, A., Yamaoka, Y., Mahachai, V., 2020. Predictors for development of complete and incomplete intestinal metaplasia (IM) associated with *H. pylori* infection: A large-scale study from low prevalence area of gastric cancer (IM-HP trial). PLoS One 15, e0239434.

Babu, S.D., Jayanthi, V., Devaraj, N., Reis, C.A., Devaraj, *H.*, 2006. Expression profile of mucins (MUC2, MUC5AC and MUC6) in *Helicobacter pylori* infected pre-neoplastic and neoplastic human gastric epithelium. Mol Cancer 5, 10.

Backert, S., Tegtmeyer, N., 2017. Type IV Secretion and Signal Transduction of *Helicobacter pylori* CagA through Interactions with Host Cell Receptors. Toxins (Basel) 9, 115.

Backert, S., Tegtmeyer, N., 2010. The Versatility of the *Helicobacter pylori* Vacuolating Cytotoxin VacA in Signal Transduction and Molecular Crosstalk. Toxins (Basel) 2, 69–92.

Bakhti, S.Z., Latifi-Navid, S., 2021. Oral microbiota and *Helicobacter pylori* in gastric carcinogenesis: what do we know and where next? BMC Microbiology 21, 71.

Baliga, S., Muglikar, S., Kale, R., 2013. Salivary pH: A diagnostic biomarker. J Indian Soc Periodontol 17, 461–465.

Balkovetz, D.F., Katz, J., 2003. Bacterial invasion by a paracellular route: divide and conquer. Microbes and Infection 5, 613–619.

Ball, J.B., McNulty, C.J., Green-Fulgham, S.M., Dragavon, J.M., Correia Rocha, I.R., Finch, M.R., Prévost, E.D., Siddique, I.I., Woodall, B.J., Watkins, L.R., Baratta, M.V., Root, D.*H.*, 2023. Combining RNAscope and immunohistochemistry to visualise inflammatory gene products in neurons and microglia. Front. Mol. Neurosci. 16.

Banks, M., Graham, D., Jansen, M., Gotoda, T., Coda, S., di Pietro, M., Uedo, N., Bhandari, P., Pritchard, D.M., Kuipers, E.J., Rodriguez-Justo, M., Novelli, M.R., Ragunath, K., Shepherd, N., Dinis-Ribeiro, M., 2019a. British Society of Gastroenterology guidelines on the diagnosis and management of patients at risk of gastric adenocarcinoma. Gut 68, 1545–1575.

Barker, N., Huch, M., Kujala, P., Wetering, M. van de, Snippert, *H.*J., Es, J.*H.* van, Sato, T., Stange, D.E., Begthel, *H.*, Born, M. van den, Danenberg, E., Brink, S. van den, Korving, J., Abo, A., Peters, P.J., Wright, N., Poulsom, R., Clevers, *H.*, 2010. Lgr5+ve Stem Cells Drive Self-Renewal in the Stomach and Build Long-Lived Gastric Units In Vitro. Cell Stem Cell 6, 25–36.

Bartfeld, S., Bayram, T., van de Wetering, M., Huch, M., Begthel, *H.*, Kujala, P., Vries, R., Peters, P.J., Clevers, *H.*, 2015. In Vitro Expansion of Human Gastric Epithelial Stem Cells and Their Responses to Bacterial Infection. Gastroenterology 148, 126-136.e6.

Batts, K.P., Ketover, S., Kakar, S., Krasinskas, A.M., Mitchell, K.A., Wilcox, R., Westerhoff, M., Rank, J., Gibson, J., Mattia, A.R., Cummings, O.W., Davison, J.M., Naini, B.V., Dry, S.M., Yantiss, R.K., 2013a. Appropriate Use of Special Stains for Identifying *Helicobacter pylori*: Recommendations From the Rodger C. Haggitt Gastrointestinal Pathology Society. The American Journal of Surgical Pathology 37, e12.

Bauman, A.L., Scott, J.D., 2002. Kinase- and phosphatase-anchoring proteins: Harnessing the dynamic duo. 182, e2.

Bazzi, A.M., Al-Tawfiq, J.A., Rabaan, A.A., 2017. Misinterpretation of Gram Stain from the Stationary Growth Phase of Positive Blood Cultures for Brucella and Acinetobacter Species. Open Microbiol J 11, 126–131.

Bebb, J.R., Leach, L., Zaitoun, A., Hand, N., Letley, D.P., Thomas, R., Atherton, J.C., 2006. Effects of *Helicobacter pylori* on the cadherin–catenin complex. J Clin Pathol 59, 1261–1266.

Becerra, S.C., Roy, D.C., Sanchez, C.J., Christy, R.J., Burmeister, D.M., 2016a. An optimized staining technique for the detection of Gram positive and Gram negative bacteria within tissue. BMC Research Notes 9, 216.

Bednarek, R., 2022. In Vitro Methods for Measuring the Permeability of Cell Monolayers. Methods and Protocols 5, 17.

Bergstrom, K.S.B., Kissoon-Singh, V., Gibson, D.L., Ma, C., Montero, M., Sham, *H.*P., Ryz, N., Huang, T., Velcich, A., Finlay, B.B., Chadee, K., Vallance, B.A., 2010a. Muc2 Protects against Lethal Infectious Colitis by Disassociating Pathogenic and Commensal Bacteria from the Colonic Mucosa. PLoS Pathog 6, e1000902.

Bernard, M. de, Papini, E., Filippis, V. de, Gottardi, E., Telford, J., Manetti, R., Fontana, A., Rappuoli, R., Montecucco, C., 1995. Low pH Activates the Vacuolating Toxin of *Helicobacter pylori*, Which Becomes Acid and Pepsin Resistant (∗). Journal of Biological Chemistry 270, 23937–23940.

Bernardo, G., Le Noci, V., Ottaviano, E., De Cecco, L., Camisaschi, C., Guglielmetti, S., Di Modica, M., Gargari, G., Bianchi, F., Indino, S., Sartori, P., Borghi, E., Sommariva, M., Tagliabue, E., Triulzi, T., Sfondrini, L., 2023. Reduction of Staphylococcus epidermidis in the mammary tumor microbiota induces antitumor immunity and decreases breast cancer aggressiveness. Cancer Lett 555, 216041.

Betge, J., Schneider, N.I., Harbaum, L., Pollheimer, M.J., Lindtner, R.A., Kornprat, P., Ebert, M.P., Langner, C., 2016. MUC1, MUC2, MUC5AC, and MUC6 in colorectal cancer: expression profiles and clinical significance. Virchows Arch 469, 255–265.

Bhaumik, S., Boyer, J., Banerjee, C., Clark, S., Sebastiao, N., Vela, E., Towne, P., 2020. Fluorescent multiplexing of 3D spheroids: Analysis of biomarkers using automated immunohistochemistry staining platform and multispectral imaging. J Cell Biochem 121, 4974–4990.

Bibiloni, R., Mangold, M., Madsen, K.L., Fedorak, R.N., Tannock, G.W., 2006. The bacteriology of biopsies differs between newly diagnosed, untreated, Crohn's disease and ulcerative colitis patients. J Med Microbiol 55, 1141–1149.

Bik, E.M., Eckburg, P.B., Gill, S.R., Nelson, K.E., Purdom, E.A., Francois, F., Perez-Perez, G., Blaser, M.J., Relman, D.A., 2006. Molecular analysis of the bacterial microbiota in the human stomach. Proc Natl Acad Sci U S A 103, 732–737.

Bizzozero, G., 1893. Ueber die schlauchförmigen Drüsen des Magendarmkanals und die Beziehungen ihres Epithels zu dem Oberflächenepithel der Schleimhaut Dritte Mittheilung: Hierzu Tafel VII-X.

Black, C.J., Paine, P.A., Agrawal, A., Aziz, I., Eugenicos, M.P., Houghton, L.A., Hungin, P., Overshott, R., Vasant, D.*H.*, Rudd, S., Winning, R.C., Corsetti, M., Ford, A.C., 2022. British Society of Gastroenterology guidelines on the management of functional dyspepsia. Gut 71, 1697–1723.

Blaser, M.J., Perez-Perez, G.I., Kleanthous, *H.*, Cover, T.L., Peek, R.M., Chyou, P.*H.*, Stemmermann, G.N., Nomura, A., 1995. Infection with *Helicobacter pylori* strains possessing cagA is associated with an increased risk of developing adenocarcinoma of the stomach. Cancer Res 55, 2111–2115.

Boccellato, F., Woelffling, S., Imai-Matsushima, A., Sanchez, G., Goosmann, C., Schmid, M., Berger, *H.*, Morey, P., Denecke, C., Ordemann, J., Meyer, T.F., 2019. Polarised epithelial monolayers of the gastric mucosa reveal insights into mucosal homeostasis and defence against infection. Gut 68, 400–413.

Bocci, V., 1992. The neglected organ: bacterial flora has a crucial immunostimulatory role. Perspect Biol Med 35, 251–260.

Boltin, D., Niv, Y., 2013. Mucins in Gastric Cancer – An Update. J Gastrointest Dig Syst 3, 15519.

Bonifacio, J.P.P., Schmolke, M., 2021. Visualisation of Respiratory Commensal Bacteria in Context of Their Natural Host Environment. Front. Microbiol. 12.

Bonnier, F., Keating, M.E., Wróbel, T.P., Majzner, K., Baranska, M., Garcia-Munoz, A., Blanco, A., Byrne, *H.*J., 2015. Cell viability assessment using the Alamar blue assay: A comparison of 2D and 3D cell culture models. Toxicology in Vitro 29, 124–131.

Borgognone, A., Serna, G., Noguera-Julian, M., Alonso, L., Parera, M., Català-Moll, F., Sanchez, L., Fasani, R., Paredes, R., Nuciforo, P., 2021. Performance of 16S Metagenomic Profiling in Formalin-Fixed Paraffin-Embedded versus Fresh-Frozen Colorectal Cancer Tissues. Cancers (Basel) 13, 5421.

Bosman, F.T., Carneiro, F., Hruban, R.*H.*, Theise, N.D., 2010. WHO classification of tumours of the digestive system. WHO classification of tumours of the digestive system.

Bourzac, K.M., Botham, C.M., Guillemin, K., 2007. *Helicobacter pylori* CagA Induces AGS Cell Elongation through a Cell Retraction Defect That Is Independent of Cdc42, Rac1, and Arp2/3. Infection and Immunity 75, 1203–1213.

Bradshaw, D.J., Marsh, P.D., Watson, G.K., Allison, C., 1998. Role of Fusobacterium nucleatum and Coaggregation in Anaerobe Survival in Planktonic and Biofilm Oral Microbial Communities during Aeration. Infect Immun 66, 4729–4732.

Bravo, D., Hoare, A., Soto, C., Valenzuela, M.A., Quest, A.F., 2018. *Helicobacter pylori* in human health and disease: Mechanisms for local gastric and systemic effects. World J Gastroenterol 24, 3071–3089.

Brown, J.H., and L. Brenn, 1931. “A Method for the Differential Staining of Gram Positive and Gram Negative Bacteria in Tissue Sections”. Bulletin of The Johns Hopkins 69-73.

Brown, R C, and H C Hopps. 1973 “Staining of bacteria in tissue sections: a reliable gram stain method. American Journal of Clinical Pathology. Volume 60,2. 234-40. doi:10.1093/ajcp/60.2.234

Bryrup, T., Thomsen, C.W., Kern, T., Allin, K.*H.*, Brandslund, I., Jørgensen, N.R., Vestergaard, *H.*, Hansen, T., Hansen, T.*H.*, Pedersen, O., Nielsen, T., 2019. Metformin-induced changes of the gut microbiota in healthy young men: results of a non-blinded, one-armed intervention study. Diabetologia 62, 1024–1035.

Buckley, K.*H.*, Beyries, K.A., Ryeom, S., Yoon, S.S., Katona, B.W., 2024. Establishment and Characterization of Patient-derived Gastric Organoids from Biopsies of Benign Gastric Body and Antral Epithelium. J Vis Exp.

Burne, R.A., Marquis, R.E., 2000. Alkali production by oral bacteria and protection against dental caries. FEMS Microbiology Letters 193, 1–6.

Buti, L., Ruiz-Puig, C., Sangberg, D., Leissing, T.M., Brewer, R.C., Owen, R.P., Sgromo, B., Royer, C., Ebner, D., Lu, X., 2020. CagA–ASPP2 complex mediates loss of cell polarity and favors *H. pylori* colonization of human gastric organoids. Proc. Natl. Acad. Sci. U.S.A. 117, 2645–2655.

Buttgereit, F., Dejaco, C., Matteson, E.L., Dasgupta, B., 2016. Polymyalgia Rheumatica and Giant Cell Arteritis: A Systematic Review. JAMA 315, 2442–2458.

Calderillo-Ruíz, G., Díaz-Romero, M.C., Carbajal-López, B., Herrera-Martínez, M., Ruiz-García, E., Leon-Takahashi, A.M., López-Basave, *H.*N., Meneses-García, A., Herrera-Gomez, Á., 2023a. Latin American young patients with gastric adenocarcinoma: worst prognosis and outcomes. Journal of Gastrointestinal Oncology 14.

Camargo, M.C., Goto, Y., Zabaleta, J., Morgan, D.R., Correa, P., Rabkin, C.S., 2012. Sex hormones, hormonal interventions, and gastric cancer risk: a meta-analysis. Cancer Epidemiol Biomarkers Prev 21, 20–38.

Canadas-Ortega, M., Mühlbacher, I., Posselt, G., Diechler, S., Ferner, C.D., Boccellato, F., Koch, O.O., Neureiter, D., Weitzendorfer, M., Emmanuel, K., Wessler, S., 2024. HtrA-Dependent E-Cadherin Shedding Impairs the Epithelial Barrier Function in Primary Gastric Epithelial Cells and Gastric Organoids. Int J Mol Sci 25, 7083.

Cancer Research UK, 2024. Research opportunities in cancers of unmet need (website article, accessed 08.18.2024).

Cancer Statistics, 2024 - Siegel - 2024 - CA: A Cancer Journal for Clinicians - Wiley Online Library. (accessed 4.16.24).

Cancer Survival in England, cancers diagnosed 2016 to 2020, followed up to 2021 NHS England Digital. (accessed 9.12.24).

Cao, Y., Yang, W., Tyler, M.A., Gao, X., Duan, C., Kim, S.O., Aronson, J.F., Popov, V., Takahashi, *H.*, Saito, *H.*, Evers, B.M., Chao, C., Hellmich, M.R., Ko, T.C., 2013. Noggin Attenuates Cerulein-Induced Acute Pancreatitis and the Impaired Autophagy. Pancreas 42, 301–307.

Capurro, M.I., Greenfield, L.K., Prashar, A., Xia, S., Abdullah, M., Wong, *H.*, Zhong, X.Z., Bertaux-Skeirik, N., Chakrabarti, J., Siddiqui, I., O'Brien, C., Dong, X., Robinson, L., Peek Jr, R.M., Philpott, D.J., Zavros, Y., Helmrath, M., Jones, N.L., 2019a. VacA generates a protective intracellular reservoir for *Helicobacter pylori* that is eliminated by activation of the lysosomal calcium channel TRPML1. Nat Microbiol 4, 1411–1423.

Carll, T., Fuja, C., Antic, T., Lastra, R., Poon, R., McGary, R., Pytel, P., 2022. Tissue Contamination During Transportation of Formalin-Fixed, Paraffin-Embedded Blocks. American Journal of Clinical Pathology 158, 96–104.

Carvalho, M.R., Yan, L.-P., Li, B., Zhang, C.-*H.*, He, Y.-L., Reis, R.L., Oliveira, J.M., 2023. Gastrointestinal organs and organoids-on-a-chip: advances and translation into the clinics. Biofabrication 15, 042004.

Castaño-Rodríguez, N., Goh, K.-L., Fock, K.M., Mitchell, *H.*M., Kaakoush, N.O.,2017. Dysbiosis of the microbiome in gastric carcinogenesis. Sci Rep 7, 15957.

Caston, R.R., Sierra, J.C., Foegeding, N.J., Truelock, M.D., Campbell, A.M., Frick-Cheng, A.E., Bimczok, D., Wilson, K.T., McClain, M.S., Cover, T.L., 2020. Functional Properties of *Helicobacter pylori* VacA Toxin m1 and m2 Variants. Infect Immun 88, e00032-20.

Castro, J., Lima, Â., Sousa, L.G.V., Rosca, A.S., Muzny, C.A., Cerca, N., 2022. Crystal Violet Staining Alone Is Not Adequate to Assess Synergism or Antagonism in Multi-Species Biofilms of Bacteria Associated With Bacterial Vaginosis. Front Cell Infect Microbiol 11, 795797.

Celli, J.P., Turner, B.S., Afdhal, N.*H.*, Keates, S., Ghiran, I., Kelly, C.P., Ewoldt, R.*H.*, McKinley, G.*H.*, So, P., Erramilli, S., Bansil, R., 2009a. *Helicobacter pylori* moves through mucus by reducing mucin viscoelasticity. Proceedings of the National Academy of Sciences 106, 14321–14326.

Chassaing, B., Gewirtz, A.T., 2018. Identification of Inner Mucus-Associated Bacteria by Laser Capture Microdissection. Cell Mol Gastroenterol Hepatol 7, 157–160.

Chaudhry, S.R., Liman, M.N.P., Peterson, D.C., 2021. Anatomy, Abdomen and Pelvis, Stomach, in: StatPearls. StatPearls Publishing, Treasure Island (FL).

Chen, D., Guo, J., Li, A., Sun, C., Lin, Huibin, Lin, Hongyu, Yang, C., Wang, W., Gao, J., n.d. Metabolic fluorine labeling and hotspot imaging of dynamic gut microbiota in mice. Sci Adv 9, eabg6808.

Chen, S.-Y., Zhang, R.-G., Duan, G.-C., 2016. Pathogenic mechanisms of the oncoprotein CagA in *H. pylori*-induced gastric cancer (Review). Oncology Reports 36, 3087–3094.

Chen, Y.-C., Malfertheiner, P., Yu, *H.*-T., Kuo, C.-L., Chang, Y.-Y., Meng, F.-T., Wu, Y.-X., Hsiao, J.-L., Chen, M.-J., Lin, K.-P., Wu, C.-Y., Lin, J.-T., O'Morain, C., Megraud, F., Lee, W.-C., El-Omar, E.M., Wu, M.-S., Liou, J.-M., 2024. Global Prevalence of *Helicobacter pylori* Infection and Incidence of Gastric Cancer Between 1980 and 2022. Gastroenterology 166, 605–619.

Chen, Yi-Hsing, Tsai, W.-*H.*, Wu, *H.*-Y., Chen, C.-Y., Yeh, W.-L., Chen, Ya-Hui, Hsu, *H.*-Y., Chen, W.-W., Chen, Y.-W., Chang, W.-W., Lin, T.-L., Lai, *H.*-C., Lin, Y.-*H.*, Lai, C.-*H.*, 2019. Probiotic Lactobacillus spp. Act Against *Helicobacter pylori*-induced Inflammation. J Clin Med 8, 90.

Chey, W.D., Leontiadis, G.I., Howden, C.W., Moss, S.F., 2017. ACG Clinical Guideline: Treatment of *Helicobacter pylori* Infection. Am J Gastroenterol 112, 212–239.

Choi, Y., Lichterman, J.N., Coughlin, L.A., Poulides, N., Li, W., Del Valle, P., Palmer, S.N., Gan, S., Kim, J., Zhan, X., Gao, Y., Evers, B.M., Hooper, L.V., Pasare, C., Koh, A.Y., 2023. Immune checkpoint blockade induces gut microbiota translocation that augments extraintestinal anti-tumor immunity. Sci Immunol 8, eabo2003.

Chu, S., Cheng, Z., Yin, Z., Xu, J., Wu, F., Jin, Y., Yang, G., 2022. Airway Fusobacterium is Associated with Poor Response to Immunotherapy in Lung Cancer. Onco Targets Ther 15, 201–213.

Chu, Y.-T., Wang, Y.-*H.*, Wu, J.-J., Lei, *H.*-Y., 2010. Invasion and Multiplication of *Helicobacter pylori* in Gastric Epithelial Cells and Implications for Antibiotic Resistance. Infect Immun 78, 4157–4165.

Cifuentes, J.D.G., Sparkman, J., Graham, D.Y., 2022. Management of upper gastrointestinal symptoms in patients with autoimmune gastritis. Curr Opin Gastroenterol 38, 600–606.

Claus, D., 1992a. A standardised Gram staining procedure. World J Microbiol Biotechnol 8, 451–452.

Clevers, *H.*, 2016. Modeling Development and Disease with Organoids. Cell 165, 1586–1597.

Clinton, S.K., Giovannucci, E.L., Hursting, S.D., 2020. The World Cancer Research Fund/American Institute for Cancer Research Third Expert Report on Diet, Nutrition, Physical Activity, and Cancer: Impact and Future Directions. J Nutr 150, 663–671.

Coker, O.O., Dai, Z., Nie, Y., Zhao, G., Cao, L., Nakatsu, G., Wu, W.K., Wong, S.*H.*, Chen, Z., Sung, J.J.Y., Yu, J., 2018. Mucosal microbiome dysbiosis in gastric carcinogenesis. Gut 67, 1024–1032.

Conze, T., Carvalho, A.S., Landegren, U., Almeida, R., Reis, C.A., David, L., Söderberg, O., 2010. MUC2 mucin is a major carrier of the cancer-associated sialyl-Tn antigen in intestinal metaplasia and gastric carcinomas. Glycobiology 20, 199–206.

Corbacho, I., Teixidó, F., Velázquez, R., Hernández, L. m., Olivero, I., 2010. Yeast vacuole staining using quinacrine and neutral red, in: Microorganisms in Industry and Environment. WORLD SCIENTIFIC, pp. 659–661.

Correa, P., 2004. The biological model of gastric carcinogenesis. IARC Sci Publ 01–310.

Correa, P., Houghton, J., 2007. Carcinogenesis of *Helicobacter pylori*. Gastroenterology 133, 659–672.

Correa, P., Piazuelo, M.B., 2012. The gastric precancerous cascade. Journal of Digestive Diseases 13, 2–9.

Cover, T.L., Blaser, M.J., 1992. Purification and characterization of the vacuolating toxin from *Helicobacter pylori*. J Biol Chem 267, 10570–10575.

Cover, T.L., Halter, S.A., Blaser, M.J., 1992. Characterization of HeLa cell vacuoles induced by *Helicobacter pylori* broth culture supernatant. Hum Pathol 23, 1004–1010.

Cover, T.L., Tummuru, M.K., Cao, P., Thompson, S.A., Blaser, M.J., 1994. Divergence of genetic sequences for the vacuolating cytotoxin among *Helicobacter pylori* strains. J Biol Chem 269, 10566–10573.

Crabtree, J. E., Wyatt, J.I., Trejdosiewicz, L.K., Peichl, P., Nichols, P.*H.*, Ramsay. N., Primrose, J.N., Lindley, I.J., 1994. Interleukin-8 expression in *Helicobacter pylori* infected, normal, and neoplastic gastroduodenal mucosa. J Clin Pathol 47, 61–66.

Criss, Z.K., Bhasin, N., Di Rienzi, S.C., Rajan, A., Deans-Fielder, K., Swaminathan, G., Kamyabi, N., Zeng, X.-L., Doddapaneni, *H.*, Menon, V.K., Chakravarti, D., Estrella, C., Yu, X., Patil, K., Petrosino, J.F., Fleet, J.C., Verzi, M.P., Christakos, S., Helmrath, M.A., Arimura, S., DePinho, R.A., Britton, R.A., Maresso, A.W., Grande-Allen, K.J.,

Behrens S, Fuchs BM, Mueller F, Amann R, 2003. Is the in situ accessibility of the 16S rRNA of Escherichia coli for Cy3-labeled oligonucleotide probes predicted by a three-dimensional structure model of the 30S ribosomal subunit. Appl Environ Microbiol. 69(8):4935-41

Blutt, S.E., Crawford, S.E., Estes, M.K., Ramani, S., Shroyer, N.F., 2021. Drivers of transcriptional variance in human intestinal epithelial organoids. Physiol Genomics 53, 486–508.

Cullen, C.M., Aneja, K.K., Beyhan, S., Cho, C.E., Woloszynek, S., Convertino, M., McCoy, S.J., Zhang, Y., Anderson, M.Z., Alvarez-Ponce, D., Smirnova, E., Karstens, L., Dorrestein, P.C., Li, *H.*, Sen Gupta, A., Cheung, K., Powers, J.G., Zhao, Z., Rosen, G.L., 2020. Emerging Priorities for Microbiome Research. Front. Microbiol. 11.

Daims H, Brühl A, Amann R, Schleifer KH, Wagner M, 1999. The Domain-specific Probe EUB338 is Insufficient for the Detection of all Bacteria: Development and Evaluation of a more Comprehensive Probe Set, Systematic and Applied Microbiology,Volume 22, Issue 3, Pages 434-444,

de Steenhuijsen Piters, W.A.A., Bogaert, D., 2020. Bacterial DNA in Fetal Lung Samples May Be Explained by Sample Contamination. Am J Respir Crit Care Med 201, 1310–1311.

Debesa-Tur, G., Pérez-Brocal, V., Ruiz-Ruiz, S., Castillejo, A., Latorre, A., Soto, J.L., Moya, A., 2021. Metagenomic analysis of formalin-fixed paraffin-embedded tumor and normal mucosa reveals differences in the microbiome of colorectal cancer patients. Sci Rep 11, 391.

DeGruttola, A.K., Low, D., Mizoguchi, A., Mizoguchi, E., 2016. Current understanding of dysbiosis in disease in human and animal models. Inflamm Bowel Dis 22, 1137–1150.

Dheer, R., Davies, J.M., Quintero, M.A., Damas, O.M., Deshpande, A.R., Kerman, D.*H.*, Sawyer, W.P., Pignac-Kobinger, J., Ban, Y., Fernandez, I., Burgueno, J.F., Phillips, M.C., Abreu, M.T., 2019. Microbial Signatures and Innate Immune Gene

Expression in Lamina Propria Phagocytes of Inflammatory Bowel Disease Patients. Cell Mol Gastroenterol Hepatol 9, 387–402.

Diaconu, S., Predescu, A., Moldoveanu, A., Pop, C., Fierbințeanu-Braticevici, C., 2017. *Helicobacter pylori* infection: old and new. J Med Life 10, 112–117.

Díaz, P., Valenzuela Valderrama, M., Bravo, J., Quest, A.F.G., 2018. *Helicobacter pylori* and Gastric Cancer: Adaptive Cellular Mechanisms Involved in Disease Progression. Front Microbiol 9, 5.

Dixon, M.F., Genta, R.M., Yardley, J.*H.*, Correa, P., the Participants in the international Workshop on the Histopathology of Gastritis, *H.* 1994, 1996. Classification and Grading of Gastritis: The Updated Sydney System. The American Journal of Surgical Pathology 20, 1161.

Doenges, J.L., 1938. Spirochetes in Gastric Glands of Macacus rhesus and Humans without Definite History of Related Disease. Proceedings of the Society for Experimental Biology and Medicine 38, 536–538.

Doorakkers E, Lagergren J, Santoni G, Engstrand L and Brusselaers N., 2020. *Helicobacter pylori* eradication treatment and the risk of Barrett's esophagus and esophageal adenocarcinoma. *Helicobacter*. 25:e12688.

Đorđević, M., Životić, M., Radojević Škodrić, S., Nešović Ostojić, J., Marković Lipkovski, J., Filipović, J., Ćirović, S., Kovačević, S., Dunđerović, D., 2021. Effects of Automation on Sustainability of Immunohistochemistry Laboratory. Healthcare (Basel) 9, 866.

Dubois, A., Berg, D.E., Incecik, E.T., Fiala, N., Heman-Ackah, L.M., Perez-Perez, G.I., Blaser, M.J., 1996. Transient and persistent experimental infection of nonhuman primates with *Helicobacter pylori*: implications for human disease. Infect Immun 64, 2885–2891.

Durazzi, F., Sala, C., Castellani, G., Manfreda, G., Remondini, D., Cesare, A., 2021a. Comparison between 16S rRNA and shotgun sequencing data for the taxonomic characterization of the gut microbiota. Scientific Reports 11.

East, J.E., Vleugels, J.L., Roelandt, P., Bhandari, P., Bisschops, R., Dekker, E., Hassan, C., Horgan, G., Kiesslich, R., Longcroft-Wheaton, G., Wilson, A., Dumonceau, J.-M., 2016. Advanced endoscopic imaging: European Society of Gastrointestinal Endoscopy (ESGE) Technology Review. Endoscopy 48, 1029–1045.

Eaton, K.A., Brooks, C.L., Morgan, D.R., Krakowka, S., 1991. Essential role of urease in pathogenesis of gastritis induced by *Helicobacter pylori* in gnotobiotic piglets. Infection and Immunity 59, 2470–2475.

Eaton, K.A., Morgan, D.R., Krakowka, S., 1992. Motility as a factor in the colonisation of gnotobiotic piglets by *Helicobacter pylori*. J Med Microbiol 37, 123–127.

Eftang, L.L., Esbensen, Y., Tannæs, T.M., Bukholm, I.R., Bukholm, G., 2012. Interleukin-8 is the single most up-regulated gene in whole genome profiling of *H. pylori* exposed gastric epithelial cells. BMC Microbiology 12, 9.

El Miedany, Y., Elgaafary, M., Toth, M., Azim, A.A., Palmer, D., Dolbear, G., Abu-zaid, M.*H.*, Affam, D., Hassan, W., Elnady, B., Tabra, S. abdAlhamed, Saber, S., 2023. Development of outcome measures for giant cell arteritis for use in clinical trials and standard practice. Clin Rheumatol 42, 3049–3057.

Elghannam, M.T., Hassanien, M.*H.*, Ameen, Y.A., Turky, E.A., ELattar, G.M., ELRay, A.A., ELTalkawy, M.D., 2024a. *Helicobacter pylori* and oral–gut microbiome: clinical implications. Infection 52, 289–300.

Elzayat, *H.*, Mesto, G., Al-Marzooq, F., 2023. Unraveling the Impact of Gut and Oral Microbiome on Gut Health in Inflammatory Bowel Diseases. Nutrients 15, 3377.

Engbaek, K., Johansen, K.S., Jensen, M.E., 1979. A new technique for Gram staining paraffin-embedded tissue. J Clin Pathol 32, 187–190.

Eun, C.S., Kim, B.K., Han, D.S., Kim, S.Y., Kim, K.M., Choi, B.Y., Song, K.S., Kim, Y.S., Kim, J.F., 2014. Differences in gastric mucosal microbiota profiling in patients with chronic gastritis, intestinal metaplasia, and gastric cancer using pyrosequencing methods. *Helicobacter* 19, 407–416.

Fallis, A.G., 2013. Janeways IMMUNOLOGY, Journal of Chemical Information and Modeling. 5, 19.

Fan, C., Chen, C., Chou, C., Kao, T., Cheng, A.N., Lee, A.Y., Kuo, C., 2019. A time-saving–modified Giemsa stain is a better diagnostic method of *Helicobacter pylori* infection compared with the rapid urease test. J Clin Lab Anal 34, e23110.

Farouk, W.I., Hassan, N.*H.*, Ismail, T.R., Daud, I.S., Mohammed, F., 2018. Warthin-Starry Staining for the Detection of *Helicobacter pylori* in Gastric Biopsies. Malays J Med Sci 25, 92–99.

Fenoglio-Preiser, C. m., Wang, J., Stemmermann, G. n., Noffsinger, A., 2003. TP53 and gastric carcinoma: A review. Human Mutation 21, 258–270.

Ferlay, J., Colombet, M., Soerjomataram, I., Parkin, D.M., Piñeros, M., Znaor, A., Bray, F., 2021. Cancer statistics for the year 2020: An overview. Int J Cancer.

Ferreira, D.A., Conde, J.P., Rothbauer, M., Ertl, P., Granja, P.L., Oliveira, C., 2023. Bioinspired human stomach-on-a-chip with in vivo like function and architecture. Lab Chip 23, 495–510.

Ferreira, R.M., Pereira-Marques, J., Pinto-Ribeiro, I., Costa, J.L., Carneiro, F., Machado, J.C., Figueiredo, C., 2018. Gastric microbial community profiling reveals a dysbiotic cancer-associated microbiota. Gut 67, 226–236.

Feyisa, Z.T., Woldeamanuel, B.T., 2021. Prevalence and associated risk factors of gastritis among patients visiting Saint Paul Hospital Millennium Medical College, Addis Ababa, Ethiopia. PLoS One 16, e0246619.

Filipe, M.I., Muñoz, N., Matko, I., Kato, I., Pompe-Kirn, V., Jutersek, A., Teuchmann, S., Benz, M., Prijon, T., 1994. Intestinal metaplasia types and the risk of gastric cancer: a cohort study in Slovenia. Int J Cancer 57, 324–329.

Fischer, A.*H.*, Jacobson, K.A., Rose, J., Zeller, R., 2008. Hematoxylin and eosin staining of tissue and cell sections. CSH Protoc 2008, pdb.prot4986.

Fischer, W., Buhrdorf, R., Gerland, E., Haas, R., 2001. Outer Membrane Targeting of Passenger Proteins by the Vacuolating Cytotoxin Autotransporter of *Helicobacter pylori*. Infect Immun 69, 6769–6775.

Fischetti, V.A., 2016. M Protein and Other Surface Proteins on Streptococci, in: Ferretti, J.J., Stevens, D.L., Fischetti, V.A. (Eds.), Streptococcus Pyogenes: Basic Biology to Clinical Manifestations. University of Oklahoma Health Sciences Center, Oklahoma City (OK).

Foegeding, N.J., Caston, R.R., McClain, M.S., Ohi, M.D., Cover, T.L., 2016a. An Overview of *Helicobacter pylori* VacA Toxin Biology. Toxins (Basel) 8, 173.

Foegeding, N.J., Raghunathan, K., Campbell, A.M., Kim, S.W., Lau, K.S., Kenworthy, A.K., Cover, T.L., Ohi, M.D., 2019. Intracellular Degradation of *Helicobacter pylori* VacA Toxin as a Determinant of Gastric Epithelial Cell Viability. Infection and Immunity 87.

Freedberg, A.S., Barron, L.E., 1940. The presence of spirochetes in human gastric mucosa; American journal of digestive diseases, 7, 443-445.

Fu, K., Cheung, A.*H.*K., Wong, C.C., Liu, W., Zhou, Y., Wang, F., Huang, P., Yuan, K., Coker, O.O., Pan, Y., Chen, D., Lam, N.M., Gao, M., Zhang, X., Huang, *H.*, To, K.F., Sung, J.J.Y., Yu, J., 2024a. Streptococcus anginosus promotes gastric inflammation, atrophy, and tumorigenesis in mice. Cell 187, 882-896.e17.

Fujii, M., Matano, M., Toshimitsu, K., Takano, A., Mikami, Y., Nishikori, S., Sugimoto, S., Sato, T., 2018. Human Intestinal Organoids Maintain Self-Renewal Capacity and Cellular Diversity in Niche-Inspired Culture Condition. Cell Stem Cell 23, 787-793.e6.

Fung, C., Tan, S., Nakajima, M., Skoog, E.C., Camarillo-Guerrero, L.F., Klein, J.A., Lawley, T.D., Solnick, J.V., Fukami, T., Amieva, M.R., 2019. High-resolution mapping reveals that microniches in the gastric glands control *Helicobacter pylori* colonization of the stomach. PLoS Biol 17, e3000231.

Gaddy, J.A., Radin, J.N., Loh, J.T., Zhang, F., Washington, M.K., Peek, R.M., Algood, *H.*M.S., Cover, T.L., 2013. High Dietary Salt Intake Exacerbates *Helicobacter pylori*-Induced Gastric Carcinogenesis. Infect Immun 81, 2258–2267.

Galeano Niño, J.L., Wu, *H.*, LaCourse, K.D., Kempchinsky, A.G., Baryiames, A., Barber, B., Futran, N., Houlton, J., Sather, C., Sicinska, E., Taylor, A., Minot, S.S., Johnston, C.D., Bullman, S., 2022a. Effect of the intratumoral microbiota on spatial and cellular heterogeneity in cancer. Nature 611, 810–817.

Galeano Niño, J.L., Wu, *H.*, LaCourse, K.D., Kempchinsky, A.G., Baryiames, A., Barber, B., Futran, N., Houlton, J., Sather, C., Sicinska, E., Taylor, A., Minot, S.S., Johnston, C.D., Bullman, S., 2022b. Effect of the intratumoral microbiota on spatial and cellular heterogeneity in cancer. Nature 611, 810–817.

Gantuya, B., El-Serag, *H.*B., Matsumoto, T., Ajami, N.J., Oyuntsetseg, K., Azzaya, D., Uchida, T., Yamaoka, Y., 2019. Gastric Microbiota in *Helicobacter pylori*-Negative and -Positive Gastritis Among High Incidence of Gastric Cancer Area. Cancers 11, 504.

García Carmona, S., Arango Viana, J.C., Ahumada Rodríguez, E.J., Agudelo Mesa, J., Pérez Cala, T.L., Martínez, A., Ospina Ospina, S., Salazar Giraldo, B.E., 2022. Utilidad de la coloración de Giemsa para diagnosticar *Helicobacter pylori* en pacientes con lesiones preneoplásicas. Rev. colomb. Gastroenterol. 37, 402–409.

García-Morales, N., Pérez-Aísa, Á., Fiorini, G., Tepes, B., Castro-Fernández, M., Lucendo, A., Voynovan, I., Bujanda, L., Garre, A., Rodrigo, L., Martínez Domínguez, S.J., Denkovski, M., Huguet Malavés, J.M., Jonaitis, L., Bumane, R., Zaytsev, O., Mata Romero, P., Barrio, J., Fernández-Salazar, L., Sarsenbaeva, A.S., Ortiz Polo, I., Alekseenko, S., Saracino, I.M., Vaira, D., Keco-Huerga, A., Bordin, D., Gasbarrini, A., Lerang, F., Rokkas, T., Kupčinskas, J., Leja, M., Babayeva, G., Marcos Pinto, R., Tonkić, A., Smith, S., Phull, P., Buzas, G.M., Simsek, *H.*, Boltin, D., Gridnyev, O., Venerito, M., Milivojevic, V., Torà, N., Cano-Català, A., Moreira, L., Nyssen, O.P., Mégraud, F., O'Morain, C., Gisbert, J.P., Puig, I., 2023. *Helicobacter pylori* Diagnostic Tests Used in Europe: Results of over 34,000 Patients from the European Registry on *Helicobacter pylori* Management. J Clin Med 12, 4363.

Gardos, G., Cole, J.O., 1976. Maintenance antipsychotic therapy: is the cure worse than the disease? Am J Psychiatry 133, 32–36.

Garner, J.A., Cover, T.L., 1996. Binding and internalization of the *Helicobacter pylori* vacuolating cytotoxin by epithelial cells. Infect Immun 64, 4197–4203.

Gastric cancer occurrence in preneoplastic lesions: A long-term follow-up in a high-risk area in Spain - González - 2010 - International Journal of Cancer - Wiley Online Library.

Gaudino, S.J., Kumar, P., 2019. Cross-talk between antigen presenting cells and T cells impacts intestinal homeostasis, bacterial infections, and tumorigenesis.

Geisinger, E., Isberg, R.R., 2015. Antibiotic Modulation of Capsular Exopolysaccharide and Virulence in Acinetobacter baumannii. PLOS Pathogens 11, e1004691.

Gellrich, S., Ventura, R., Jones, M., Tan, S.-Y., Mason, D.Y., 2004. Immunofluorescent and FISH analysis of skin biopsies. Am J Dermatopathol 26, 242–247.

Gerhard, M., Lehn, N., Neumayer, N., Borén, T., Rad, R., Schepp, W., Miehlke, S., Classen, M., Prinz, C., 1999. Clinical relevance of the *Helicobacter pylori* gene for blood-group antigen-binding adhesin. Proceedings of the National Academy of Sciences 96, 12778–12783.

Gerli, R., Lunardi, C., Vinante, F., Bistoni, O., Pizzolo, G., Pitzalis, C., 2001. Role of CD30+ T cells in rheumatoid arthritis: A counter-regulatory paradigm for Th1-driven diseases.

Geuze, *H.*J., 1998. The role of endosomes and lysosomes in MHC class II functioning. 98, 201.

Ghiara, P., Marchetti, M., Blaser, M.J., Tummuru, M.K., Cover, T.L., Segal, E.D., Tompkins, L.S., Rappuoli, R., 1995. Role of the *Helicobacter pylori* virulence factors vacuolating cytotoxin, CagA, and urease in a mouse model of disease. Infect Immun 63, 4154–4160.

Giddings, H.J., Teodósio, A., Jones, J., McMurray, J.L., Hunter, K., Alame, R., Gardiner, I., Abdawn, Z., Butterworth, W., Henderson, I.R., Cole, J.A., Shannon-Lowe, C.D. and Rossiter-Pearson, A.E. (2025), The Gastric Microbiota Invade the Lamina Propria in *Helicobacter pylori*-Associated Gastritis and Precancer. Helicobacter, 30: e70016.

Gilbert, M.T.P., Haselkorn, T., Bunce, M., Sanchez, J.J., Lucas, S.B., Jewell, L.D., Marck, E.V., Worobey, M., 2007. The Isolation of Nucleic Acids from Fixed, Paraffin-Embedded Tissues–Which Methods Are Useful When? PLOS ONE 2, e537.

Gillooly, J.F., Hayward, A., Hou, C., Burleigh, J.G., 2012. Explaining differences in the lifespan and replicative capacity of cells: a general model and comparative analysis of vertebrates. Proc Biol Sci 279, 3976–3980.

Glassing, A., Dowd, S.E., Galandiuk, S., Davis, B., Chiodini, R.J., 2016. Inherent bacterial DNA contamination of extraction and sequencing reagents may affect interpretation of microbiota in low bacterial biomass samples. Gut Pathog 8, 24.

Global Cancer Statistics 2020: GLOBOCAN Estimates of Incidence and Mortality Worldwide for 36 Cancers in 185 Countries – PubMed. Accessed 09.01.24.

Glover, B., Teare, J., Ashrafian, *H.*, Patel, N., 2020. The endoscopic predictors of *Helicobacter pylori* status: a meta-analysis of diagnostic performance. Ther Adv Gastrointest Endosc 13, 2631774520950840.

Gonciarz, W., Walencka, M., Moran, A.P., Hinc, K., Obuchowski, M., Chmiela, M., 2019. Upregulation of MUC5AC production and deposition of LEWIS determinants by *H. pylori* facilitate gastric tissue colonization and the maintenance of infection. Journal of Biomedical Science 26, 23.

González, C.A., López-Carrillo, L., 2010. *Helicobacter pylori*, nutrition and smoking interactions: their impact in gastric carcinogenesis. Scand J Gastroenterol 45, 6–14.

González, C.A., Pardo, M.L., Ruiz Liso, J.M., Alonso, P., Bonet, C., Garcia, R.M., Sala, N., Capella, G., Sanz-Anquela, J.M., 2010. Gastric cancer occurrence in preneoplastic lesions: A long-term follow-up in a high-risk area in Spain. International Journal of Cancer 127, 2654–2660.

González-Rivera, C., Algood, *H.*M.S., Radin, J.N., McClain, M.S., Cover, T.L., 2012. The Intermediate Region of *Helicobacter pylori* VacA Is a Determinant of Toxin Potency in a Jurkat T Cell Assay. Infect Immun 80, 2578–2588.

Goodell, V., dela Rosa, C., Slota, M., MacLeod, B., Disis, M.L., 2007. Sensitivity and specificity of tritiated thymidine incorporation and ELISPOT assays in identifying antigen specific T cell immune responses. BMC Immunology.

Goodman, K.J., Correa, P., 2000. Transmission of *Helicobacter pylori* among siblings. Lancet 355, 358–362.

Goodwin, A.C., Weinberger, D.M., Ford, C.B., Nelson, J.C., Snider, J.D., Hall, J.D., Paules, C.I., Peek, R.M., Forsyth, M.*H.*, 2008. Expression of the *Helicobacter pylori* adhesin SabA is controlled via phase variation and the ArsRS signal transduction system. Microbiology (Reading) 154, 2231–2240.

Goodwin, C.S., 1994. How *Helicobacter pylori* acquired its name, and how it overcomes gastric defence mechanisms. J Gastroenterol Hepatol 9 Suppl 1, S1-3.

Goyal, R.K., Guo, Y., Mashimo, *H.*, 2019. Advances in the physiology of gastric emptying. Neurogastroenterology & Motility 31, e13546.

Gram, H.C. 1884. Uber die isolierte Farbung der Schizomyceten in Schnittund Trocken praparaten. Fortschritte der Medizin, 2, 185-189.

Griswold, A., Chen, Y.-Y.M., Snyder, J.A., Burne, R.A., 2004. Characterization of the Arginine Deiminase Operon of Streptococcus rattus FA-1. Appl Environ Microbiol 70, 1321–1327.

Gu, *H.*, 2017. Role of Flagella in the Pathogenesis of *Helicobacter pylori*. Curr Microbiol 74, 863–869.

Guilford, P.J., Hopkins, J.B.W., Grady, W.M., Markowitz, S.D., Willis, J., Lynch, *H.*, Rajput, A., Wiesner, G.L., Lindor, N.M., Burgart, L.J., Toro, T.T., Lee, D., Limacher, J.-M., Shaw, D.W., Findlay, M.P.N., Reeve, A.E., 1999. E-cadherin germline mutations define an inherited cancer syndrome dominated by diffuse gastric cancer. Human Mutation 14, 249–255.

Han, Y.W., 2015. Fusobacterium nucleatum: a commensal-turned pathogen. Curr Opin Microbiol 0, 141–147.

Harris, P.R., Cover, T.L., Crowe, D.R., Orenstein, J.M., Graham, M.F., Blaser, M.J., Smith, P.D., 1996. *Helicobacter pylori* cytotoxin induces vacuolation of primary human mucosal epithelial cells. Infect Immun 64, 4867–4871.

Hatakeyama, M., 2017. Structure and function of *Helicobacter pylori* CagA, the first-identified bacterial protein involved in human cancer. Proc Jpn Acad Ser B Phys Biol Sci 93, 196–219.

He, X.-X., Li, Y.-*H.*, Yan, P.-G., Meng, X.-C., Chen, C.-Y., Li, K.-M., Li, J.-N., 2021. Relationship between clinical features and intestinal microbiota in Chinese patients with ulcerative colitis. World J Gastroenterol 27, 4722–4737.

Hennies, C.M., Lehn, M.A., Janssen, E.M., 2015. Quantitating MHC class II trafficking in primary dendritic cells using imaging flow cytometry. Journal of Immunological Methods.

Herrera, J.A., Mallikarjun, V., Rosini, S., Montero, M.A., Lawless, C., Warwood, S., O'Cualain, R., Knight, D., Schwartz, M.A., Swift, J., 2020a. Laser capture microdissection coupled mass spectrometry (LCM-MS) for spatially resolved analysis of formalin-fixed and stained human lung tissues. Clin Proteomics 17, 24.

Higashi, *H.*, Nakaya, A., Tsutsumi, R., Yokoyama, K., Fujii, Y., Ishikawa, S., Higuchi, M., Takahashi, A., Kurashima, Y., Teishikata, Y., Tanaka, S., Azuma, T., Hatakeyama,

M., 2004. *Helicobacter pylori* CagA induces Ras-independent morphogenetic response through SHP-2 recruitment and activation. J Biol Chem 279, 17205–17216.

Hirschl, A.M., Richter, M., Makristathis, A., Prückl, P.M., Willinger, B., Schütze, K., Rotter, M.L., 1994. Single and multiple strain colonization in patients with *Helicobacter pylori*-associated gastritis: detection by macrorestriction DNA analysis. J Infect Dis 170, 473–475.

Holland, R.L., Bosi, K.D., Harpring, G.*H.*, Luo, J., Wallig, M., Phillips, *H.*, Blanke, S.R., 2020. Chronic in vivo exposure to *Helicobacter pylori* VacA: Assessing the efficacy of automated and long-term intragastric toxin infusion. Sci Rep 10, 9307.

Hoy, B., Löwer, M., Weydig, C., Carra, G., Tegtmeyer, N., Geppert, T., Schröder, P., Sewald, N., Backert, S., Schneider, G., Wessler, S., 2010. *Helicobacter pylori* HtrA is a new secreted virulence factor that cleaves E-cadherin to disrupt intercellular adhesion. EMBO reports 11, 798–804.

Hoyt, C.C., 2021. Multiplex Immunofluorescence and Multispectral Imaging: Forming the Basis of a Clinical Test Platform for Immuno-Oncology. Front Mol Biosci 8, 674747.

Hu, Y., Wan, J.-*H.*, Li, X.-Y., Zhu, Y., Graham, D.Y., Lu, N.-*H.*, 2017. Systematic review with meta-analysis: the global recurrence rate of *Helicobacter pylori*. Alimentary Pharmacology & Therapeutics 46, 773–779.

Hu, Y.-L., Pang, W., Huang, Y., Zhang, Y., Zhang, C.-J., 2018. The Gastric Microbiome Is Perturbed in Advanced Gastric Adenocarcinoma Identified Through Shotgun Metagenomics. Front. Cell. Infect. Microbiol. 8.

Huang, Y., Wang, Q., Cheng, D., Xu, W., Lu, N., 2016. Adhesion and Invasion of Gastric Mucosa Epithelial Cells by *Helicobacter pylori*. Frontiers in Cellular and Infection Microbiology 6, 159.

Hutt-Fletcher, L.M., 2017. The Long and Complicated Relationship between Epstein-Barr Virus and Epithelial Cells. J Virol 91, e01677-16.

Hybiske, K., Stephens, R.S., 2008. Exit strategies of intracellular pathogens. NatComs, 5, 201.

Ibrahim, S., Al-Saryi, N., Al-Kadmy, I.M.S., Aziz, S.N., 2021. Multidrug-resistant Acinetobacter baumannii as an emerging concern in hospitals. Mol Biol Rep 48, 6987–6998.

Idowu, S., Bertrand, P.P., Walduck, A.K., 2022. Gastric organoids: Advancing the study of *H. pylori* pathogenesis and inflammation. *Helicobacter* 27, e12891.

Iino, C., Shimoyama, T., Chinda, D., Arai, T., Chiba, D., Nakaji, S., Fukuda, S. 2018. Infection of *Helicobacter pylori* and Atrophic Gastritis Influence Lactobacillus in Gut Microbiota in a Japanese Population. Front. Immunol. 9.

Ishihara, K., Miura, T., Kimizuka, R., Ebihara, Y., Mizuno, Y., Okuda, K., 1997. Oral bacteria inhibit *Helicobacter pylori* growth. FEMS Microbiology Letters 152, 355–361.

Ito, 1967. Anatomic structure of the gastric mucosa. American Physiological Society, Washington, D.C. Alimentary Canal, 705–741.

Ito, T., Kobayashi, D., Uchida, K., Takemura, T., Nagaoka, S., Kobayashi, I., Yokoyama, T., Ishige, I., Ishige, Y., Ishida, N., Furukawa, A., Muraoka, *H.*, Ikeda, S., Sekine, M., Ando, N., Suzuki, Y., Yamada, T., Suzuki, T., Eishi, Y., 2008. *Helicobacter pylori* invades the gastric mucosa and translocates to the gastric lymph nodes. Laboratory Investigation 88, 664–681.

Iwai, K., Watanabe, I., Yamamoto, T., Kuriyama, N., Matsui, D., Nomura, R., Ogaya, Y., Oseko, F., Adachi, K., Takizawa, S., Ozaki, E., Koyama, T., Nakano, K., Kanamura, N., Uehara, R., Watanabe, Y., 2019. Association between *Helicobacter pylori* infection and dental pulp reservoirs in Japanese adults. BMC Oral Health 19, 267.

Iwasaki, A., Medzhitov, R., 2015. Control of adaptive immunity by the innate immune system.

Jacobs, A.C., Hood, I., Boyd, K.L., Olson, P.D., Morrison, J.M., Carson, S., Sayood, K., Iwen, P.C., Skaar, E.P., Dunman, P.M., 2010. Inactivation of Phospholipase D Diminishes Acinetobacter baumannii Pathogenesis. Infect Immun 78, 1952–1962.

Jafar A Al Souz, M.A., 2019. Use of modified peptides for live tracking of peptide-MHCII complexes during antigenspecific T cell-dendritic cell interactions. The Journal of Immunology 202.

Jang, B.G., Lee, B.L., Kim, W.*H.*, 2015. Intestinal Stem Cell Markers in the Intestinal Metaplasia of Stomach and Barrett's Esophagus. PLoS One 10, e0127300.

Jemilohun, A.C., Otegbayo, J.A., 2016. *Helicobacter pylori* infection: past, present and future. The Pan African Medical Journal 23.

Jencks, D.S., Adam, J.D., Borum, M.L., Koh, J.M., Stephen, S., Doman, D.B., 2018. Overview of Current Concepts in Gastric Intestinal Metaplasia and Gastric Cancer. Gastroenterol Hepatol (N Y) 14, 92–101.

Jeroch, J., Riedlinger, T., Schmitt, C., Ebner, S., Winkelmann, R., Wild, P.J., Demes, M., 2023. A Comparison of Two Different FFPE Tissue Dissection Methods for Routine Diagnostics in Molecular Pathology: Manual Macrodissection versus Automated

Microdissection Using the Roche “AVENIO Millisect” System. Cancers (Basel) 15, 3249.

Johansson, M.E.V., Phillipson, M., Petersson, J., Velcich, A., Holm, L., Hansson, G.C., 2008. The inner of the two Muc2 mucin-dependent mucus layers in colon is devoid of bacteria. Proc Natl Acad Sci U S A 105, 15064–15069.

Johnson, G.L., Lapadat, R., 2002. Mitogen-activated protein kinase pathways mediated by ERK, JNK, and p38 protein kinases.

Johnson, J.S., Spakowicz, D.J., Hong, B.-Y., Petersen, L.M., Demkowicz, P., Chen, L., Leopold, S.R., Hanson, B.M., Agresta, *H.*O., Gerstein, M., Sodergren, E., Weinstock, G.M., 2019b. Evaluation of 16S rRNA gene sequencing for species and strain-level microbiome analysis. Nat Commun 10, 5029.

Jones, B.C., Calà, G., De Coppi, P., Giobbe, G.G., 2021. Paediatric gastric organoids as a tool for disease modelling and clinical translation. Pediatr Surg Int 37, 317–324.

Jones, K.R., Whitmire, J.M., Merrell, D.S., 2010. A Tale of Two Toxins: *Helicobacter* Pylori CagA and VacA Modulate Host Pathways that Impact Disease. Front Microbiol 1, 115.

Jonkers, D., Gisbertz, I., de Bruine, A., Bot, F., Arends, J.W., Stobberingh, E., Schouten, *H.*, Stockbrügger, R., 1997. *Helicobacter pylori* and non-*Helicobacter pylori* bacterial flora in gastric mucosal and tumour specimens of patients with primary gastric lymphoma. Eur J Clin Invest 27, 885–892.

Jurado-Martín, I., Sainz-Mejías, M., McClean, S., 2021. Pseudomonas aeruginosa: An Audacious Pathogen with an Adaptable Arsenal of Virulence Factors. International Journal of Molecular Sciences 22.

Kachuei, V., Talebi Bezmin Abadi, A., Rahimi, F., Forootan, M., 2020b. Colonization by Pseudomonas aeruginosa and Staphylococcus aureus of Antral Biopsy Specimens from Gastritis Patients Uninfected with *Helicobacter* Pylori. Infect Drug Resist 13, 1411–1417.

Kalhor, K., Chen, C.-J., Lee, *H.*S., Cai, M., Nafisi, M., Que, R., Palmer, C., Yuan, Y., Zhang, Y., Song, J., Knoten, A., Lake, B.B., Gaut, J.P., Keene, D., Lein, E., Kharchenko, P.V., Chun, J., Jain, S., Fan, J.-B., Zhang, K., 2023. Mapping Human Tissues with Highly Multiplexed RNA in situ Hybridisation. bioRxiv 2023.08.16.553610.

Kang, W., Jia, Z., Tang, D., Zhang, Z., Gao, *H.*, He, K., Feng, Q., 2019. Fusobacterium nucleatum Facilitates Apoptosis, ROS Generation, and Inflammatory Cytokine Production by Activating AKT/MAPK and NF-κB Signaling Pathways in Human Gingival Fibroblasts. Oxid Med Cell Longev 2019, 1681972.

Kao, C.-Y., Sheu, B.-S., Sheu, S.-M., Yang, *H.*-B., Chang, W.-L., Cheng, *H.*-C., Wu, J.-J., 2012. Higher Motility Enhances Bacterial Density and Inflammatory Response in Dyspeptic Patients Infected with *Helicobacter pylori*. *Helicobacter* 17, 411–416.

Kao, C.-Y., Sheu, B.-S., Wu, J.-J., 2016. *Helicobacter pylori* infection: An overview of bacterial virulence factors and pathogenesis. Biomed J 39, 14–23.

Kavitt, R.T., Lipowska, A.M., Anyane-Yeboa, A., Gralnek, I.M., 2019. Diagnosis and Treatment of Peptic Ulcer Disease. Am J Med 132, 447–456.

Kelly, M., Pitcher, C.L., Farmery, M., Gibson', R., n.d. Isolation of Hekobacter *pylori* From Feces of Patients With Dyspepsia in the United Kingdom 107.

Khoramian-Falsafi, T., Harayama, S., Kutsukake, K., Pechère, J.C., 1990. Effect of motility and chemotaxis on the invasion of Salmonella typhimurium into HeLa cels.

Khosravi, Y., Dieye, Y., Poh, B.*H.*, Ng, C.G., Loke, M.F., Goh, K.L., Vadivelu, J., 2014. Culturable Bacterial Microbiota of the Stomach of *Helicobacter pylori* Positive and Negative Gastric Disease Patients. The Scientific World Journal 2014, 610421.

Kianoush, N., Adler, C.J., Nguyen, K.-A.T., Browne, G.V., Simonian, M., Hunter, N., 2014. Bacterial Profile of Dentine Caries and the Impact of pH on Bacterial Population Diversity. PLoS One 9, e92940.

Kim, J., Kim, *H.*, Lee, M.-S., Lee, *H.*, Kim, Y.J., Lee, W.Y., Yun, S.*H.*, Kim, *H.*C., Hong, *H.*K., Hannenhalli, S., Cho, Y.B., Park, D., Choi, S.S., 2023. Transcriptomes of the tumor-adjacent normal tissues are more informative than tumors in predicting recurrence in colorectal cancer patients. Journal of Translational Medicine 21, 209.

Kim, J., Koo, B.-K., Knoblich, J.A., 2020. Human organoids: model systems for human biology and medicine. Nat Rev Mol Cell Biol 21, 571–584.

Kim, S.-M., Kim, R., Ryu, J.-*H.*, Jho, E.-*H.*, Song, K.-J., Jang, S.-I., Kee, S.-*H.*, 2005. Multinuclear giant cell formation is enhanced by down-regulation of Wnt signaling in gastric cancer cell line, AGS. Experimental Cell Research 308, 18–28.

Kimura, M., Goto, S., Wada, A., Yahiro, K., Niidome, T., Hatakeyama, T., Aoyagi, *H.*, Hirayama, T., Kondo, T., 1999. Vacuolating cytotoxin purified from*Helicobacter pylori*causes mitochondrial damage in human gastric cells. Microbial Pathogenesis 26, 45–52.

Kinchen, J.M., Ravichandran, K.S., 2008. Phagosome maturation: Going through the acid test.

Kool, J., Tymchenko, L., Shetty, S.A., Fuentes, S., 2023. Reducing bias in microbiome research: Comparing methods from sample collection to sequencing. Front Microbiol 14, 1094800.

Kozlowski, W., Jochymski, C., Markiewicz, T., Kozlowski, W., Jochymski, C., Markiewicz, T., 2011. Chronic Gastritis, in: Gastritis and Gastric Cancer - New Insights in Gastroprotection, Diagnosis and Treatments. IntechOpen.

KR Vinod, Jones, D., Udupa, V., 2016. A simple and effective heat induced antigen retrieval method. MethodsX 3, 315–319.

Krenacs, L., Krenacs, T., Stelkovics, E., Raffeld, M., 2010. Heat-Induced Antigen Retrieval for Immunohistochemical Reactions in Routinely Processed Paraffin Sections. Methods Mol Biol 588, 103–119.

Krienitz, W., 1906. Ueber das Auftreten von Spirochäten verschiedener Form im Mageninhalt bei Carcinoma ventriculi. Dtsch Med Wochenschr 32, 872–872.

Kuck, D., Kolmerer, B., Iking-Konert, C., Krammer, P.*H.*, Stremmel, W., Rudi, J., 2001a Vacuolating Cytotoxin of *Helicobacter pylori* Induces Apoptosis in the Human Gastric Epithelial Cell Line AGS. Infect Immun 69, 5080–5087.

Kufe, D.W., 2009. Mucins in cancer: function, prognosis and therapy. Nat Rev Cancer 9, 874–885.

Kulasinghe, A., Wood, F., Belz, G., 2023. The seductive allure of spatial biology: accelerating new discoveries in the life sciences. Immunology & Cell Biology 101, 798–804.

Kusters, J.G., van Vliet, A.*H.*M., Kuipers, E.J., 2006. Pathogenesis of *Helicobacter pylori* Infection. Clin Microbiol Rev 19, 449–490.

Lakoduk A, Lee, C, Chen P., 2021. Gain-of-“endocytic’ function in mutant p53 cancer cells, Int J of Biochem & Cell Bio,131,105905,1357-2725..

Lam, S.Y., Ioannou, A., Konstanti, P., Visseren, T., Doukas, M., Peppelenbosch, M.P., Belzer, C., Fuhler, G.M., 2021. Technical challenges regarding the use of formalin-fixed paraffin embedded (FFPE) tissue specimens for the detection of bacterial alterations in colorectal cancer. BMC Microbiol 21, 297.

Langford, C.A., Cuthbertson, D., Ytterberg, S.R., Khalidi, N., Monach, P.A., Carette, S., Seo, P., Moreland, L.W., Weisman, M., Koening, C.L., Sreih, A., Spiera, R., McAlear, C.A., Warrington, K.J., Pagnoux, C., McKinnon, K., Forbess, L.J., Hoffman, G.S., Borchin, R., Krischer, J.P., Merkel, P.A., 2017. A RANDOMISED, DOUBLE-BLIND TRIAL OF ABATACEPT (CTLA4-IG) FOR THE TREATMENT OF GIANT CELL ARTERITIS. Arthritis Rheumatol 69, 837–845.

Lau, J.T., Whelan, F.J., Herath, I., Lee, C.*H.*, Collins, S.M., Bercik, P., Surette, M.G., 2016. Capturing the diversity of the human gut microbiota through culture-enriched molecular profiling. Genome Med 8, 72.

Lauwers, G.Y., Riddell, R.*H.*, 1999. Gastric epithelial dysplasia. Gut 45, 784–784.

Lee, A., O'Rourke, J., De Ungria, M., Robertson, B., Daskalopoulos, G., Dixon, M., 1997. A standardised mouse model of *Helicobacter pylori* infection: Introducing the Sydney strain. Gastroenterology 112, 1386–1397.

Lee, *H.*S., Lee, *H.*K., Kim, *H.*S., Yang, *H.*K., Kim, Y.I., Kim, W.*H.*, 2001. MUC1, MUC2, MUC5AC, and MUC6 expressions in gastric carcinomas. Cancer 92, 1427–1434.

Lee, J.*H.*, Chang, K.K., Yoon, C., Tang, L.*H.*, Strong, V.E., Yoon, S.S., 2018. Lauren histologic type is the most important factor associated with pattern of recurrence following resection of gastric adenocarcinoma. Ann Surg 267, 105–113.

Lee, J.J., Rosenberg, *H.*F., 2012. Eosinophils in Health and Disease. Academic Press.

Lee, J.Y., Kim, N., 2015. Diagnosis of *Helicobacter pylori* by invasive test: histology. Ann Transl Med 3, 10.

Lee, K.E., Khoi, P.N., Xia, Y., Park, J.S., Joo, Y.E., Kim, K.K., Choi, S.Y., Jung, Y.D., 2013. *Helicobacter pylori* and interleukin-8 in gastric cancer. World Journal of Gastroenterology: WJG 19, 8192.

Lee, J & Kim, N (2015). Diagnosis of Helicobacter pylori by invasive test: Histology. Annals of translational medicine. 3. 10. 10.3978/j.issn.2305-5839.2014.11.03.

Lee, K.K., McCauley, *H.*A., Broda, T.R., Kofron, M.J., Wells, J.M., Hong, C.I., 2018. Human stomach-on-a-chip with luminal flow and peristaltic-like motility. Lab Chip 18, 3079–3085.

Lehouritis, P., Cummins, J., Stanton, M., Murphy, C.T., McCarthy, F.O., Reid, G., Urbaniak, C., Byrne, W.L., Tangney, M., 2015. Local bacteria affect the efficacy of chemotherapeutic drugs. Sci Rep 5, 14554.

Letley, D.P., Rhead, J.L., Twells, R.J., Dove, B., Atherton, J.C., 2003. Determinants of Non-toxicity in the Gastric Pathogen *Helicobacter pylori* *. Journal of Biological Chemistry 278, 26734–26741.

Leunk, R.D., Johnson, P.T., David, B.C., Kraft, W.G., Morgan, D.R., 1988. Cytotoxic activity in broth-culture filtrates of Campylobacter *pylori*. J Med Microbiol 26, 93–99.

Li, J., Perez-Perez, G.I., 2018. *Helicobacter pylori* the Latent Human Pathogen or an Ancestral Commensal Organism. Front Microbiol 9, 609.

Li, N., Batzer, A., Daly, R., Yajnik, V., Skolnik, E., Chardin, P., Bar-Sagi, D., Margolis, B., Schlessinger, J., 1993. Guanine-nucleotide-releasing factor hSos1 binds to Grb2 and links receptor tyrosine kinases to Ras signalling. Nature 363, 85–88.

Li, N., Xie, C., Lu, N.-*H.*, 2016. p53, a potential predictor of *Helicobacter pylori* infection-associated gastric carcinogenesis? Oncotarget 7, 66276–66286.

Li X-X, Wong GL-H, To K-F, et al. Bacterial microbiota profiling in gastritis without *Helicobacter pylori* infection or non-steroidal anti-inflammatory drug use. PLoS.

Li, X.-X., Wong, G.L.-*H.*, To, K.-F., Wong, V.W.-S., Lai, L.*H.*, Chow, D.K.-L., Lau, J.Y.-W., Sung, J.J.-Y., Ding, C., 2009. Bacterial microbiota profiling in gastritis without *Helicobacter pylori* infection or non-steroidal anti-inflammatory drug use. PLoS One 4, e7985.

Liang, S., Wang, C., Shao, Y., Wang, Y., Xing, D., Geng, Z., 2022. Recent advances in bacteria-mediated cancer therapy. Front. Bioeng. Biotechnol. 10.

Lim, J.J., Grinstein, S., Roth, Z., 2017. Diversity and versatility of phagocytosis: Roles in innate immunity, tissue remodeling, and homeostasis. Frontiers in Cellular and Infection Microbiology.

Lin, A., Loughman, J.A., Zinselmeyer, B.*H.*, Miller, M.J., Caparon, M.G., 2009. Streptolysin S inhibits neutrophil recruitment during the early stages of Streptococcus pyogenes infection. Infection and Immunity.

Linares, R., Francés, R., Gutiérrez, A., Juanola, O., 2021. Bacterial Translocation as Inflammatory Driver in Crohn's Disease. Front Cell Dev Biol 9, 703310.

Linz B, Balloux F, Moodley Y, Manica A, Liu H, Roumagnac P, Falush D, Stamer C, Prugnolle F, van der Merwe SW, Yamaoka Y, Graham DY, Perez-Trallero E, Wadstrom T, Suerbaum S, Achtman M. An African origin for the intimate association between humans and *Helicobacter pylori.* Nature. 2007 Feb 22;445(7130):915-918. doi: 10.1038/nature05562. Epub 2007 Feb 7. PMID: 17287725.

Liu, A., 2010. Laser Capture Microdissection in the Tissue Biorepository. J Biomol Tech 21, 120–125.

Liu, D., Chen, S., Gou, Y., Yu, W., Zhou, *H.*, Zhang, R., Wang, J., Ye, F., Liu, Y., Sun, B., Zhang, K., 2021a. Gastrointestinal Microbiota Changes in Patients With Gastric Precancerous Lesions. Front Cell Infect Microbiol 11, 749207.

Liu, J., Tan, Y., Cheng, *H.*, Zhang, D., Feng, W., Peng, C., 2022. Functions of Gut Microbiota Metabolites, Current Status and Future Perspectives. Aging Dis 13, 1106–1126.

Liu, J., Xue, Y., Zhou, L., 2018. Detection of gastritis-associated pathogens by culturing of gastric juice and mucosa. Int J Clin Exp Pathol 11, 2214–2220.

Liu, M., Wang, Y. & Du, B. 2024. Update on the association between Helicobacter pylori infection and asthma in terms of microbiota and immunity. *Allergy Asthma Clin Immunol*. 0.1186/s13223-024-00870-2.

Liu, S., Wang, S., Zhang, N., Li, P., 2024. The oral microbiome and oral and upper gastrointestinal diseases. Journal of Oral Microbiology 16, 2355823.

Li, T., Qin, Y., Sham, P. *et al.* 2017.Alterations in Gastric Microbiota After *H. Pylori* Eradication and in Different Histological Stages of Gastric Carcinogenesis. *Sci Rep* **7**, 44935. https://doi.org/10.1038/srep44935

Liu, X., Liu, H., Luo, X., Zhang, P., Gao, Y., Xie, S., Xu, K., Chang, J., Ma, L., 2017. Strains of Group B streptococci from septic patients induce platelet activation via Toll-like Receptor 2. Clin Exp Pharmacol Physiol 44, 335–343.

Liu, Y., Ma, Y., Huang, C., 2022. Evaluation of the Gastric Microbiome in Patients with Chronic Superficial Gastritis and Intestinal Metaplasia. Chinese Medical Sciences Journal 37, 44–51.

Llopis, M., Cassard, A.M., Wrzosek, L., Boschat, L., Bruneau, A., Ferrere, G., Puchois, V., Martin, J.C., Lepage, P., Le Roy, T., Lefèvre, L., Langelier, B., Cailleux, F., González-Castro, A.M., Rabot, S., Gaudin, F., Agostini, *H.*, Prévot, S., Berrebi, D., Ciocan, D., Jousse, C., Naveau, S., Gérard, P., Perlemuter, G., 2016. Intestinal microbiota contributes to individual susceptibility to alcoholic liver disease. Gut 65, 830–839.

Lo, C.-*H.*, Wu, D.-C., Jao, S.-W., Wu, C.-C., Lin, C.-Y., Chuang, C.-*H.*, Lin, Y.-B., Chen, C.-*H.*, Chen, Ying-Ting, Chen, J.-*H.*, Hsiao, K.-*H.*, Chen, Y.-J., Chen, Yuan-Tsong, Wang, J.-Y., Li, L.-*H.*, 2022a. Enrichment of Prevotella intermedia in human colorectal cancer and its additive effects with Fusobacterium nucleatum on the malignant transformation of colorectal adenomas. Journal of Biomedical Science 29, 88.

Löfling, J., Diswall, M., Eriksson, S., Borén, T., Breimer, M.E., Holgersson, J., 2008. Studies of Lewis antigens and *H. pylori* adhesion in CHO cell lines engineered to express Lewis b determinants. Glycobiology 18, 494–501.

Loong, T.*H.*, Soon, N.C., Nik Mahmud, N.R.K., Naidu, J., Rani, R.A., Abdul Hamid, N., Elias, M.*H.*, Mohamed Rose, I., Tamil, A., Mokhtar, N.M., Raja Ali, R.A., 2017. Serum pepsinogen and gastrin-17 as potential biomarkers for pre-malignant lesions in the gastric corpus. Biomed Rep 7, 460–468.

López-Valverde, N., Macedo de Sousa, B., López-Valverde, A., Suárez, A., Rodríguez, C., Aragoneses, J.M., 2022. Possible Association of Periodontal Diseases With

Helicobacter pylori Gastric Infection: A Systematic Review and Meta-Analysis. Front. Med. 9.

Loricera, J., Blanco, R., Hernández, J.L., Castañeda, S., Mera, A., Pérez-Pampín, E., Peiró, E., Humbría, A., Calvo-Alén, J., Aurrecoechea, E., Narváez, J., Sánchez-Andrade, A., Vela, P., Díez, E., Mata, C., Lluch, P., Moll, C., Hernández, Í., Calvo-Río, V., Ortiz-Sanjuán, F., González-Vela, C., Pina, T., González-Gay, M.Á., 2015. Tocilizumab in giant cell arteritis: Multicenter open-label study of 22 patients. Semin Arthritis Rheum 44, 717–723.

Lousada, M.B., Edelkamp, J., Lachnit, T., Fehrholz, M., Jimenez, F., Paus, R., 2023b. Laser capture microdissection as a method for investigating the human hair follicle microbiome reveals region-specific differences in the bacteriome profile. BMC Res Notes 16, 29.

Louw, J.A., Kidd, M.S., Kummer, A.F., Taylor, K., Kotze, U., Hanslo, D., 2001. The relationship between *Helicobacter pylori* infection, the virulence genotypes of the infecting strain and gastric cancer in the African setting. *Helicobacter* 6, 268–273.

Löwer, M., Weydig, C., Metzler, D., Reuter, A., Starzinski-Powitz, A., Wessler, S., Schneider, G., 2008. Prediction of Extracellular Proteases of the Human Pathogen *Helicobacter pylori* Reveals Proteolytic Activity of the Hp1018/19 Protein HtrA. PLOS ONE 3, e3510.

Lu, R., Voigt, R.M., Zhang, Y., Kato, I., Xia, Y., Forsyth, C.B., Keshavarzian, A., Sun, J., 2017. Alcohol Injury Damages Intestinal Stem Cells. Alcoholism: Clinical and Experimental Research 41, 727–734.

Lytton, S.D., Fischer, W., Nagel, W., Haas, R., Beck, F.X., 2005. Production of ammonium by *Helicobacter pylori* mediates occludin processing and disruption of tight junctions in Caco-2 cells. Microbiology (Reading) 151, 3267–3276.

Mahdavi, J., Sondén, B., Hurtig, M., Olfat, F.O., Forsberg, L., Roche, N., Ångström, J., Larsson, T., Teneberg, S., Karlsson, K.-A., Altraja, S., Wadström, T., Kersulyte, D., Berg, D.E., Dubois, A., Petersson, C., Magnusson, K.-E., Norberg, T., Lindh, F., Lundskog, B.B., Arnqvist, A., Hammarström, L., Borén, T., 2002b. *Helicobacter pylori* SabA Adhesin in Persistent Infection and Chronic Inflammation. Science 297, 573–578.

Mailhe, M., Ricaboni, D., Vitton, V., Gonzalez, J.-M., Bachar, D., Dubourg, G., Cadoret, F., Robert, C., Delerce, J., Levasseur, A., Fournier, P.-E., Angelakis, E., Lagier, J.-C., Raoult, D., 2018. Repertoire of the gut microbiota from stomach to colon using culturomics and next-generation sequencing. BMC Microbiol 18, 157.

Malaty, *H.*M., El-Kasabany, A., Graham, D.Y., Miller, C.C., Reddy, S.G., Srinivasan, S.R., Yamaoka, Y., Berenson, G.S., 2002. Age at acquisition of *Helicobacter pylori* infection: a follow-up study from infancy to adulthood. The Lancet 359, 931–935.

Maldonado-Contreras, A., Goldfarb, K., Godoy-Vitorino, F. 2011. Structure of the human gastric bacterial community in relation to Helicobacter pylori status. ISME J 5, 574–579. https://doi.org/10.1038/ismej.2010.149

Malfertheiner, P., Megraud, F., O'Morain, C.A., Gisbert, J.P., Kuipers, E.J., Axon, A.T., Bazzoli, F., Gasbarrini, A., Atherton, J., Graham, D.Y., Hunt, R., Moayyedi, P., Rokkas, T., Rugge, M., Selgrad, M., Suerbaum, S., Sugano, K., El-Omar, E.M., European *Helicobacter* and Microbiota Study Group and Consensus panel, 2017. Management of *Helicobacter pylori* infection-the Maastricht V/Florence Consensus Report. Gut 66, 6–30.

Markou, P., Apidianakis, Y., 2014. Pathogenesis of intestinal Pseudomonas aeruginosa infection in patients with cancer. Front Cell Infect Microbiol 3, 115.

Marques, M.S., Melo, J., Cavadas, B., Mendes, N., Pereira, L., Carneiro, F., Figueiredo, C., Leite, M., 2018. Afadin Downregulation by *Helicobacter pylori* Induces Epithelial to Mesenchymal Transition in Gastric Cells. Front Microbiol 9, 2712.

Marshall, B., Adams, P.C., 2008. *Helicobacter pylori*: A Nobel pursuit? Can J Gastroenterol 22, 895–896.

Marshall, B., Warren, J.R., 1984. UNIDENTIFIED CURVED BACILLI IN THE STOMACH OF PATIENTS WITH GASTRITIS AND PEPTIC ULCERATION. The Lancet, originally published as Volume 1, Issue 8390 323, 1311–1315.

Marshall, B.J., 2001. One Hundred Years of Discovery and Rediscovery of *Helicobacter pylori* and Its Association with Peptic Ulcer Disease, in: Mobley, *H.*L., Mendz, G.L., Hazell, S.L. (Eds.), *Helicobacter* Pylori: Physiology and Genetics. ASM Press, Washington (DC).

Marshall, B.J., Armstrong, J.A., McGechie, D.B., Glancy, R.J., 1985. Attempt to fulfil Koch's postulates for *pyloric* Campylobacter. Med J Aust 142, 436–439.

Marshall, B.J., Warren, J.R., 1984. Unidentified curved bacilli in the stomach of patients with gastritis and peptic ulceration. Lancet 1, 1311–1315.

Martel, C. de, Georges, D., Bray, F., Ferlay, J., Clifford, G.M., 2020. Global burden of cancer attributable to infections in 2018: a worldwide incidence analysis. The Lancet Global Health 8, e180–e190.

Martínez, L.E., Hardcastle, J.M., Wang, J., Pincus, Z., Tsang, J., Hoover, T.R., Bansil, R., Salama, N.R., 2016. elicobacter *pylori* strains vary cell shape and flagellum number

to maintain robust motility in viscous environments. Molecular Microbiology 99, 88–110.

Matozaki, T., Sakamoto, C., Matsuda, K., Suzuki, T., Konda, Y., Nakano, O., Wada, K., Uchida, T., Nishisaki, *H.*, Nagao, M., Kasuga, M., 1992. Missense mutations and a deletion of the p53 gene in human gastric cancer. Biochemical and Biophysical Research Communications 182, 215–223.

McClain, M.S., Cao, P., Iwamoto, *H.*, Vinion-Dubiel, A.D., Szabo, G., Shao, Z., Cover, T.L., 2001. A 12-amino-acid segment, present in type s2 but not type s1 *Helicobacter pylori* VacA proteins, abolishes cytotoxin activity and alters membrane channel formation. J Bacteriol 183, 6499–6508.

McCracken, K.W., Wells, J.M., 2017. Mechanisms of embryonic stomach development. Semin Cell Dev Biol 66, 36–42.

Mendall, M.A., Goggin, P.M., Molineaux, N., Levy, J., Toosy, T., Strachan, D., Northfield, T.C., 1992. Childhood living conditions and *Helicobacter pylori* seropositivity in adult life. Lancet 339, 896–897.

Meyer, R.D., 1993. Book Review Medical Mycology By K.J. Kwon-Chung and John E. Brennett. 866 pp., illustrated. Philadelphia, Lea and Febiger, 1992. $69.50. 0-8121-1463-9. New England Journal of Medicine.

Mi, M., Wu, F., Zhu, J., Liu, F., Cui, G., Wen, X., Hu, Y., Deng, Z., Wu, X., Zhang, Z., Qi, T., Chen, Z., 2021. Heterogeneity of *Helicobacter pylori* Strains Isolated from Patients with Gastric Disorders in Guiyang, China. Infect Drug Resist 14, 535–545.

Mills, J., Shivdasani, R., 2011. Gastric Epithelial Stem Cells. Gastroenterology 140, 412–424.

Miller A, Williams S., 2021. *Helicobacter pylori* infection causes both protective and deleterious effects in human health and disease. Genes Immun. 2021 Aug;22(4):218-226. doi: 10.1038/s41435-021-00146- Jul 9. PMID: 34244666.

Minor, D., Cavon, J., Johnson, T., Ontiveros, S., Gao, D., Quinn, M.T., Lei, B., 2022. Host-to-Host Group A Streptococcus Transmission Causes Infection of the Lamina Propria but Not Epithelium of the Upper Respiratory Tract in MyD88-Deficient Mice. Infection and Immunity 90, e00423-21.

Mishra, A., Lai, G.C., Yao, L.J., Aung, T.T., Shental, N., Rotter-Maskowitz, A., Shepherdson, E., Singh, G.S.N., Pai, R., Shanti, A., Wong, R.M.M., Lee, A., Khyriem, C., Dutertre, C.A., Chakarov, S., Srinivasan, K.G., Shadan, N.B., Zhang, X.-M., Khalilnezhad, S., Cottier, F., Tan, A.S.M., Low, G., Chen, P., Fan, Y., Hor, P.X., Lee, A.K.M., Choolani, M., Vermijlen, D., Sharma, A., Fuks, G., Straussman, M. Pavelka, N., Malleret, B., McGovern, N., Albani, S., Chan, J.K.Y., Ginhoux, F., 2021. Microbial

exposure during early human development primes fetal immune cells. Cell 184, 3394-3409.e20.

Mizote, T., Yoshiyama, *H.*, Nakazawa, T., 1997. Urease-independent chemotactic responses of *Helicobacter pylori* to urea, urease inhibitors, and sodium bicarbonate. Infection and Immunity 65, 1519–1521.

Mohammadi, M., 2020. Role of Obesity in the Tumorigenesis of Gastric Cancer. Int J Prev Med 11, 148.

Mohammadi, S., Morell-Perez, C., Wright, C.W., Wyche, T.P., White, C.*H.*, Sana, T.R., Lieberman, L.A., 2021. Assessing donor-to-donor variability in human intestinal organoid cultures. Stem Cell Reports 16, 2364–2378.

Monstein, *H.*, Tiveljung, A., Kraft, C.*H.*, Borch, K., Jonasson, J., 2000. Profiling of bacterial flora in gastric biopsies from patients with *Helicobacter pylori*-associated gastritis and histologically normal control individuals by temperature gradient gel electrophoresis and 16S rDNA sequence analysis. Journal of Medical Microbiology 49, 817–822.

Morgan, E., Arnold, M., Camargo, M.C., Gini, A., Kunzmann, A.T., Matsuda, T., Meheus, F., Verhoeven, R.*H.*A., Vignat, J., Laversanne, M., Ferlay, J., Soerjomataram, I., 2022. The current and future incidence and mortality of gastric cancer in 185 countries, 2020–40: A population-based modelling study. eClinicalMedicine 47.

Morita, C., Sumioka, R., Nakata, M., Okahashi, N., Wada, S., Yamashiro, T., Hayashi, M., Hamada, S., Sumitomo, T., Kawabata, S., 2014. Cell wall-anchored nuclease of Streptococcus sanguinis contributes to escape from neutrophil extracellular trap-mediated bacteriocidal activity. PLoS ONE.

Morris, F.C., Dexter, C., Kostoulias, X., Uddin, M.I., Peleg, A.Y., 2019. The Mechanisms of Disease Caused by Acinetobacter baumannii. Front. Microbiol. 10.

Moschioni, M., Pansegrau, W., Barocchi, M.A., 2010. Adhesion determinants of the Streptococcus species. Microb Biotechnol 3, 370–388.

Müller, A.J., Kaiser, P., Dittmar, K.E.J., Weber, T.C., Haueter, S., Endt, K., Songhet, P., Zellweger, C., Kremer, M., Fehling, *H.*-J., Hardt, W.-D., 2012. Salmonella Gut Invasion Involves TTSS-2-Dependent Epithelial Traversal, Basolateral Exit, and Uptake by Epithelium-Sampling Lamina Propria Phagocytes. Cell Host & Microbe 11, 19–32.

Murakami, M., Fukuzawa, M., Yamamoto, M., Hamaya, K., Tamura, Y., Sugiyama, A., Takahashi, R., Murakami, T., Amagase, K., Takeuchi, K., 2013. Effects of *Helicobacter pylori* infection on gastric parietal cells and E-cadherin in Mongolian gerbils. J Pharmacol Sci 121, 305–311.

Murata-Kamiya, N., Kurashima, Y., Teishikata, Y., Yamahashi, Y., Saito, Y., Higashi, *H.*, Aburatani, *H.*, Akiyama, T., Peek, R.M., Azuma, T., Hatakeyama, M., 2007. *Helicobacter pylori* CagA interacts with E-cadherin and deregulates the β-catenin signal that promotes intestinal transdifferentiation in gastric epithelial cells. Oncogene 26, 4617–4626.

Nearing, J.T., Douglas, G.M., Hayes, M.G., MacDonald, J., Desai, D.K., Allward, N., Jones, C.M.A., Wright, R.J., Dhanani, A.S., Comeau, A.M., Langille, M.G.I., 2022a. Microbiome differential abundance methods produce different results across 38 datasets. Nat Commun 13, 342.

Nedrud, J.G., 1999. Animal models for gastric *Helicobacter* immunology and vaccine studies. FEMS Immunology & Medical Microbiology 24, 243–250.

Neiman, A.M., 2005. Ascospore Formation in the Yeast Saccharomyces cerevisiae. Microbiology and Molecular Biology Reviews 69, 565–584.

Nejati, S., Karkhah, A., Darvish, *H.*, Validi, M., Ebrahimpour, S., Nouri, *H.*R., 2018. Influence of *Helicobacter pylori* virulence factors CagA and VacA on pathogenesis of gastrointestinal disorders. Microbial Pathogenesis 117, 43–48.

Ng, K.M., Tropini, C., 2021. Visualisation of Gut Microbiota-host Interactions via Fluorescence In Situ Hybridisation, Lectin Staining, and Imaging. J Vis Exp.

Nguyen, D.-*H.*, Chong, A., Hong, Y., Min, J.-J., 2023. Bioengineering of bacteria for cancer immunotherapy. Nat Commun 14, 3553.

Nogueira, C., Figueiredo, C., Carneiro, F., Taveira Gomes, A., Barreira, R., Figueira, P., Salgado, C., Belo, L., Peixoto, A., Bravo, J.C., Bravo, L.E., Realpe, J.L., Plaisier, A.P., Quint, W.G.V., Ruiz, B., Correa, P., van Doorn, L.-J., 2001a. *Helicobacter pylori* Genotypes May Determine Gastric Histopathology. Am J Pathol 158, 647–654.

Nomura, R., Kadota, T., Ogaya, Y., Matayoshi, S., Iwashita, N., Okawa, R., Nakano, K., 2020. Contribution of Streptococcus mutans to *Helicobacter pylori* colonisation in oral cavity and gastric tissue. Sci Rep 10, 12540.

Noto, J.M., Jr, R.M.P., 2017. The gastric microbiome, its interaction with *Helicobacter pylori*, and its potential role in the progression to stomach cancer. PLOS Pathogens 13, e1006573.

Nunes, P., Demaurex, N., 2010. The role of calcium signaling in phagocytosis. Journal of Leukocyte Biology.

Ofori-Darko, E., Zavros, Y., Rieder, G., Tarlé, S.A., Van Antwerp, M., Merchant, J.L., 2000. An OmpA-Like Protein from Acinetobacterspp. Stimulates Gastrin and Interleukin-8 Promoters. Infection and Immunity 68, 3657–3666.

Ohnishi, N., Yuasa, *H.*, Tanaka, S., Sawa, *H.*, Miura, M., Matsui, A., Higashi, *H.*, Musashi, M., Iwabuchi, K., Suzuki, M., Yamada, G., Azuma, T., Hatakeyama, M., 2008. Transgenic expression of *Helicobacter pylori* CagA induces gastrointestinal and hematopoietic neoplasms in mouse. Proc Natl Acad Sci U S A 105, 1003–1008.

Okada, K., Takezawa, K., Tsujimura, G., Imanaka, T., Kuribayashi, S., Ueda, N., Hatano, K., Fukuhara, S., Kiuchi, *H.*, Fujita, K., Motooka, D., Nakamura, S., Koyama, Y., Shimada, S., Nonomura, N., 2022. Localization and potential role of prostate microbiota. Front. Cell. Infect. Microbiol. 12.

Oliphant, K., Allen-Vercoe, E., 2019. Macronutrient metabolism by the human gut microbiome: major fermentation by-products and their impact on host health. Microbiome 7, 91.

Oosterlinck, B., Ceuleers, *H.*, Arras, W., De Man, J.G., Geboes, K., De Schepper, *H.*, Peeters, M., Lebeer, S., Skieceviciene, J., Hold, G.L., Kupcinskas, J., Link, A., De Winter, B.Y., Smet, A., 2023. Mucin-microbiome signatures shape the tumor microenvironment in gastric cancer. Microbiome 11, 86.

Ootani, A., Toda, S., Fujimoto, K., Sugihara, *H.*, 2003. Foveolar Differentiation of Mouse Gastric Mucosa in Vitro. Am J Pathol 162, 1905–1912.

Ootani, A., Toda, S., Fujimoto, K., Sugihara, *H.*, 2000. An Air–Liquid Interface Promotes the Differentiation of Gastric Surface Mucous Cells (GSM06) in Culture. Biochemical and Biophysical Research Communications 271, 741–746.

Ophir, T., Gutnick, D.L., 1994. A role for exopolysaccharides in the protection of microorganisms from desiccation.

O'Rourke, J.L., Lee, A., 2003. Animal models of *Helicobacter pylori* infection and disease. Microbes and Infection, *Helicobacter pylori*: epidemiology, virulence, immune responses, and vaccine approaches 5, 741–748.

Osaki, T., Mabe, K., Hanawa, T., Kamiya, S., 2008. Urease-positive bacteria in the stomach induce a false-positive reaction in a urea breath test for diagnosis of *Helicobacter pylori* infection. J Med Microbiol 57, 814–819.

Pachathundikandi, S.K., Tegtmeyer, N., Backert, S., 2013. Signal transduction of *Helicobacter pylori* during interaction with host cell protein receptors of epithelial and immune cells. Gut Microbes 4, 454–474.

Pagliaccia, C., de Bernard, M., Lupetti, P., Ji, X., Burroni, D., Cover, T.L., Papini, E., Rappuoli, R., Telford, J.L., Reyrat, J.M., 1998. The m2 form of the *Helicobacter pylori* cytotoxin has cell type-specific vacuolating activity. Proc Natl Acad Sci U S A 95, 10212–10217.

Palframan, S.L., Kwok, T., Gabriel, K., 2012. Vacuolating cytotoxin A (VacA), a key toxin for *Helicobacter pylori* pathogenesis. Front Cell Infect Microbiol 2, 92.

Palmer, E.D., 1954. Investigation of the Gastric Mucosa Spirochetes of the Human. Gastroenterology 27, 218–220.

Papastergiou, V., Georgopoulos, S.D., Karatapanis, S., 2014. Treatment of *Helicobacter pylori* infection: meeting the challenge of antimicrobial resistance. World J Gastroenterol 20, 9898–9911.

Papini, E., de Bernard, M., Milia, E., Bugnoli, M., Zerial, M., Rappuoli, R., Montecucco, C., 1994. Cellular vacuoles induced by *Helicobacter pylori* originate from late endosomal compartments. Proc Natl Acad Sci U S A 91, 9720–9724.

Papini, E., Zoratti, M., Cover, T.L., 2001. In search of the *Helicobacter pylori* VacA mechanism of action. Toxicon 39, 1757–1767.

Parente, F., Porro, G.B., 2001. The 13C-urea breath test for non-invasive diagnosis of *Helicobacter pylori* infection: which procedure and which measuring equipment? European Journal of Gastroenterology & Hepatology 13, 803.

Pareti, G., Cerletti, C., Gaetano, G. de, 2002. How old is *Helicobacter pylori*? The Lancet 359, 1700–1701.

Parsons, B.N., Ijaz, U.Z., D'Amore, R., Burkitt, M.D., Eccles, R., Lenzi, L., Duckworth, C.A., Moore, A.R., Tiszlavicz, L., Varro, A., Hall, N., Pritchard, D.M., 2017. Comparison of the human gastric microbiota in hypochlorhydric states arising as a result of *Helicobacter pylori*-induced atrophic gastritis, autoimmune atrophic gastritis and proton pump inhibitor use. PLOS Pathogens 13, e1006653.

Patel, N.M., Geropoulos, G., Patel, P.*H.*, Bhogal, R.*H.*, Harrington, K.J., Singanayagam, A., Kumar, S., 2023. The Role of Mucin Expression in the Diagnosis of Oesophago-Gastric Cancer: A Systematic Literature Review. Cancers 15, 5252.

Patil, R., Blankenship, L., 2013. Proton Pump Inhibitors and Clostridium Difficile Infection: Are We Propagating an Already Rapidly Growing Healthcare Problem? Gastroenterology Res 6, 171–173.

Pavlova, S.I., Jin, L., Gasparovich, S.R., Tao, L., 2013. Multiple alcohol dehydrogenases but no functional acetaldehyde dehydrogenase causing excessive acetaldehyde production from ethanol by oral streptococci. Microbiology (Reading) 159, 1437–1446.

Peng, C., Ouyang, Y., Lu, N., Li, N., 2020. The NF-κB Signaling Pathway, the Microbiota, and Gastrointestinal Tumorigenesis: Recent Advances. Front Immunol 11, 1387.

Pennelli, G., Grillo, F., Galuppini, F., Ingravallo, G., Pilozzi, E., Rugge, M., Fiocca, R., Fassan, M., Mastracci, L., 2020. Gastritis: update on etiological features and histological practical approach. Pathologica 112, 153–165.

Piazuelo, M.B., Correa, P., 2013. Cáncer Gastrico: Punto de vista. Colombia Médica 44, 10.

Piazuelo, M.B., Haque, S., Delgado, A., Du, J.X., Rodriguez, F., Correa, P., 2004. Phenotypic differences between esophageal and gastric intestinal metaplasia. Mod Pathol 17, 62–74.

Piwocka, O., Musielak, M., Ampuła, K., Piotrowski, I., Adamczyk, B., Fundowicz, M., Suchorska, W.M., Malicki, J., 2024. Navigating challenges: optimising methods for primary cell culture isolation. Cancer Cell Int 24, 28.

Plummer, M., Franceschi, S., Vignat, J., Forman, D., de Martel, C., 2015. Global burden of gastric cancer attributable to *Helicobacter pylori*. Int J Cancer 136, 487–490.

Png, C.W., Lee, W.J.J., Chua, S.J., Zhu, F., Yeoh, K.G., Zhang, Y., 2022. Mucosal microbiome associates with progression to gastric cancer. Theranostics 12, 48–58.

Poulsen, K., Reinholdt, J., Jespersgaard, C., Boye, K., Brown, T.A., Hauge, M., Kilian, M., 1998. A Comprehensive Genetic Study of Streptococcal Immunoglobulin A1 Proteases: Evidence for Recombination within and between Species. Infect Immun 66, 181–190.

Pourvali, K., Monji, *H.*, 2021. Obesity and intestinal stem cell susceptibility to carcinogenesis. Nutr Metab (Lond) 18, 37.

Prasad, A., Ene, A., Jablonska, S., Du, J., Wolfe, A.J., Putonti, C., 2023. Comparative Genomic Study of Streptococcus anginosus Reveals Distinct Group of Urinary Strains. mSphere 8, e00687-22.

Pyo, J.-S., Sohn, J.*H.*, Kang, G., Kim, D.-*H.*, Kim, K., Do, I.-G., Kim, D.*H.*, 2015. MUC2 Expression Is Correlated with Tumor Differentiation and Inhibits Tumor Invasion in Gastric Carcinomas: A Systematic Review and Meta-analysis. J Pathol Transl Med 49, 249–256.

Qi, Y.-F., Sun, J.-N., Ren, L.-F., Cao, X.-L., Dong, J.-*H.*, Tao, K., Guan, X.-M., Cui, Y.-N., Su, W., 2019. Intestinal Microbiota Is Altered in Patients with Gastric Cancer from Shanxi Province, China. Dig Dis Sci 64, 1193–1203.

Rahman, M.M., McFadden, G., 2011. Modulation of NF-κB signalling by microbial pathogens. Nat Rev Microbiol 9, 291–306.

Rajilic-Stojanovic, M., Figueiredo, C., Smet, A., Hansen, R., Kupcinskas, J., Rokkas, T., Andersen, L., Machado, J.C., Ianiro, G., Gasbarrini, A., Leja, M., Gisbert, J.P., Hold, G.L., 2020. Systematic review: gastric microbiota in health and disease. Alimentary Pharmacology & Therapeutics 51, 582–602.

Rashid, M., Teixeira, A.S., Qureshi, U., Pereira, S.P., Novelli, M.R., Swallow, D.M., 2013. Apical MUC1 expression revealed on the foveolar epithelium in *H. pylori* gastritis. Br J Cancer 108, 1113–1118.

Rathinavelu, S., Zavros, Y., Merchant, J.L., 2003. Acinetobacter lwoffii infection and gastritis. Microbes and Infection 5, 651–657.

Reis, C.A., David, L., Correa, P., Carneiro, F., Bolós, C. de, Garcia, E., Mandel, U., Clausen, *H.*, Sobrinho-Simões, M., 1999. Intestinal Metaplasia of Human Stomach Displays Distinct Patterns of Mucin (MUC1, MUC2, MUC5AC, and MUC6) Expression1. Cancer Research 59, 1003–1007.

Repetto, G., del Peso, A., Zurita, J.L., 2008. Neutral red uptake assay for the estimation of cell viability/cytotoxicity. Nat Protoc 3, 1125–1131.

Resende, T.P., Marshall Lund, L., Rossow, S., Vannucci, F.A., 2019. Next-Generation Sequencing Coupled With in situ Hybridisation: A Novel Diagnostic Platform to Investigate Swine Emerging Pathogens and New Variants of Endemic Viruses. Front Vet Sci 6, 403.

Reynolds, D.E., Sun, Y., Wang, X., Vallapureddy, P., Lim, J., Pan, M., Fernandez Del Castillo, A., Carlson, J.C.T., Sellmyer, M.A., Nasrallah, M., Binder, Z., O'Rourke, D.M., Ming, G., Song, *H.*, Ko, J., 2024. Live Organoid Cyclic Imaging. Advanced Science 11, 2309289.

Rhee, K.-*H.*, Park, J.-S., Cho, M.-J., 2014. *Helicobacter pylori*: Bacterial Strategy for Incipient Stage and Persistent Colonization in Human Gastric Niches. Yonsei Medical Journal 55, 1453–1466.

Ricci, V., Sommi, P., Cova, E., Fiocca, R., Romano, M., Ivey, K.J., Solcia, E., Ventura, U., 1993. Na+,K(+)-ATPase of gastric cells. A target of *Helicobacter pylori* cytotoxic activity. FEBS Lett 334, 158–160.

Rico, S.D., Mahnken, M., Büscheck, F., Dum, D., Luebke, A.M., Kluth, M., Hube-Magg, C., Hinsch, A., Höflmayer, D., Möller-Koop, C., Fraune, C., Möller, K., Menz, A., Bernreuther, C., Jacobsen, F., Lebok, P., Clauditz, T.S., Sauter, G., Uhlig, R., Wilczak, W., Simon, R., Steurer, S., Minner, S., Burandt, E., Krech, T., Marx, A.*H.*, 2021. MUC5AC Expression in Various Tumor Types and Nonneoplastic Tissue: A Tissue Microarray Study on 10 399 Tissue Samples. Technol Cancer Res Treat 20, 15330338211043328.

Rieder, G., Tessier, A.J., Qiao, X.T., Madison, B., Gumucio, D.L., Merchant, J.L., 2005. *Helicobacter*-induced Intestinal Metaplasia in the Stomach Correlates with Elk-1 and Serum Response Factor Induction of Villin *. Journal of Biological Chemistry 280, 4906–4912.

Rivest, F., Eroglu, D., Pelz, B., Kowal, J., Kehren, A., Navikas, V., Procopio, M.G., Bordignon, P., Pérès, E., Ammann, M., Dorel, E., Scalmazzi, S., Bruno, L., Ruegg, M., Campargue, G., Casqueiro, G., Arn, L., Fischer, J., Brajkovic, S., Joris, P., Cassano, M., Dupouy, D., 2023. Fully automated sequential immunofluorescence (seqIF) for hyperplex spatial proteomics. Sci Rep 13, 16994.

Rocha R, Almeida C, Azevedo NF, 2018. Influence of the fixation/permeabilization step on peptide nucleic acid fluorescence in situ hybridization (PNA-FISH) for the detection of bacteria. PLoS One. 13(5):e0196522

Roche, P.A., Furuta, K., 2015. The ins and outs of MHC class II-mediated antigen processing and presentation.

Rosenplänter, C., Sommer, F., Kleemann, P., Belkovets, A., Schmidt, A., Lohoff, M., 2007. *Helicobacter pylori* polyclonally activates murine CD4+ T cells in the absence of antigen-presenting cells. European Journal of Immunology 37, 1905–1915.

Røyset, E.S., Sahlin Pettersen, *H.*P., Xu, W., Larbi, A., Sandvik, A.K., Steigen, S.E., Catalan-Serra, I., Bakke, I., 2022. Deep learning-based image analysis reveals significant differences in the number and distribution of mucosal CD3 and γδ T cells between Crohn's disease and ulcerative colitis. J Pathol Clin Res 9, 18–31.

Sadeghi, A., Dehdari Ebrahimi, N., 2023. Global prevalence of *Helicobacter pylori* infection among individuals with obesity: A protocol for a systematic review and meta-analysis. Health Science Reports 6, e1505.

Sáenz, J.B., Mills, J.C., 2018. Acid and the basis for cellular plasticity and reprogramming in gastric repair and cancer. Nat Rev Gastroenterol Hepatol 15, 257–273.

Safadi, M.F., Shamma, *H.*, Berger, M., n.d. The Visible Stomach: Elusive Diffuse-Type Adenocarcinoma Presents With Gastric Outlet Obstruction. Cureus 14, e25554.

Safaralizadeh, R., Dastmalchi, N., Hosseinpourfeizi, M., Latifi-Navid, S., 2017. *Helicobacter pylori* virulence factors in relation to gastrointestinal diseases in Iran. Microbial Pathogenesis 105, 211–217.

Saito, *H.*, Tatebayashi, K., 2004. Regulation of the osmoregulatory HOG MAPK cascade in yeast.

Sakagami, T., Dixon, M., O'Rourke, J., Howlett, R., Alderuccio, F., Vella, J., Shimoyama, T., Lee, A., 1996. Atrophic gastric changes in both *Helicobacter* felis and *Helicobacter pylori* infected mice are host dependent and separate from antral gastritis. Gut 39, 639–648.

Sakamoto, *H.*, Yonezawa, S., Utsunomiya, T., Tanaka, S., Kim, Y.S., Sato, E., 1997. Mucin antigen expression in gastric carcinomas of young and old adults. Human Pathology 28, 1056–1065.

Salter, S.J., Cox, M.J., Turek, E.M., Calus, S.T., Cookson, W.O., Moffatt, M.F., Turner, P., Parkhill, J., Loman, N.J., Walker, A.W., 2014a. Reagent and laboratory contamination can critically impact sequence-based microbiome analyses. BMC Biology 12, 87.

Sanchez-Alvarez, C., Bond, M., Soowamber, M., Camellino, D., Anderson, M., Langford, C.A., Dejaco, C., Touma, Z., Ramiro, S., 2023. Measuring treatment outcomes and change in disease activity in giant cell arteritis: a systematic literature review informing the development of the EULAR-ACR response criteria on behalf of the EULAR-ACR response criteria in giant cell arteritis task force. RMD Open 9, e003233.

Sanduleanu, S., Jonkers, D., De Bruine, A., Hameeteman, W., Stockbrügger, R.W., 2001. Non-*Helicobacter pylori* bacterial flora during acid-suppressive therapy: differential findings in gastric juice and gastric mucosa. Alimentary Pharmacology & Therapeutics 15, 379–388.

Santucci, C., Mignozzi, S., Malvezzi, M., Boffetta, P., Collatuzzo, G., Levi, F., La Vecchia, C., Negri, E., 2024. European cancer mortality predictions for the year 2024 with focus on colorectal cancer. Annals of Oncology 35, 308–316.

Sarnecka, A.K., Nawrat, D., Piwowar, M., Ligęza, J., Swadźba, J., Wójcik, P., 2019. DNA extraction from FFPE tissue samples – a comparison of three procedures. Contemp Oncol (Pozn) 23, 52–58.

Sartor, R.B., 2008. Microbial Influences in Inflammatory Bowel Diseases. Gastroenterology 134, 577–594.

Saruuljavkhlan, B., Alfaray, R.I., Oyuntsetseg, K., Gantuya, B., Khangai, A., Renchinsengee, N., Matsumoto, T., Akada, J., Azzaya, D., Davaadorj, D., Yamaoka, Y., 2023. Study of *Helicobacter pylori* Isolated from a High-Gastric-Cancer-Risk Population: Unveiling the Comprehensive Analysis of Virulence-Associated Genes including Secretion Systems, and Genome-Wide Association Study. Cancers 15.

Sasazuki, S., Sasaki, S., Tsugane, S., Japan Public Health Center Study Group, 2002. Cigarette smoking, alcohol consumption and subsequent gastric cancer risk by subsite and histologic type. Int J Cancer 101, 560–566.

Scaglione, L., Gambino, R., Rolfo, E., Lillaz, E., Gai, M., Cassader, M., Pagano, G., Cavallo-Perin, P., 2002. Plasma homocysteine, methylenetetrahydrofolate reductase gene polymorphism and carotid intima-media thickness in Italian type 2 diabetic patients. European Journal of Clinical Investigation 32, 24–28.

Schlaermann, P., Toelle, B., Berger, *H.*, Schmidt, S.C., Glanemann, M., Ordemann, J., Bartfeld, S., Mollenkopf, *H.*J., Meyer, T.F., 2016. A novel human gastric primary cell culture system for modelling *Helicobacter pylori* infection in vitro. Gut 65, 202–213.

Schmidt, W.A., Dasgupta, B., Sloane, J., Giannelou, A., Xu, Y., Unizony, S.*H.*, Mackie, S.L., Gonzalez-Gay, M.A., Spiera, R., Warrington, K.J., Villiger, P.M., Nivens, M.C., Akinlade, B., Lin, Y., Buttgereit, F., Stone, J.*H.*, 2023. A phase 3 randomised, double-blind, placebo-controlled study to evaluate the efficacy and safety of sarilumab in patients with giant cell arteritis. Arthritis Res Ther 25, 199.

Schmitt, W., Haas, R., 1994. Genetic analysis of the *Helicobacter pylori* vacuolating cytotoxin: structural similarities with the IgA protease type of exported protein. Mol Microbiol 12, 307–319.

Schneider, S., Carra, G., Sahin, U., Hoy, B., Rieder, G., Wessler, S., 2011. Complex Cellular Responses of *Helicobacter pylori*-Colonized Gastric Adenocarcinoma Cells ▿. Infect Immun 79, 2362–2371.

Schoep, T.D., Fulurija, A., Good, F., Lu, W., Himbeck, R.P., Schwan, C., Choi, S.S., Berg, D.E., Mittl, P.R.E., Benghezal, M., Marshall, B.J., 2010. Surface properties of *Helicobacter pylori* urease complex are essential for persistence. PLoS One 5, e15042.

Schönhuber W, Fuchs B, Juretschko S, Amann R, 1997. Improved sensitivity of whole-cell hybridization by the combination of horseradish peroxidase-labeled oligonucleotides and tyramide signal amplification. Appl Environ Microbiol. Aug;63(8):3268-73

Schrader, K.A., Masciari, S., Boyd, N., Wiyrick, S., Kaurah, P., Senz, J., Burke, W., Lynch, *H.*T., Garber, J.E., Huntsman, D.G., 2008. Hereditary diffuse gastric cancer: association with lobular breast cancer. Fam Cancer 7, 73–82.

Schreider, C., Peignon, G., Thenet, S., Chambaz, J., Pinçon-Raymond, M., 2002. Integrin-mediated functional polarization of Caco-2 cells through E-cadherin--actin complexes. J Cell Sci 115, 543–552.

Schultsz*, C., Berg‡, F.M. van den, Kate‡, F.W. ten, Tytgat§, G.N.J., Dankert*, J., 1999. The intestinal mucus layer from patients with inflammatory bowel disease

harbors high numbers of bacteria compared with controls. Gastroenterology 117, 1089–1097.

Schulz, C., Schütte, K., Mayerle, J., Malfertheiner, P., 2019. The role of the gastric bacterial microbiome in gastric cancer: *Helicobacter pylori* and beyond. Therap Adv Gastroenterol 12, 1756284819894062.

Schwab, B., Hülskamp, M., 2010. Neutral red staining for plant vacuoles. Cold Spring Harb Protoc 2010, pdb.prot4953.

Sekido, Y., Nishimura, J., Nakano, K., Osu, T., Chow, C.-E.T., Matsuno, *H.*, Ogino, T., Fujino, S., Miyoshi, N., Takahashi, *H.*, Uemura, M., Matsuda, C., Kayama, *H.*, Mori, M., Doki, Y., Takeda, K., Uchino, M., Ikeuchi, *H.*, Mizushima, T., 2020. Some GammaPseudomonadota are enriched within CD14+ macrophages from intestinal lamina propria of Crohn's disease patients versus mucus. Sci Rep 10, 2988.

Serrano, C., Harris, P.R., Smith, P.D., Bimczok, D., 2021. Interactions between *H. pylori* and the Gastric Microbiome: Impact on Gastric Homeostasis and Disease. Curr Opin Physiol 21, 57–64.

Seto, K., Hayashi-Kuwabara, Y., Yoneta, T., Suda, *H.*, Tamaki, *H.*, 1998. Vacuolation induced by cytotoxin from *Helicobacter pylori* is mediated by the EGF receptor in HeLa cells. FEBS Lett 431, 347–350.

Sewald, X., Fischer, W., Haas, R., 2008. Sticky socks: *Helicobacter pylori* VacA takes shape. Trends in Microbiology 16, 89–92.

Sharafutdinov, I., Tegtmeyer, N., Linz, B., Rohde, M., Vieth, M., Tay, A.C.-Y., Lamichhane, B., Tuan, V.P., Fauzia, K.A., Sticht, *H.*, Yamaoka, Y., Marshall, B.J., Backert, S., 2023a. A single-nucleotide polymorphism in *Helicobacter pylori* promotes gastric cancer development. Cell Host & Microbe 31, 1345-1358.e6.

Sharma, S. A., Tummuru, M.K., Blaser, M.J., Kerr, L.D., 1998. Activation of IL-8 gene expression by *Helicobacter pylori* is regulated by transcription factor nuclear factor-kappa B in gastric epithelial cells. J Immunol 160, 2401–2407.

Shi, D., Xi, X.-X., 2021. Regulation of MUC6 Methylation Correlates with Progression of Gastric Cancer. Yonsei Med J 62, 1005–1015.

Shimbori, C., De Palma, G., Baerg, L., Lu, J., Verdu, E.F., Reed, D.E., Vanner, S., Collins, S.M., Bercik, P., n.d. Gut bacteria interact directly with colonic mast cells in a humanized mouse model of IBS. Gut Microbes 14, 2105095.

Shinozaki, A., Sakatani, T., Ushiku, T., Hino, R., Isogai, M., Ishikawa, S., Uozaki, *H.*, Takada, K., Fukayama, M., 2010. Downregulation of microRNA-200 in EBV-associated gastric carcinoma. Cancer Res 70, 4719–4727.

Siegel, R.L., Miller, K.D., Fuchs, *H.*E., Jemal, A., 2021. Cancer Statistics, 2021. CA Cancer J Clin 71, 7–33.

Singh, *H.*, Narayan, B., Urs, A.B., Kumar Polipalli, S., Kumar, S., 2020. A novel approach for extracting DNA from formalin-fixed paraffin-embedded tissue using microwave. Med J Armed Forces India 76, 307–311.

Sjöstedt, S., Heimdahl, A., Kager, L., Nord, C.E., 1985. Microbial colonization of the oropharynx, esophagus and stomach in patients with gastric diseases. Eur. J, Clin. Microbiol. 4, 49–51.

Skirrow, M.B., 1977. Campylobacter enteritis: a “new” disease. Br Med J 2, 9–11.

Skorko-Glonek, J., Zurawa-Janicka, D., Koper, T., Jarzab, M., Figaj, D., Glaza, P., Lipinska, B., 2013. HtrA Protease Family as Therapeutic Targets. Current Pharmaceutical Design 19, 977–1009.

Slavin, T.P., Weitzel, J.N., Neuhausen, S.L., Schrader, K.A., Oliveira, C., Karam, R., 2019. Genetics of gastric cancer: what do we know about the genetic risks? Transl Gastroenterol Hepatol 4, 55.

Smirnov, K.S., Maier, T.V., Walker, A., Heinzmann, S.S., Forcisi, S., Martinez, I., Walter, J., Schmitt-Kopplin, P., 2016. Challenges of metabolomics in human gut microbiota research. Int J Med Microbiol 306, 266–279.

Smith, M.G., Hold, G.L., Tahara, E., El-Omar, E.M., 2006. Cellular and molecular aspects of gastric cancer. World J Gastroenterol 12, 2979–2990.

Soares, G.A.S., Moraes, F.A. de S., Ramos, A.F.P.L., Santiago, S.B., Germano, J.N., Fernandes, G.A., Curado, M.P., Barbosa, M.S., 2023. Dietary habits and *Helicobacter pylori* infection: is there an association? Therap Adv Gastroenterol 16, 17562848231160620.

Song, M., Chan, A.T., Sun, J., 2020. Influence of the Gut Microbiome, Diet, and Environment on Risk of Colorectal Cancer. Gastroenterology 158, 322–340.

Song, X., Xin, N., Wang, W., Zhao, C., 2015. Wnt/β-catenin, an oncogenic pathway targeted by *H. pylori* in gastric carcinogenesis. Oncotarget 6, 35579–35588.

Soyfoo, D.M., Doomah, Y.*H.*, Xu, D., Zhang, C., Sang, *H.*-M., Liu, Y.-Y., Zhang, G.-X., Jiang, J.-X., Xu, S.-F., 2021a. New genotypes of *Helicobacter* Pylori VacA d-region identified from global strains. BMC Molecular and Cell Biology 22, 4.

Srinivasan, B., Kolli, A.R., Esch, M.B., Abaci, *H.*E., Shuler, M.L., Hickman, J.J., 2015. TEER Measurement Techniques for In Vitro Barrier Model Systems. J Lab Autom. 20, 107–126.

Steer, *H.*W., Colin-Jones, D.G., 1975. Mucosal changes in gastric ulceration and their response to carbenoxolone sodium. Gut 16, 590–597.

Sung, Joseph J Y, Coker, O.O., Chu, E., Szeto, C.*H.*, Luk, S.T.Y., Lau, *H.*C.*H.*, Yu, J., 2020. Gastric microbes associated with gastric inflammation, atrophy and intestinal metaplasia 1 year after *Helicobacter pylori* eradication. Gut 69, 1572–1580.

Sung, J.K., 2016. Diagnosis and management of gastric dysplasia. Korean J Intern Med 31, 201–209.

Swart, A.L., Laventie, B.-J., Sütterlin, R., Junne, T., Lauer, L., Manfredi, P., Jakonia, S., Yu, X., Karagkiozi, E., Okujava, R., Jenal, U., 2024a. Pseudomonas aeruginosa breaches respiratory epithelia through goblet cell invasion in a microtissue model. Nat Microbiol 9, 1725–1737.

Swart, A.L., Laventie, B.-J., Sütterlin, R., Junne, T., Yu, X., Karagkiozi, E., Okujava, R., Jenal, U., 2023. Goblet cell invasion promotes breaching of respiratory epithelia by an opportunistic human pathogen.

Sz, B., S, L.-N., 2021. Oral microbiota and *Helicobacter pylori* in gastric carcinogenesis: what do we know and where next? BMC microbiology 21.

Taillieu, E., Chiers, K., Amorim, I., Gärtner, F., Maes, D., Van Steenkiste, C., Haesebrouck, F., 2022. Gastric *Helicobacter* species associated with dogs, cats and pigs: significance for public and animal health. Vet Res 53, 42.

Takahashi, M., Ogura, K., Maeda, S., Mori, K., Mafune, K., Mikami, Y., Terano, A., Omata, M., 1997. Promoters of epithelialization induce expression of vascular endothelial growth factor in human gastric epithelial cells in primary culture. FEBS Lett 418, 115–118.

Taniguchi, K., Karin, M., 2018. NF-κB, inflammation, immunity and cancer: coming of age. Nat Rev Immunol 18, 309–324.

Tartaglia, M., Martinelli, S., Stella, L., Bocchinfuso, G., Flex, E., Cordeddu, V., Zampino, G., Burgt, I. van der, Palleschi, A., Petrucci, T.C., Sorcini, M., Schoch, C., Foa, R., Emanuel, P.D., Gelb, B.D., 2006. Diversity and functional consequences of germline and somatic PTPN11 mutations in human disease. Am J Hum Genet 78, 279–290.

Taylor, N.S., Fox, J.G., 2012. Animal Models of *Helicobacter*-Induced Disease: Methods to Successfully Infect the Mouse. Methods Mol Biol 921, 131–142.

Tegtmeyer, N., Zabler, D., Schmidt, D., Hartig, R., Brandt, S., Backert, S., 2009. Importance of EGF receptor, HER2/Neu and Erk1/2 kinase signalling for host cell

elongation and scattering induced by the *Helicobacter pylori* CagA protein: antagonistic effects of the vacuolating cytotoxin VacA. Cellular Microbiology 11, 488–505.

Telford, J.L., Ghiara, P., Dell'Orco, M., Comanducci, M., Burroni, D., Bugnoli, M., Tecce, M.F., Censini, S., Covacci, A., Xiang, Z., 1994b. Gene structure of the *Helicobacter pylori* cytotoxin and evidence of its key role in gastric disease. J Exp Med 179, 1653–1658.

ten Broeke, T., Wubbolts, R., Stoorvogel, W., 2013. MHC class II antigen presentation by dendritic cells regulated through endosomal sorting. Cold Spring Harbor Perspectives in Biology.

Thurnheer, T., Gmür, R., Guggenheim, B., 2004. Multiplex FISH analysis of a six-species bacterial biofilm. Journal of Microbiological Methods 56, 37–47.

Tomb, J.F., White, O., Kerlavage, A.R., Clayton, R.A., Sutton, G.G., Fleischmann, R.D., Ketchum, K.A., Klenk, *H.*P., Gill, S., Dougherty, B.A., Nelson, K., Quackenbush, J., Zhou, L., Kirkness, E.F., Peterson, S., Loftus, B., Richardson, D., Dodson, R., Khalak, *H.*G., Glodek, A., McKenney, K., Fitzegerald, L.M., Lee, N., Adams, M.D., Hickey, E.K., Berg, D.E., Gocayne, J.D., Utterback, T.R., Peterson, J.D., Kelley, J.M., Cotton, M.D., Weidman, J.M., Fujii, C., Bowman, C., Watthey, L., Wallin, E., Hayes, W.S., Borodovsky, M., Karp, P.D., Smith, *H.*O., Fraser, C.M., Venter, J.C., 1997a. The complete genome sequence of the gastric pathogen *Helicobacter pylori*. Nature 388, 539–547.

Tombola, F., Carlesso, C., Szabò, I., de Bernard, M., Reyrat, J.M., Telford, J.L., Rappuoli, R., Montecucco, C., Papini, E., Zoratti, M., 1999. *Helicobacter pylori* vacuolating toxin forms anion-selective channels in planar lipid bilayers: possible implications for the mechanism of cellular vacuolation. Biophys J 76, 1401–1409.

Torres, V.J., Ivie, S.E., McClain, M.S., Cover, T.L., 2005. Functional Properties of the p33 and p55 Domains of the *Helicobacter pylori* Vacuolating Cytotoxin. Journal of Biological Chemistry 280, 21107–21114.

Tripathi, N., Sapra, A., 2024a. Gram Staining, in: StatPearls. StatPearls Publishing, Treasure Island (FL).

Troncoso, C et al. 2020. "MALDI-TOF MS and 16S RNA Identification of Culturable Gastric Microbiota: Variability Associated with the Presence of Helicobacter pylori." Microorganisms vol. 8,11 1763, doi:10.3390/microorganisms8111763

Tsai, Y.-Y., Franca, M., Camus, A., Stabler, L.J., Barbieri, N., Logue, C.M., 2023. Laser Capture Microdissection, Culture Analysis, and Bacterial Sequencing to Evaluate the Microbiota of Focal Duodenal Necrosis in Egg Layers. avdi 67, 177–185.

Tseng, C.-*H.*, Lin, J.-T., Ho, *H.*J., Lai, Z.-L., Wang, C.-B., Tang, S.-L., Wu, C.-Y., 2016. Gastric microbiota and predicted gene functions are altered after subtotal gastrectomy in patients with gastric cancer. Sci Rep 6, 20701.

Tsutsumi, R., Takahashi, A., Azuma, T., Higashi, *H.*, Hatakeyama, M., 2006. Focal adhesion kinase is a substrate and downstream effector of SHP-2 complexed with *Helicobacter pylori* CagA. Mol Cell Biol 26, 261–276.

Turnbaugh, P.J., Ley, R.E., Hamady, M., Fraser-Liggett, C., Knight, R., Gordon, J.I., 2007. The human microbiome project: exploring the microbial part of ourselves in a changing world. Nature 449, 804–810.

UK NSC, 2021. Adult screening programme: Stomach cancer. Website article; (accessed 09.01.2024).

Vagin, O., Tokhtaeva, E., Larauche, M., Davood, J., Marcus, E.A., 2024. *Helicobacter pylori*-Induced Decrease in Membrane Expression of Na,K-ATPase Leads to Gastric Injury. Biomolecules 14, 772.

Valente, P., Garrido, M., Gullo, I., Baldaia, *H.*, Marques, M., Baldaque-Silva, F., Lopes, J., Carneiro, F., 2015. Epithelial dysplasia of the stomach with gastric immunophenotype shows features of biological aggressiveness. Gastric Cancer 18, 720–728.

van Beest, M., Robben, J.*H.*, Savelkoul, P.J.M., Hendriks, G., Devonald, M.A.J., Konings, I.B.M., Lagendijk, A.K., Karet, F., Deen, P.M.T., 2006. Polarisation, key to good localisation. Biochimica et Biophysica Acta (BBA) - Biomembranes, Aquaporins 1758, 1126–1133.

Van der Sluis, M., De Koning, B.A.E., De Bruijn, A.C.J.M., Velcich, A., Meijerink, J.P.P., Van Goudoever, J.B., Büller, *H.*A., Dekker, J., Van Seuningen, I., Renes, I.B., Einerhand, A.W.C., 2006. Muc2-Deficient Mice Spontaneously Develop Colitis, Indicating That MUC2 Is Critical for Colonic Protection. Gastroenterology 131, 117–129.

Villiger, P.M., Adler, S., Kuchen, S., Wermelinger, F., Dan, D., Fiege, V., Bütikofer, L., Seitz, M., Reichenbach, S., 2016. Tocilizumab for induction and maintenance of remission in giant cell arteritis: a phase 2, randomised, double-blind, placebo-controlled trial. Lancet 387, 1921–1927.

Wakatsuki, K., Yamada, Y., Narikiyo, M., Ueno, M., Takayama, T., Tamaki, *H.*, Miki, K., Matsumoto, S., Enomoto, K., Yokotani, T., Nakajima, Y., 2008. Clinicopathological and prognostic significance of mucin phenotype in gastric cancer. J Surg Oncol 98, 124–129.

Walker, A.W., Duncan, S.*H.*, McWilliam Leitch, E.C., Child, M.W., Flint, *H.*J., 2005. pH and peptide supply can radically alter bacterial populations and short-chain fatty acid ratios within microbial communities from the human colon. Appl Environ Microbiol 71, 3692–3700.

Wang, D, et al. 2022 “Helicobacter pylori infection affects the human gastric microbiome, as revealed by metagenomic sequencing.” FEBS open bio vol. 12,6. 1188-1196. doi:10.1002/2211-5463.13390

Wang, P.-L., Xiao, F.-T., Gong, B.-C., Liu, F.-N., 2017. Alcohol drinking and gastric cancer risk: a meta-analysis of observational studies. Oncotarget 8, 99013–99023.

Wang, Y., Antonopoulos, D.A., Zhu, X., Harrell, L., Hanan, I., Alverdy, J.C., Meyer, F., Musch, M.W., Young, V.B., Chang, E.B., 2010. Laser capture microdissection and metagenomic analysis of intact mucosa-associated microbial communities of human colon. Appl Microbiol Biotechnol 88, 10.1007/s00253-010-2921–8.

Wang, Z., Gao, X., Zeng, R., Wu, Q., Sun, *H.*, Wu, W., Zhang, X., Sun, G., Yan, B., Wu, L., Ren, R., Guo, M., Peng, L., Yang, Y., 2020. Changes of the Gastric Mucosal Microbiome Associated With Histological Stages of Gastric Carcinogenesis. Front Microbiol 11, 997.

Waskiewicz, A.J., Cooper, J.A., 1995. Mitogen and stress response pathways: MAP kinase cascades and phosphatase regulation in mammals and yeast. Current Opinion in Cell Biology.

Waskito, L.A., Rezkitha, Y.A.A., Vilaichone, R., Sugihartono, T., Mustika, S., Dewa Nyoman Wibawa, I., Yamaoka, Y., Miftahussurur, M., 2022. The role of non-*Helicobacter pylori* bacteria in the pathogenesis of gastroduodenal diseases. Gut Pathog 14, 19.

Weersma, R.K., Zhernakova, A., Fu, J., 2020. Interaction between drugs and the gut microbiome. Gut 69, 1510–1519.

Wen, S., Moss, S.F., 2009. *Helicobacter pylori* virulence factors in gastric carcinogenesis. Cancer Lett 282, 1–8.

Willet, S.G., Mills, J.C., 2016. Stomach Organ and Cell Lineage Differentiation: From Embryogenesis to Adult Homeostasis. Cellular and Molecular Gastroenterology and Hepatology 2, 546–559.

Willner, D., Daly, J., Whiley, D., Grimwood, K., Wainwright, C.E., Hugenholtz, P., 2012. Comparison of DNA Extraction Methods for Microbial Community Profiling with an Application to Pediatric Bronchoalveolar Lavage Samples. PLoS One 7, e34605.

Winter, J.A., Letley, D.P., Cook, K.W., Rhead, J.L., Zaitoun, A.A.M., Ingram, R.J.M., Amilon, K.R., Croxall, N.J., Kaye, P.V., Robinson, K., Atherton, J.C., 2014. A Role for the Vacuolating Cytotoxin, VacA, in Colonization and *Helicobacter pylori*–Induced Metaplasia in the Stomach. The Journal of Infectious Diseases 210, 954–963.

Wong, *H.*P.S., Yu, L., Lam, E.K.Y., Tai, E.K.K., Wu, W.K.K., Cho, C.*H.*, 2007. Nicotine promotes cell proliferation via alpha7-nicotinic acetylcholine receptor and catecholamine-synthesizing enzymes-mediated pathway in human colon adenocarcinoma HT-29 cells. Toxicol Appl Pharmacol 221, 261–267.

Wortel, I.M.N., Kim, S., Liu, A.Y., Ibarra, E.C., Miller, M.J., 2022. Listeria motility increases the efficiency of epithelial invasion during intestinal infection. PLoS Pathog 18, e1011028.

Xiao, S., Zhou, L., 2020. Gastric Stem Cells: Physiological and Pathological Perspectives. Front. Cell Dev. Biol. 0.

Xie, X., He, Z., Chen, N., Tang, Z., Wang, Q., Cai, Y., 2019. The Roles of Environmental Factors in Regulation of Oxidative Stress in Plant.

Xiong, X., Wen, Y.-A., Fairchild, R., Zaytseva, Y.Y., Weiss, *H.*L., Evers, B.M., Gao, T., 2020. Upregulation of CPT1A is essential for the tumor-promoting effect of adipocytes in colon cancer. Cell Death Dis 11, 736.

Xu, A.A., Graham, D.Y., 2021. Things We Do for No ReasonTM: Serum Serologic *Helicobacter pylori* Testing. J Hosp Med 16, 691–693.

Yadav, R., Sagar, M., n.d. Comparison of Different Histological Staining Methods for Detection of *Helicobacter pylori* Infection in Gastric Biopsy. Cureus 14, e27316.

Yamamura, R., Inoue, K.Y., Nishino, K., Yamasaki, S., 2023. Intestinal and fecal pH in human health. Front. Microbiomes 2.

Yamazaki, K., 2023. Oral-gut axis as a novel biological mechanism linking periodontal disease and systemic diseases: A review. Jpn Dent Sci Rev 59, 273–280.

Yao, D., Dai, W., Dong, M., Dai, C., Wu, S., 2021a. MUC2 and related bacterial factors: Therapeutic targets for ulcerative colitis. EBioMedicine 74, 103751.

Yildiz, S., Pereira Bonifacio Lopes, J.P., Bergé, M., González-Ruiz, V., Baud, D., Kloehn, J., Boal-Carvalho, I., Schaeren, O.P., Schotsaert, M., Hathaway, L.J., Rudaz, S., Viollier, P.*H.*, Hapfelmeier, S., Francois, P., Schmolke, M., n.d. Respiratory tissue-associated commensal bacteria offer therapeutic potential against pneumococcal colonization. eLife 9, e53581.

Yisireyili, M., Alimujiang, A., Aili, A., Li, Y., Yisireyili, S., Abudureyimu, K., 2020. Chronic Restraint Stress Induces Gastric Mucosal Inflammation with Enhanced Oxidative Stress in a Murine Model. Psychol Res Behav Manag 13, 383–393.

Yokoyama, K., Higashi, *H.*, Ishikawa, S., Fujii, Y., Kondo, S., Kato, *H.*, Azuma, T., Wada, A., Hirayama, T., Aburatani, *H.*, Hatakeyama, M., 2005. Functional antagonism between *Helicobacter pylori* CagA and vacuolating toxin VacA in control of the NFAT signaling pathway in gastric epithelial cells. Proceedings of the National Academy of Sciences 102, 9661–9666.

Yusuf, K., Sampath, V., Umar, S., 2023. Bacterial Infections and Cancer: Exploring This Association And Its Implications for Cancer Patients. Int J Mol Sci 24, 3110.

Zamani, M., Ebrahimtabar, F., Zamani, V., Miller, W.*H.*, Alizadeh-Navaei, R., Shokri-Shirvani, J., Derakhshan, M.*H.*, 2018. Systematic review with meta-analysis: the worldwide prevalence of *Helicobacter pylori* infection. Alimentary Pharmacology & Therapeutics 47, 868–876.

Zaręba, K.P., Zińczuk, J., Dawidziuk, T., Pryczynicz, A., Guzińska-Ustymowicz, K., Kędra, B., 2019. Stomach cancer in young people – a diagnostic and therapeutic problem. Prz Gastroenterol 14, 283–285.

Zepeda-Rivera, M., Minot, S.S., Bouzek, *H.*, Wu, *H.*, Blanco-Míguez, A., Manghi, P., Jones, D.S., LaCourse, K.D., Wu, Y., McMahon, E.F., Park, S.-N., Lim, Y.K., Kempchinsky, A.G., Willis, A.D., Cotton, S.L., Yost, S.C., Sicinska, E., Kook, J.-K., Dewhirst, F.E., Segata, N., Bullman, S., Johnston, C.D., 2024a. A distinct Fusobacterium nucleatum clade dominates the colorectal cancer niche. Nature 628, 424–432.

Zepeda-Rivera, M., Minot, S.S., Bouzek, *H.*, Wu, *H.*, Blanco-Míguez, A., Manghi, Zhang, J., Zhang, F., Niu, R., 2015. Functions of Shp2 in cancer. J Cell Mol Med 19, 2075–2083.

Zhang, L., Ren, J.W., Wong, C.C.M., Wu, W.K.K., Ren, S.X., Shen, J., Chan, R.L.Y., Cho, C.*H.*, 2012. Effects of cigarette smoke and its active components on ulcer formation and healing in the gastrointestinal mucosa. Curr Med Chem 19, 63–69.

Zhang, L., Zhao, M., Fu, X., 2023. Gastric microbiota dysbiosis and *Helicobacter pylori* infection. Front. Microbiol. 14.

Zi, M., Zhang, Y., Hu, C., Zhang, S., Chen, J., Yuan, L., Cheng, X., 2022. A literature review on the potential clinical implications of streptococci in gastric cancer. Front Microbiol 13, 1010465.

Appendix A. Supplementary patient information

Assigned Patient Number	Patient group	Gender	Diagnosis	PPI use	H&E Inflammation grade	Invasion Score (0-4)
1	CG *H. pylori* positive	Male	Mild active *H. pylori* associated gastritis	None	Moderate	3
2	CG *H. pylori* positive	Male	Active chronic gastritis	None	Mild	1
3	CG *H. pylori* positive	Male	Mild active *H. pylori* associated gastritis	None	Moderate	3
4	CG *H. pylori* positive	Male	Mild active chronic gastritis	Lansoprazole	Moderate	2
5	CG *H. pylori* positive	Male	*H. pylori* associated active chronic gastritis	Missing	Moderate	2
6	CG *H. pylori* positive	Male	Persistent *H. pylori* associated gastritis	Missing	Mild	3
7	CG *H. pylori* positive	Male	Active chronic gastritis	Missing	Moderate to Se	0
8	CG *H. pylori* positive	Male	*H. pylori* gastritis	Missing	Missing	3
9	CG *H. pylori* positive	Male	Gatritis, non-erosive	Missing	Missing	1
10	CG *H. pylori* negativ	Male	Mild reactive gastropathy	None	Mild	1
11	CG *H. pylori* negativ	Male	Mild chronic gastritis	None	Mild	0
12	CG *H. pylori* negativ	Male	Mild non-specific chronic inflammation	None	Mild	1
13	CG *H. pylori* negativ	Male	Mild chronic inactive gastritis	Lansoprazole	Moderate	1
14	CG *H. pylori* negativ	Male	Corrobative of inflamed Barretts mucosa	Lansoprazole	Moderate	0
15	CG *H. pylori* negativ	Male	Gastric atrophy	Missing	Missing	0
16	GIM *H. pylori* positiv	Male	Severe active chronic infection with gastritis/atrophy	None	Severe	2
17	GIM *H. pylori* positiv	Male	Chronic active gastritis and intestinal metaplasia	None	Severe	3
18	GIM *H. pylori* positiv	Male	Mild active *H. pylori* associated gastritis and intestinal metaplasia	None	Patchy severe	3
19	GIM *H. pylori* positiv	Male	*H. pylori* associated gastritis and intestinal metaplasia	None	Moderate	1
20	GIM *H. pylori* positiv	Male	Intestinal metaplasia with squamous and columnar mucosa	Lansoprazole	Moderate	2
21	GIM *H. pylori* positiv	Male	*H. pylori* associated gastritis and intestinal metaplasia	None	Mild	3
22	GIM *H. pylori* positiv	Male	*H. pylori* associated active chronic gastritis with intestinal metaplasia	Missing	Mild to Modera	0
23	GIM *H. pylori* positiv	Male	Chronic Gastritis with intestinal metaplasia	Missing	Mild to Modera	3
24	GIM *H. pylori* positiv	Male	*H. pylori* associated gastritis with focal intestinal metaplasia	Missing	Moderate	3
25	GIM *H. pylori* positiv	Male	Active chronic gastritis with associated *H. pylori* and focal intestinal metaplasia	Missing	Mild	3
26	GIM *H. pylori* negati	Male	Chronic gastritis and intestinal metaplasia	None	Moderate	0
27	GIM *H. pylori* negati	Male	N/C	None	Mild	0
28	GIM *H. pylori* negati	Female	Mild active gastritis and focal intestinal metaplasia	None	Missing	1
29	GIM *H. pylori* negati	Female	Active chronic gastritis and intestinal metaplasia	None	Missing	1
30	GIM *H. pylori* negati	Male	Focal active chronic gastritis and intestinal metaplasia/atrophy	None	Moderate	1
31	GIM *H. pylori* negati	Male	Mild chronic gastritis and intestinal metaplasia	Rabeprazole	Mild	2
32	GIM *H. pylori* negati	Male	Gastric intestinal metaplasia	Missing	Missing	0
33	GAC	Male	Gastric adenocarcinoma	N/A	N/A	4
33	NAT	Male	Healthy tissue adjacent to tumour	N/A	N/A	3
34	GAC	Male	Gastric adenocarcinoma	N/A	N/A	3
34	NAT	Male	Healthy tissue adjacent to tumour	N/A	N/A	0
35	GAC	Male	Gastric adenocarcinoma	N/A	N/A	3
35	NAT	Male	Healthy tissue adjacent to tumour	N/A	NA	1

Appendix B. Manuscript accepted and subsequently published in Helicobacter, February 2025

The gastric microbiota invade the lamina propria in *Helicobacter pylori*-associated gastritis and pre-cancer

Harriet J. Giddings[1,2], Ana Teodósio[3], Jordanne Jones[3], Jack L. McMurray[3,4], Kelly Hunter[3], Riad Alame[5], Isaac Gardiner[1,2], Zainab Abdawn[5], William Butterworth[7], Ian R. Henderson[6], , Jeffrey A. Cole[1], Claire D. Shannon-Lowe[7] and Amanda E. Rossiter-Pearson[1,2*]

Affiliations: [1]Institute of Microbiology and Infection, University of Birmingham, UK. [2] Department of Microbes, Infection and Microbiomes, School of Infection, Inflammation and Immunology, College of Medicine and Health, University of Birmingham, UK. [3]Birmingham Tissue Analytics, [4]Rheumatology Research Group, University of Birmingham, UK. [5]Queen Elizabeth Hospital, University Hospital Birmingham NHS Foundation Trust, UK. [6]Institute for Molecular Biosciences, University of Queensland, Australia. [7]Department of Immunology and Immunotherapy, School of Infection, Inflammation and Immunology, College of Medicine and Health, University of Birmingham, UK.

*Corresponding author: Amanda E. Rossiter-Pearson

Email: a.e.rossiter@bham.ac.uk

Author Contributions: Conceptualisation: C.D.S-L. & A.E.R-P. Methodology: H.J.G, A.T., J.L.M, R.A., I.G. & A.E.R-P. Data analysis: H.J.G., A.T., J.L.M., K.H., Z.A., I.R.H., J.A.C. & A.E.R-P. Writing: H.J.G., J.A.C. & A.E.R-P. Funding acquisition: A.E.R-P.

Acknowledgments We thank the Royal Society (RGS\R2\192312), the University of Birmingham Cancer Research UK Centre Development Fund (A.E.R-P.), Cancer Research UK (EDDPMA-Nov21\100008) (A.E.R-P.) and the Medical Research Council IMPACT Doctoral Training Programme (H.J.G. and A.E.R-P.) for funding. We thank the patients who have donated samples to HBRC. We also thank Michael Russell, Emma Hurlestone, Shalom Simende and Shannon Smallman at HBRC for patient sample retrieval. We thank Dr. Gary Reynolds for tissue sample sectioning. We thank Joe Flint at Birmingham Tissue Analytics for whole slide scanning.

Conflict of interest statement: The authors declare no conflict of interest.

Keywords: *Helicobacter pylori,* gastric adenocarcinoma, microbiome, spatial biology.

Abstract

Background
Stomach cancer is the fourth leading cause of cancer-related deaths worldwide. *Helicobacter pylori* is the main risk factor for gastric adenocarcinoma (GAC), yet the precise mechanism underpinning this association remains controversial. Gastric intestinal metaplasia (GIM) represents the pre-cancerous stage and follows *H. pylori*-associated chronic gastritis (CG). Sequencing studies have revealed fewer *H. pylori* and more non-*H. pylori* bacteria in GAC. However, the spatial organisation of the gastric microbiota in health and disease is unknown.

Materials and Methods
Here, we have combined RNA *in situ* hybridisation and immunohistochemistry to detect *H. pylori,* non-*H. pylori* bacteria and host cell markers (E-cadherin, Mucins 5AC and 2) on tissue sections from patients with CG (n=15) and GIM (n=17).

Results
Quantitative analysis of whole slide scans revealed significant correlations of *H. pylori* and other bacteria in CG and GIM. In contrast to sequencing studies, significantly fewer non-*H. pylori* bacteria were detected in *H. pylori*-negative patients. Importantly, whilst *H. pylori* exclusively colonised the gastric glands, non-*H. pylori* bacteria invaded the lamina propria in 6/9 CG and 8/10 GIM *H. pylori*-positive patients. A rapid and cost-effective modified Gram stain was used to confirm these findings and enabled detection of non-*H. pylori* bacteria in GIM samples.

Conclusions
The invasion of the gastric lamina propria by non-*H. pylori* bacteria during *H. pylori*-associated CG and GIM represents an overlooked phenomenon in cancer progression. Future work must determine the mechanisms underlying the synergistic roles of *H. pylori* and other bacteria in carcinogenesis. This observation should redirect attempts to prevent, diagnose and treat GAC.

1 INTRODUCTION

Gastric adenocarcinoma (GAC) is the fourth leading cause of cancer-related deaths, accounting for 7.7% of cancer mortalities worldwide (1). *Helicobacter pylori* infection is associated with approximately 70% of GAC cases and the global prevalence of *H. pylori* infection is 43.9% (2). Correa's cascade describes the histopathological changes to the gastric mucosa during progression to GAC (3). *H. pylori* first triggers chronic gastritis (CG), which can lead to gastric intestinal metaplasia (GIM), dysplasia and finally GAC. Although genotypes of *H. pylori* that encode the virulence factors CagA, VacA and HtrA (4) are more associated with severe disease outcomes, the mechanism by which a minority of *H. pylori* infections (1%) develop GAC is not fully understood. In recent years, multiple 16S ribosomal RNA (16S rRNA) and metagenomic sequencing studies have profiled the human gastric microbiota during health and *H. pylori*-associated disease (5-8). The proposed model is that the healthy human stomach harbours a distinct microbial community structure and that upon *H. pylori* infection, this community structure shifts towards a dominance of *H. pylori* in CG. As carcinogenesis progresses, multiple other bacterial species displace *H. pylori* and dominate the GAC microbiota. However, sequencing studies are often prone to issues with contamination (9) and do not offer spatial resolution. A longstanding question is whether the gastric microbiota play a causative or correlative role in GAC. Here, we provide high resolution spatial images of *H. pylori* and non-*H. pylori* bacteria in patients with *H. pylori*-positive or negative CG and GIM. Importantly, we provide direct evidence of non-*H. pylori* bacteria invading the lamina propria in the early to middle stages of Correa's cascade, suggesting that non-*H. pylori* bacteria might play a synergistic role in the cause of these disease states.

2 MATERIALS AND METHODS

2.1 Sample preparation and pre-treatment protocol for automated tissue staining

Punch biopsy gastric corpus tissue samples were collected from consenting patients at the Queen Elizabeth Hospital, Birmingham fixed in formalin and prepared at the Human Biomaterial Resource Centre (HBRC), University of Birmingham by embedding in paraffin (Ethics #17-285) and retrieved from archived stocks at the Human Biomaterials Research Centre (HBRC). Exclusion criteria were previous *H. pylori* eradication therapy, antibiotic treatment 4 weeks prior to endoscopy and tissue from the cardia, fundus or antrum and patients under 30 years old. Routine histologic evaluation of H&E-stained gastric mucosal sections was used for *H. pylori* diagnosis. Tissue sections 4 μM thick were then prepared for RNAscope and immunohistochemistry staining, using a Leica BOND RX Fully Automated Research Stainer. Prior to staining, sections were prepared in the BOND RX, following three short protocols: 1) Deparaffinisation, rehydration, hydrogen peroxide and distilled water wash. 2) Heating to 100°C in target retrieval buffer ER2 (pH9; AR9640) for 45 min and manual washing with distilled water followed by 100% ethanol and drying at 60°C. 3) Incubation in protease III solution for 30 min, followed by a final wash in distilled water.

2.2 Optimisation of RNAscope treatments and immunohistochemistry (IHC) antibody concentrations for 5-plex automated staining

Automated RNAscope C1 and C2 probes against *H. pylori* (ACD-Bio, #542938) and Eubacteria (ACD-Bio; #464468), respectively, were first tested on healthy colon tissue in a fluorescent multiplex assay, using an RNAscope LS Multiplex Fluorescent Reagent Kit (ACD Bio; 322800), following the standard protocol recommended for this platform. Pre-treatment of tissue slides for automated tissue staining with lysozyme was not used as this was found to affect tissue integrity. However, automated tissue staining with lysozyme (micro bacteria detection protocol provided by ACD-Bio) and a 3-plex panel (E-Cadherin and RNAscope probes against *H. pylori* and Eubacteria) was used on all samples to ensure bacterial signal was not underestimated in comparison to 5-plex stained images (data not shown). A positive and negative control probe section was used on every RNAscope run to validate and assess its quality and the sensitivity of the assay. The bacterial gene *dapB* (ACD Bio; 312038) was used as negative control to confirm the absence of background noise and a cocktail of housekeeping genes *polr2A* C1, *ppiB* C2 and *ubc* C3 (ACD Bio; 320868) was used as positive control to validate the detection of the signal and the tissue integrity. *H. pylori* gene sequences can bind to both 16S rRNA probes against *H. pylori* and Eubacteria, whilst non-*H. pylori* bacteria stain with only the Eubacteria probe.All antibodies used in IHC steps were optimised prior, using chromogenic DAB staining of healthy colon tissue in addition to a Leica Bond Polymer Refine Detection kit (Leica; DS9800). Antigen retrieval was tested using pH6 (Leica Bond TM Epitope Retrieval 1; AR9961) and pH9 (Leica Bond TM Epitope Retrieval 2; AR9640) buffers by heating to 100°C for 20 min. Three different dilutions were tested for each antibody, as recommended by manufacturer. Ideal staining pattern and intensity was assessed and approved by a pathologist, whereby slides were then used as reference throughout the validation process. All antibodies were then tested for compliance with the RNAscope pre-treatment, to ensure stability after protease III digestion. Once each antibody was assigned an Opal fluorophore, single fluorescence assays were directly compared against DAB-stained colon tissue to optimise Opal concentration. To assess epitope stability during the following heat steps and to define the order of the addition of antibodies in the multiplex sequence, each antibody was tested individually in the different positions of the panel. Further probe and antibody information can be found in Supporting information Table 2.

2.3 Automated 5-plex co-RNAscope *in situ* hybridisation/immunohistochemistry protocol

The automated RNAscope Multiplex Fluorescent LS assay (ACD Bio, 322800) was conducted using a Leica BOND RX according to manufacturer's instructions, incubating the sections with C1 and C2 probes against *H. pylori* and Eubacteria, respectively, for 2 h. An automated immunohistochemistry staining protocol was immediately followed to fluorescently label E-cadherin, MUC5AC and MUC2. Between each staining cycle, a heat induced stripping step with pH6 solution was added. Images were acquired using a Vectra Polaris Multispectral whole slide scanner. Exposure times on the Vectra Polaris Slide scanner for the DAPI, 480, 520, 570, 620 and 690

channels were 1.13 ms, 2.47 ms, 36.06 ms, 5.61 ms, 29.58 ms, and 7.46 ms, respectively.

2.4 Counterstaining and section visualisation

Sections were counterstained with spectral DAPI (Akoya Biosciences) and mounted with ProLong Diamond Antifade Mountant, according to manufacturer's instructions. Mounted sections were stored in the dark at 4°C until viewing. During optimisation steps, sections were visualised using a Zeiss LSM 900 confocal microscope or Mantra 2 Quantitative Pathology Digital Workstation (Akoya Biosciences) and final images were obtained on a Vectra Polaris Whole Slide Scanner (Akoya Biosciences) and saved as a qptiff file. Images were viewed at 40x magnification using Phenochart Whole Slide Viewer with PhenoImager HT (Akoya Biosciences) or open source QuPath software (Version 0.4.3) (10). All .qptiff image files were spectrally unmixed by importing and stamping in Phenochart Whole Slide Viewer (Akoya Biosciences), unmixed and exported in InForm software (Akoya Biosciences) and finally restitched as a BIGTIFF file using Visiopharm software (Visiopharm, Hørsholm, Denmark).

2.5 Qualitative and quantitative image analysis

For quantitation of target markers in whole slide tissue sections, manual image analysis was conducted using Qupath. For each whole-slide scan, tissue regions were first annotated and defined as a region of interest (ROI). Tissue detection was then performed based on the average values of all channels using pixel thresholders. A pixel thresholder was used to calculate mean tissue area (μM²), which was exported. Separate pixel thresholders were then created for each individual Opal channel, corresponding to *H. pylori*, Eubacteria, MUC5AC or MUC2. The thresholders were saved, and average area annotation measurements (μM²) were obtained for each channel. To account for *H. pylori* double staining and detection in both the *H. pylori* and Eubacteria channels, Eubacteria area was quantified by calculating total Eubacteria channel area minus combined *H. pylori* and Eubacteria channel areas. For each whole slide scan, average percentage area coverage of each marker of interest was calculated by dividing individual channel area over total tissue area x 100. Data were exported from Excel to GraphPad Prism 9 (Version 9.5.1). For qualitative scoring of bacterial invasion, images were viewed using Phenochart Whole Slide Viewer (Akoya Biosciences) or QuPath. Invasion was scored, whereby 0 = no invasion, 1 = sparse invasion, 2 = moderate invasion (patches of bacteria across sample) and 3 = high invasion (multiple clear regions of bacterial invasion across sample). A Mann-Whitney test was used for statistical analysis in which * indicates $p<0.05$, ** indicates $p<0.01$, *** indicates $p<0.001$ and ns indicates non-significant. Data are presented as median ± SEM, for each group.

2.6 H&E and Modified Gram staining

Additional sections were stained with H&E for further inflammation analysis and scoring by an independent pathologist. A modified Gram stain was also followed for staining of bacteria in additional tissue sections (11).

3 RESULTS

3.1 Localisation of *H. pylori* and the gastric microbiota in chronic gastritis and gastric intestinal metaplasia

Due to anatomical differences and unique microenvironments within the gastric mucosa driving microbial variation (12), archived formalin-fixed paraffin-embedded (FFPE) tissue blocks from only gastric corpus tissue were retrieved from the Human Biomaterials Research Centre (n=32) for the purpose of this study. The associated clinical pathology reports confirmed samples were *H. pylori*-positive CG (n=9) or GIM (n=10) and *H. pylori*-negative CG (n=6) or GIM (n=7). H&E-stained tissue sections were prepared from the archived FFPE gastric corpus tissue blocks. Again, using routine histologic evaluation, an independent pathologist confirmed *H. pylori* status and graded all samples for inflammation (Supporting information Table 1). There was no significant difference in inflammation between *H. pylori*-positive and *H. pylori*-negative samples (data not shown). To detect *H. pylori* or non-*H. pylori* bacteria, sections were stained using RNAscope *in situ* hybridisation (ISH) probes against *H. pylori*-specific or conserved sequences of the 16S rRNA gene, respectively. The probe 'Eubacteria' was used to detect non-*H. pylori* bacteria. IHC enabled detection of the host cell markers E-cadherin, Mucins 5AC (MUC5AC) and 2 (MUC2) using automated tissue staining for CG and GIM samples. Goblet cells, present only in GIM, secrete MUC2, whereas MUC5AC is found in both healthy and diseased gastric mucus. Representative images of GIM and CG samples are presented in Figure 1 and Figure S1, respectively. Quantification of indicated markers are shown in Figure 2. Comparable levels of MUC5AC were observed across the patient groups and, as expected, there was a significant increase in MUC2 in GIM patients (Figure 2 C&D). Consistent with previous studies (13, 14), *H. pylori* exclusively colonised the gastric glands (Figure 1B). The presence of Eubacteria correlated with *H. pylori* infection in CG and GIM but were significantly reduced in the absence of *H. pylori* infection (n=13) (Figure 2B). This contrasts with the current dogma that there is a unique microbiota in *H. pylori*-negative individuals (5). Interestingly, there was an increase in levels of Eubacteria in *H. pylori*-positive GIM samples compared with *H. pylori*-positive CG. Although this was not statistically significant, this raised the possibility that the presence of GIM-specific MUC2 could provide intestinal-like microniches within the stomach that promote bacterial colonisation. As such, we observed co-localisation of non-*H. pylori* bacteria with MUC2 in 2/10 *H. pylori*-positive and 1/7 *H. pylori*-negative GIM patients (Figure S2).

3.2 Association of *Helicobacter pylori* with invasion of non-*H. pylori* bacteria to the lamina propria

Bacterial invasion is associated with multiple diseases of the gastrointestinal tract, causing damage to the epithelial architecture by triggering inflammatory responses (15-17). Whilst *H. pylori* colonised the gastric glands, non-*H. pylori* bacteria invaded the lamina propria in 6/9 patients with *H. pylori*-associated CG and 8/10 *H. pylori*-positive patients with GIM (Figure 3A-D). Qualitative scoring of Eubacterial invasion showed significantly more invasion in *H. pylori*-positive CG and GIM than *H. pylori*-negative CG and GIM (Figure 3G). Representative images of *H. pylori*-positive CG and

GIM patients with an invasion score of 3 are shown in Figure 3A-D, and *H. pylori*-negative patients with an invasion score of 0 can be seen in Figure 3E-F. Very few Eubacteria are seen in samples with an invasion score of 0. It is most likely that these rare occurrences of Eubacteria in the stomach represent transient bacteria, rather than stable colonisation (18). Invasion of *H. pylori* into the lamina propria is very rare across all patient samples, yet an instance of this can be seen in Figure 3C. Representative images of samples with invasion scores of 1-2 can be seen in Figure S3.

3.3 Visualisation of non-*H. pylori* bacteria using a modified Gram stain

Next, we aimed to confirm bacterial invasion at the cellular level in patients with *H. pylori*-positive CG (n=4) or GIM (n=4). As can be seen in Figure 4A-D, microniches of Gram-positive bacteria could be identified in all 4 *H. pylori*-positive GIM patients. Visualisation of Gram-negative bacteria with this technique was not clear and H&E-stained sections were superior for identifying *H. pylori* (data not shown). Bacteria could not readily be identified in *H. pylori*-positive CG patients using this technique (data not shown). This is consistent with the lower levels of non-*H. pylori* bacteria that were detected in CG patients in comparison to GIM patients (Figure 2B). Although further work is required to understand the biological consequences of invasive bacteria in carcinogenesis, this modified Gram stain technique could be used alongside the current histological diagnostic tools to stratify patients at higher risk for developing GAC.

4 DISCUSSION

Sequencing technologies have enabled characterisation of the human microbiota in health and disease in multiple organs. However, applying 16S rRNA PCR-based sequencing to low biomass samples, such as the skin and the stomach, can introduce sampling and technical errors in comparison to higher biomass samples (9) and do not offer spatial resolution. Here, we have circumvented these issues by applying advanced imaging technologies to directly visualise the gastric microbiota in CG and GIM. By combining detection of targeted sequences within the bacterial 16S rRNA gene with immunostaining against host cell markers E-cadherin, MUC5AC and MUC2 we show that *H. pylori* exclusively occupies the gastric glandular niche, which is in agreement with previous studies (13, 14). We have also shown the presence of significantly more non-*H. pylori* bacteria in *H. pylori*-infected CG and GIM patients, whereas there are barely detectable levels in *H. pylori*-negative CG patients and only slightly more present in *H. pylori*-negative GIM patients. This is in contrast to sequencing studies, which suggest a distinct microbiome exists in *H. pylori*-negative disease states (5-8). These discrepancies may be due many factors contributing to an over-representation of the gastric microbiota using sequencing techniques, such as amplification-based methods capturing bacterial DNA remnants, contamination issues (9) and detection of transient rather than persistent bacteria (18). Indeed, this study highlights the crucial need for researchers to use a combination of sequencing, spatial profiling and culture techniques to fully resolve the ecology of the gastric microbiota during health and disease. The most important observation made in this study was that non-*H. pylori* bacteria invaded the lamina propria in 67% of *H. pylori*-positive CG and

80% of *H. pylori*-positive GIM. The high prevalence of invasive bacteria in *H. pylori*-positive patients amongst this cohort of patients was surprising. However, this could be explained by these patients being symptomatic and therefore attending for further clinical investigations. Our preliminary studies using intestinal-type GAC tissue from gastrectomy samples highlighted that comparisons between CG and GIM gastric punch biopsy samples and gastrectomy samples are incredibly difficult to make with spatial biology approaches. The size, stage and molecular subtypes of GAC samples demands that three-dimensional reconstructions of consecutive tissue sections are required to fully resolve intratumoral microbial communities. As such, these samples were excluded from this study until this comprehensive analysis of GAC samples can be made.

The gastrointestinal tract provides an important barrier to pathogen invasion. Translocation of bacteria and their metabolites across the intestinal epithelial barrier is associated with gastrointestinal infections and a range of diseases, such as inflammatory bowel diseases and metabolic diseases (16, 17). Activation of immune cells in the lamina propria drives pathology in these disorders via the production of pro-inflammatory cytokines and reactive oxygen species. Thus, it is conceivable that invasive bacteria within the gastric lamina propria synergistically activate the immune response in *H. pylori*-associated CG and GIM. Further work is underway to triangulate the immune response to invasive bacteria within the gastric mucosa. Given that these archived gastric tissue samples were retrieved via the local tissue bank (HBRC), we did not have access to the associated *H. pylori* clinical isolates from these patients. Recently, Sharafutdinov and colleagues reported that *H. pylori* strains encoding the trimeric form of the HtrA serine protease, which proteolytically cleaves the cell junction proteins occludin, claudin-8 and E-cadherin, are associated with a higher GAC risk than strains encoding the monomeric form (4). It is therefore conceivable that individuals infected with strains of *H. pylori* that secrete the trimeric HtrA cause the gastric epithelial cell barrier to become ‘leakier’, thereby facilitating invasion of bacteria to the lamina propria. However, it is also possible that *H. pylori*-associated inflammation can cause disruption to the epithelial barrier by direct and indirect interactions between gastric epithelial cells and mucosal immune cells (19). Thus, we propose that *H. pylori* facilitates opportunistic invasion of the lamina propria by transiting microbes. Further work is required to compare bacterial invasion in patients that are infected with strains of *H. pylori* encoding the trimeric or monomeric HtrA. Unfortunately, we did not have access to healthy patients for endoscopy and so the microbial landscape in the healthy, *H. pylori*-negative gastric mucosa is yet to be determined using imaging-based approaches. Additionally, the prevalence and precise identity of invasive bacteria during the carcinogenic cascade must be determined in a larger cohort of patients.

Interestingly, we have also shown that the levels of non-*H. pylori* bacteria increased from CG to GIM (Figure 2B) and that microniches of MUC2 with non-*H. pylori* bacteria are apparent in GIM tissue samples (Figure S2). The region of non-*H. pylori* bacteria shown in Figure S1A represents the largest single region of non-*H. pylori* bacteria detected amongst all patient samples. Although the levels of Eubacteria was relatively low in this patient (0.14%), it is conceivable that this microniche of bacterial colonisation could be due to their use of the proton pump inhibitor, Rabeprazole (Table S1). However, our relatively low number of patients with known PPI use (Table S1) limits

our ability to correlate the use of PPI with changes in the gastric microbiota. Nonetheless, our data provides the first observation of non-*H. pylori* bacteria with MUC2 within the gastric mucosa. Further work is required to understand whether these unique pre-cancer microenvironments contribute to the estimated 0-10% of GIM patients who progress to developing GAC (21). Limitations of this study were that 94% of patients were male, cases of autoimmune gastritis within the *H. pylori*-negative CG samples is unknown and PPI use is only known for a small number of patients (5) within this cohort (Table S1). Future studies should address these important considerations, particularly the use of proton pump inhibitors, when assessing the role of *H. pylori* and the microbiota in gastric cancer.

Clinically, GIM has been termed the 'point of no return', given that antibiotic eradication of *H. pylori* in GIM provides only minimal benefit to patient's risk of developing GAC, in comparison to treatment of *H. pylori*-associated CG (21). Additionally, patients with GIM are monitored for progression to GAC with 3-yearly endoscopic surveillance due to a lack of convincing evidence on the use of biomarkers (21). Here, we show that a rapid and cost-effective modified Gram stain could identify non-*H. pylori* bacteria in GIM, whilst it was less superior at visualising *H. pylori* than H&E staining (data not shown). Therefore, further work could focus on optimising the modified Gram stain to better visualise Gram-negative bacteria, or, modified Gram staining in conjunction with H&E staining of consecutive tissue sections could be utilised for the diagnosis of invasive bacteria and *H. pylori,* respectively. Although future studies must determine whether invasive bacteria drive progression to GAC, it is possible that this represents a novel biomarker for GAC and that antibiotic treatment of GIM patients to eradicate both *H. pylori* and invasive bacteria could be implemented as a preventative treatment for GAC.

In conclusion, we have observed that invasive bacteria are associated with *H. pylori* infection in the early and middle stages of Correa's carcinogenic cascade and therefore represent an attractive target for microbiome-based interventions in the prevention, diagnosis and management of GAC.

REFERENCES

1. H. Sung, J. Ferlay*, et al.*, Global Cancer Statistics 2020: GLOBOCAN Estimates of Incidence and Mortality Worldwide for 36 Cancers in 185 Countries. *CA Cancer J Clin*. 71(3), 209-49 (2021).
2. Y. C. Chen, P. Malfertheiner*, et al.*, Global Prevalence of *Helicobacter pylori* Infection and Incidence of Gastric Cancer Between 1980 and 2022. *Gastroenterology*. 166(4), 605-19 (2024).
3. P. Correa, Human gastric carcinogenesis: a multistep and multifactorial process--First American Cancer Society Award Lecture on Cancer Epidemiology and Prevention. *Cancer Res*. 52(24), 6735-40 (1992).
4. I. Sharafutdinov, N. Tegtmeyer*, et al.*, A single-nucleotide polymorphism in *Helicobacter pylori* promotes gastric cancer development. *Cell Host Microbe*. 31(8), 1345-58 e6 (2023).
5. J. M. Noto, R. M. Peek, Jr., The gastric microbiome, its interaction with *Helicobacter pylori*, and its potential role in the progression to stomach cancer. *PLoS Pathog*. 13(10), e1006573 (2017).
6. R. M. Ferreira, J. Pereira-Marques*, et al.*, Gastric microbial community profiling reveals a dysbiotic cancer-associated microbiota. *Gut*. 67(2), 226-36 (2018).
7. S. Delgado, R. Cabrera-Rubio*, et al.*, Microbiological survey of the human gastric ecosystem using culturing and pyrosequencing methods. *Microb Ecol*. 65(3), 763-72 (2013).
8. Y. Li, Y. Ouyang*, et al.*, Research trends on the relationship between *Helicobacter pylori* and microbiota: A bibliometric analysis. *Helicobacter*. 28(6), e13021 (2023).
9. S. J. Salter, M. J. Cox*, et al.*, Reagent and laboratory contamination can critically impact sequence-based microbiome analyses. *BMC Biol*. 12, 87 (2014).
10. P. Bankhead, M. B. Loughrey*, et al.*, QuPath: Open source software for digital pathology image analysis. *Sci Rep*. 7(1), 16878 (2017).
11. R. D. Taylor, Modification of the Brown and Brenn gram stain for the differential staining of gram-positive and gram-negative bacteria in tissue sections. *Am J Clin Pathol*. 46(4), 472-4 (1966).
12. D. J. Wilkinson, B. Dickins*, et al.*, Genomic diversity of Helicobacter pylori populations from different regions of the human stomach. *Gut Microbes*. 14(1), 2152306 (2022).
13. C. Fung, S. Tan*, et al.*, High-resolution mapping reveals that microniches in the gastric glands control *Helicobacter pylori* colonization of the stomach. *PLoS Biol*. 17(5), e3000231 (2019).
14. D. Keilberg, Y. Zavros*, et al.*, Spatial and Temporal Shifts in Bacterial Biogeography and Gland Occupation during the Development of a Chronic Infection. *mBio*. 7(5), (2016).
15. R. S. Aleman, M. Moncada*, et al.*, Leaky Gut and the Ingredients That Help Treat It: A Review. *Molecules*. 28(2), (2023).
16. F. Schreiber, I. Balas*, et al.*, Border Control: The Role of the Microbiome in Regulating Epithelial Barrier Function. *Cells*. 13(6), (2024).
17. C. A. Thaiss, M. Levy*, et al.*, Hyperglycemia drives intestinal barrier dysfunction and risk for enteric infection. *Science*. 359(6382), 1376-83 (2018).

18. M. R. Spiegelhauer, J. Kupcinskas*, et al.*, Transient and Persistent Gastric Microbiome: Adherence of Bacteria in Gastric Cancer and Dyspeptic Patient Biopsies after Washing. *J Clin Med*. 9(6), (2020).
19. A. C. Luissint, C. A. Parkos*, et al.*, Inflammation and the Intestinal Barrier: Leukocyte-Epithelial Cell Interactions, Cell Junction Remodeling, and Mucosal Repair. *Gastroenterology*. 151(4), 616-32 (2016).
20. B. Ghaddar, M. J. Blaser*, et al.*, Denoising sparse microbial signals from single-cell sequencing of mammalian host tissues. *Nat Comput Sci*. 3(9), 741-7 (2023).
21. M. Banks, D. Graham*, et al.*, British Society of Gastroenterology guidelines on the diagnosis and management of patients at risk of gastric adenocarcinoma. *Gut*. 68(9), 1545-75 (2019).

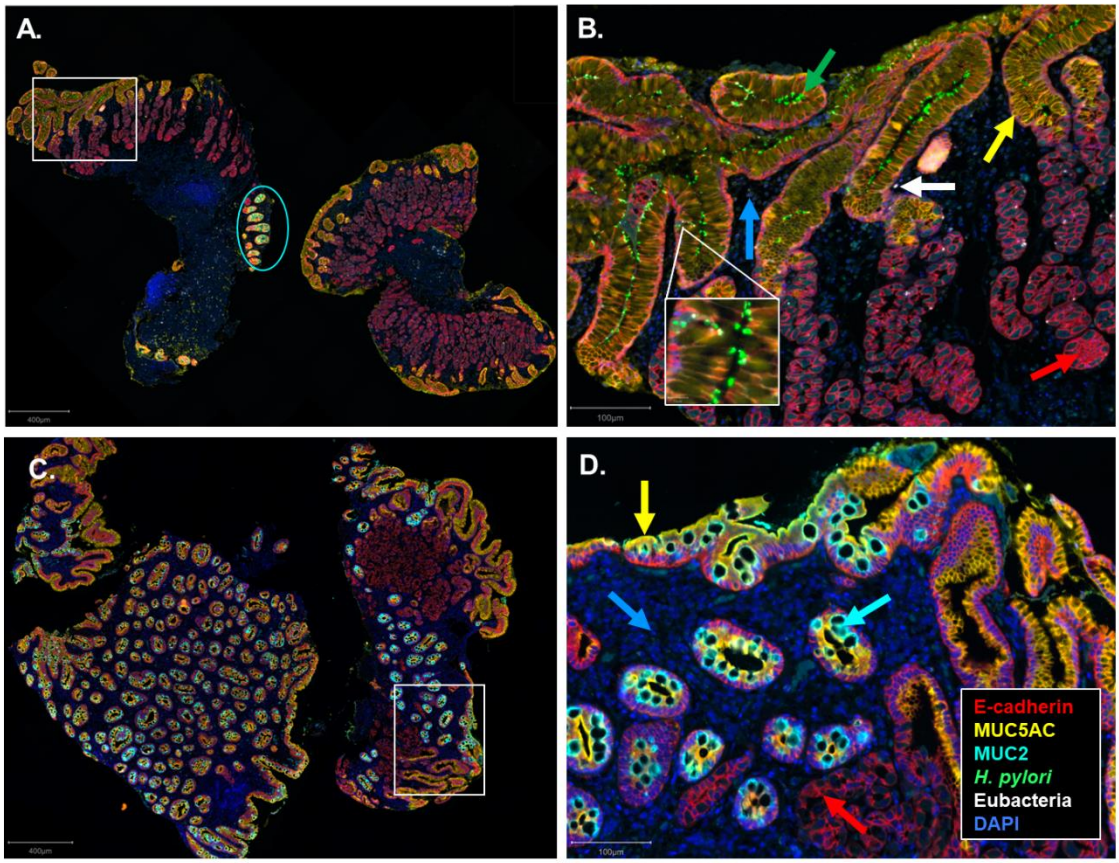

Figure 1. Spatial localisation of *H. pylori* and non-*H. pylori* bacteria in GIM revealed by RNAscope *in situ* hybridisation (ISH) and immunohistochemistry (IHC). Whole slide scans of stained patient tissue sections were obtained using a Vectra whole slide scanner. Images were spectrally unmixed, viewed and quantified using QuPath. **A & C)** A representative whole slide scan of a GIM *H. pylori*-positive (A) or *H. pylori*-negative (C) section showing RNAscope ISH probes '*H. pylori*' and 'Eubacteria' to detect *H. pylori* (green) and non-*H. pylori* bacteria (white), respectively. IHC staining against E-cadherin (red), MUC5AC (yellow) and MUC2 (turquoise) are also shown. **B & D)** A higher magnification of regions highlighted with a white box from panels A and C, respectively. The coloured arrows show the indicated markers and a region of MUC2 is highlighted within the cyan circle in Panel A.

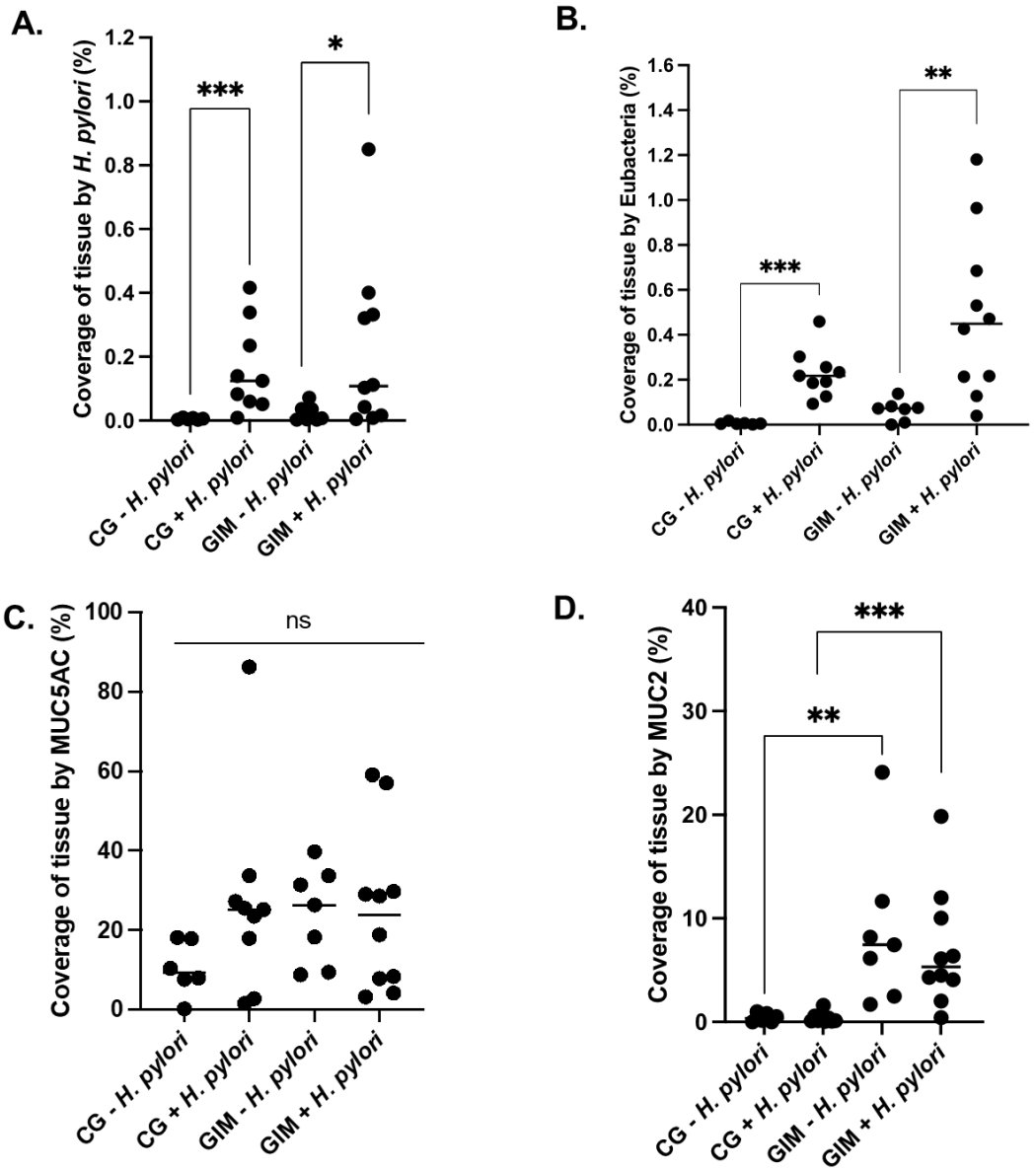

Figure 2. Quantification of target markers in tissue from whole slide scans, using QuPath. The percentage coverage of tissue for each patient group is shown for H. pylori (A), Eubacteria (B) MUC5AC (C) and MUC2 (D). Horizontal bars indicate the median for each indicated patient group. A Mann Whitney test was used to determine significance where * = $p<0.05$, ** = $p<0.01$ and *** = $p<0.001$.

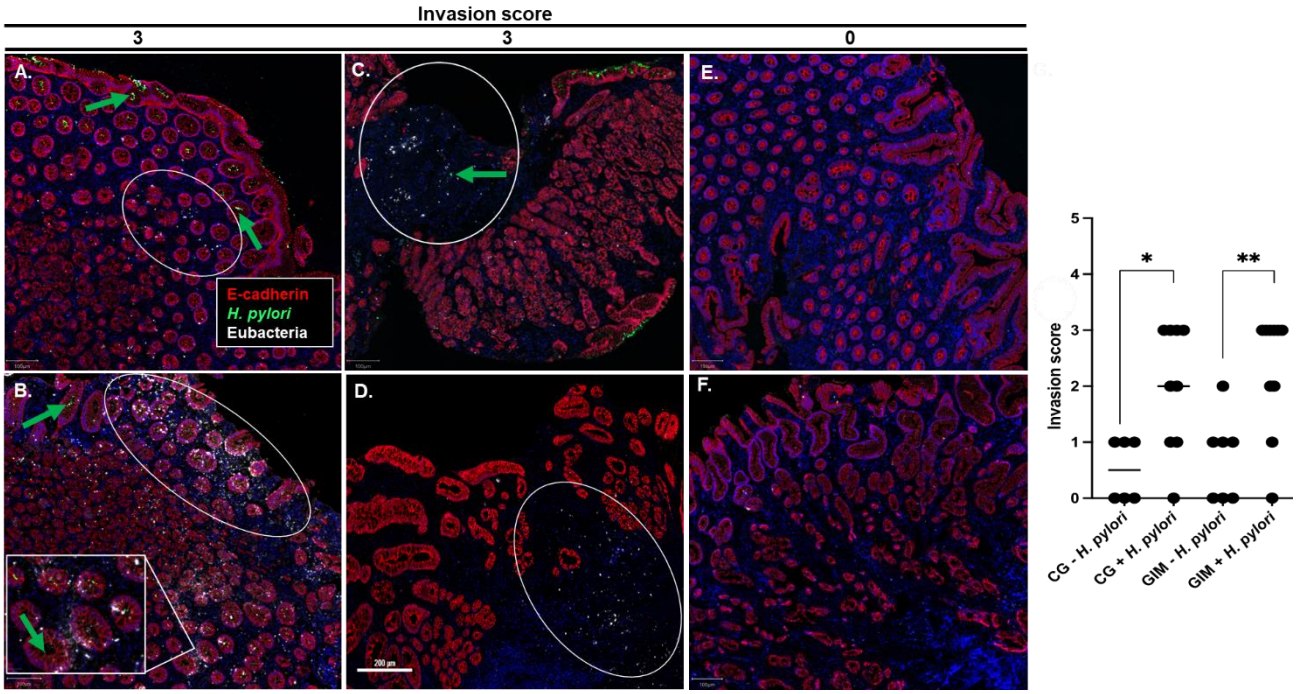

Figure 3. Non-*H. pylori* bacteria invade the gastric lamina propria in CG and GIM. Whole slide scans were obtained using a Vectra whole slide scanner. Images were spectrally unmixed and viewed using QuPath. **A-F)** Representative images showing Eubacterial (white) invasion in patients with CG (A-B), GIM (C-D), *H. pylori* negative CG (E) and GIM (F). Only E-cadherin (red), *H. pylori* (green), Eubacteria (white) and DAPI (blue) are shown for visualisation purposes. Arrows indicate the target markers. Eubacterial invasion is highlighted in white ovals for CG and GIM. A rare occurrence of *H. pylori* invasion to the lamina propria is indicated by the green arrow in (C). Qualitative invasion ISH scoring of Eubacterial invasion was determined for each patient as follows; 0 = no invasion, 1 = sparse, 2 = moderate and 3 = high invasion. Invasion scores for representative images are indicated above each column and qualitative scores for each patient group are shown in **(G).** Horizontal bars indicate the mean for each indicated patient group. A Mann-Whitney test was used to determine significance where * = $p<0.05$ and ** = $p<0.01$.

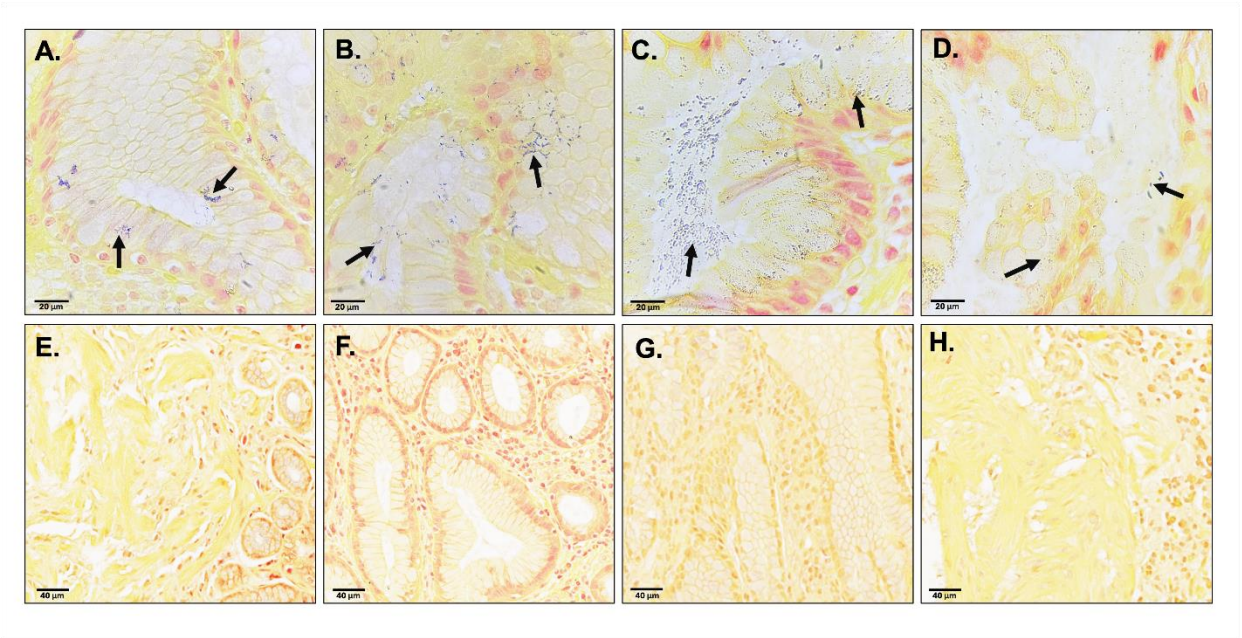

Figure 4. A modified Gram stain detects non-*H. pylori* bacteria in GIM. Archived FFPE biopsy tissue from *H. pylori*-positive GIM patients (n=4) were obtained from the Human Biomaterials Resource Centre (HBRC). After applying a modified Gram stain, slides were viewed at 100x magnification with oil immersion using a light microscope. Images A-D show a single representative image for each GIM *H. pylori*-positive patient. Images E-H show a region on the same patient where bacteria are not present. Black arrows in Panels A-D indicate purple stained bacteria.

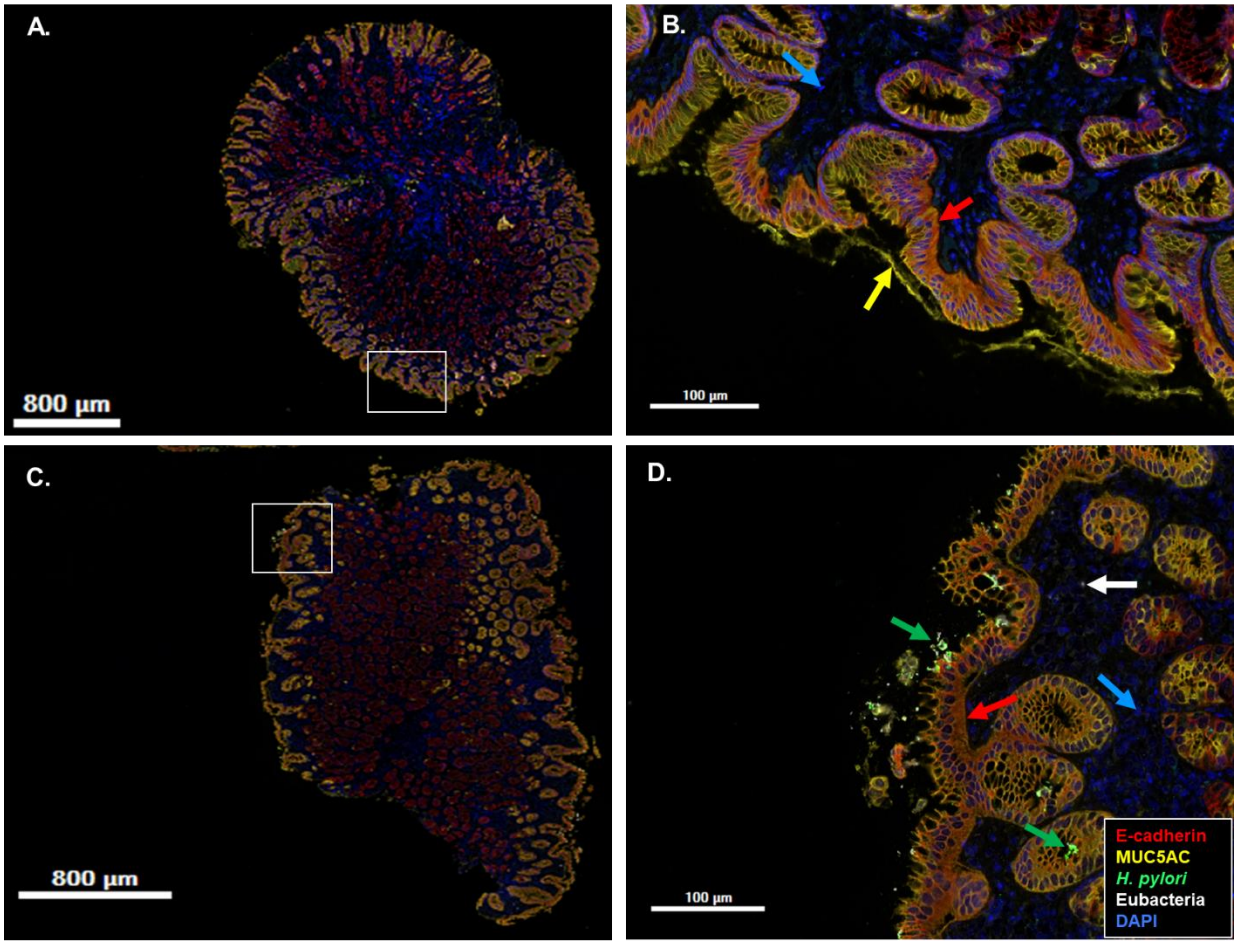

Figure S1. Spatial localisation of *H. pylori* and non-*H. pylori* bacteria in CG revealed by RNAscope *in situ* hybridisation (ISH) and immunohistochemistry (IHC). Whole slide scans of stained patient tissue sections were obtained using a Vectra whole slide scanner. Images were spectrally unmixed, viewed and quantified using QuPath. A & C) A representative whole slide scan of a CG *H. pylori*-negative (A) or *H. pylori-positive* (C) section showing RNAscope ISH probes '*H. pylori*' and 'Eubacteria' to detect *H. pylori* (green) and non-*H. pylori* bacteria (white), respectively. IHC staining against E-cadherin (red) and MUC5AC (yellow) are also shown. B & D) A higher magnification of regions highlighted with a white box from panels A and C, respectively. The coloured arrows show the indicated markers.

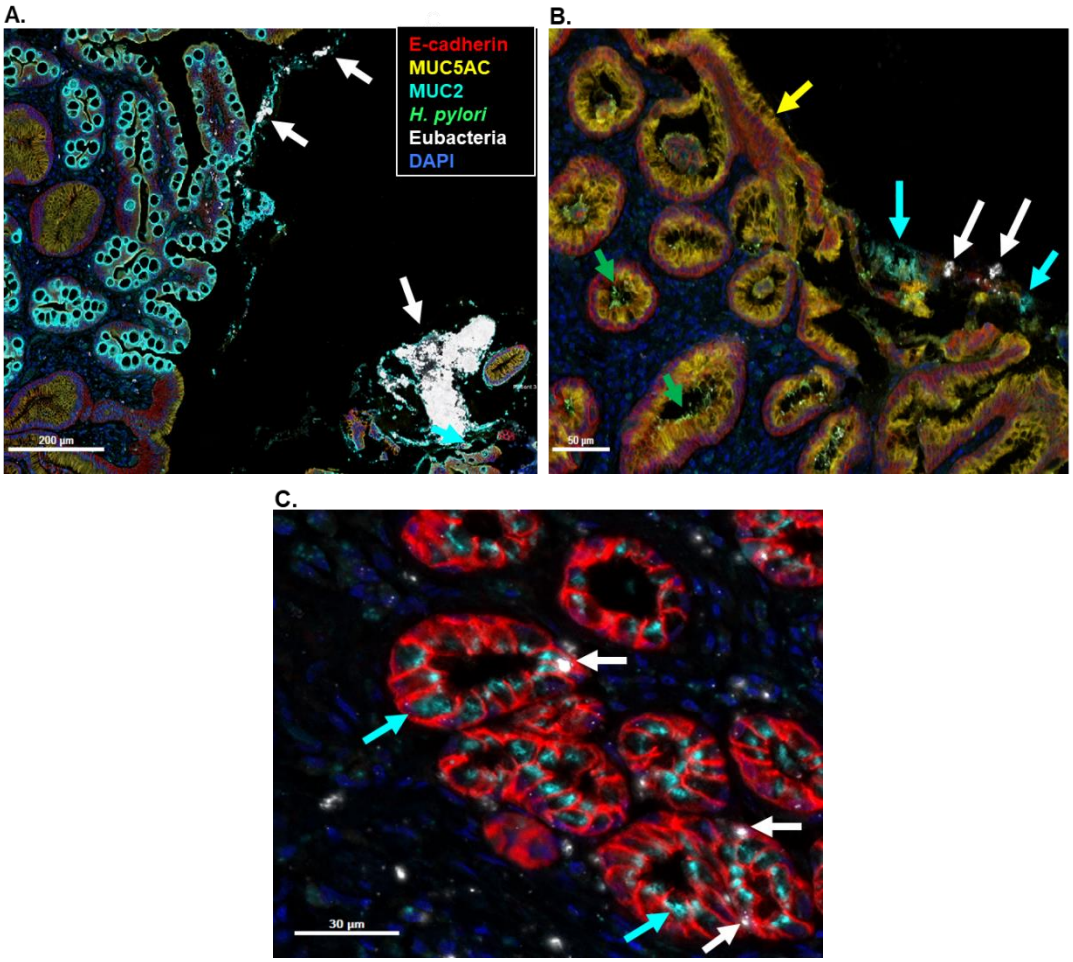

Figure S2. Co-localisation of non-*H. pylori* bacteria and Muc2 in GIM. (A-C) Whole slide scans of stained patient tissue sections were obtained using a Vectra whole slide scanner. Images were spectrally unmixed, viewed and quantified using QuPath. *H. pylori-negative* (A) or *H. pylori*-positive (B-C) GIM patient samples are shown. RNAscope *in situ* hybridisation probes '*H. pylori*' and 'Eubacteria' were used to detect *H. pylori* (green) and non-*H. pylori* bacteria (white), respectively. Immunohistochemistry staining against E-cadherin (red), MUC5AC (yellow) and MUC2 (turquoise) are also shown. The coloured arrows show the indicated markers.

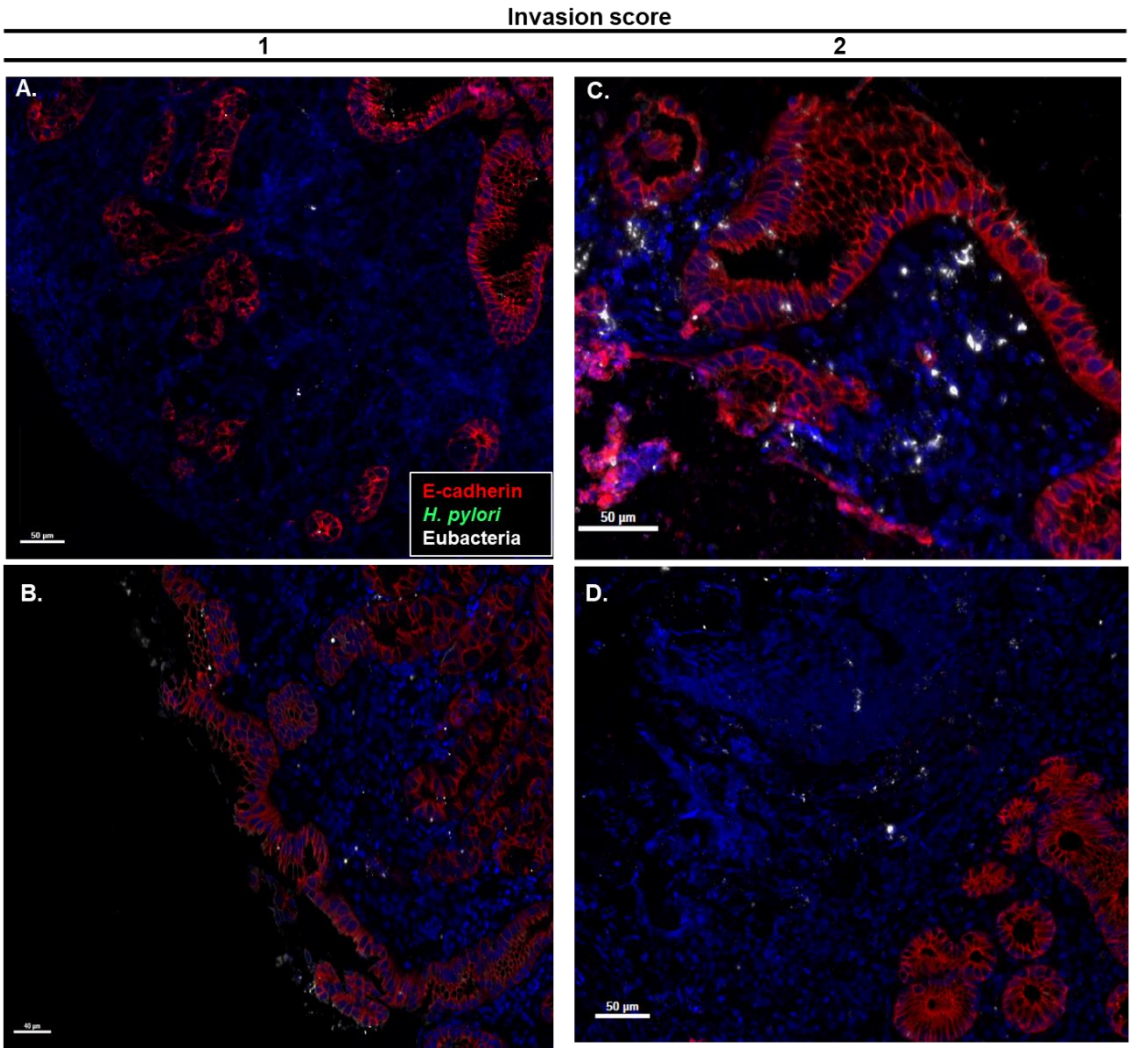

Figure S3. Representative images of scoring system for invasion of non-*H. pylori* bacteria to the gastric lamina propria. Whole slide scans were obtained using a Vectra whole slide scanner. Images were spectrally unmixed and viewed using QuPath. A-D) Representative images showing Eubacterial (white) invasion in patients with *H.* pylori-positive CG (A-B) or GIM (C-D). Eubacterial invasion was determined for each patient as follows; 1 = sparse and 2 = moderate invasion. Invasion scores for each image is indicated at the top of each column. Only E-cadherin (red), *H. pylori* (green), Eubacteria (white) and DAPI (blue) are shown for visualisation purposes.